BUBBLE INDUCED HEAT TRANSFER IN TWO-PHASE SYSTEMS

by

JIRI KUBIE

A thesis submitted in fulfilment of the requirements
for the degree of Doctor of Philosophy.

Department of Mechanical Engineering
The University of Aston in Birmingham

May 1974

SUMMARY

The two-phase theory of fluidization has been extended to cover heat transfer at surfaces by introducing the concept of a property boundary layer in the vicinity of the surface. The property boundary layer is a consequence of changed voidage and hence of changed thermophysical properties of the emulsion phase at the surface. A method of defining and calculating this boundary layer has been developed. A model of heat transfer from a surface to a gas fluidized bed based on the extended theory has been developed.

Aggregative gas fluidized beds and bubbling gas-liquid systems can be unified from the point of view of heat transfer by defining a general two-phase system consisting of a discrete gas bubble phase and a continuous dense phase. The thickness of the property boundary layer of the dense phase, which is in the vicinity of the surface, differentiates between bubbling liquids and aggregative gas fluidized beds since it is zero in the former case and non-zero in the latter one.

To investigate the mechanism of the bubble induced heat transfer, the multi-bubbling system has been simplified by generating a single continuous stream of gas bubbles in a stationary dense phase. Furthermore, a special probe which can be used to discriminate between conductive and convective modes of heat transfer has been designed. A model of the bubble induced heat transfer in the simplified system based on the surface renewal and penetration theory has been developed. It has been found that transient conduction into the dense phase is the most important mechanism of the bubble induced heat transfer. In the case of aggregative gas fluidized beds of small particles operating below the radiative temperature level, it is responsible for at least 90% of heat transfer; in the case of bubbling gas-liquid systems for about 75% of heat transfer. In the former case the remainder is contributed by superimposed gas convection, and in the latter case by liquid convection.

ACKNOWLEDGEMENTS

The author would like to thank and acknowledge:

Professor D.E. Elliott, under whose supervision this work was carried out, for his help and advice throughout the course of this work.

Mr J.R. Howard, Dr J. Broughton and other colleagues in the Department of Mechanical Engineering for their help in the preparation of this thesis.

The technical staff of the Department of Mechanical Engineering for their assistance in the experimental work.

The University of Aston in Birmingham for providing the financial support for this work.

TABLE OF CONTENTS

page

List of Tables viii

List of Figures ix

Notation xiv

1. INTRODUCTION 1

2. THE ANALOGY BETWEEN FLUIDIZED BEDS AND LIQUIDS 4

2.1. Introduction 4
2.2. Regimes of bed behaviour 4
2.3. Liquid analogy 6
2.4. Distribution of gas between emulsion and bubble phases 7
2.5. Heat transfer 8
  2.5.1. Analogy 8
  2.5.2. Heat transfer in bubbling liquids 9
    2.5.2.1. Theoretical analysis 10
    2.5.2.2. Experimental 12
    2.5.2.3. Discussion 14
2.6. Conclusions 15

3. EXTENSION OF THE ANALOGY, A MODEL OF HEAT TRANSFER IN GAS FLUIDIZED BEDS 16

3.1. Introduction 16
3.2. Basic models, their limitations and extensions 17
  3.2.1. General considerations 17
  3.2.2. Single particle models 18
  3.2.3. Emulsion phase models 19
3.3. Proposed model for surface to bed heat transfer 20
  3.3.1. Assumptions for the theoretical treatment 20
  3.3.2. Formulation of the model 21
  3.3.3. Voidage variations in the vicinity of a constraining wall 22
  3.3.4. Functions H(Z) and L(Z) 24
3.4. Theoretical heat transfer coefficients 25
  3.4.1. Numerical calculations 25
  3.4.2. The instantaneous Nusselt number 26
  3.4.3. The time-mean Nusselt number 26
3.5. Comparison with experimental data 27
  3.5.1. Current experimental methods 27
  3.5.2. Comparison 29

3.6. Discussion 29
3.7. Conclusions 31
3.8. Notation 32

4. BUBBLE INDUCED HEAT TRANSFER IN A UNIFIED TWO-PHASE SYSTEM 34

4.1. Introduction 34
4.2. General considerations 34
4.3. The heat transfer probe 36
  4.3.1. Requirements and design 36
  4.3.2. Application 37
4.4. A model of the bubble induced heat transfer 39
  4.4.1. Assumptions used in the theoretical model 39
  4.4.2. Full differential description of the system 41
  4.4.3. Non-steady heat transfer mechanism 42
  4.4.4. Influence of the initial wire temperature 43
  4.4.5. First approximation to the wire temperature 46
  4.4.6. Temperature field due to initial wire temperature 49
  4.4.7. Full solution for the average wire temperature 50
  4.4.8. Conduction model of the bubble induced heat transfer 51
4.5. Experimental technique and instrumentation 52
4.6. Conclusions 56

5. BUBBLE INDUCED HEAT TRANSFER IN GAS-LIQUID SYSTEMS 57

5.1. Introduction 57
5.2. Theoretical analysis 57
  5.2.1. Response to a step heating input 57
  5.2.2. Bubble induced heat transfer 58
5.3. Apparatus, instrumentation and experimental technique 60
  5.3.1. Experimental apparatus and instrumentation 60
  5.3.2. Experimental technique 61
5.4. Experimental results 62
  5.4.1. Response of the wire to a step heating input 62
  5.4.2. Instantaneous bubble induced heat transfer 63
  5.4.3. Time-mean bubble induced heat transfer 63
5.5. Discussion 64
  5.5.1. The heat transfer probe 64
  5.5.2. Bubble induced instantaneous average wire temperature 65
  5.5.3. Surface renewal and other assumptions 67
  5.5.4. Bubble induced heat transfer 69

5.5.5. Influence of the wire length/bubble diameter ratio 71
5.6. Conclusions 73

6. BUBBLE INDUCED HEAT TRANSFER IN GAS FLUIDIZED BEDS 75

6.1. Introduction 75
6.2. Theoretical analysis 75
6.2.1. Heat transfer mechanisms 75
6.2.2. The functions H(R) and L(R) 76
6.2.3. Response to a step heating input 78
6.2.4. Bubble induced heat transfer 79
6.3. Apparatus, instrumentation and experimental technique 80
6.3.1. Experimental apparatus and instrumentation 80
6.3.2. Experimental technique 81
6.4. Experimental results 82
6.4.1. Response of the wire to a step heating input 82
6.4.2. Instantaneous bubble induced heat transfer 83
6.4.3. Time-mean bubble induced heat transfer 83
6.5. Discussion 84
6.5.1. The influence of gas convection 84
6.5.2. The concept of the property boundary layer 85
6.5.3. Bubble induced instantaneous average wire temperature 87
6.5.4. Bubble induced heat transfer 88
6.6. Conclusions 92

7. GENERAL CONCLUSIONS AND SUGGESTIONS FOR FURTHER WORK 95

Tables 101

Figures 103

References 149

APPENDICES 153

1. Equivalent conductivity of the first slab 153
2. Space average wire temperature 155
3. Simplification of equations (4.16) to (4.25) 156
4. Method of numerical solution of equations (4.41) to (4.45) 157
5. Method of solution of equations (4.58) to (4.62) 162
6. Calibration of the UV-recorder traces 167
7. Voidage distribution in the wire vicinity 170
8. Programme for the numerical solution of equations (4.41) to (4.45) 172
9. Programme for the numerical solution of equations (4.67) to (4.76) 176

List of Tables.

page

3.1. Thermophysical properties of solid particles and gases at 25^{o}C. 101

3.2. Calculated values of thermal conductivity of the emulsion phase for $\varepsilon_E = 0.41$. (Method of Kunii and Smith[43].) 101

5.1. Thermophysical properties of liquids at 25^{o}C. 102

6.1. Thermophysical properties of solid particles and gases at 25^{o}C. 102

List of Figures.

page

2.1. Schematic diagram of the experimental apparatus used for the investigation of heat transfer in gas-liquid systems. 103

2.2. Probe used in the experimental investigation of heat transfer in two-phase gas-liquid systems. 104

2.3. A plot of a typical variation of the instantaneous surface temperature of the probe in a two-phase air-water system. 105

2.4. Comparison of experimental data with the theoretical result for the time-mean heat transfer in a two-phase air-water system. 105

3.1. Variation of the emulsion phase voidage in the vicinity of a flat surface. 106

3.2. Variation of the dimensionless conductivity b(Z) with Z for emulsion phase voidage $\varepsilon_E = 0.40$. 107

3.3. Variation of the dimensionless conductivity b(Z) with Z for emulsion phase voidage $\varepsilon_E = 0.50$. 107

3.4. Considerations for deriving b_{eq} used in the numerical calculations. 108

3.4a. Considerations for describing the voidage distribution in the vicinity of a constraining surface. 109

3.5. A plot of the instantaneous Nusselt number as a function of the instantaneous Fourier number. (Emulsion phase voidage is assumed to be $\varepsilon_E = 0.41$.) 110

3.6. A plot of the time-mean Nusselt number as a function of the time-mean Fourier number. (Emulsion phase voidage is assumed to be $\varepsilon_E = 0.41$.) 111

3.7. Instantaneous heat transfer in the system glass ballotini-air. Comparison of the present theory with experimental data of Antonishin *et al*[2]. 112

3.8. Instantaneous heat transfer in the system glass ballotini-carbon dioxide. Comparison of the present theory with experimental data of Antonishin *et al*[2]. 112

3.9. Instantaneous heat transfer in the system glass ballotini-freon 12. Comparison of the present theory with experimental data of Antonishin *et al*[2]. 113

3.10. Time-mean heat transfer in the system copper shot-helium. Comparison of the present theory with experimental data of Hampshire[30]. 114

3.11. Time-mean heat transfer in the system copper shot-air. Comparison of the present theory with experimental data of Butt[12], Desai[20] and Hampshire[30]. 114

3.12. Time-mean heat transfer in the system copper shot-carbon dioxide. Comparison of the present theory with experimental data of Desai[20]. 115

3.13. Time-mean heat transfer in the system glass ballotini-helium. Comparison of the present theory with experimental data of Hampshire[30] and Harakas & Beatty[31]. 115

3.14. Time-mean heat transfer in the system glass ballotini-air. Comparison of the present theory with experimental data of Butt[12], Cain[13], Hampshire[30], Harakas & Beatty[31] and Williams & Smith[60]. 116

3.15. Time-mean heat transfer in the system glass ballotini-freon 12. Comparison of the present theory with experimental data of Cain[13]. 116

3.16. Time-mean heat transfer in the system steel shot-helium. Comparison of the present theory with experimental data of Hampshire[30]. 117

3.17. Time-mean heat transfer in the system steel shot-air. Comparison of the present theory with experimental data of Butt[12] and Hampshire[30]. 117

3.18. Time-mean heat transfer in the system slag spheres-air. Comparison of the present theory with experimental data of Dunsky *et al*[21]. 118

3.19. Time-mean heat transfer in the system silica sand-air. Comparison of the present theory with experimental data of Desai[20] and Ernst[24]. 118

4.1. Schematic diagram of the probe used for the investigation of the bubble induced heat transfer. 119

4.2. Supporting bridge and instrumentation of the heat transfer probe. 120

5.1. Photograph of the experimental apparatus. 121

5.2. Line diagram of the experimental apparatus. 122

5.3. Response of the probe wire, placed in stationary water, to a step heating input (a = 152.5 μm, A = 113, T_∞ = 20°C). 123

5.4. Variation of the instantaneous average wire temperature with time (water, a = 20.6 μm, A = 108, T_∞ = 20°C, ξ = 1.0 to 1.1). From top to bottom: f = 0.8, 1.2, 2.3, 3.8 and 10.4 1/sec. 124

5.5. Instantaneous bubble induced heat transfer from a 41.15 μm dia wire into water (A = 108, ξ = 1.1, T_F = 25°C). 125

5.6. Instantaneous bubble induced heat transfer from a 41.15 μm dia wire into 50% glycerol solution (A=108, ξ=1.1, T_F=25°C). 125

5.7. Instantaneous bubble induced heat transfer from a 125 μm dia wire into water (A = 35.6, ξ = 1.1, T_F = 25°C). 126

5.8. Instantaneous bubble induced heat transfer from a 125 μm dia wire into n-heptane ($A = 35.6$, $\xi = 1.3$, $T_F = 25^{o}C$). 126

5.9. Time-mean bubble induced heat transfer from a 305 μm dia wire into water ($A = 14.6$, $\xi = 1.1$, $T_F = 25^{o}C$). 127

5.10. Time-mean bubble induced heat transfer from a 125 μm dia wire into water ($A = 35.6$, $\xi = 1.1$, $T_F = 25^{o}C$). 127

5.11. Time-mean bubble induced heat transfer from a 41.15 μm dia wire into water ($A = 108$, $\xi = 1.1$, $T_F = 25^{o}C$). 128

5.12. Time-mean bubble induced heat transfer from a 125 μm dia wire into n-heptane ($A = 35.6$, $\xi = 1.3$, $T_F = 25^{o}C$). 128

5.13. Time-mean bubble induced heat transfer from a 41.15 μm dia wire into n-heptane ($A = 108$, $\xi = 1.3$, $T_F = 25^{o}C$). 129

5.14. Time-mean bubble induced heat transfer from a 125 μm dia wire into 50% solution of glycerol ($A=35.6, \xi=1.1, T_F=25^{o}C$). 129

5.15. Time-mean bubble induced heat transfer from a 41.15 μm dia wire into 50% solution of glycerol ($A=108, \xi=1.1, T_F=25^{o}C$). 130

5.16. Influence of elevated film temperatures on the time-mean bubble induced heat transfer from a 125 μm dia wire into water ($A = 35.6$, $\xi = 1.1$ to 1.3). 130

5.17. Influence of ξ on the time-mean bubble induced heat transfer from a 101 μm dia wire into water ($A=128, \xi=2.8, T_F=25^{o}C$). 131

5.18. Influence of ξ on the time-mean bubble induced heat transfer from a 101 μm dia wire into water ($A=264, \xi=5.8, T_F=25^{o}C$). 131

5.19. Influence of ξ on the time-mean bubble induced heat transfer from a 101 μm dia wire into water ($A=264, \xi=9.1, T_F=25^{o}C$). 132

5.20. A typical plot of the instantaneous average wire temperature as a function of time. 132

6.1. A spherical particle in the wire vicinity
Equation of the wire $r = a$.
Equation of the spherical particle $(r - a - a_p)^2 + x^2 = a_p^2$ 133

6.2. Variation of the emulsion phase voidage in the wire vicinity for three different values of σ and $\varepsilon_E = 0.40$. 133

6.3. Variation of the dimensionless conductivity $b(R)$ in the wire vicinity for $\varepsilon_E = 0.40$, $k_p/k_G = 10$ and three values of σ. 134

6.4. Variation of the dimensionless conductivity $b(R)$ in the wire vicinity for $\varepsilon_E= 0.40$, $k_p/k_G= 10\ 000$ and three values of σ. 134

6.5. Photograph of the experimental apparatus. 135

6.6. Line diagram of the experimental apparatus. 136

6.7. Influence of gas velocity on the response of the wire, placed in the emulsion phase of silica sand 4 - air, to a step heating input. 137

6.8. Response of the wire, placed in an incipiently fluidized bed of silica sand 1 - air, to a step heating input. (Experimentally obtained value of the emulsion phase voidage.) 138

6.8a. Response of the wire, placed in an incipiently fluidized bed of silica sand 1 - air, to a step heating input. (Results are based on an assumed value of the emulsion phase voidage.) 138

6.9. Response of the wire, placed in an incipiently fluidized bed of silica sand 2 - air, to a step heating input. 139

6.10. Response of the wire, placed in an incipiently fluidized bed of silica sand 3 - air, to a step heating input. 139

6.11. Response of the wire, placed in an incipiently fluidized bed of silica sand 4 - air, to a step heating input. 140

6.12. Response of the wire, placed in an incipiently fluidized bed of silica sand 1 - helium, to a step heating input. 140

6.13. Response of the wire, placed in an incipiently fluidized bed of silica sand 1 - freon 12, to a step heating input. 141

6.14. Response of the wire, placed in an incipiently fluidized bed of silica sand 2 - helium, to a step heating input. 141

6.15. Response of the wire, placed in an incipiently fluidized bed of silica sand 2 - carbon dioxide, to a step heating input. 142

6.16. Variation of the instantaneous average wire temperature with time (incipiently fluidized bed of copper shot - air). From top to bottom: f = 1.7, 1.1, .83, .49, .33 and .13 1/sec. 143

6.17. Instantaneous bubble induced heat transfer from the wire into an incipiently fluidized bed of silica sand 1 - air. 144

6.18. Instantaneous bubble induced heat transfer from the wire into an incipiently fluidized bed of silica sand 2 - air. 144

6.19. Instantaneous bubble induced heat transfer from the wire into an incipiently fluidized bed of silica sand 3 - air. 145

6.20. Instantaneous bubble induced heat transfer from the wire into an incipiently fluidized bed of silica sand 1 - helium. 145

6.21. Instantaneous bubble induced heat transfer from the wire into an incipiently fluidized bed of silica sand 1 - argon. 146

6.22. Instantaneous bubble induced heat transfer from the wire into an incipiently fluidized bed of silica sand 1 - freon 12. 146

6.23. Time-mean bubble induced heat transfer from the wire into an incipiently fluidized bed of silica sand 1 - helium. 147

6.24. Time-mean bubble induced heat transfer from the wire into an incipiently fluidized bed of silica sand 1 - air. 147

6.25. Time-mean bubble induced heat transfer from the wire into an incipiently fluidized bed of silica sand 1 - argon. 148

6.26. Time-mean bubble induced heat transfer from the wire into an incipiently fluidized bed of silica sand 1 - freon 12. 148

A4.1. Grid used for the numerical calculation. 158

A5.1. Contour used for the inversion of function (A5.23). 165

A6.1. Schematic diagram of the bridge incorporating the heat transfer probe. 168

Notation.

Note: Symbols listed below are used in Chapters 1,2,4,5,6 and 7 only. Chapter 3 uses a separate list of symbols (Section 3.8). Additional or modified symbols used in Appendices are defined in the appropriate place in each Appendix.

a	Wire radius, radius of the heat transfer probe [m]
a_p	Particle radius [m]
A	L/a, aspect ratio of the wire (or probe) [-]
$b(R)$	Function defined by equation (4.51) [-]
c_p	Specific heat [J/kgK]
$c_p(R)$	Specific heat of the dense phase at point R [J/kgK]
d_b	Bubble diameter [m]
d_p	$2a_p$, particle diameter [m]
f	Frequency of bubble generation (or surface renewal) [1/s]
$fn(x)$	Function defined by equation (4.65) [-]
f_s	Surface flux [W/m^2]
Fo	$\kappa_D t/a^2$, instantaneous Fourier number [-]
Fo_m	κ_D/fa^2, time-mean Fourier number [-]
$g(R)$	Function defined be equation (4.50) [-]
h	Time-mean heat transfer coefficient between the wire and the pool [W/m^{2}K]
h_m	Time-mean heat transfer coefficient defined by eqn. (2.7) [W/m^{2}K]
$H(R)$	Function defined by equation (4.52) [-]
I	Current [A]
k	Thermal conductivity [W/mK]
$k(R)$	Thermal conductivity of the dense phase at point R [W/mK]
k_0	k_D/k_W, dimensionless thermal conductivity [-]
L	Wire (or probe) halflength [m]
$L(R)$	Function defined by equation (4.53) [-]
n	Summation parameter [-]
Nu	Nusselt number defined by equation (4.92) [-]
Nu_1	Nusselt number defined by equation (4.90) [-]
Nu_B	$2ah_B/k_L$, bubble induced Nusselt number [-]
Nu_N	$2ah_N/k_L$, natural convection Nusselt number [-]
Nu_S	$2ah_m/k_L$, Nusselt number used in Chapter 2 [-]
Nu_T	$2ah_T/k_L$, overall Nusselt number [-]
Nu_X	$Qa^2/k_D\Delta T$, experimentally obtained Nusselt number [-]

Q	Rate of heat generation per unit volume of the wire [W/m^3]
r	Space coordinate [m]
Δr	$r - a$, distance from the surface of the probe [m]
R	Dimensionless space coordinate (r/a) [-]
Re	$2aU/\nu_L$, Reynolds number [-]
R_W	Wire resistance [Ω]
s	$(2n + 1)\pi/2$, parameter [-]
t	Time [s]
T	Space average wire temperature [K]
T_D	Temperature of the dense phase [K]
T_{D1}	First approximation to the dense phase temperature [K]
T_{D2}	Dense phase temperature due to non-zero initial wire temperature [K]
T_E	Temperature of the emulsion phase [K]
T_F	$0.5(T_\infty + T_m)$ or $0.5(T_\infty + T_S)$, film temperature [K]
T_L	Temperature of the liquid [K]
T_{L1}	First approximation to the liquid temperature [K]
T_{L2}	Liquid temperature due to non-zero initial wire temperature [K]
T_0	Initial wire temperature [K]
T_{0A}	Initial space average wire temperature [K]
T_S	Surface temperature of the probe [K]
T_W	Temperature of the wire [K]
T_{W1}	First approximation to the wire temperature [K]
T_{W2}	Wire temperature due to non-zero initial wire temperature [K]
T_X	Experimentally obtained average wire temperature [K]
T_∞	Pool temperature [K]
ΔT	$T_X - T_\infty$, temperature difference [K]
U	Superficial gas velocity [m/s]
U_b	Bubble velocity [m/s]
U_{mf}	Minimum fluidizing velocity [m/s]
U_r, U_θ, U_x	Components of the dense phase velocity [m/s]
V_p	Particle volume [m^3]
W	Tk_D/Qa^2, dimensionless temperature [-]
W_1	T_1k_D/Qa^2, dimensionless temperature [-]
W_2	T_2/T_{0A}, dimensionless temperature [-]
W_{D1}	Dimensionless temperature defined by equation (4.46) [-]
W_{D2}	Dimensionless temperature defined by equation (4.77) [-]
W_{L1}	Temperature W_{D1} with liquid as the dense phase [-]
W_{W2}	Dimensionless temperature defined by equation (4.78) [-]
x	Space coordinate [m]

y	Integration parameter [-]
y_1	$y^2 + s^2/A^2$, parameter [-]
Z	x/L, dimensionless coordinate [-]
ΔZ	Space incremental size [-]
β	$1 - \varepsilon$, solid concentration [-]
$\beta(R)$	Solid concentration in emulsion phase at point R [-]
ε	Voidage [-]
$\varepsilon(R)$	Voidage of emulsion phase at point R [-]
θ	Space coordinate [-]
κ	Thermal diffusivity [m^2/s]
κ_0	κ_D/κ_W, dimensionless thermal diffusivity [m^2/s]
μ	Viscosity [kg/ms]
ν	Kinematic viscosity [m^2/s]
ξ	$2L/d_b$, parameter defined by equation (5.12) [-]
ρ	Density [kg/m^3]
$\rho(R)$	Density of the dense phase at point R [kg/m^3]
σ	a/a_p, parameter [-]
τ	$1/f$, periodic time [s]
τ_b	Bubble residence time on the surface of the probe [s]
ϕ	Function defined by equation (A5.27) [-]
ψ	Function defined by equation (A5.28) [-]
Ψ	Function defined by equation (4.89) [-]

Subscripts

1	First approximation to
2	Due to the non-zero initial wire temperature
B	Bubble induced
CORRECTED	The error in calculating the property boundary layer is accounted for (used in Chapter 6)
D	Dense phase
E	Emulsion phase
G	Gas phase
i	Instantaneous
L	Liquid phase
m	Time-mean
N	Due to natural convection
P	Particle of the emulsion phase
T	Overall quantity
W	Wire
X	Experimentally obtained

Definitions

liquid phase - continuous phase of a bubbling gas-liquid system

emulsion phase - continuous phase of an aggregative gas fluidized system

dense phase - continuous phase of a unified bubbling two-phase system

Chapter 1.

INTRODUCTION

Fluidization is an operation by which fine solid particles are transformed into a liquid-like state through contact with gas or liquid. The contact between the solid particles and the fluid (and hence the transformation into a liquid-like state) is usually accomplished by passing the fluid through a bed of fine solid particles. At low flow rates, fluid merely percolates through the void spaces between the stationary particles. When the flow rate is increased, a point is reached when the frictional force between solid particles in the bed and the upward flowing fluid is exactly counterbalanced by the particles weight. The particles are suspended in the upward flowing fluid. The bed is then considered to be just fluidized and is referred to as a bed at minimum fluidization[42]. At this point bed behaviour exhibits many of the features which are characteristic of the behaviour of liquids; namely, the free surface remains horizontal, solid bodies float in the bed, liquid-like flow properties of the bed etc. At even higher fluid flow rates, the bed behaviour generally depends on the properties of used fluid. For liquid fluidized beds, the bed progressively and uniformly expands, for gas fluidized beds a different behaviour is observed. With gas flow rates increased beyond minimum fluidizing conditions, large instabilities occur and bubbles rising through the bed are observed. The two-phase theory of fluidization suggests[17,56] that all gas in excess of that necessary for minimum fluidization rises through the bed as bubbles. Hence a gas fluidized bed can be regarded as analogous to a bubbling liquid.

Bubbles rising through a fluidized bed cause its continuous and vigorous mixing. This mixing is responsible for the high rates of heat transfer between a surface and a fluidized bed. Because of the rapid replacement of solids at the heat transfer surface, heat transfer coefficients at cooling or heating of surfaces are of the order of magnitude higher than in equivalent fixed beds or in comparable single phase gas flow. A heat transfer mechanism based on the liquid analogy has been developed[46], giving a good qualitative agreement between theoretical and experimental data, but failing completely for certain conditions. On the other hand, the liquid analogy (and the two-phase theory of fluidization) gives an excellent agreement between theoretical and experimental data in other aspects of fluidization, as for example, in the case of the rising velocity of gas bubbles[18].

The object of the present work is to examine the analogy between fluidized beds and liquids from the point of view of heat transfer and to investigate the mechanism of the bubble induced heat transfer in both systems (gas-liquid systems and gas fluidized beds).

In Chapter 2, the analogy between liquids and fluidized beds is discussed in more details and it is shown that in order to obtain a quantitative understanding of the problem of the bubble induced heat transfer, simplified systems must be used and a special heat transfer probe must be developed.

In Chapter 3, the analogy is extended by introducing the concept of a property boundary layer in the vicinity of the heat transfer surface in a fluidized bed and a new model of heat transfer in fluidized beds is developed and the theoretical results are compared with the experimental data available in the literature.

In Chapter 4, gas-liquid systems and gas fluidized beds are unified, the development of the special heat transfer probe is described and the general multi-bubbling system is simplified. Furthermore, a model of the bubble induced heat transfer, based on the surface renewal and penetration theory, is developed for the unified bubbling system.

In Chapter 5, the theory derived in Chapter 4 is applied on gas-liquid systems and is compared with experimental data. Similarly, in Chapter 6, the theory is applied on gas fluidized beds and is again compared with appropriate experimental data.

In Chapter 7, a general comparison of both systems is made and conclusions are drawn. Some suggestions for further work are also discussed.

Chapter 2.

THE ANALOGY BETWEEN FLUIDIZED BEDS AND LIQUIDS.

2.1. INTRODUCTION.

Under certain conditions a fluidized bed exhibits in many respects a liquid-like behaviour. To investigate various processes in a fluidized bed, it is sometimes convenient to use this analogy in order to assign thermophysical and transport properties to a fluidized bed. Thus one can speak, for example, about viscosity and thermal conductivity of a fluidized bed. The analogy is briefly discussed; it is shown that in many aspects the agreement between the theoretical results, based on the analogy, and the experimental data is very good, but that in the case of heat transfer the analogy gives only qualitative agreement. Hence it is proposed that the analogy must be extended to cover also this aspect of fluidization.

It is further shown, that even an analogous bubbling gas-liquid system (with well defined thermophysical and transport properties) is very complicated for theoretical investigation. It is suggested that a special heat transfer probe must be developed and that the mechanism of the bubble induced heat transfer can be best determined in simplified bubbling systems.

2.2. REGIMES OF BED BEHAVIOUR.

If a fluid is forced upward through a bed of fine solid particles, depending on the fluid velocity, several distinct regimes of bed behaviour can be observed. First, at low fluid flow rates, fluid merely percolates through the void spaces between the stationary particles. This is a fixed (or packed) bed. As the fluid flow rate increases, the drag forces on individual particles (and the total frictional force produced by the flowing fluid) increase too. Finally a point is reached when the frictional force between any particle in the bed and the fluid exactly counterbalances the weight of the particle. At this point particles become suspended in the fluid and rearrange to offer less resistance to the flow, giving rise to an incipiently fluidized bed. The bed is considered to be at minimum fluidization[42]. There are many theoretical equations and experimental correlations for the calculation of the minimum fluidizing velocity available in the literature[17,18,42].

If the flow rate of the fluid is increased above that required for incipient fluidization, the behavior of fluidized beds generally depends on the fluidizing agent. The bed will either continue to expand, so that the average distance between particles will become greater, or some of the excess fluid (above the flow rate required for minimum fluidization) will pass through the bed in form of bubbles[18]. In the former case, which is typical of liquid fluidized beds, flow instabilities are damped, and large scale instabilities are not usually observed - the bed is termed particulately (or homogeneously) fluidized. In the latter case, which is typical of gas fluidized beds, flow instabilities grow and bubbling and chanelling of the gas is observed. In addition, the aggitation of the bed increases with increasing gas flow rate, the movement of the solids becomes more vigorous and the bed usually does not expand much beyond its volume at minimum fluidization. The bed is then called aggregatively (or heterogeneously) fluidized bed. Parameters which affect the fluidized bed behaviour are many and are widely discussed in the literature. A criterion for distinguishing between particulate and aggregative fluidization was developed by Wilhelm and Kwauk[59]. The effect of a small void or perturbation in a fluidized bed has been considered mathematically[35,49,55]. A void once formed due to a flow instability can be either absorbed by the bed or grow into a larger void. The stability of a bed with respect to a small void can be used as yet another criterion to distinguish between particulate and aggregative fluidization.

At very high flow rates, the drag force on an isolated particle will be greater than its weight and the particles will be transported from the fluidized bed in the fluid stream. This regime is called dilute (or lean phase) fluidized bed with pneumatic transport of solids. Hence a fluidized bed can exist in only a certain range of fluid velocities - bounded at the minimum by the minimum fluidizing velocity and at the maximum by the terminal fluid velocity.

This work is mainly concerned with aggregative gas fluidized beds.

2.3. LIQUID ANALOGY.

The resemblence of fluidized systems to bubbling or boiling liquids is one of their most readily observable features. The literature about the analogy has been reviewed elsewhere[18]. There are many different aspects of the analogy and only some of them (mostly those related to the present work) are summarized here.

Solid bodies immersed in fluidized beds obey the laws of floating bodies, the upper surface of the bed remains horizontal and when two beds are connected their levels equalize. When a fluidized bed is disturbed, waves appear on the surface of the bed and behave like waves on the free surface of a liquid[18]. Further, particles in fluidized beds are in random motion which in many ways resembles Brownian motion of molecules in liquids[37]. The similarity between a number of phenomena in a liquid and in a fluidized bed results from the analogy between the energetic states of both systems. The measure of kinetic energy of molecules in liquids is the liquid temperature and the measure of kinetic energy of particles in fluidized beds is the velocity of the fluid. Hence the temperature of the liquid and the fluid velocity may be regarded as analogous[25].

The analogy between liquids and fluidized beds can be used to assign certain flow properties to fluidized systems. The most obvious one is the viscosity. Many investigators measured viscosity of fluidized beds. The direct method of Schugerl *et al*[53] using a rotating cylinder appears to be most satisfactory since it offers least disturbance to the bed. Grace[29] used the analogy between bubbles in liquids and in fluidized beds to calculate the viscosity of fluidized systems indirectly. The fact that the values of viscosities, obtained by so different methods, are similar confirms indirectly the analogy. The analogy is even more succesful in comparing rise velocities of bubbles in liquids and fluidized beds. This is discussed in the next Section.

2.4. DISTRIBUTION OF GAS BETWEEN EMULSION AND BUBBLE PHASES.

A gas fluidized bed contains regions of low (and sometimes zero) solid density, which are called gas bubbles. The region of higher solid density is called the emulsion phase. Bubbles in fluidized beds are very important for they are responsible for most of the features which differentiate a fixed from a fluidized bed. Because they modify gas flow through the system and induce and influence particle movement and mixing, which are responsible for high heat transfer rates between the bed and immersed surfaces, it is important to know the distribution of gas between emulsion and bubble phases. The simplest two-phase theory of fluidization, due to Toomey and Johnstone[56], suggests that all gas in excess of that required just to fluidize the system will pass in the form of bubbles, leaving the emulsion phase of the bed at the point of incipient fluidization. The direct evidence on the merit or otherwise of the simple two-phase theory of fluidization is scarce. There is some experimental evidence that for a number of gas-solid systems, the two-phase theory of fluidization is an oversimplification[19,27,28]. Because of its usefulness and simplicity it will be assumed as correct in the present work and where necessary it will be used in the following modified form: It is assumed that for a particular gas flow rate through the bed some of the gas will pass through the bed in the form of gas bubbles, leaving the emulsion phase at uniform voidage (not necessarily the voidage at minimum fluidization), which can be determined experimentally.

Basically, a fluidized bed is a two-phase system, where the continuous phase is provided by the gas and the discrete phase by solid particles. Using the two-phase theory of fluidization, the bed is still considered a two-phase system, but the characteristics and the functions of the two phases are different - gas bubbles constitute the discrete phase and the emulsion phase provides the continuous phase.

Gas bubbles have been investigated by many workers, both theoretically[18,35,48] and experimentally[18]. Gas bubbles in liquids and in gas fluidized beds are in many respects analogous, the main difference being that, as opposed to gas-liquid systems, there is an interchange of gas between discrete and continuous phases in gas fluidized beds. The validity of the analogy is perhaps best demonstrated on the agreement between rise velocities of bubbles in liquids and in gas fluidized beds, which for the same dimensionless descriptions are, within the experimental error, identical[18]. The analogy can also be demonstrated in other aspects of bubble behaviour, as for example, the wall effect and the bubble generation from a single orifice, where excellent quantitative agreement between behaviour of gas bubbles in liquids and in gas fluidized beds can be also observed.

2.5. HEAT TRANSFER.

2.5.1. ANALOGY.

Heat transfer in aggregative gas fluidized beds is of the order of magnitude higher than heat transfer in fixed beds or in single phase flow under similar flow rate conditions. Similarly, it has also been observed that two-phase gas-liquid flow is usually associated with large increase in heat transfer rates, as compared with single phase flow under similar flow conditions[41]. Hence the following analogy can be postulated. First, because the voidage of the emulsion phase is uniform, it is assumed that certain average thermophysical properties can be assigned to it. Then the emulsion phase can be regarded as analogous to liquid and thus a bed at minimum fluidization is analogous to stationary liquid and an aggregative gas fluidized bed to a liquid through which gas is bubbled. The heat transfer mechanism in the above described bubbling systems has been long established. Bubbles act as stirring agents and thus cause a continual mixing of the system (bubbling liquids or gas fluidized beds). The regions of high heat capacity (liquid or emulsion phase) are brought into contact with the heat transfer surface where they act as local heat sources or sinks. While the regions of high heat capacity are in contact with the heat transfer surface, heat is transferred by a non-steady heat transfer process. After a certain time they are replaced and the process is repeated. Models of heat transfer in gas fluidized beds, based on this analogy[46], give good qualitative agreement between theory and experiment, and good quantitative agreement can also be obtained if certain empiricism is included. (The situation is discussed more fully in Chapter 3.) The qualitative agreement between both systems (bubbling liquids and gas fluidized beds) can also be observed by comparing correlations for heat transfer from horizontal circular cylinders to bubbling liquids[41] and to gas fluidized beds[58]. Similar dimensionless groups occur in both correlations and trends of both correlations are also similar.

The analogy, as it stands, gives a good qualitative description to the mechanism of heat transfer in gas fluidized beds, but to obtain also quantitative agreement, the liquid analogy must be extended. This is further discussed in Chapter 3.

2.5.2. HEAT TRANSFER IN BUBBLING LIQUIDS.

It seems now appropriate to demonstrate the difficulties in theoretical investigations of mechanism of heat transfer in multi-bubbling systems. The problem discussed is one of heat transfer from circular cylinders into bubbling liquids (which are simpler, because the thermophysical properties of the continuous phase - liquid, are well known and tabulated).

The method of solution and the experimental apparatus have been described by the present author in more details elsewhere[41]. The solution described in[41] will be closely followed here.

2.5.2.1. Theoretical analysis.

Heat transfer from horizontal circular cylinders to bubbling liquids is investigated as follows: The presence of gas bubbles causes turbulence of the liquid. This turbulence is responsible for the continuous mixing of the liquid in the bulk of the pool (the mixture of gas and liquid inside the containing vessel). Because of the continuous mixing in the bulk of the pool, the bulk of the pool remains isothermal. Without loss of generality the pool temperature ,T_∞, is set at the reference zero. Due to mixing in the pool, liquid elements are continually brought into contact with the surface of the heat transfer probe. (A liquid element is defined as an elemental volume of liquid only, containing no gas bubbles.) While a liquid element is in contact with the heat transfer surface, heat is transferred by a non-steady heat transfer process. The amount of heat transferred depends on the duration of the contact time between the surface of the heat transfer probe and the liquid element. After a certain time, known as the 'residence time', each element on the heat transfer surface is replaced by a new element from the bulk of the pool. In this way the liquid elements on the surface of the probe are being periodically replaced. It is assumed that gas does not come into contact with the surface of the probe and that the time taken for the liquid elements to be transferred to and from the surface is negligible, although their residence time on the probe surface is finite. It is further assumed that a liquid element remains stationary, once it is brought into contact with the surface of the probe and that there are no convection currents within the element. This implies that the only mechanism of heat transfer from the probe into the liquid element is transient conduction.

To obtain the time-mean coefficient of heat transfer from the probe to the pool, it is necessary to know the residence time of each liquid element on the surface of the probe. It is assumed that the frequency of surface renewal is constant and that the residence time of all liquid elements on the surface is the same. Hence the Higbie uniform age distribution function[32], is used to calculate the time-mean heat transfer coefficient.

The walls of the heat transfer probe are thin and of low heat capacity. It is further assumed that the heat flux provided by the probe over its outer surface is uniform and constant with time. It is also assumed that the heat is transferred in the radial direction only and that the heat never penetrates beyond the outer boundary of the liquid element. Hence the one-dimensional heat diffusion equation in a semi-infinite medium is used for the mathematical description of the problem.

To obtain the instantaneous temperature field in a liquid element, subject to the above assumptions, requires the solution of the following equations:

$$t \geq 0,\ r \geq a \qquad \frac{\partial T_L}{\partial t} = \kappa_L \left(\frac{\partial^2 T_L}{\partial r^2} + \frac{1}{r} \frac{\partial T_L}{\partial r} \right) \tag{2.1}$$

subject to

$$t = 0,\ r \geq a \qquad T_L = 0 \tag{2.2}$$

$$t \geq 0,\ r = a \qquad -k_L \frac{\partial T_L}{\partial r} = f_s \tag{2.3}$$

A complete solution of equations (2.1) to (2.3) is given by Carslaw and Jaeger[15]. For small values of the Fourier number ,Fo, the instantaneous surface temperature of the probe may be approximated by:

$$(T_S)_i = \frac{2af_s}{k_L} Fo^{0.5} \left(\frac{1}{\pi^{0.5}} - 0.25\ Fo^{0.5} \right) \tag{2.4}$$

The time-mean surface temperature of the probe, using the Higbie uniform age distribution function, is calculated as

$$(T_S)_m = f \int_0^{1/f} (T_S)_i \, dt \tag{2.5}$$

where f is the frequency of the surface renewal of the liquid elements.

Substituting equation (2.4) into equation (2.5), the time-mean surface temperature of the probe is given by

$$(T_S)_m = \frac{2af_s}{k_L} \left(\frac{2}{3\pi^{0.5}} Fo_m^{0.5} - 0.125\, Fo_m \right) \quad . \qquad (2.6)$$

The experimental time-mean heat transfer coefficient is calculated by dividing the surface heat flux by the experimentally obtained temperature difference between the time-mean surface temperature of the probe and the temperature of the pool. The theoretical time-mean heat transfer coefficient is defined accordingly as

$$h_m = f_s/(T_S)_m \quad . \qquad (2.7)$$

Substituting equation (2.6) into (2.7), the expression for the theoretical time-mean heat transfer coefficient is, for small Fourier numbers ($Fo_m < 1$), obtained in the following form:

$$Nu_S = \frac{1}{\frac{2}{3\pi^{0.5}} Fo_m^{0.5} - 0.125\, Fo_m} \qquad (2.8)$$

The only non-primary parameter on the right hand side of equation (2.8) is the mean frequency of the surface renewal of the liquid elements, f, which is obtained experimentally. Expression (2.8) is valid for small Fourier numbers only. Similar, but more complicated expressions can be also found for large and intermediate Fourier numbers.

2.5.2.2. Experimental.

The experimental apparatus is shown in Figure 2.1. It consists of a bubbling column (BC), a distributor plate (DP), placed between the bubbling column and the distributor (DS), a cylindrical heat transfer probe (HT) and a cooling element (CE). Gas is introduced through a filter and a system of valves and flowmeters (VF). The direction of the heat flow is chosen for convenience from the heat transfer probe to the gas-liquid pool, because electrical heating of the probe is used. A schematic diagram of the heat transfer probe is shown in Figure 2.2. A hollow cylinder (HC), 138 mm long, made of stainless steel and 2.15 mm in diameter is used as the heat transfer probe. The temperature of the outer surface of the cylindrical probe is measured by at least five surface thermocouples which are soldered into it and insulated from the gas-liquid pool by a thin layer of 'Araldite'. This results in a slight local roughness of the outer surface of the probe, but its effect is negligible because the rough area is much smaller than the total surface area of the probe. The temperature of the gas-liquid pool is measured by shielded thermocouples.

Heat is supplied to the heat transfer probe by a heating element (HE) made from a nichrome wire. The rate of heat generation in the heating element is measured by a wattmeter. The temperature of the pool is kept constant by placing a cooling element (CE) inside it and by adjusting its cooling water flow rate in such a way as to counteract the high rate of heat supplied to the pool by the heat transfer probe. Because of the practically isothermal characteristic of the pool, no distortions of the temperature field within it are introduced by inserting the cooling element. Furthermore, the cooling element does not change the flow pattern. This can be verified by comparing heat transfer coefficients from the probe to the pool with and without the cooling element.

To place the probe across the bubbling column (BC), a 'perspex' support (PS) is used. Because of the low thermal conductivity of 'perspex', heat losses from the ends of the probe to the 'perspex' support are low and are estimated to be below 3 % of the total heat supply to the probe. Hence the heat supplied by the heating element, corrected for the end losses, is calculated. The heat transfer coefficient from the probe to the pool is calculated from the heat supplied by the probe and from the temperature difference between the average time-mean wall temperature of the probe and the temperature of the pool.

Water-air system is used to investigate the validity of the model based on transient conduction as the only mechanism of heat transfer. The frequency of surface renewal of the liquid is determined as follows: The temperature of the surface of the probe and of the liquid element in contact with it increases with the residence time. When this particular liquid element is swept away and a 'new' cold liquid element is brought into contact with the surface of the probe, the temperature of the surface drops suddenly and then starts increasing again. Hence the frequency of the surface renewal of the liquid is identical with the frequency of oscillation of the surface temperature of the probe, which is measured by a surface thermocouple and recorded.

2.5.2.3. Discussion.

For a particular gas flow rate, the fluctuations of the surface temperature were recorded. A typical time-temperature profile is shown in Figure 2.3. The mean frequency of surface renewal was determined and the heat transfer coefficient calculated from equation (2.8) was compared with that determined by a direct experiment. Equation (2.8) was applicable, because the maximum time-mean Fourier number encountered ($Fo_m=0.13$) was below unity. Both results (in dimensionless form) are shown in Figure 2.4. Figure 2.4 shows that the trend of both theoretical and experimental results is about the same, but that the theoretical values are, on average, about 40% smaller than the experimental ones. Reasons for this discrepancy are probably twofold. First, it is possible that incorrect readings of the mean frequency of the surface renewal were taken. Secondly (and more likely) there is a probability of the presence of a mechanism of heat transfer additional to conduction which was the only mechanism of heat transfer considered in the theoretical analysis. The additional mechanism of heat transfer (liquid convection) would increase the experimentally obtained heat transfer rates and be responsible for this discrepancy.

Although it seems reasonable to assume that transient conduction is the most important mechanism of heat transfer in bubbling liquids, the evidence of its exact contribution is inconclusive. In order to get a better insight into the problem, a heat transfer probe with well defined boundary conditions and multi-bubbling systems with controlled frequency of bubble generation must be used.

2.6. CONCLUSIONS.

The analogy between liquids and gas fluidized beds is a powerful tool for the investigation of many aspects of fluidization. Some aspects of it can be described by the analogy very well (for example, the bubble behaviour), but the analogy gives only qualitative agreement between theory and experiments in the case of heat transfer at surfaces.

It has been shown that transient conduction into the liquid phase is the most important mechanism of heat transfer in freely bubbling gas-liquid systems. It has been also shown that liquid convection might be responsible for up to 40% of heat transfer in these systems.

It is desirable to determine the exact contribution of various modes to the overall mechanism of heat transfer in bubbling systems, but it has been demonstrated that the investigation of the mechanism of heat transfer is very difficult in multi-bubbling systems. Hence simplified systems must be used in order to shed some more light on the precise mechanism of the bubble induced heat transfer.

Chapter 3.

EXTENSION OF THE ANALOGY. A MODEL OF HEAT TRANSFER IN GAS FLUIDIZED BEDS.

(Note: This Chapter uses separate notation listed in Section 3.8.)

3.1. INTRODUCTION.

Models for heat transfer between fluidized beds and surfaces are discussed in this Chapter. The approach to theoretical investigation is either to look at the behaviour of a single particle in the vicinity of the heat transfer surface or at the behaviour of a packet of the emulsion phase there (thus applying indirectly the liquid analogy). It is shown that models based on these two approaches provide basically two asymptotic solutions. The model developed here is a variant of the surface renewal and penetration theory of heat transfer. The packet theory (liquid analogy) is modified to allow for, and to describe quantitatively, variations of the emulsion phase voidage in the vicinity of the heat transfer surface (or in general, in the vicinity of any constraining wall). The voidage variations in the vicinity of the constraining surface are estimated from simple geometrical considerations and are then used to calculate the variations of the thermophysical properties of the emulsion phase there. The model so derived shows a good agreement with available experimental data without recourse to any of the semi-empirical approximatios that are features of the previous models.

Hence it follows that in order to obtain reasonable agreement between theoretical and experimental data of heat transfer, the liquid analogy must be extended: It is still assumed that everywhere, except in the vicinity of the constraining surface, the voidage of the emulsion phase of a gas fluidized bed remains uniform. It is then further assumed that the constraining wall influences the emulsion phase voidage only locally; thus the properties of the emulsion phase in the vicinity of the constraining wall are different from those in the bulk of the fluidized bed. Hence the concept of a property boundary layer is introduced. In bubbling liquids this situation does not arise. So the extended analogy can be described completely as follows: Gas fluidized beds (bubbling liquids) consist of a discrete gas bubble phase and a continuous emulsion (liquid) phase. Emulsion (liquid) phase has constant voidage and thus constant thermophysical properties everywhere in the bed except in the vicinity of the constraining surface, where a property boundary layer must be considered. The thickness of the property boundary layer is finite in the case of the emulsion phase of a gas fluidized bed and zero in the case of the liquid phase of a bubbling liquid system. (It is important to note that the property variations are assumed to be due to the influence of the constraining surface on the packing of particles only. To simplify the subsequent analysis the influence of temperature on the properties of the continuous phase is neglected and it is assumed that the temperature associated property boundary layer may be neglected too.)

3.2. BASIC MODELS, THEIR LIMITATIONS AND EXTENSIONS.

3.2.1. GENERAL CONSIDERATIONS.

Measurements of heat transfer between fluidized beds and boundary surfaces have been carried out by many investigators and extensive experimental data are available in the literature. A number of mathematical models have been proposed for the prediction of heat transfer coefficients, the most useful types being based upon transient conduction between the particles (or the emulsion phase) and the surface. None of the models gives agreement with experimental data, even under closely controlled residence time conditions, unless some empiricism is invoked, although when coupled with experimentally derived equations most models are capable of fitting experimental data gathered under wide range of conditions. The model proposed here has the advantage over the previous models that it can fit most of the available controlled residence time data, without any *a posteriory* empirical constants being used.

Nowdays, when considering mathematical models of fluidized bed heat transfer, two basic philosophies can be discerned. Both methods use a two-phase description of the system, but for each approach the characteristics and the functions of the phases are different. The first approach is to regard the bed as a fundamental system consisting of a continuous phase, provided by the fluidizing agent, and a discrete phase which is provided by the solid particles, and sets out to solve the transient heat transfer equations for single particles during their residence on the surface. The second approach uses the analogy between fluidized beds and liquids, so considers the emulsion phase to be the continuous phase and gas bubbles to constitute the discrete phase. The transient conduction equations are solved for a packet of emulsion phase swept up to the surface by the bubbles, a stirrer or by flowing the particles over the surface. Each of these approaches has some inherent advantages over the other.

3.2.2. SINGLE PARTICLE MODELS.

The simplest model based on this approach was developed by Botterill and Williams[10], who assumed that an isolated particle surrounded by gas contacts the heat transfer surface for a certain time during which the heat is transferred to it by transient conduction. The solution was necessarily numerical and the experimental results gathered from closely controlled residence time experiments were much lower than those predicted theoretically. This shortcoming was removed by the expedient of introducing a gas film between the particle and the surface. With this adjustment a good agreement between predicted and experimental data was possible for short particle residence times on the heat transfer surface. This is the major limitation on the use of this type of models, since even if the position and the residence time of particles near the surface are known precisely, there are still mathematical limitations in the basic model. The model will be accurate only if the heat from the heat transfer surface does not penetrate beyond the first layer of particles. The depth of heat penetration is given by[7]:

$$L_d \propto (\kappa_E t)^{0\cdot5} \tag{3.1}$$

and hence

$$\frac{L_d}{d_p} \propto Fo^{0\cdot5} \tag{3.2}$$

Where κ_E is the thermal diffusivity of the emulsion phase. Thus the single particle approach can be expected to be accurate at low Fourier numbers only. This limitation has been long recognised and Botterill *et al*[8] and Gabor[26] have solved the heat diffusion equations for additional layers of particles, however, the mathematical modelling of individual layers of particles has limitations and it is doubtful if the extension of the domain to further layers can be justified physically.

3.2.3. EMULSION PHASE MODELS.

The models based on the liquid analogy stem from the work of Mickley and Fairbanks[46], who consider a packet of constant voidage emulsion phase being swept into contact with the heat transfer surface for a period of time. During this time, known as the packet residence time, the heat is transferred by a non-steady conduction until the packet is replaced by a fresh packet from the bulk of the bed. Even assuming that all thermophysical properties of the packet can be determined accurately, the model still has limitations in that the presence of the heat transfer surface changes the voidage distribution of the packet in its vicinity and hence the packet properties in the vicinity of the surface differ from those in the bed. For this surface effect to be negligible, the heat penetration depth must be much greater than the layer of altered thermophysical properties (which is usually of the order of one particle diameter). Hence this model will be accurate for large values of the Fourier number only.

Models based on this approach have been considerably refined to extend their validity to low Fourier numbers. The methods used are either to introduce a time independent contact resistance at the bed-surface interface to account for the increased voidage in the vicinity of the surface[3], or, to consider the packet to have a limited depth (thus setting a boundary constraint)[61]. The concept of the time independent contact resistance appears to be a good first approximation to the problem, as it enables good curve fitting of the available data[4], however the physical reasoning behind it is somewhat tenuous and its introduction the result of mathematical expedience, rather than physical considerations[26]. The evaluation of this contact resistance is based upon empirical considerations, which enable a good data-fit to be obtained.

In conclusion, each of the basic approaches has limitations: the first being reasonable at low values of the Fourier number, the latter at large values. Extensions of these asymptotic solutions rely upon empirical considerations which somewhat reduce their theoretical validities. The model developed here is based upon the extended liquid analogy, by using the penetration theory on the emulsion phase with a modification to allow for variable properties in the vicinity of the heat transfer surface.

3.3. PROPOSED MODEL FOR SURFACE TO BED HEAT TRANSFER.

3.3.1. ASSUMPTIONS FOR THE THEORETICAL TREATMENT.

The assumptions are similar to those introduced by Mickley and Fairbanks[46]:

i) The emulsion phase has constant voidage and is isothermal when in the bulk of the bed. Without loss of generality the temperature of the bed is set at the reference zero.

ii) Packets of emulsion phase, initially isothermal, are transferred to the heat transfer surface, either by bubble induced circulation, by stirring or by flowing the solids. The heat transfer mechanism is one of transient conduction during the time of packet residence on the surface.

iii) The only constraint on the position of particles at the surface is provided by the surface itself[52], which influences the local packing and hence alters the local thermophysical properties of the packet.

iv) The variation of the packet voidage is confined to the plane normal to the wall.

3.3.2. FORMULATION OF THE MODEL.

Consider that the heat transfer is confined to the direction normal to the surface in the semi-infinite layer of the emulsion phase. The Fourier equation then takes the following form:

$$\rho(x)c_p(x)\frac{\partial T}{\partial x} = \frac{\partial}{\partial x}[k(x)\frac{\partial T}{\partial x}] \tag{3.3}$$

subject to

$$t = 0,\ x \geq 0 \qquad T = 0 \tag{3.4}$$

$$t \geq 0,\ x = 0 \qquad -k(x)\frac{\partial T}{\partial x} = f_s \tag{3.5}$$

All thermophysical properties refer to the emulsion phase and are functions of position.

These equations can be rewritten in dimensionless form

$$\frac{\partial W}{\partial Fo} = H(Z)\frac{\partial^2 W}{\partial Z^2} + L(Z)\frac{\partial W}{\partial Z} \tag{3.6}$$

subject to

$$Fo = 0,\ Z \geq 0 \qquad W = 0 \tag{3.7}$$

$$Fo \geq 0,\ Z = 0 \qquad \frac{\partial W}{\partial Z} = -1/b(0) \tag{3.8}$$

by using the following transformations

$$W = Tk_E/f_s d_p \tag{3.9}$$

$$Z = x/d_p \tag{3.10}$$

$$Fo = \kappa_E t/d_p^2 \tag{3.11}$$

$$g(Z) = \rho(Z)c_p(Z)/(\rho c_p)_E \tag{3.12}$$

$$b(Z) = k(Z)/k_E \tag{3.13}$$

$$H(Z) = b(Z)/g(Z) \tag{3.14}$$

$$L(Z) = \frac{db(Z)}{dZ} / g(Z) \tag{3.15}$$

where suffix E refers to those properties of the emulsion phase which are un-influenced by the constraining surface (properties of the packet beyond the property boundary layer).

In order to solve equations (3.6) to (3.8), the functions defined by equations (3.14) and (3.15) must be evaluated. These evaluations require a knowledge of the voidage variations in the vicinity of the heat transfer surface. This is discussed in the next Section.

3.3.3. VOIDAGE VARIATIONS IN THE VICINITY OF A CONSTRAINING WALL.

The variations of local voidage of fixed beds in the vicinity of a constraining wall have been investigated by several workers[6,40,51,52]. Using spherical particles the usual observation is that the voidage variation with distance from the constraining surface takes the form of a damped oscillation curve with a voidage minimum occurring at about one particle radius from the surface. In the case of fluidized beds, the oscillations of the voidage appear to be damped much more rapidly[39,40] and the voidage minimum is shifted further from the constraining surface. This situation is further amplified for non-spherical particles: the voidage remaining practically constant after a distance of one particle diameter from the wall and its minimum occurring at about 0.75 d_p from the surface.

As mentioned previously, particles at the same distance from the constraining surface will be influenced by it in the same way. Hence the mean voidage at any plane parallel to the constraining surface is a function of the distance of the plane from the constraining surface. The area mean voidage of these planes is defined as

$$\varepsilon(x) = 1 - \beta(x) \tag{3.16}$$

where $\beta(x)$, the solid concentration is given by

$$\beta(x) = \frac{A(x)}{A_B} \tag{3.17}$$

and where $A(x)$ is the solids cross sectional area at a reference plane, which is situated at a distance x from the constraining surface. In order to calculate the solid cross sectional area at any distance from the constraining surface, it is assumed that the particles in the bed can be approximated by uniform spherical particles having the diameter equal to the mean equivalent diameter of the actual particles, without affecting the voidage distribution within the packet of emulsion phase.

It is now postulated that for a bed of uniform spherical particles, the particles cross sectional area A(x) at a distance x from the constraining surface is proportional to the cross sectional area of a cylinder whose volume and height are identical to those of the segment of a spherical particle which can be found between the reference plane and the constraining surface while touching the constraining surface (Figure 3.4a).

When the reference plane is situated beyond one particle diameter from the surface, the fraction of a spherical particle which can be found between it and the surface is constant and equal to the entire particle. Thus it is implied that the asymptotic material cross section ,β_E, is attained at a distance of one particle diameter from the surface. The voidage variation can then be calculated as

$$x \le d_p \qquad A(x) \;\alpha\; V(x)/x \tag{3.18}$$

$$x > d_p \qquad A(x) \;\alpha\; V_p/d_p \tag{3.19}$$

where V(x) is the volume of that segment of a spherical particle between the surface and the reference plane and V_p is the volume of the whole particle.

Equations (3.18) and (3.19) can be rewritten as

$$x \le d_p \qquad \beta(x) = C\, V(x)/x \tag{3.20}$$

$$x > d_p \qquad \beta(x) = C\, V_p/d_p \tag{3.21}$$

where C is a constant of proportionality. The right hand side of equation (3.21) is a constant, un-influenced by the constraining surface, equal to the material concentration within the emulsion phase.

Hence

$$C\, V_p/d_p = 1 - \varepsilon_E = \beta_E \tag{3.22}$$

and the following forms of equations (3.20) and (3.21) can be obtained:

$$x \le d_p \qquad \beta(x) = (1 - \varepsilon_E)\,\frac{d_p}{x}\,\frac{V(x)}{V_p} \tag{3.23}$$

$$x > d_p \qquad \beta(x) = (1 - \varepsilon_E) \tag{3.24}$$

where V(x), the volume of the segment of a spherical particle between the reference plane and the constraining surface, is given as[50]:

$$V(x) = \frac{1}{3}\pi x^2(1.5d_p - x) \tag{3.25}$$

Equations (3.23) and (3.24) can be rewritten in dimensionless form:

$$Z \le 1 \qquad \varepsilon(Z) = 1 - 3(1 - \varepsilon_E)(Z - \tfrac{2}{3}Z^2) \tag{3.26}$$

$$Z > 1 \qquad \varepsilon(Z) = \varepsilon_E \tag{3.27}$$

The predicted variations of the voidage for two values of the emulsion voidage ,ε_E, are plotted in Figure 3.1. These predictions agree well with the experimental data of other investigators[39,40].

Equations (3.26) and (3.27) are used in the next Section to calculate the functions H(Z) and L(Z).

3.3.4. FUNCTIONS H(Z) AND L(Z).

i) When the fluidizing agent is a gas, then its heat capacity can be neglected as compared with that of the solids, so that

$$\rho(Z)c_p(Z) = (\rho c_p)_P \cdot \beta(Z) \tag{3.28}$$

and

$$(\rho c_p)_E = (\rho c_p)_P \cdot \beta_E \tag{3.29}$$

and hence

$$g(Z) = \beta(Z)/\beta_E \quad . \tag{3.30}$$

ii) The effective thermal conductivity of a packet of emulsion phase can be calculated from one of the models available in the literature. In this work the method proposed by Kunii and Smith[43] is used and it is assumed that its validity can be extended into regions of high voidage, as suggested by them[43]. The local effective thermal conductivity of a packet of emulsion phase can then be expressed in the following form:

$$k(Z) = \text{fn}[\ k_P\ ,\ k_G\ ,\ \varepsilon(Z)\ ] \tag{3.31}$$

Using equations (3.13) and (3.31), function b(Z) can be readily calculated; but k(Z) can be more easily evaluated graphically than from its explicit form[43]. Figures 3.2 and 3.3 show the behaviour of function b(Z) for various ratios of particle and gas thermal conductivities and two values of the emulsion phase voidage ε_E.

iii) Function H(Z) is then calculated from equation (3.14). In order to calculate function L(Z), function b(Z) must be differentiated either graphically (using Figures 3.2 and 3.3) or, as in this work, by numerical differentiation. Function L(Z) is then given by equation (3.15).

3.4. THEORETICAL HEAT TRANSFER COEFFICIENTS.

3.4.1. NUMERICAL CALCULATIONS.

Equations (3.6) to (3.8) were solved numerically using the voidage distribution given by equations (3.26) and (3.27). The calculated thermophysical properties vary very rapidly close to the heat transfer surface, which type of variations lends itself most readily to constant flux boundary conditions. The physical situation is somewhere between constant surface temperature and constant surface flux, however the solutions obtained by either approach are very similar[15]. In order to solve the equations accurately, very small space (and hence time) increments must be used because of these large variations of properties close to the surface. The size of increments needed makes computer times requirements extremely large.

In order to overcome this complication while not sacrificing much accuracy, it is assumed that the first space increment from the surface remains at steady state, so that the situation is as shown in Figure 3.4, and the dimensionless wall temperature ,W_W, can then be calculated, as shown in Appendix 1, from

$$W_W = W(0) = W(\Delta Z) + \frac{\Delta Z}{b_{eq}} \qquad (3.32)$$

where

$$b_{eq} = \frac{b(\Delta Z) - b(0)}{\ln \dfrac{b(\Delta Z)}{b(0)}} \qquad (3.33)$$

The temperature field in the packet is calculated for each time increment by a standard numerical technique[15], until a point is reached at which the dimensionless temperature ,W, becomes smaller than 10^{-10}. At this point the calculation is terminated and restarted for the next time increment. The space incremental size used is $\Delta Z = 0.05$. The solution thus obtained was checked for accuracy by halving and quartering the step-size. This demonstrated both, the adequacy of the original step-size and that the simplification (equations (3.32) and (3.33)) was numerically reasonable, leading to a great saving in computer time, while incurring a negligible loss of accuracy.

3.4.2. THE INSTANTANEOUS NUSSELT NUMBER.

The instantaneous Nusselt number is defined as

$$Nu_i = \frac{h_i d_P}{k_E} \qquad (3.34)$$

where h_i, the instantaneous heat transfer coefficient can be expressed as

$$h_i = \frac{f_s}{(T_W)_i} \qquad (3.35)$$

so that

$$Nu_i = \frac{d_P f_s}{k_E (T_W)_i} \quad . \qquad (3.36)$$

Thus from equation (3.9),

$$Nu_i = 1/(W_W)_i \qquad (3.37)$$

Figure 3.5 shows the variation of the instantaneous Nusselt number with the instantaneous Fourier number, Fo. It should be noted that the instantaneous surface temperature ,$(W_W)_i$, is equal to the packet temperature ,W, obtained from equations (3.6) to (3.8), calculated at the point $Z = 0$.

3.4.3. THE TIME-MEAN NUSSELT NUMBER.

The time-mean heat transfer coefficient (and hence the time-mean Nusselt number) can be calculated, it the mean residence time of the packets and their age distribution function on the surface are known, as

$$h_m = f_s/(T_W)_m \quad . \qquad (3.38)$$

In order to evaluate $(T_W)_m$ a certain age distribution function must be used. The simplest form for fluidized beds appears to be the uniform age distribution function[3,61], although many other forms can be used[1,16,61]. The effect of the distribution function is not numerically large[38,61], so that using the uniform age distribution function,

$$(T_W)_m = \frac{1}{\tau} \int_0^{\tau} (T_W)_i \, dt \tag{3.39}$$

where τ is the periodic time of packet renewal on the heat transfer surface (mean packet residence time). The time-mean Nusselt number is

$$Nu_m = 1/(W_W)_m \tag{3.40}$$

where

$$(W_W)_m = \frac{1}{Fo_m} \int_0^{Fo_m} (W_W)_i \, dFo \quad . \tag{3.41}$$

Figure 3.6 shows the variation of the time-mean Nusselt number with the time-mean Fourier number for various solid-gas combinations.

3.5. COMPARISON WITH EXPERIMENTAL DATA.

3.5.1. CURRENT EXPERIMENTAL METHODS.

The discrepancies amongst the available experimental data, obtained in freely bubbling beds under apparently identical conditions of fluidization, can be of several orders of magnitudes[44], reflecting the many parameters which can influence fluidized bed heat transfer rates. Hence in order to test various theories or develop new models, simplified systems, in which the bed behaviour is closely controlled, are used. The experimental systems can be classified as follows:

i) The low thermal capacity probe. In this technique a small, low heat capacity heating foil is used to measure both heat transfer coefficients and packet residence times in freely bubbling beds[47]. While this technique is very useful, the results obtained are subject to errors, because the surface boundary conditions are not usually well defined, and further, because the packet voidage at the surface is disturbed by the passing bubbles.

ii) Stirred beds. The heat transfer probe is moved through the bed on a stirrer[21], or the bed is stirred past the heat transfer probe[10], in order to effect the residence time control. However this technique involves two questionable assumptions. First, that particle replacement over the entire surface is complete, and secondly, that the bed structure is uneffected by the stirring. Each of these assumptions has been shown to be of limited validity[26].

iii) Flowing packed beds. According to the two-phase theory of fluidization, the emulsion phase of a fluidized bed is considered to be under approximately incipiently fluidized conditions. The incipiently fluidized bed has many of the characteristics of a packed (fixed) bed[18], so that the emulsion phase can be for many purposes simulated by a packed (fixed) bed. Many experimental data have been gathered for packed beds flowing over heat transfer surfaces. The main experimental limitation of this technique is that particle spin has been observed under some conditions[9].

iv) Transient response. In this technique a heat transfer probe of known heat capacity and initial temperature is submerged into an incipiently fluidized, or packed, bed[2]. The variation of the heat transfer coefficient with time, obtained from the temperature response of the probe, is analogous to the response of a packet of particles (or emulsion phase) at a heat transfer surface in a fluidized bed over the same time interval. This technique suffers from the same disadvantage as the first method because, again, the boundary conditions might be difficult to define, however the packing at the surface is not, in this case, disturbed by the passing bubbles.

Experimental data, obtained under all of the above conditions, are available in the literature. In comparing these data with the prediction of this work, it was sometimes necessary to use assumed values for the emulsion phase voidage. The voidage then used was $\varepsilon_E = 0.41$ and the thermophysical properties were calculated as outlined in Section 3.3.4. The properties of the solid particles and gases, used in this comparison are set-out in Table 3.1. Calculated thermal conductivities of the emulsion phase are shown in Table 3.2.

3.5.2. COMPARISON.

The predictions for the instantaneous Nusselt numbers, obtained here, are compared with the results of Antonishin *et al*[2] in Figures 3.7 to 3.9. The asymptotic Mickley and Fairbanks solution[46], assuming a constant surface flux boundary condition, and given by Carslaw and Jaeger[15] as

$$Nu_i = 0.5\ \pi^{0.5} Fo^{-0.5} \quad , \qquad (3.42)$$

is also included.

The experimental results of a number of workers for the time-mean Nusselt numbers are compared with the predictions of the present theory in Figures 3.10 to 3.19. Again the Mickley and Fairbanks solutions, calculated from equations (3.38), (3.39) and (3.42) as

$$Nu_m = 0.75\ \pi^{0.5}\ Fo_m^{-0.5} \quad , \qquad (3.43)$$

are included.

3.6. DISCUSSION.

As the present model involves the use of the experimental and theoretical results of several workers, for example in calculating voidage variations near surfaces or emulsion phase properties, it is very satisfying to observe the very good agreement between the present theory and the experimental data available in the literature. It is significant that the best agreement between theory and experiment was obtained using the results from experiments conducted under very carefully controlled conditions, with materials of well known thermophysical properties. This suggests that where the disagreement is most pronounced, the true experimental conditions may not have been known. These errors may be due to:

i) The stirrer not being 100% efficient.

ii) In flowing packed beds some particle rotation could occur.

iii) The voidage of the emulsion phase was not reported in many of these experiments and the value of $\varepsilon_E = 0.41$, assumed here, may not be correct.

iv) Because of the relative lack of knowledge about the thermal conductivity of the emulsion phase, the calculated thermal conductivity of the emulsion phase is probably the biggest single source of error. This error is indicated by the fact that in cases where the disagreement is strongest, the results of a particular study fall systematically either above or below the theoretical curve.

v) In the case of fluidized metals a further complication is that a microlayer of oxides on the surface of the particles would considerably effect their conductivity and hence also the effective thermal conductivity of the emulsion phase.

Some of these effects could be eliminated by calculating the effective thermal conductivity of the emulsion phase from heat transfer results for long packet residence times, using the asymptotic Mickley and Fairbanks solution[46]. However, the agreement obtained without using this method seems to make such a refinment unnecessary.

None of the previous models of heat transfer in fluidized beds (Section 3.2) has been capable of producing acceptable agreement with experimental results over the full range of experimental data without the introduction of some form of a semi-empirical approximation . While these approximations, such as a gas film or a finite penetration depth, have obvious physical significance, they are ad hoc expedients rather than solutions to the real problem of behaviour of particle packets in the vicinity of a heat transfer surface. The model developed here is similar to the variable wall properties approach, long used in single phase heat transfer[45].

Since most of the experimental data used in the comparison (Section 3.5.2) were obtained from experiments conducted in fluidized beds of small particles, the contribution of gas convection to the overall mechanism of heat transfer can be neglected[5,54]. Figures 3.7 to 3.19 then demonstrate that the model developed here gives good agreement with experimental data in cases where conduction is the predominant mode of heat transfer. In principle this model could be extended to more complicated mixed-mode heat transfer situations, for example to high pressure systems where gas convection heat transfer becomes significant[9].

The voidage variation in the vicinity of a surface could probably be described by a more accurate expression than that developed here and the theoretical solution and numerical calculations could be improved, however it is doubtful whether the increase in precision of the theoretical solutions could be justified in terms of experimental limitations. In order to get further justification of the present model, it is desirable to obtain some more experimental results, particularly in the range where the property boundary layer is controlling. This is done in Chapter 6.

Bubbling liquids and gas fluidized beds can be unified from the point of view of heat transfer by introducing the concept of the property boundary layer. Bubbling liquids differ from the gas fluidized beds in the thickness of the property boundary layer. Because the voidage variations are confined to a distance of one particle diameter from the surface, the property boundary layer is of the same thickness - i.e. one particle diameter. Hence the thickness of the property boundary layer varies from relatively large (for gas fluidized beds of coarse particles), through relatively small (for gas fluidized beds of fine particles) to zero (for bubbling liquids).

3.7. CONCLUSIONS.

Bubbling liquids and gas fluidized beds have been unified from the point of view of heat transfer by introducing the concept of the property boundary layer in the vicinity of the heat transfer surface. The concept of the property boundary layer results from the presence of the heat transfer surface and its effect on the local voidage of the emulsion phase there. The thickness of the property boundary layer is assumed to be one particle diameter. The thickness of the property boundary layer differentiates between liquids and fluidized beds: - it is zero for bubbling liquids and non-zero (equal to the particle diameter) for fluidized beds.

The model of heat transfer derived here, based on the packet theory, extended to take into account the property boundary layer, agrees well with experimental data available in the literature.

3.8. NOTATION.

(Note: This notation is applicable to this Chapter only.)

A_B	bed cross sectional area $[m^2]$
$A(x)$	cross sectional area of solid particles at point x $[m^2]$
b_{eq}	equivalent dimensionless conductivity - eqn.(3.33) [-]
$b(Z)$	function defined by eqn. (3.13) [-]
c_p	specific heat [J/kgK]
$c_p(x)$	specific heat of emulsion phase at point x [J/kgK]
C	constant of proportionality $[1/m^2]$
d_p	particle diameter [m]
f_s	surface flux $[W/m^2]$
$fn(x)$	function of x
Fo	$\kappa_E t/d_p^2$, instantaneous Fourier number [-]
Fo_m	$\kappa_E \tau/d_p^2$, time-mean Fourier number [-]
$g(Z)$	function defined by eqn. (3.12) [-]
h	heat transfer coefficient $[W/m^2K]$
$H(Z)$	function defined by eqn. (3.14) [-]
k	thermal conductivity [W/mK]
$k(x)$	thermal conductivity of emulsion phase at point x [W/mK]

L_d	heat penetration depth [m]
$L(Z)$	function defined by eqn. (3.15) [-]
Nu	hd_p/k_E, particle Nusselt number [-]
t	contact time [s]
T	emulsion phase temperature [K]
T_W	surface temperature [K]
V	volume [m^3]
$V(x)$	volume of the particle segment - eqn. (3.25) [m^3]
W	dimensionless temperature defined be equation (3.9) [-]
$W(Z)$	dimensionless emulsion phase temperature at point Z [-]
x	distance from the surface [m]
Z	x/d_p, dimensionless distance from the surface [-]
ΔZ	step-size used in the numerical calculation [-]

Greek symbols

β	solid concentration [-]
$\beta(x)$	solid concentration in the emulsion phase at point x [-]
ε	voidage [-]
$\varepsilon(x)$	voidage of the emulsion phase at point x [-]
κ	thermal diffusivity [m^2/s]
ρ	specific density [kg/m^3]
$\rho(x)$	specific density of the emulsion phase at point x [kg/m^3]
τ	mean packet residence time [s]

Subscripts

E	emulsion phase un-influenced by the constraining surface
G	gas
i	instantaneous value at time t
m	time-mean value
P	particle
W	wall, heat transfer surface

Chapter 4.

BUBBLE INDUCED HEAT TRANSFER IN A UNIFIED TWO-PHASE SYSTEM.

4.1. INTRODUCTION.

It has been shown in Chapter 3 that the analogy between gas fluidized beds and bubbling liquids can be extended to cover heat transfer at surfaces as well as other processes, by introducing the concept of a property boundary layer in the vicinity of the heat transfer surface. Hence a unified two-phase bubbling system can be defined. It has been shown in Chapter 2, that rising gas bubbles are the agents responsible for the high rates of heat transfer in such a system; it has been further shown that bubble coalescence and interactions make it very difficult to determine the mechanism of the bubble induced heat transfer in multi-bubbling systems.

In this Chapter it is shown that more detailed knowledge of the heat transfer processes involved can be obtained if the multi-bubbling two-phase system is simplified to one in which the frequency of bubble occurrence in the vicinity of the heat transfer surface can be controlled. A special heat transfer probe which can be used to discriminate between conductive and non-conductive modes of heat transfer is developed and heat transfer from the probe into the surrounding medium, when conduction is the only mode of heat transfer, is calculated. The supporting instrumentation of the probe is also discussed and the application of the probe is described. Finally, a general model of bubble induced heat transfer in two-phase systems, based on the surface renewal and penetration theory, is developed.

4.2. GENERAL CONSIDERATIONS.

It has been shown that the analogy between gas fluidized beds and bubbling liquids can be extended to cover heat transfer at surfaces, by introducing the concept of a property boundary layer in the vicinity of any constraining surface, (and particularly, the heat transfer surface). The thickness of the property boundary layer depends on the bubbling system used; it is finite for fluidized beds and zero for bubbling liquids. Hence both systems can be unified by defining a general two-phase system, consisting of a discrete gas bubble phase and a continuous dense phase. The dense phase has constant thermophysical properties everywhere in the bed except in the vicinity of any constraining surface, where a localized property boundary layer must be considered. In the case of bubbling liquids, the liquid constitutes the dense phase and the thickness of the property boundary layer is zero, in the case of gas fluidized beds, the dense phase is provided by the continuous emulsion phase and the thickness of the property boundary layer is finite.

In order to describe the mechanism of the bubble induced heat transfer precisely, one must know the behaviour of the dense and the bubble phases in the vicinity of the heat transfer surface. The parameters which must be known are, for example, residence times of the dense and the bubble phases on the heat transfer surface, the frequency of bubble occurrence on the heat transfer surface and the age distribution function of the elements of the dense phase on the heat transfer surface. In a multi-bubbling system, it is very difficult to measure precisely any of the above listed parameters[41], hence to get more insight into the problem of the bubble induced heat transfer, it has been decided to simplify the general multi-bubbling system by generating a single continuous stream of discrete gas bubbles into a stationary dense phase. The bubble volumes and the frequency of their generation are measured and thus known. (The mixture of the dense phase and gas bubbles within the system, will be referred to as the 'pool' throughout this work.)

It was suggested in Chapter 2, that transient conduction into the dense phase is the most important mechanism of the bubble induced heat transfer in two-phase bubbling systems, however the evidence was inconclusive. To compare the contributions of the various modes of heat transfer, a heat transfer probe which can be used to discriminate between conductive and convective modes of heat transfer must be developed. This is described in the next Section.

4.3. THE HEAT TRANSFER PROBE.

4.3.1. REQUIREMENTS AND DESIGN.

Ideally, any heat transfer probe should be of such construction that the boundary conditions met in its experimental application are well defined mathematically and hence identical to those for which the solution of the governing equations has been obtained. Additionally, the solution of the governing equations should be in such a form that the parameters required for its evaluation are directly measurable.

In order to satisfy the above requirements and to achieve maximum sensitivity of the probe, the smallest bubble likely to be encountered in the system should envelop the entire surface area of the probe, thus setting its maximum permissible dimension. Furthermore, the smallest dimension of the probe, its diameter in the case of cylindrical probes, must be large enough to be sufficiently strong to withstand the stresses induced in it by the violent bubbling and eddying normally encountered in two-phase flows. The probe should also have a certain symmetry, so as to make the mathematical description, and the subsequent solution, simpler.

The probe developed here and used later is a thin wire of finite length but, unlike conventional probes, with well defined boundary conditions, which will arise in its practical use. The schematic design of the probe is shown in Figure 4.1. A thin platinum wire (serving as the heat transfer probe) is stretched between two flat copper supports, the wire being electrically heated and the copper supports serving as electrical leads. The length of the wire is equal (or about equal) to the diameter of generated bubbles. The bubble generating orifice (described later) is placed below the centre of the platinum wire. The probe and the generating orifice are submerged into the stationary dense phase.

To obtain experimental data from the probe, the wire has been incorporated into one branch of a standard Wheatstone bridge - Figure 4.2. The current through the bridge is supplied by a 12 V battery and regulated by the variable resistor R1. The digital voltmeter (DV) is used to measure the voltage across the wire. The bridge is balanced by the variable resistor R2. More detailed description of the experimental application of the wire is discussed in Section 4.5.

4.3.2. APPLICATION.

It is usually difficult to distinguish between conductive and non-conductive modes of heat transfer from a heat transfer probe to the surrounding dense phase, but due to the special features of the present probe, it can be used to discriminate between conductive and non-conductive modes. This is due to the fact that heat transfer from the probe to the surrounding dense phase, when conduction is the only mode of heat transfer, can be calculated theoretically to a high degree of accuracy. Hence the compound effect of heat transfer modes other than conduction, can be determined by comparing the experimentally observed heat transfer rates from the probe under mixed-mode conditions (conductive and non-conductive modes) with those determined theoretically, in which conduction is the only mode of heat transfer. The contribution of the non-conductive modes of heat transfer can therefore be assessed from the difference between experimental and theoretical results.

As mentioned previously, it is desirable to express the theoretical solution in terms of directly measurable parameters. These will be obtained by considering the experimental application of the probe. It is not practicable to detect the local wire temperature; in practice the wire temperature is determined from the electrical resistance of its entire length. If, as in the present case, the wire is used in a similar way to a constant current anemometer, a certain space-average wire temperature will be measured. This space-average wire temperature is the directly measurable parameter upon which the theoretical solution should be based. It is therefore necessary to find the relationship between the local wire temperature distribution ,T_W, at any time t and the space-average wire temperature ,T, at the same instant. Hereafter the term 'average wire temperature' will be used to denote the space-average wire temperature. It is shown in Appendix 2, that the average wire temperature is given as

$$T = \frac{1}{2L} \int_{L}^{-L} T_W \, dx \qquad (4.1)$$

where L is the wire halflength.

As a result of the probe construction, the following assumptions about its behaviour, which are used in the subsequent analysis, are made:

i) Since the electrical and thermal resistances of the copper supports (Figure 4.1) are small compared with those of the wire material and their surface area is large compared with that of the wire, it is assumed that they remain at the pool temperature ,T_∞, throughout the process.

ii) It is further assumed that the radial extent of the copper supports and of the medium between them is infinite, compared with the very small radius of the wire (heat transfer probe). Hence the system can be regarded as axisymmetric about the x-axis.

iii) Since the length of the probe wire is many times greater than the thickness of the property boundary layer and since, from the point of view of heat transfer, the copper supports provide only secondary heat transfer surfaces, it is assumed that the thickness of the property boundary layer of the dense phase in the vicinity of the copper supports is zero. Hence the concept of the property boundary layer will be applied on the probe wire only, resulting in the assumption that the thermophysical properties of the dense phase vary in the radial direction only.

iv) Since the wire is very thin and is made of material whose thermal conductivity is very much greater than that of its surrounding medium, the radial distribution of temperature within the wire will be nearly uniform. The wire then may be for many purposes regarded as a finite rod with heat generated within it and being dissipated (a) from the outer surface to the surrounding medium and (b) from its ends by conduction to the copper supports[36].

v) It is further assumed that all wire material properties remain constant and that only Joule heating (I^2R_W) of the wire is considered.

4.4. A MODEL OF THE BUBBLE INDUCED HEAT TRANSFER.

4.4.1. ASSUMPTIONS USED IN THE THEORETICAL MODEL.

A theoretical model of the bubble induced heat transfer in the present system, based on the surface renewal and penetration theory[16,32], has been developed. The model is based on the following assumptions, some of which are similar to those used in Section 2.5.2.1:

i) The heat transfer process is periodic with period $\tau = 1/f$, where f is the frequency of bubble generation.

ii) The presence of gas bubbles in the pool causes turbulence of the dense phase, which is responsible for the continuous mixing of the dense phase in the pool. Because of the continual mixing in the bulk of the pool, the temperature of the dense phase throughout the bulk of the pool remains constant. When a bubble passes the surface of the heat transfer probe, the 'old' dense phase, which has been heated by the wire prior to the bubble arrival is replaced by 'fresh' dense phase from the bulk of the pool, which was brought by the passing bubble in its wake. While this dense phase is in contact with the surface of the heat transfer probe, heat is transferred to it by a non-steady heat transfer process. For a particular case the amount of heat transferred to it depends on the duration of the contact time between the surface of the heat transfer probe and the dense phase. After a certain time, known as the 'residence time' of the dense phase on the surface of the heat transfer probe, the next bubble arrives and the now 'old' dense phase is again replaced by the fresh dense phase from the bulk of the pool. In this way the dense phase on the surface of the heat transfer probe is being replaced periodically at frequency f.

iii) The diameter of passing bubbles is approximately equal to the length of the probe. Hence it is assumed that the dense phase is being effectively replaced over the whole surface area of the heat transfer probe. It is further assumed that the residence time of gas bubbles on the surface of the heat transfer probe is negligible compared with the residence time of the dense phase there. This implies that only dense phase is in contact with the surface of the heat transfer probe and hence that only dense phase is responsible for the heat transfer from the probe to the pool. On the other hand, gas bubbles cause the surface renewal of the dense phase and hence they are (neglecting natural convection) entirely responsible for mass transport in the pool.

iv) Since heat supplied by the probe wire to the pool is negligible compared with the heat capacity of the pool, it is assumed that the temperature of the pool ,T_∞, remains constant not only in space but also with time. Without loss of generality, T_∞ is set at the reference zero.

v) It is further assumed that all wire material properties and dense phase properties outside the property boundary layer, remain constant, that the property boundary layer is formed on the wire surface only (Section 4.3.2) and that the properties there are functions of the radial position only.

vi) Finally it is assumed that the dissipation of mechanical energy and the radiative heat transfer can be neglected.

4.4.2. FULL DIFFERENTIAL DESCRIPTION OF THE SYSTEM.

Only the slab of the dense phase between the two copper supports (Figure 4.1) is considered and it is assumed that each heating period of the dense phase and of the wire starts at the moment when the dense phase on the wire surface has just been renewed. Cylindrical coordinates are used to describe the system during each period. Using the assumption for the mechanism of the bubble induced heat transfer (Section 4.4.1) and for the behaviour of the probe (Section 4.3.2), the following energy equations apply^{22}:

$t \geq 0,\ r \geq a,\ |x| \leq L$

$$\rho(r)c_p(r)\left(\frac{\partial T_D}{\partial t} + U_r\frac{\partial T_D}{\partial r} + \frac{U_\theta}{r}\frac{\partial T_D}{\partial \theta} + U_x\frac{\partial T_D}{\partial x}\right) =$$

$$= k(r)\left(\frac{\partial^2 T_D}{\partial r^2} + \frac{1}{r}\frac{\partial T_D}{\partial r} + \frac{1}{r^2}\frac{\partial^2 T_D}{\partial \theta^2} + \frac{\partial^2 T_D}{\partial x^2}\right) + \frac{dk(r)}{dr}\frac{\partial T_D}{\partial r} \tag{4.2}$$

$t \geq 0,\ r \leq a,\ |x| \leq L$

$$(\rho c_p)_W\frac{\partial T_W}{\partial t} = k_W\left(\frac{\partial^2 T_W}{\partial r^2} + \frac{1}{r}\frac{\partial T_W}{\partial r} + \frac{1}{r^2}\frac{\partial^2 T_W}{\partial \theta^2} + \frac{\partial^2 T_W}{\partial x^2}\right) + Q \tag{4.3}$$

subject to

$$t = 0,\ r > a,\ |x| \leq L \qquad T_D = 0 \tag{4.4}$$

$$t = 0,\ r \leq a,\ |x| \leq L \qquad T_W = T_0(r,\theta,x) \tag{4.5}$$

$$t \geq 0,\ r \geq a,\ |x| = L \qquad T_D = 0 \tag{4.6}$$

$$t \geq 0,\ r \leq a,\ |x| = L \qquad T_W = 0 \tag{4.7}$$

$$t \geq 0,\ r \geq a,\ x = 0 \qquad \frac{\partial T_D}{\partial x} = 0 \tag{4.8}$$

$$t \geq 0,\ r \leq a,\ x = 0 \qquad \frac{\partial T_W}{\partial x} = 0 \tag{4.9}$$

$$t \geq 0,\ r = a,\ |x| \leq L \qquad T_D = T_W \tag{4.10}$$

$$t \geq 0,\ r = a,\ |x| \leq L \qquad -k(a)\frac{\partial T_D}{\partial r} = -k_W\frac{\partial T_W}{\partial r} \tag{4.11}$$

These energy equations together with the momentum and continuity equations provide the complete description of the system. Neglecting natural convection the momentum and the energy equations are uncoupled and the momentum equations can be readily written down. Thus, at least in principle, the solution could be obtained.

4.4.3. NON-STEADY HEAT TRANSFER MECHANISM.

The system of differential equations, describing the bubble induced heat transfer in the present system (Section 4.4.2), is very complex and to solve it, even numerically, would be extremely difficult. So an alternative method of attack must be developed. The method is based on separating conductive and convective modes of heat transfer.

While the wire is in contact with the surrounding dense phase, the heat is transferred from the wire to the dense phase by a non-steady heat transfer process. In equations (4.2) and (4.3) this non-steady heat transfer mechanism is defined generally as consisting of a conductive and a convective components. The convective component of the heat transfer mechanism can be calculated only after the velocity field in the dense phase in the wire vicinity has been determined. The calculation of the velocity field in the wire vicinity (and hence the contribution of the convective component to the total mechanism of heat transfer) causes the main difficulties in finding a full theoretical solution. As mentioned previously (Section 4.3.2), the present probe can be used to discriminate between conductive and convective components of heat transfer. In order to achieve this, heat transfer from the probe to the surrounding dense phase, when conduction is the only mode of heat transfer, must be calculated. Hence in the subsequent analysis the effect of additional convection is neglected and it is assumed that conduction is the only mode of the bubble induced heat transfer.

The neglect of the convective mode of heat transfer implies the following simplifying assumption: Gas bubbles cause the renewal of the dense phase on the wire surface only, and the dense phase remains stationary once in contact with the surface of the probe (there are no convection currents within the dense phase). This is clearly the most controversial assumption and its validity will be discussed later. If the experimental heat transfer rates are higher than the theoretical ones, which assume that conduction is the only mechanism of the bubble induced heat transfer, the assumption does not hold. In that case convection provides an important contribution to the bubble induced heat transfer and its importance can be assessed from the difference between experimental and theoretical results, (the greater the relative difference, the greater the contribution of convection).

The implication of neglecting convection is that

$$U_r = U_\theta = U_x = 0 \tag{4.12}$$

which simplifies equation (4.2) to

$$\rho(r)c_p(r)\,\frac{\partial T_D}{\partial t} = k(r)\left(\frac{\partial^2 T_D}{\partial r^2} + \frac{1}{r}\frac{\partial T_D}{\partial r} + \frac{1}{r^2}\frac{\partial^2 T_D}{\partial \theta^2} + \frac{\partial^2 T_D}{\partial x^2}\right) + \frac{dk(r)}{dr}\frac{\partial T_D}{\partial r} \quad \ldots. \; (4.13)$$

Hence equations (4.13) and (4.3) subject to equations (4.4) to (4.11) give the solution of the conductive heat transfer from the probe to the surrounding dense phase. Because the heat transfer probe and the surrounding dense phase are, at least in the vicinity of the probe, symmetrical about the x-axis (axisymmetric), temperatures T_D and T_W are independent of θ and hence equations (4.13) and (4.3) can be simplified further by putting the θ - derivatives equal to zero.

4.4.4. INFLUENCE OF THE INITIAL WIRE TEMPERATURE.

At the start of each heating cycle, when the dense phase has just been replaced on the surface of the heat transfer probe, the initial temperature of the dense phase in the wire vicinity is the same as the temperature of the dense phase in the bulk of the pool, T_∞. The initial temperature of the wire is different. Because the probe wire has finite heat capacity, finite times are required for finite changes of the wire temperature. Hence the initial wire temperature is different from the initial temperature of the dense phase. The initial wire temperature depends on many factors, such as the bubble residence time on the wire surface, thermophysical properties of the bubble gas etc. To discuss the influence of the initial wire temperature ,T_0, equations (4.13) and (4.3) are rearranged in the following way, (assuming the system to be axisymmetric about the x-axis):

Let

$$T_D = T_{D1} + T_{D2} \tag{4.14}$$

$$T_W = T_{W1} + T_{W2} \tag{4.15}$$

such that

$t \geq 0,\ r \geq a,\ |x| \leq L$

$$\rho(r) c_p(r) \frac{\partial T_{D1}}{\partial t} = k(r) (\frac{\partial^2 T_{D1}}{\partial r^2} + \frac{1}{r} \frac{\partial T_{D1}}{\partial r} + \frac{\partial^2 T_{D1}}{\partial x^2}) + \frac{dk(r)}{dr} \frac{\partial T_{D1}}{\partial r} \tag{4.16}$$

$t \geq 0,\ r \leq a,\ |x| \leq L$

$$(\rho c_p)_W \frac{\partial T_{W1}}{\partial t} = k_W (\frac{\partial^2 T_{W1}}{\partial r^2} + \frac{1}{r} \frac{\partial T_{W1}}{\partial r} + \frac{\partial^2 T_{W1}}{\partial x^2}) + Q \tag{4.17}$$

subject to

$t = 0,\ r > a,\ |x| \leq L \qquad T_{D1} = 0 \qquad (4.18)$

$t = 0,\ r \leq a,\ |x| \leq L \qquad T_{W1} = 0 \qquad (4.19)$

$t \geq 0,\ r > a,\ |x| = L \qquad T_{D1} = 0 \qquad (4.20)$

$t \geq 0,\ r \leq a,\ |x| = L \qquad T_{W1} = 0 \qquad (4.21)$

$t \geq 0,\ r > a,\ x = 0 \qquad \partial T_{D1}/\partial x = 0 \qquad (4.22)$

$t \geq 0,\ r \leq a,\ x = 0 \qquad \partial T_{W1}/\partial x = 0 \qquad (4.23)$

$t \geq 0,\ r = a,\ |x| \leq L \qquad T_{D1} = T_{W1} \qquad (4.24)$

$t \geq 0,\ r = a,\ |x| \leq L \qquad -k(a) \frac{\partial T_{D1}}{\partial r} = -k_W \frac{\partial T_{W1}}{\partial r} \qquad (4.25)$

and

$t \geq 0,\ r \geq a,\ |x| \leq L$

$$\rho(r) c_p(r) \frac{\partial T_{D2}}{\partial t} = k(r) (\frac{\partial^2 T_{D2}}{\partial r^2} + \frac{1}{r} \frac{\partial T_{D2}}{\partial r} + \frac{\partial^2 T_{D2}}{\partial x^2}) + \frac{dk(r)}{dr} \frac{\partial T_{D2}}{\partial r} \tag{4.26}$$

$t \geq 0,\ r \leq a,\ |x| \leq L$

$$(\rho c_p)_W \frac{\partial T_{W2}}{\partial t} = k_W\left(\frac{\partial^2 T_{W2}}{\partial r^2} + \frac{1}{r}\frac{\partial T_{W2}}{\partial r} + \frac{\partial^2 T_{W2}}{\partial x^2} \right) \tag{4.27}$$

subject to

$t = 0,\ r > a,\ |x| \leq L$ $\qquad T_{D2} = 0$ (4.28)

$t = 0,\ r \leq a,\ |x| \leq L$ $\qquad T_{W2} = T_0(r,x)$ (4.29)

$t \geq 0,\ r > a,\ |x| = L$ $\qquad T_{D2} = 0$ (4.30)

$t \geq 0,\ r \leq a,\ |x| = L$ $\qquad T_{W2} = 0$ (4.31)

$t \geq 0,\ r > a,\ x = 0$ $\qquad \partial T_{D2}/\partial x = 0$ (4.32)

$t \geq 0,\ r \leq a,\ x = 0$ $\qquad \partial T_{W2}/\partial x = 0$ (4.33)

$t \geq 0,\ r = a,\ |x| \leq L$ $\qquad T_{D2} = T_{W2}$ (4.34)

$t \geq 0,\ r = a,\ |x| \leq L$ $\qquad -k(a)\dfrac{\partial T_{D2}}{\partial r} = -k_W \dfrac{\partial T_{W2}}{\partial r}$ (4.35)

The solution of equations (4.26) and (4.27) provides only a transient non-trivial temperature field, due to the non-zero initial wire temperature. The importance of this solution will be greater for larger wire diameters (the larger the wire diameter the greater the amount of heat stored in it at the beginning of each heating cycle), smaller thermoconductivities of the dense phase (heat transfer from the wire increases with increasing thermal conductivity of the dense phase) and smaller times of contact between the dense phase and the wire surface. This can be summarized by the following statement: The greater the instantaneous Fourier number ,Fo, the smaller the influence of the non-zero initial wire temperature on the total temperature field in and around the wire. Hence the solution of equations (4.16) to (4.25) will provide the first approximation to the temperature field in and around the wire when conduction is the only mechanism of heat transfer between the wire and the dense phase, and its accuracy will increase with increasing values of the instantaneous Fourier number. This approximation implies the assumption that at the beginning of each heating cycle the temperature of the wire drops instantaneously to the initial temperature of the dense phase ,T_∞, which is set at the reference zero (Section 4.4.1).

4.4.5. FIRST APPROXIMATION TO THE WIRE TEMPERATURE.

Equations (4.16) to (4.25) provide the first approximation to the temperature field in and around the wire when conduction is the only mode of heat transfer between the probe and the surrounding dense phase. They can be solved numerically but to simplify the numerical calculations without incurring much loss of accuracy it is advantageous to separate the temperature fields within the wire and in the dense phase (Appendix 3). It has been argued that the wire can be approximated by a rod with uniform radial temperature distribution (Section 4.3.2). It is shown in Appendix 3 that the differential equation (4.17) and boundary conditions (4.24) and (4.25) then simplify into one boundary condition (4.40). Hence the original system of equations (equations (4.16) to (4.25)) can be approximated by the following equations:

$t \geq 0,\ r \geq a,\ |x| \leq L$

$$\rho(r)c_p(r)\frac{\partial T_{D1}}{\partial t} = k(r)\left(\frac{\partial^2 T_{D1}}{\partial r^2} + \frac{1}{r}\frac{\partial T_{D1}}{\partial r} + \frac{\partial^2 T_{D1}}{\partial x^2}\right) + \frac{dk(r)}{dr}\frac{\partial T_{D1}}{\partial r} \tag{4.36}$$

subject to

$$t = 0,\ r \geq a, |x| \leq L \qquad T_{D1} = 0 \tag{4.37}$$

$$t \geq 0,\ r \geq a, |x| = L \qquad T_{D1} = 0 \tag{4.38}$$

$$t \geq 0,\ r \geq a,\ x = 0 \qquad \partial T_{D1}/\partial x = 0 \tag{4.39}$$

$$t \geq 0,\ r = a, |x| \leq L \qquad \frac{1}{\kappa_W}\frac{\partial T_{D1}}{\partial t} = \frac{\partial^2 T_{D1}}{\partial x^2} + \frac{2k(a)}{ak_W}\frac{\partial T_{D1}}{\partial r} + \frac{Q}{k_W} \tag{4.40}$$

Equations (4.36) to (4.40) can be rewritten in dimensionless form as

$Fo \geq 0,\ R \geq 1,\ |Z| \leq 1$

$$\frac{\partial W_{D1}}{\partial Fo} = H(R)\left(\frac{\partial^2 W_{D1}}{\partial R^2} + \frac{1}{R}\frac{\partial W_{D1}}{\partial R} + \frac{1}{A^2}\frac{\partial^2 W_{D1}}{\partial Z^2}\right) + L(R)\frac{\partial W_{D1}}{\partial R} \tag{4.41}$$

subject to

$$Fo = 0,\ R \geq 1,\ |Z| \leq 1 \qquad W_{D1} = 0 \tag{4.42}$$

$$\text{Fo} \geq 0,\ R \geq 1,\ |Z| = 1 \qquad W_{D1} = 0 \tag{4.43}$$

$$\text{Fo} \geq 0,\ R \geq 1,\ Z = 0 \qquad \partial W_{D1}/\partial Z = 0 \tag{4.44}$$

$$\text{Fo} \geq 0,\ R = 1,\ |Z| \leq 1 \qquad \frac{\partial W_{D1}}{\partial \text{Fo}} = \frac{1}{\kappa_0 A^2}\frac{\partial^2 W_{D1}}{\partial Z^2} + \frac{2k_0 b(1)}{\kappa_0}\frac{\partial W_{D1}}{\partial R} + \frac{k_0}{\kappa_0} \tag{4.45}$$

by using the following transformations,

$$W_{D1} = T_{D1}k_D/Qa^2 \tag{4.46}$$

$$\text{Fo} = \kappa_D t/a^2 \tag{4.47}$$

$$R = r/a \tag{4.48}$$

$$Z = x/L \tag{4.49}$$

$$g(R) = \rho(R)c_p(R)/(\rho c_p)_D \tag{4.50}$$

$$b(R) = k(R)/k_D \tag{4.51}$$

$$H(R) = b(R)/g(R) \tag{4.52}$$

$$L(R) = \frac{db(R)}{dR} \bigg/ g(R) \tag{4.53}$$

$$k_0 = k_D/k_W \tag{4.54}$$

$$\kappa_0 = \kappa_D/\kappa_W \tag{4.55}$$

$$A = L/a \tag{4.56}$$

where suffix D refers to those properties of the dense phase which are un-influenced by the heat transfer surface (properties of the dense phase in the bulk of the pool, beyond the boundary of the property boundary layer).

If all parameters of a particular system are known, functions H(R) and L(R) can be defined (similarly to Section 3.3.4) and equations (4.41) to (4.45) can be solved numerically. The method of numerical solution is briefly described in Appendix 4 and a typical computer programme is shown in Appendix 8. Finally, the first approximation to the dimensionless instantaneous average wire temperature ,$(W_1)_i$, (defined analogously to equation (4.1)) can be obtained. From the point of view of the overall time-mean heat transfer, the time-mean average wire temperature is of far greater importance. The time-mean average wire temperature can be calculated only if the age distribution function of the elements of the dense phase on the surface of the heat transfer probe is known (compare with Section 3.4.3). It is assumed that the dense phase on the wire surface is stationary (Section 4.4.3) and this implies that the required age distribution function is the Higbie's uniform age distribution function[32] with the mean residence time of the dense phase on the wire surface given by the frequency of bubble generation. Hence the first approximation to the dimensionless time-mean average wire temperature ,$(W_1)_m$, is defined (Section 3.4.3) by

$$(W_1)_m = \frac{1}{Fo_m} \int_0^{Fo_m} (W_1)_i \, dFo \tag{4.57}$$

and can be calculated.

In a special case when the thickness of the property boundary layer is zero and hence properties of the dense phase are constant throughout, an analytical solution of equations (4.41) to (4.45) can be obtained. Since zero thickness of the property boundary layer defines a liquid dense phase, subscript L will be used instead of subscript D.

First, equations (4.41) to (4.45) simplify to

$Fo \geq 0,\ R \geq 1,\ |Z| \leq 1$

$$\frac{\partial W_{L1}}{\partial Fo} = \frac{\partial^2 W_{L1}}{\partial R^2} + \frac{1}{R}\frac{\partial W_{L1}}{\partial R} + \frac{1}{A^2}\frac{\partial^2 W_{L1}}{\partial Z^2} \tag{4.58}$$

subject to

$Fo = 0,\ R \geq 1,\ |Z| \leq 1 \qquad W_{L1} = 0$ (4.59)

$Fo \geq 0,\ R \geq 1,\ |Z| = 1 \qquad W_{L1} = 0$ (4.60)

$Fo \geq 0,\ R \geq 1,\ Z = 0 \qquad \partial W_{L1}/\partial Z = 0$ (4.61)

$Fo \geq 0,\ R = 1,\ |Z| \leq 1 \qquad \dfrac{\partial W_{L1}}{\partial Fo} = \dfrac{1}{\kappa_0 A^2}\dfrac{\partial^2 W_{L1}}{\partial Z^2} + \dfrac{2k_0}{\kappa_0}\dfrac{\partial W_{L1}}{\partial R} + \dfrac{k_0}{\kappa_0}$ (4.62)

The method of solution of equations (4.58) to (4.62) is shown in Appendix 5. The first approximations to the dimensionless instantaneous,$(W_1)_i$, and time-mean ,$(W_1)_m$, average wire temperatures are then given by the following equations (Appendix 5):

$$(W_1)_i = \frac{4}{\pi^2} \sum_{n=0}^{\infty} \frac{1}{s^2} \int_0^{\infty} [1 - e^{-y_1 Fo}] \frac{y\,dy}{y_1(\phi^2 + \psi^2)} \tag{4.63}$$

$$(W_1)_m = \frac{4}{\pi^2}\sum_{n=0}^{\infty}\frac{1}{s^2}\int_0^{\infty}\{1 - \frac{1}{y_1 Fo_m}[1 - e^{-y_1 Fo_m}]\}\frac{y\,dy}{y_1(\phi^2 + \psi^2)} \qquad (4.64)$$

If then all properties of the system and wire dimensions are known, temperatures $(W_1)_i$ and $(W_1)_m$ are calculated as functions of Fourier numbers by numerical integration. The exact solution, given by equation (4.63), is later used (Section 5.5.1) to test some of the assumptions used for the theoretical model of heat transfer developed in this Chapter.

4.4.6. TEMPERATURE FIELD DUE TO INITIAL WIRE TEMPERATURE.

The temperature field due to the influence of the initial wire temperature is given by the solution of equations (4.26) to (4.35). It is again assumed that the radial distribution of the wire temperature is nearly uniform (Section 4.3.2) and hence the initial wire temperature can be rewritten as

$$T_0(r,x) = T_{0A} \cdot fn(x) \qquad (4.65)$$

where fn(x) is normalized such that

$$\frac{1}{2L}\int_{-L}^{L} fn(x)\,dx = 1 \qquad (4.66)$$

and hence T_{0A} is the initial average wire temperature. Equations (4.26) to (4.35) can be rewritten in dimensionless form as

$Fo \geq 0,\ R \geq 1,\ |Z| \leq 1$

$$\frac{\partial W_{D2}}{\partial Fo} = H(R)\left(\frac{\partial^2 W_{D2}}{\partial R^2} + \frac{1}{R}\frac{\partial W_{D2}}{\partial R} + \frac{1}{A^2}\frac{\partial^2 W_{D2}}{\partial Z^2}\right) + L(R)\frac{\partial W_{D2}}{\partial R} \qquad (4.67)$$

$Fo \geq 0,\ R \leq 1,\ |Z| \leq 1$

$$\frac{\partial W_{W2}}{\partial Fo} = \frac{1}{\kappa_0}\left(\frac{\partial^2 W_{W2}}{\partial R^2} + \frac{1}{R}\frac{\partial W_{W2}}{\partial R} + \frac{1}{A^2}\frac{\partial^2 W_{W2}}{\partial Z^2}\right) \qquad (4.68)$$

subject to

$Fo = 0,\ R > 1,\ |Z| \leq 1 \qquad W_{D2} = 0 \qquad (4.69)$

$Fo = 0,\ R \leq 1,\ |Z| \leq 1 \qquad W_{W2} = fn(Z) \qquad (4.70)$

$Fo \geq 0,\ R \geq 1,\ |Z| = 1 \qquad W_{D2} = 0 \qquad (4.71)$

$Fo \geq 0,\ R \leq 1,\ |Z| = 1 \qquad W_{W2} = 0 \qquad (4.72)$

$Fo \geq 0,\ R > 1,\ Z = 0 \qquad \partial W_{D2}/\partial Z = 0 \qquad (4.73)$

$$\mathrm{Fo} \geq 0,\ R \leq 1,\ Z = 0 \qquad \partial W_{W2}/\partial Z = 0 \tag{4.74}$$

$$\mathrm{Fo} \geq 0,\ R = 1,\ |Z| \leq 1 \qquad W_{D2} = W_{W2} \tag{4.75}$$

$$\mathrm{Fo} \geq 0,\ R = 1,\ |Z| \leq 1 \qquad k_0 b(1) \frac{\partial W_{D2}}{\partial R} = \frac{\partial W_{W2}}{\partial R} \tag{4.76}$$

using the following transformations

$$W_{D2} = T_{D2}/T_{0A} \tag{4.77}$$

$$W_{W2} = T_{W2}/T_{0A} \tag{4.78}$$

in addition to those defined by equations (4.47) to (4.56).

Function fn(Z) is the normalized dimensionless initial temperature distribution over the wire length. It is either known or it must be estimated. Once function fn(Z) is known, equations (4.67) to (4.76) can be solved numerically. The numerical method used here is similar to that discussed in Appendix 4, the main difference being that the convergence conditions are much stricter and hence that larger computer times are required for numerical calculations. A typical computer programme is shown in Appendix 9.

The radial distribution of the wire temperature is nearly uniform and hence equation (4.1) can be used to calculate the average wire temperature. Finally, as in Section 4.4.5, the dimensionless instantaneous ,$(W_2)_i$, and time-mean ,$(W_2)_m$, average wire temperatures due to the influence of the initial wire temperature can be calculated.

4.4.7. FULL SOLUTION FOR THE AVERAGE WIRE TEMPERATURE.

Full solution for the temperature field in and around the wire is defined by equations (4.14) and (4.15). Similarly the instantaneous and the time-mean average wire temperatures can be defined as

$$T_i = (T_1)_i + (T_2)_i \tag{4.79}$$

$$T_m = (T_1)_m + (T_2)_m \tag{4.80}$$

respectively. Equations (4.79) and (4.80) can be rewritten in dimensionless forms as

$$W_i = (W_1)_i + (W_2)_i \cdot \Psi \tag{4.81}$$

$$W_m = (W_1)_m + (W_2)_m \cdot \Psi \tag{4.82}$$

using the following transformations

$$W_i = T_i k_D/Qa^2 \tag{4.83}$$

$$W_m = T_m k_D/Qa^2 \tag{4.84}$$

$$(W_1)_i = (T_1)_i k_D/Qa^2 \tag{4.85}$$

$$(W_1)_m = (T_1)_m k_D/Qa^2 \tag{4.86}$$

$$(W_2)_i = (T_2)_i/T_{0A} \tag{4.87}$$

$$(W_2)_m = (T_2)_m/T_{0A} \tag{4.88}$$

$$\Psi = T_{0A} k_D/Qa^2 \quad . \tag{4.89}$$

Similarly to function fn(Z), function Ψ must be also estimated or experimentally measured. The determination of functions fn(Z) and Ψ provides the main difficulties in finding the complete theoretical solution to the problem. On the other hand, the first approximation to the wire temperature can be determined theoretically to a high degree of accuracy. It will be shown later (Section 4.5), that under certain circumstances boundary condition (4.19) can be satisfied experimentally, so that the first approximation to the wire temperature will be identical with the exact wire temperature which is given by the full solution to the problem. This is the main reason for separating the temperature fields in and around the wire.

4.4.8. CONDUCTION MODEL OF BUBBLE INDUCED HEAT TRANSFER.

It can be shown that $Qa/2(T_1)_i$ and $Qa/2(T_1)_m$ can be regarded as first approximations to the instantaneous and the time-mean heat transfer coefficients for the conduction model of the bubble induced heat transfer in the present system respectively. Similarly $Qa^2/k_D(T_1)_i$ and $Qa^2/k_D(T_1)_m$ can be regarded as first approximations to the instantaneous and the time-mean Nusselt numbers respectively.

Hence

$$(Nu_1)_i = 1/(W_1)_i \tag{4.90}$$

$$(Nu_1)_m = 1/(W_1)_m \tag{4.91}$$

and similarly

$$Nu_i = 1/W_i \tag{4.92}$$

$$Nu_m = 1/W_m \tag{4.93}$$

where Nu_i and Nu_m are full solutions for the instantaneous and the time-mean Nusselt numbers respectively (assuming that conduction is the only mode of heat transfer).

If then the properties of the dense phase and of the wire material and the wire dimensions are known, the Nusselt number can be calculated as a function of the Fourier number. As mentioned previously, the calculation must usually be done numerically, but in one special case (equations (4.63) and (4.64)) an analytical solution can be obtained.

4.5. EXPERIMENTAL TECHNIQUE AND INSTRUMENTATION.

Only experimental techniques and instrumentation concerning the application of the heat transfer probe are discussed in this Section. The design of the bubble generator depends on the character of the dense phase used and is described later (Chapters 5 and 6).

The heat transfer probe has three basic functions:

i) it serves as a heat transfer probe,

ii) using the principles of anemometry it is employed to measure its own instantaneous average temperature,

iii) it is used to measure the frequency of bubble generation.

This has been achieved by incorporating the probe into one branch of a standard Wheatstone bridge - Figure 4.2. The current through the bridge is supplied by a 12 V battery (BT) and regulated by a variable resistor R1. The digital voltmeter (DV) is used to measure the voltage across the wire and the UV-recorder to record voltage fluctuations across the bridge. The bridge is balanced by the variable resistor R2. To obtain accurate measurements of the wire resistance, the resistance of the connecting leads of the probe should be as small as possible. Using heavy copper leads their total resistance is about 0.0029 Ω, which is much less than even the smallest resistance of the wire. Wire materials of high temperature coefficient of resistance (as, for example, tungsten or platinum) must be used in the design of the probe. Because of the simplicity of handling platinum, platinum wire probes are used throughout this work.

To measure the instantaneous average wire temperature, principles of anemometry are applied[11]. The wire is calibrated in liquid at known temperatures and the relationship between the average wire temperature and the resistance of R2 (Figure 4.2) is obtained. During the calibration the current through the wire is very low and thus the rate of heat generation in it is negligible. (This is accomplished by connecting the switch S1 with a high resistance variable resistor R3 in its branch and by disconnecting the switch S2.) Because heat transfer coefficients for wires are very large, the difference between the wire temperature and the known temperature of the calibrating liquid is small and can be neglected. Hence the wire temperature is identical, within a small error, with the temperature of the liquid. Because the bridge is balanced by the variable resistor R2, the calibration curve of the wire (average wire temperature versus the resistance of R2) is then determined. The same method, but in reverse, is used to determine the temperature of the pool during experimental runs. If during an experiment the value of resistance of R2 for a balanced bridge is known, the average wire temperature may then be determined from the calibration curve.

It has been mentioned previously (Section 4.4.7) that under certain circumstances boundary condition (4.19) can be satisfied experimentally. Since this implies that the initial wire temperature is equal to the initial temperature of the dense phase, the first approximation to the conductive model of heat transfer is then identical with the exact description of it. Boundary condition (4.19) can be satisfied experimentally in the following way: It has been suggested above that the temperature of the wire remains equal to the temperature of the dense phase surrounding it, even with switch S1 connected. Hence the switch S1 can be connected throughout the process, supplying the base current which is necessary to determine the initial temperature of the dense phase and of the wire. Then at certain time t = 0, switch S2 is connected too, thus supplying the full working current through the bridge and hence also the full working heating load into the probe wire. The heating input generated within the wire can be approximated very well by a step function starting at time t = 0. Thus, if conduction is the only mechanism of heat transfer between the heat transfer probe and the surrounding dense phase, equations (4.16) to (4.25) can be satisfied experimentally and their solution provides the full description of the problem. This finding will be used later (Section 5.5.1) to test some of the assumptions used in this Chapter.

Assume that a heating input is applied into the wire which is a part of an originally balanced bridge. Because of the heat generated within the wire its temperature and hence also its resistance start to rise, the bridge becomes un-balanced and finite potential across the bridge is formed. The changes of potential across the wire are recorded by the UV-recorder. It is shown in Appendix 6, that from the known values of all resistors in the circuit (Figure 4.2), the known calibration curve of the wire, the known voltage across the wire (measured by the digital voltmeter), the sensitivity of the galvanometer in the UV-recorder and the UV-recorder traces, it is possible to determine the instantaneous average wire temperature.

To investigate the mechanism of the bubble induced heat transfer, the procedure is as follows: For a given frequency of bubble generation (from the bubble generating orifice placed below the centre of the probe - Section 4.3.1), the time-mean average wire temperature is set approximately at the required level by setting the resistor R2 at the value corresponding to this temperature and by adjusting the current through the bridge (with the switch S2 connected) in such a way that the bridge is approximately in balance. The current through the bridge is regulated by the resistor R1. Once the bridge is roughly balanced, the UV-recorder traces are obtained. Using the known calibration constant for the UV-recorder traces (Appendix 6), the variations of the instantaneous average wire temperature are obtained.

The exact time-mean average wire temperature is then calculated by graphical integration. Because of the surface renewal character of the bubble induced heat transfer mechanism, the wire is periodically heated and cooled (Section 4.4.1) and hence the frequency of the periodic fluctuation of the wire temperature is equal to the frequency of bubble occurrence on the wire surface.

The voltage across the wire, corrected for the potential drop across its leads, is obtained from the digital voltmeter readings. For set values of resistors R1 and R3, the variation of this voltage with time is small and can be neglected. The rate of heat generation per unit volume of the wire, Q, is assumed constant and is calculated from the constant voltage across the wire and the average wire resistance corresponding to the time-mean average wire temperature. The change of the average wire resistance with time is also neglected. (The error introduced by these two approximations is small and can be estimated for each particular case.)

The experimental instantaneous Nusselt number ,$(Nu_X)_i$, corresponding to a particular value of the instantaneous Fourier number, is then calculated from the known values of the rate of heat generation per unit volume of the wire ,Q, and the instantaneous average wire temperature difference $\Delta T_i = (T_X)_i - T_\infty$. Similarly the experimental time-mean Nusselt numbers are calculated as functions of the time-mean Fourier numbers.

It should be noted that the temperature difference used in the definition of Nu_X, the experimentally determined Nusselt number, is the temperature difference between the experimentally determined average wire temperature, T_X, and the temperature of the pool ,T_∞ . This temperature difference corresponds to the average wire temperature calculated from the theory developed in Section 4.4, in which the temperature of the pool is set at the reference zero.

4.6. CONCLUSIONS.

It has been shown that in order to investigate the mechanism of the bubble induced heat transfer in bubbling two-phase systems in more details, the multi-bubbling system must be simplified, in this work by generating a single continuous stream of discrete gas bubbles in a stationary dense phase. A special heat transfer probe has been developed. Finally, a theoretical model of the bubble induced heat transfer in the present system, based on the surface renewal and penetration theory, has been derived.

In this Chapter, bubble induced heat transfer in a unified two-phase system has been considered. The purpose of this Chapter has been to present some of the theoretical analyses which are necessary for the subsequent work. In Chapter 5 this analysis is applied on gas-liquid systems and in Chapter 6 on gas fluidized beds. In Chapter 7 the unification is discussed and final conclusions are made.

Chapter 5.

BUBBLE INDUCED HEAT TRANSFER IN GAS-LIQUID SYSTEMS.

5.1. INTRODUCTION.

The general system and analysis developed in the preceeding Chapter will be applied on the bubble induced heat transfer in gas-liquid systems. Since the thermophysical properties of the dense phase (called liquid in this Chapter) are assumed constant even in the vicinity of the heat transfer surface, these systems are characterised by the zero thickness of the property boundary layer. This feature of gas-liquid systems will be utilized to check on some of the assumptions used in the preceeding Chapter.

It will be further shown that in the present system, where a single continuous stream of gas bubbles is generated into a stationary liquid, transient conduction is the predominant mode of heat transfer. Transient conduction is responsible for about 75% of heat transfer and the remainder is contributed by the convective mode of heat transfer.

5.2. THEORETICAL ANALYSIS.

5.2.1. RESPONSE TO A STEP HEATING INPUT.

Assuming that liquid properties are constant with temperature, they are then uniform in the vicinity of the heat transfer surface. Functions b(R) and g(R) are then constant and equal to unity (equations 4.50 and 4.51) and hence from equations (4.52) and (4.53):

$$H(R) = 1 \tag{5.1}$$

$$L(R) = 0 \tag{5.2}$$

The first approximation to the dimensionless instantaneous average wire temperature, assuming that conduction is the only mode of heat transfer, can then be expressed in an analytical form and is given by equation (4.63).

It has been demonstrated in Section 4.5 that if conduction is the only mechanism of heat transfer between the heat transfer probe and the surrounding liquid, by generating a step heating input in the wire, the first approximation to the wire temperature is identical with the exact temperature of the wire, which is obtained from the full description of the problem.

Furthermore, if the wire is placed in the stationary liquid there are no forced convection currents within the liquid and, because of the liquid inertia, finite times after applying the step heating input into the wire are necessary for the development of natural convection currents. For small diameter wires these times are of the order of seconds. (This can be expressed more precisely as follows: If, as in the present case, the Rayleigh number of the wire in the liquid is smaller than one, the time necessary for the development of the natural convection currents is of the order of seconds.)

Hence for short times after applying the step heating input into the wire, which is placed in the stationary liquid, there are no convection currents within the liquid and conduction is the only mode of heat transfer between the wire and the surrounding liquid. Then, provided the assumptions for the probe behaviour (Sections 4.3.2 and 4.4.1) are correct, equations (4.58) to (4.62) give the full energy description of the system and their solution, given by equation (4.63), constitutes an exact solution to the problem. Using the experimental technique discussed in Section 4.5 experimental data can be obtained and from the agreement (or otherwise) between the theoretical results, (equation 4.63), and these experimental data, the merit (or otherwise) of the assumptions used to describe the probe behaviour can be ascertained.

5.2.2. BUBBLE INDUCED HEAT TRANSFER.

The first approximations to the dimensionless instantaneous, $(W_1)_i$, and time-mean ,$(W_1)_m$, average wire temperatures are given by equations (4.63) and (4.64) respectively. The full solution to the problem can be determined only after the temperature field in and around the wire due to the initial wire temperature ,T_0, has been calculated. If the initial temperature distribution within the wire ,T_0, is known, the temperature field in and around the wire is obtained from equations (4.67) to (4.76), with H(R)=1 and L(R)=0, by numerical calculations. Hence in order to obtain the full solution to the problem, the initial temperature distribution ,T_0, within the wire must be determined. In this work the initial wire temperature distribution is defined by the initial average wire temperature ,T_{0A}, and the normalized dimensionless wire temperature distribution fn(Z) - equation (4.65).

It will be confirmed experimentally (Section 5.5.2, Figure 5.4) that the initial average wire temperature is approximately equal to the experimentally determined time-mean average wire temperature , $(T_X)_m$. Because the theoretical analysis developed in this work is based on the assumption (Section 4.4.1) that the pool (initial liquid) temperature ,T_∞, is zero, the initial average wire temperature which must be used here is given by the temperature difference between the experimentally determined time-mean average wire temperature ,$(T_X)_m$, and the pool temperature ,T_∞:

$$T_{0A} = (T_X)_m - T_\infty \tag{5.3}$$

It is difficult to determine the initial wire temperature distribution ,T_0, and hence it is assumed that T_0 is uniform across the cross section of the wire (Sections 4.3.2 and 4.4.6). Furthermore, the simplest form of the function fn(Z), satisfying all boundary conditions, is assumed. Hence a parabolic function is chosen, so that (Section 4.4.6):

$$\mathrm{fn}(Z) = 1.5\ (1 - Z^2) \tag{5.4}$$

Equations (4.67) to (4.76) can now be solved numerically (a typical computer programme is shown in Appendix 9) and the instantaneous and the time-mean average wire temperatures due to the initial wire temperature ,T_0, can be calculated.

It should be noted that for the above value of the initial average wire temperature ,T_{0A}, the function Ψ (equation 4.89) takes the following form

$$\Psi = \frac{[(T_X)_m - T_\infty]\ k_L}{Qa^2} \tag{5.5}$$

which can be rewritten as

$$\Psi = 1/(Nu_X)_m \tag{5.6}$$

where $(Nu_X)_m$ is the experimentally determined time-mean Nusselt number (Sections 4.4.8 and 4.5). Hence finally, the instantaneous and the time-mean Nusselt numbers can be calculated as (Section 4.4.8)

$$Nu_i = 1/W_i \tag{5.7}$$

$$Nu_m = 1/W_m \tag{5.8}$$

where

$$W_i = (W_1)_i + (W_2)_i/(Nu_X)_m \tag{5.9}$$

$$W_m = (W_1)_m + (W_2)_m/(Nu_X)_m \tag{5.10}$$

and where all variables have their usual meanings.

5.3. APPARATUS, INSTRUMENTATION AND EXPERIMENTAL TECHNIQUE.

5.3.1. EXPERIMENTAL APPARATUS AND INSTRUMENTATION.

A photograph of the experimental equipment is shown in Figure 5.1, and its line diagram in Figure 5.2. The gas is supplied through a system of valves (V) and rotameters (R), which are used to measure the gas flow rate. The liquid is contained in a glass vessel (GV), which is separated from the plenum chamber (GC) by a 'perspex' plate (PP), in the middle of which is situated the bubble generator (BG). The bubble generator consists of a thin stainless steel tube with a valve (GV) at one end. Three different bubble generator diameters are used - 0.8 mm, 1.6 mm and 2.8 mm. The maximum frequency of bubble generation (for convenience referred to henceforth as 'frequency') is obtained with the smallest diameter bubble generator and is of the order of 40 bubbles per second.

The heat transfer probe (HT) (described in Chapter 4) is placed above the generating orifice. Using additional glass sections (AS) it is possible to adjust the distance between the probe wire and the generating orifice. The smallest distance between the wire and the generating orifice is about

1 mm. Four different wire diameters ranging from 41 μm to 305 μm are used. From the point of view of the accuracy of the theoretical solution to the problem, the platinum wire diameter should be as small as possible; however it was found that the wake following each bubble imposed a constraint since it damaged those platinum wires whose diameters were very small. The shortest length of the probe wire is 4.2 mm, so as to be comparable with the diameter of the generated gas bubbles.

5.3.2. EXPERIMENTAL TECHNIQUE.

Three different liquids (water, n-heptane and 50% aqueous solution of glycerol) were used for the experimental investigation of the phenomenon. Their thermophysical properties calculated at the film temperature $T_F=25^oC$ are shown in Table 5.1. Air was used as the gas phase.

The frequency of bubble generation and their size depend on the diameter of the generating orifice, the gas flowrate through this orifice and the properties of the liquid phase. A coarse adjustment of bubble frequency was achieved by adjusting the opening of the end valve (GV). Fine adjustment was effected by adjusting the gas back pressure. The maximum frequency was about 40 bubbles per second and the minimum was effectively zero when no bubbles were generated and only stationary liquid was present. Some difficulties were encountered when the biggest generating orifice was used in liquids of small surface tension, because the frequency then fluctuated with time. In these cases the bubbles were counted over a longer period of time and the time-mean frequency of bubble generation was used as a parameter to describe the situation. (The frequency was measured by the heat transfer probe - Section 4.5.)

Volumes of generated bubbles were determined from the known gas flowrate and from the known frequency of bubble generation. Because the bubbles were small it was assumed that they were of a spherical shape and their diameters were calculated from their volumes.

For the basic experiments the length of the wire was 4.45 mm, but for some additional experiments wires up to 27 mm long were used. The distance between the wire and the generating orifice was chosen as 10 mm. When this distance was too small, the currents in the liquid, caused by bubbles growing at the orifice (local source effect in the liquid) tended to distort the temperature field near the wire. When this distance was too large, the rising bubbles sometimes by-passed the wire because of the oscillatory character of the horizontal component of their velocity. It was found experimentally that when this distance was about 10 mm the distortions of the temperature field were very small (the bubble induced heat transfer was influenced by rising bubbles only and bubbles growing at the orifice had negligible effect on it). The bubbles then always hit the wire and were nearly always bisected by it instead of rolling over the wire surface or completely missing it.

For the basic experiments the working time-mean temperature difference between the time-mean average temperature of the wire and the temperature of the pool was chosen by a compromise: the time-mean temperature difference being big enough to keep the error of its measurement small, but small enough for the assumption of constant wire and liquid properties (Sections 4.3.2 and 5.2.1) to hold. For the basic experiments the time-mean temperature difference was set at about $10^{o}C$ and the film temperature ,T_F, was kept at about $25^{o}C$. In some additional experiments the film temperature ,T_F, was increased in order to investigate its influence on the mechanism of the bubble induced heat transfer.

The use of the probe and the method of evaluating the experimental data are described in Section 4.5.

5.4. EXPERIMENTAL RESULTS.

5.4.1. RESPONSE OF THE WIRE TO A STEP HEATING INPUT.

A typical plot of the instantaneous Nusselt number as a function of the instantaneous Fourier number obtained from the temperature response of the probe wire to a step heating input is shown in Figure 5.3. The experimental data were obtained using 305 μm diameter, 34.6 mm long platinum wire in water. The solid line is the theoretical result given by equation (4.63).

5.4.2. INSTANTANEOUS BUBBLE INDUCED HEAT TRANSFER.

For standard conditions experiments the length of the wire was 4.45 mm (i.e. of the same order as the diameter of the generated bubbles). The distance between the wire and the generating orifice was 10 mm. The liquid temperature was kept at 20°C and the time-mean temperature difference was set at about 10°C ($\Delta T_m = 10^{o}C$).

The variation of the instantaneous average wire temperature with time is shown in Figure 5.4. This Figure was obtained by photographing some of the UV-recorder traces. The ripples on these traces are due to noise. These temperature variations were obtained using a platinum wire of 41.15 μm diameter in water. The choice of the liquid in the pool had little effect on the general character of the temperature curves, but the influence of the wire diameter was profound. The greatest sensitivity to bubble frequency, and hence the clearest outputs, was obtained with the smallest diameter wire, since its heat capacity was small and the distortions due to it were minimized.

Some experimentally obtained instantaneous Nusselt numbers are plotted against the instantaneous Fourier numbers in Figures 5.5 to 5.8. The two lines are the theoretical results given by equations (4.63) and (5.7).

5.4.3. TIME-MEAN BUBBLE INDUCED HEAT TRANSFER.

Some of the experimentally obtained time-mean Nusselt numbers, taken under standard conditions (Section 5.4.2) are plotted against the time-mean Fourier numbers in Figures 5.9 to 5.15. The solid lines are the theoretical results given by equations (4.64) and (5.8).

Experiments have been conducted to investigate the influence of elevated temperatures on the mechanism of the bubble induced heat transfer.

All experimental conditions except the film temperature ,T_F, remained the same as in the standard conditions experiments (Section 5.4.2). Only two sets of readings were taken. The liquid used was water. Experimental results are shown in Figure 5.16, the solid line being the theoretical result given by equation (4.64).

The time-mean heat transfer coefficients for wires appreciably longer than the diameter of generated bubbles were also investigated. The purpose of this series of experiments was to investigate the effectivness of the 'sweeping' action of the bubbles on the surface renewal of the liquid on wires appreciably longer than the diameter of the generated bubbles. These experiments were performed in water on a 101 μm diameter platinum wire, placed 10 mm above the generating orifice. Operating temperatures were the same as in the standard conditions experiments (Section 5.4.2). The wire length-bubble diameter ratio ,ξ, varied from 1 to about 9. Some of the experimental results are shown in Figures 5.17 to 5.19. The solid lines are the theoretical results given by equations (4.64) and (5.17).

5.5. DISCUSSION.

5.5.1. THE HEAT TRANSFER PROBE.

Figure 5.3 shows a typical plot of the instantaneous Nusselt number, obtained from the temperature response of the probe wire to a step heating input, as a function of the instantaneous Fourier number. It has been argued (Section 5.2.1) that for short liquid residence times (short contact times between the probe and the surrounding liquid after the step heating input has been applied) transient conduction is the only mechanism of heat transfer between the probe and the surrounding liquid. The solid line in Figure 5.3 is the theoretical solution of the conductive heat transfer between the probe and the surrounding liquid, given by equation (4.63). The very good agreement between the theoretical results and the experimental data obtained for short liquid residence times, demonstrates the compound validity of many assumptions discussed in Chapter 4, namely:

i) The copper supports remain at the pool temperature ,T_∞, throughout the heating process (Section 4.3.2).

ii) The radial extent of the copper supports and the liquid in between them is effectively infinite (Section 4.3.2).

iii) The radial distribution of the temperature within the wire is very near to uniform (Section 4.3.2).

iv) All wire material properties remain constant throughout the heating process (Section 4.3.2).

v) The method used for evaluation of the experimental data, which is discussed in Section 4.5, is a very good approximation to the exact situation.

Figure 5.3 demonstrates that using all of the above assumptions, the systematic error between the experimental data and the theoretical solution is very small (below 2%). Figure 5.3 also indicates the good accuracy of the experimental technique, because the scatter of the experimental data is very small.

The discrepancy between the experimental data and the theoretical solution during large liquid residence times is due to natural convection, which then provides an additional mechanism of heat transfer between the probe and the surrounding liquid and hence places the experimental data above the theoretical curve.

5.5.2. BUBBLE INDUCED INSTANTANEOUS AVERAGE WIRE TEMPERATURE.

A typical bubble induced instantaneous average wire temperature versus time diagram is shown in Figure 5.20. No simultaneous photographs of rising gas bubbles were taken. However a simple explanation of this temperature-time profile can be made.

Referring to Figure 5.20, assume that the periodic process starts at point 0, when the wake of a passing gas bubble brings fresh liquid in contact with the wire. At that moment two heat transfer processes are competing. The first is the heating of the wire by the heat generated within it, (which is present throughout the process); the second is the simultaneous rapid cooling of the wire by the fresh cool liquid. From point 0 to point 1 the cooling rate is greater than the heating rate, at point 1 they are equal, and from point 1 to point 2 the transient heating of the wire and of the liquid surrounding it is the only heat transfer process present. The transient heating of the wire and of the surrounding liquid is undisturbed until the next bubble approaches the wire. Then the nose of this bubble forces the 'old' warm liquid away and replaces it partially with the fresh liquid, causing some cooling of the wire. This corresponds to the temperature drop from point 2 to point 3. At point 3 the gas bubble itself comes into contact with the wire and at least some of the liquid in the vicinity of the wire is replaced by the gas contained inside the gas bubble. This causes a marked drop in the heat transfer rate and hence in turn a sudden rise of the wire temperature. This corresponds to the temperature rise of the wire from point 3 to point 0'. When the bubble leaves the wire, cold pool liquid in its wake hits the wire and the whole process is repeated again.

The residence time of gas bubbles on the wire ,τ_b, corresponds to the time interval necessary for a bubble to pass the wire and is of the order of 10 to 20 miliseconds. This agrees well with the experimental observations of bubble sizes and velocities. The bubble diameter was about 4.5 mm and the corresponding bubble velocity about 300 mm/sec, implying a residence time of the bubble on the wire surface of about 15 miliseconds.

Figure 5.4 demonstrates that the initial average wire temperature ,T_{0A}, (point 0, Figure 5.20) is in most cases approximately equal to the time-mean average wire temperature. This value of the initial average wire temperature is used to determine dimensionless temperatures $(W_2)_i$ and $(W_2)_m$ - Sections 4.4.6 and 5.2.2.

5.5.3. SURFACE RENEWAL AND OTHER ASSUMPTIONS.

The rate of heating of the wire during the time when a bubble is present on it (corresponding to the time interval from point 3 to point 0', Figure 5.20) was investigated. The observed rate of temperature rise of the wire was far below the value expected for heating of a bare wire in air, even when the time constants of the wire, bridge and recording instruments were allowed for. From this it was deduced that there was a liquid film attached to the wire during the bubble residence on the wire surface.

Next it was investigated if this liquid film remained attached to the wire permanently. The question about the permanent attachment of the liquid film is closely related to the question about the effectivness of the surface renewal of the liquid by the action of passing bubbles. This was investigated as follows:

Assume that when the wake of a passing bubble hits the wire (point 0, Figure 5.20) the liquid on the surface of the wire is completely replaced and that conduction is the only mechanism of the subsequent heat transfer. The instantaneous average wire temperature is then given (equation 4.79) by

$$T_i = (T_1)_i + (T_2)_i \tag{5.11}$$

where $(T_1)_i$ and $(T_2)_i$ are determined by methods described in Sections 5.2.1 and 5.2.2 respectively.

Temperature T_i goes through a minimum, the value of which is calculated theoretically from equation (5.11). This minimum has also been observed experimentally (point 1, Figure 5.20 and Figure 5.4). The experimental values of the minimum have been found on average to be about 25% lower than the theoretical ones calculated from equation (5.11) on the basis of the complete surface renewal of the liquid and conduction as the only mechanism of heat transfer. It is shown in Section 5.5.4 that when Fourier numbers are sufficiently large (i.e. when temperature $(T_2)_i$ is negligible compared with temperature $(T_1)_i$, which can be determined very accurately theoretically), convection is responsible for about 25% of the bubble induced heat transfer. This implies that for identical conditions, experimental temperatures are about 25% lower than the theoretical ones, which are calculated on the assumption that conduction is the only mechanism of the bubble induced heat transfer. It is reasonable to assume that the same situation occurs for extremely small Fourier numbers, which must be considered when investigating the effectivness of the surface renewal of the liquid. This then necessarily means that the surface renewal of the liquid on the wire surface is complete and that the liquid film does not remain attached to the wire permanently. Had this been the case, the experimentally observed minimum wire temperatures would have been nearer to, or even above, the theoretically calculated minimum wire temperatures.

Hence the liquid film is attached to the wire only during the presence of gas bubbles on it, when, perhaps, the momentum of gas bubbles is not sufficiently large to force all liquid away from the wire vicinity. When the bubble passes the wire the large momentum of the bubble wake causes a complete liquid replacement in the wire vicinity.

For the calculation of the time-mean heat transfer coefficients, it is assumed that the residence time of gas bubbles on the wire surface ,τ_b, is negligible and that only bubble wakes are responsible for the surface renewal of the liquid (Section 4.4.1). Clearly this is not the case, because the bubble residence time ,τ_b, is finite and the bubble nose is responsible for a partial liquid renewal on the wire surface (Figures 5.4 and 5.20). The influence of these two effects will be more important for higher frequencies of bubble generation when the ratio τ_b/τ is relatively large. Because of the influence of two opposing effects during the liquid renewal, which are most prominent for higher frequencies of bubble generation (Figure 5.4), the error due to the above mentioned discrepancies will be attenuated. The two opposing effects are the partial drop of the wire temperature during the approach of the bubble nose (interval 2 to 3, Figure 5.20) and the wire temperature rise during the presence on the wire of the bubble itself (interval 3 to 0', Figure 5.20). This is schematically shown in Figure 5.20. The broken line represents the case of an ideal liquid renewal. The areas A_1 and A_2 below and above the broken line respectively, do, *at least partially*, cancel each other out. This situation is most pronounced for high frequencies of bubble generation - Figure 5.4, last diagram.

5.5.4. BUBBLE INDUCED HEAT TRANSFER.

It has been shown in Section 5.5.1, that the assumptions used for the mathematical description of the heat transfer probe are satisfied to a high degree of accuracy. It has been further shown in Section 5.5.3, that bubble induced liquid replacement on the surface of the probe wire is a 100% effective mechanism of mass transport there. Hence the theoretically derived solution for the instantaneous bubble induced heat transfer from the wire to the surrounding liquid, based on transient conduction as the only mechanism of heat transfer, should result in heat transfer coefficients which are lower than those obtained experimentally. This must be the case because the additional convection in any form (forced or natural), which increases the experimentally obtained heat transfer coefficients, is neglected in the theoretical analysis. Because of the liquid moving with the bubble wake, the effect of forced convection is most prominent for short liquid residence times and hence for small values of the instantaneous Fourier number ,Fo. On the other hand, the effect of natural convection becomes important for large liquid residence times (large values of the instantaneous Fourier number). For intermediate values of liquid residence time, both types of convection are important.

Figures 5.5 to 5.8 demonstrate that the above requirement is well satisfied. The experimental results are about 25% higher than the theoretical predictions which are based on transient conduction as the only mechanism of the bubble induced heat transfer. This confirms the assumption that transient conduction is the most important mechanism of the bubble induced heat transfer. Transient conduction is responsible for about 75% of the total heat transfer and liquid convection contributes the remainder.

Situations similar to the case of the instantaneous bubble induced heat transfer can be observed on graphs of the time-mean bubble induced heat transfer (Figures 5.9 to 5.15) - all experimental results lie 20 to 30% above the theoretical prediction. The experimental results of the time-mean bubble induced heat transfer, coupled with the experimental observation that transient conduction is responsible for 75% of heat transfer also in the case of the instantaneous bubble induced heat transfer, confirm indirectly the assumption that the bubble wakes are primarily responsible for the surface renewal of the liquid on the wire surface and, furthermore, that the effect of the finite residence time of the bubbles on the wire and the effect of the bubble 'noses' cancel each other out (Section 5.5.3).

Figures 5.5 to 5.15 demonstrate that the non-zero initial wire temperature ,T_0, has with increasing values of the Fourier number decreasing influence on the full temperature of the wire. Hence for large values of the Fourier number, assuming that conduction is the only mode of heat transfer, the first approximation to the wire temperature given by W_1 is nearly identical with the exact wire temperature given by W.

Some results have been obtained from experiments conducted at higher film temperatures (Figure 5.16). These results show a slight increase in heat transfer coefficients for the case of higher film temperatures which is probably due to the increased contribution of liquid convection. These results do not differ appreciably from results obtained from experiments conducted under standard conditions and confirm once more that transient conduction is the most important mechanism of the bubble induced heat transfer.

The theoretical solution to the present problem shows (and experimental results confirm) that the frequency of bubble generation has profound effect on the time-mean bubble induced heat transfer. The time-mean heat transfer coefficient increases with the frequency of bubble generation. Hence in order to maximize the time-mean bubble induced heat transfer, the frequency of bubble generation should be as high as possible.

The influence of the liquid viscosity is also investigated. Since the liquid viscosity affects only the convective component of the bubble induced heat transfer, its influence is examined by comparing the contributions of the convective mode of heat transfer in liquids of various viscosities (n-heptane and 50% aqueous solution of glycerol). The convective contribution is given by the difference between the experimentally observed heat transfer rates, obtained under mixed mode conditions, and the theoretically derived heat transfer rates which assume conduction as the only mechanism of the bubble induced heat transfer. Since for liquids of different viscosities the convective components are all about the same, it is concluded that the influence of the liquid viscosity on the bubble induced heat transfer is small.

5.5.5. INFLUENCE OF THE WIRE LENGTH/BUBBLE DIAMETER RATIO.

The influence of ξ defined by

$$\xi = 2L/d_b \tag{5.12}$$

has been investigated. A rigorous theoretical treatment of this problem is difficult and only a numerical solution based on far reaching assumptions is possible. Hence the problem has been treated as follows.

It has been found experimentally that when ξ is smaller than 1.5, the bubble induced heat transfer does not depend upon it. So it is assumed that the replacement mechanism is completely effective on only a part of the wire (1.5 d_b long) and that natural convection is the mechanism responsible for heat transfer on the remaining portion of the wire ($2L - 1.5d_b$ long). The coefficient of the time-mean bubble induced heat transfer for the middle section of the wire is calculated from equation (4.64). (The aspect ratio, A, used in equation (4.64) is based on the total wire length.) The coefficient of natural convection heat transfer for the remaining sections of the wire ($2L - 1.5d_b$ long) is assumed equal to that for the whole wire and is determined experimentally in stationary liquid.

Assuming that the time-mean temperature difference between the wire and the liquid (pool) temperatures is approximately constant along the wire length, the total time-mean heat transfer coefficient can be found from the energy balance on the wire as

$$\xi > 1.5 \qquad 2Lh_T = 1.5\, d_b h_B + (2L - 1.5\, d_b)h_N \tag{5.13}$$

From equation (5.13) the dimensionless equations for the total time-mean Nusselt number ,Nu_T, can be obtained as

$$\xi \le 1.5 \qquad Nu_T = Nu_B \tag{5.14}$$

$$\xi > 1.5 \qquad Nu_T = \frac{1.5}{\xi} Nu_B + (1 - \frac{1.5}{\xi})\, Nu_N \tag{5.15}$$

Taking into account that conduction is responsible for about 75% of the bubble induced heat transfer and assuming that the first approximation to the conduction mechanism of the bubble induced heat transfer provides a good description of the real situation (a small diameter wire is used and hence large Fourier numbers are considered and thus the temperature field in and around the wire, due to the initial wire temperature ,T_0, can be neglected - Sections 4.4.4 and 5.5.4), the final result for Nu_T is given as

$$\xi \le 1.5 \qquad Nu_T = 1.25\, (Nu_1)_m \tag{5.16}$$

$$\xi > 1.5 \qquad Nu_T = \frac{1.9}{\xi} (Nu_1)_m + (1 - \frac{1.5}{\xi})\, Nu_N \tag{5.17}$$

where $(Nu_1)_m$ is given by equations (4.91) and (4.64) and the natural convection Nusselt number ,Nu_N, is determined experimentally. Equation (5.17) is included in Figures 5.17 to 5.19, from which a very good agreement with the experimental data is observed. Hence it follows that the above assumptions for the mechanism of the bubble induced heat transfer from wires appreciably longer than the diameter of generated bubbles are well justified.

5.6. CONCLUSIONS.

Bubble induced heat transfer in simplified gas-liquid systems with controlled frequency of bubble generation, using a special heat transfer probe has been investigated. It has been found that:

i) The assumptions used for the mathematical description of the heat transfer probe, developed in Chapter 4, are correct to a high degree of accuracy.

ii) Surface renewal and penetration theory, as developed in Section 4.4, can be used to describe the bubble induced heat transfer in the present system to a high degree of accuracy.

iii) Bubble wakes are primarily responsible for the surface renewal of the liquid.

iv) Complete surface renewal of the liquid takes place over a wire surface of up to one and half bubble diameters long.

v) Transient conduction into the liquid phase is the most important mechanism of the bubble induced heat transfer, being responsible for about 75% of the total heat transfer. Convection contributes the remainder.

vi) To maximize the time-mean bubble induced heat transfer, the frequency of bubble generation should be as high as possible.

vii) To allow high frequencies of bubble generation without bubble coalescence and to decrease the residence time of bubbles on the wire surface, the volume of generated bubbles should be as small as possible (but the ratio wire length/bubble diameter should not be greater than 1.5).

viii) The only possible advantage of larger gas bubbles is that their velocity is greater, thus increasing the contribution of the additional forced convection to the overall bubble induced heat transfer. Nevertheless, the corresponding small increase in heat transfer rates is far outweighed by the adverse effects associated with large gas bubbles, namely, large bubble residence time on the wire surface and the limit on the maximum frequency of generation of discrete gas bubbles.

ix) The direct effect of liquid viscosity on the bubble induced heat transfer is small, because liquid viscosity affects only the convective component of heat transfer which makes only a small contribution to the total bubble induced heat transfer.

Chapter 6.

BUBBLE INDUCED HEAT TRANSFER IN GAS FLUIDIZED BEDS.

6.1. INTRODUCTION.

The general system and analysis developed in Chapter 4 will be applied on the bubble induced heat transfer in gas fluidized beds. As shown in Chapter 3, these systems are characterised by a finite thickness of the property boundary layer in the vicinity of the heat transfer surface. Functions H(R) and L(R) which define the property boundary layer are calculated by a method similar to that used in Section 3.3.4. Further experimental evidence on the justification and the validity of the concept of the property boundary layer and the method of calculating functions H(R) and L(R) is presented.

It will be further shown that in the present system, where a single continuous stream of gas bubbles is generated into a stationary emulsion phase of small particles, transient conduction is the predominant mode of heat transfer responsible for about 90 to 95% of heat transfer. The remainder is contributed by emulsion convection and gas phase convection.

6.2. THEORETICAL ANALYSIS.

6.2.1. HEAT TRANSFER MECHANISMS.

After the emulsion phase on the surface of the probe wire has been renewed (or after the step heating input into the wire has been applied) the heat is transferred from the probe to the surrounding emulsion phase by a non-steady heat transfer process (Section 4.4.3). Assuming that the temperature of the system is below 600°C, the contribution of the radiative component of heat transfer can be neglected[18]. The remaining components can be defined as follows:

i) Conduction into the stationary emulsion phase. This mechanism is analogous to conduction into the stationary liquid phase (without any convection currents within it) in two-phase gas-liquid systems.

ii) Convection due to moving emulsion phase. This mechanism is analogous to convection due to moving liquid in the case of two-phase gas-liquid systems. Whereas liquid convection can be of two different forms (forced or natural), the emulsion convection is due to forced convection only (the thermal driving force necessary for the development of the natural convection velocity field is very small in gas fluidized beds). In the present system, forced emulsion convection is due to the emulsion moving with the bubble wake.

iii) Convection due to the superimposed gas flow through the interstices between the particles in the emulsion phase, called gas convection. The feature of gas fluidized beds is that the gas is flowing upward through the bed of particles (Section 2.2), providing an additional mechanism of surface to bed heat transfer. Provided that the diameter of the solid particles is small, the gas velocity is generally small too and hence the contribution of gas convection can usually be neglected[5]. This mechanism of heat transfer has no analogue in gas-liquid systems.

As discussed in Chapter 4, the heat transfer probe can be used to discriminate between conductive and non-conductive modes of heat transfer. Using an experimental technique discussed in Section 6.3.2, it is possible to discriminate also between gas and emulsion convections.

As previously (Chapters 4 and 5), the theoretical solution of the problem is based on the assumption that conduction is the only mechanism of heat transfer. The compound effect of convection is then determined by comparison with experimental results (as suggested in Section 4.3.2).

6.2.2. THE FUNCTIONS H(R) AND L(R).

If the functions H(R) and L(R) are known, the solution of the problem can be obtained by the general method described in Chapter 4. Hence functions H(R) and L(R), defined by equations (4.52) and (4.53) respectively, must be determined. Once the voidage variation in the vicinity of the probe wire (which constitutes the constraining surface) is determined, functions H(R) and L(R) can be calculated by the technique discussed in Section 3.3.4.

The method of calculating the voidage variation in the vicinity of the probe wire is analogous to that discussed in Section 3.3.3. Since the wire radius is comparable with the radius of the solid particles in the emulsion phase, the curvature of the probe wire must be taken into account when calculating the voidage distribution in the wire vicinity. As mentioned in Section 3.3.3, particles at the same distance from the constraining wall (probe wire in the present case) are influenced by it in the same way. Hence the mean voidage at any cylindrical plane, concentric with the probe wire, is a function of the distance of this cylindrical plane from the probe wire. The postulate used in Section 3.3.3 to calculate the solid cross sectional area is modified to take into account the curvature of the constraining surface in the following way: For a bed of uniform spherical particles, the solid cross sectional area on a particular cylindrical reference plane, distance Δr from the cylindrical constraining surface, is proportional to the cross sectional area of a cylinder whose volume and height are identical to those of that part of a spherical particle which can be found in the annulus of the reference and the constraining cylinders, while touching the constraining cylindrical wall- Figure 6.1.

The subsequent method of calculation of the voidage distribution in the wire vicinity is similar to that suggested in Section 3.3.3 and is described in more detail in Appendix 7. The predicted variations of the voidage in the wire vicinity for various ratios of the wire and the particles radii are plotted in Figure 6.2.

From the calculated values of the voidage in the wire vicinity, functions g(R) and b(R) can be obtained by the method described in Section 3.3.4. Similarly functions H(R) and L(R) can be calculated too. Figures 6.3 and 6.4 show the behaviour of function b(R) for various ratios of the wire and the paticles radii and for two ratios of the gas and the solid thermoconductivities.

6.2.3. RESPONSE TO A STEP HEATING INPUT.

It has been demonstrated in Section 4.5, that were conduction the only mechanism of heat transfer between the heat transfer probe and the surrounding emulsion phase, by generating a step heating input into the wire, the first approximation to the wire temperature, given by the solution of equations (4.41) to (4.45), would be identical with the exact temperature of the wire which is obtained from the full description of the problem.

If the wire is placed in a stationary emulsion phase of small particles, there are no convection currents within the emulsion phase and gas convection contribution to the overall heat transfer is small. The contribution of gas convection can be further decreased be keeping the gas flowrate as small as possible. Hence after applying a step heating input into the wire which is placed in a stationary emulsion phase of small particles, transient conduction into the emulsion phase is the only mechanism of heat transfer between the wire and the surrounding emulsion phase.

It has been shown (Section 5.5.1) that the assumptions used for the mathematical description of the heat transfer probe are correct to a high degree of accuracy. Furthermore, the design of the heat transfer probe is such that the property boundary layer of the surrounding emulsion phase has a profound and controlling influence on the mechanism of heat transfer. This is due to the inclusion of the copper supports in the design of the heat transfer probe (Section 4.3.1) which provide secondary heat transfer surfaces by acting as heat sinks. The depth of heat penetration from the wire into the surrounding emulsion phase is then kept small and comparable with the thickness of the property boundary layer.

The only parameters in equations (4.41) to (4.45) which are not well defined are the functions H(R) and L(R). Hence the agreement (or otherwise) between the theoretical results given by equations (4.41) to (4.45) with functions H(R) and L(R) calculated by the method of Section 6.2.2, and the experimental results obtained by applying a step heating input into the wire in a stationary emulsion phase of small particles, can be used as a criterion in regarding the merits (or otherwise) of the assumptions used in defining the property boundary layer, given by functions H(R) and L(R). This technique can be used to obtain further experimental evidence for justifying the concept of the property boundary layer developed in this work.

The solution for the conduction model of the instantaneous heat transfer is given by equation (4.90) as

$$(Nu_1)_i = 1/(W_1)_i \qquad (6.1)$$

where $(W_1)_i$ is the dimensionless instantaneous average wire temperature (assuming that transient conduction is the only mode of heat transfer) given by solving equations (4.41) and (4.45). The method of numerical solution is shown in Appendix 4 and a typical computer programme is shown in Appendix 8.

6.2.4. BUBBLE INDUCED HEAT TRANSFER.

As discussed in Sections 4.4.7 and 5.2.2, the full solution to the temperature field in and around the wire is determined by adding the temperature field due to the non-zero initial wire temperature to that describing the first approximation to the problem. As in Section 5.2.2, it is again assumed that the initial average wire temperature (compare with Figure 6.16) is given by

$$T_{0A} = (T_X)_m - T_\infty \qquad (6.2)$$

and that function fn(Z) is of the form given by equation (5.4). The dimensionless instantaneous and time-mean average wire temperatures, due to the non-zero initial wire temperature ,T_0, are then calculated from equations (4.67) to (4.76) by the method similar to that described in Appendix 4. A typical computer programme is shown in Appendix 9. The instantaneous and the time-mean bubble induced Nusselt numbers are then calculated from equations (5.7) to (5.10).

6.3. APPARATUS, INSTRUMENTATION AND EXPERIMENTAL TECHNIQUE.

6.3.1. EXPERIMENTAL APPARATUS AND INSTRUMENTATION.

The photograph of the experimental equipment is shown in Figure 6.5, and its line diagram in Figure 6.6. To enable good observation of the bubble motion and to ensure uniform fluidization across the bed cross section, all experiments have been performed in a two-dimensional bed. The bed, made of 'perspex', is 600 mm high, 350 mm wide and 12.7 mm thick. Solid particles are contained in this two-dimensional bed (TB). The bed is separated from the plenum chamber (GC) by a high pressure drop porous distributor (PD). The gas used to provide incipiently fluidized conditions in the bed is supplied through a valve (V1) and a rotameter (RT1), which is used to measure the gas flow rate. The bubble generator (BG) is situated in the centre of the bed cross sectional area about 30 mm above the distributor plate. The bubble generator consists of a thin stainless steel tube (1.6 mm in diameter) with a solenoid valve (SV) at one end. The triggering signal for the solenoid valve is supplied by a triggering mechanism (TM) consisting of an electrical motor, a series of cams and a microswitch. The gas to the bubble generator is supplied through a microrotameter (RT2) and a valve (V2). The tank (TK), placed between the valve (V2) and the solenoid valve (SV), is used to dampen the pressure oscillations in the gas supply line, which are initiated by the action of the solenoid valve. The maximum frequency of bubble generation (referred to henceforth as 'frequency') obtained with the present set up is about 2 bubbles per second. This is the maximum frequency with which a continuous stream of discrete gas bubbles can be maintained in the bed under present conditions using the above described bubble generator.

The heat transfer probe (HT), described in Chapter 4, is placed 80 mm above the generating orifice. The probe wire used in the present series of experiments is 125 μm in diameter and 14.2 mm long. The probe wire is shorter than the smallest observed diameter of generated gas bubbles so that the theoretical analysis developed in Section 4.4, for the mechanism of the bubble induced heat transfer, is applicable.

The instrumentation of the heat transfer probe is described in Section 4.5.

6.3.2. EXPERIMENTAL TECHNIQUE.

Silica sand particles of various size ranges and five different gases were used for the experimental investigation. Their properties, calculated at temperature of 25°C, are shown in Table 6.1. The solid particles were carefully graded on a sieving machine and very close size ranges were obtained. The mean particle diameter used is the geometric mean, calculated from the two sieve sizes which specify each particle size range. No metal particles were used for the investigation of the mechanism of heat transfer, because the metal particles available were not clean (there was a layer of metal oxides on their surface) and their thermophysical properties were not known. As discussed in Section 3.3.4, emulsion phase properties can be calculated only if the emulsion phase voidage and the properties of both phases are known. Mean emulsion voidage ,ε_E, was determined experimentally from the volume of the incipiently fluidized bed and the true density of the solid particles.

The condition of incipient fluidization was determined experimentally by a combination of pressure drop measurements through the bed and visual observations. Gas bubbles were generated into a bed incipiently fluidized by the same gas. It was found difficult to generate bubbles into an incipiently fluidized bed, since the generated bubbles were unstable and each bubble was accompanied by a swarm of smaller bubbles which followed in its wake. By a trial and error method it was found that when the bed was fluidized at about 95% of incipiently fluidized conditions, stable bubbles could still be generated and maintained, but that the smaller bubbles following the main one were eliminated. (The 95% incipiently fluidized bed is for convenience referred to henceforth as the 'incipiently fluidized bed'.) The frequency of bubble generation was controlled by the speed of the cam and their volume by the design of the cam and the gas back pressure in the tank. Volumes of the generated bubbles were determined approximately from the rate of gas supply to the tank and from the known frequency of bubble generation.

As discussed in Section 5.3.2, the working time-mean temperature difference between the time-mean average temperature of the wire and the temperature of the pool must be chosen by a compromise; in the present case it is set at between 10 and 20°C.

The use of the probe and the method of evaluating the experimental data are described in Section 4.5.

It has been shown in Section 6.2.3 that when the wire is placed in a stationary emulsion phase, emulsion convection is eliminated as a heat transfer mechanism between the wire and the surrounding emulsion phase. Hence the remaining mechanisms of heat transfer are emulsion conduction and gas convection. The influence and contribution of gas convection can be approximately determined in the following way. The probe is placed into a fixed (packed) bed and a step heating input is applied into the wire. The gas flowrate is then increased in steps and the step heating input into the wire is applied for each value of the gas flowrate. The contribution of gas convection is then obtained by comparing the responses of the wire for various values of the gas flowrate. During these experiments care must be taken to keep the bed structure undisturbed.

6.4. EXPERIMENTAL RESULTS.

6.4.1. RESPONSE OF THE WIRE TO A STEP HEATING INPUT.

A typical influence of gas velocities on the response of the probe wire, situated in a fixed bed, to a step heating input is shown in Figure 6.7. Air is used as the gas phase and silica sand 4 (size range 500 to 600 μm) provides the solid particles. Similar graphs have been obtained for other gases and particle sizes, but with a decreased particle size, the influence of gas velocity is not so marked.

The response of the probe wire submerged in an incipiently fluidized bed to a step heating input has been also studied. The experimental data obtained are plotted in dimensionless form in Figures 6.8 to 6.15. The solid lines are the theoretical solutions given by equation (6.1). The mean voidage of the emulsion phase ,ε_E, determined experimentally by the method of Section 6.3.2 and used for calculating the properties of the emulsion phase is included in each Figure. Also included are the values of the thermophysical properties of the emulsion phase.

6.4.2. INSTANTANEOUS BUBBLE INDUCED HEAT TRANSFER.

The variation of the instantaneous average wire temperature with time for various frequencies of bubble generation is shown in Figure 6.16. This Figure was obtained by photographing some of the UV-recorder traces. The ripples on these traces are due to noise. These temperature variations have been obtained by placing the probe into an incipiently fluidized bed of copper shot ($T_\infty = 20^oC$). The copper shots have been chosen because the shape of the generated bubbles is well defined and reproducible, and, further because it is relatively simple to keep the bed at incipiently fluidized conditions. Similar, but not so well defined graphs, have been obtained also for fluidized beds of silica sand.

Some experimentally obtained instantaneous Nusselt numbers ,$(Nu_X)_i$, are plotted against the instantaneous Fourier numbers ,Fo, in Figures 6.17 to 6.22. The two solid lines (in each Figure) are the theoretical results given by equations (6.1) and (5.7) - as discussed in Sections 6.2.3 and 6.2.4. The values of the mean voidage of the emulsion phase and the thermophysical properties of the emulsion phase are also included.

6.4.3. TIME-MEAN BUBBLE INDUCED HEAT TRANSFER.

Some of the experimentally obtained time-mean Nusselt numbers ,$(Nu_X)_m$, are plotted against the time-mean Fourier numbers ,Fo_m, in Figures 6.23 to 6.26. The two solid lines (in each Figure) are the theoretical results obtained by the method described in Sections 6.2.3 and 6.2.4. The values of the mean voidage of the emulsion phase and the thermophysical properties of the emulsion phase are also included.

6.5. DISCUSSION.

6.5.1. THE INFLUENCE OF GAS CONVECTION.

It has been shown in Section 6.3.2 that when a heat transfer probe is placed in a fixed bed and a step heating input is applied into the probe wire, the only mechanisms of heat transfer between the probe and the surrounding fixed bed are emulsion conduction and gas convection. Furthermore, as shown in Section 6.2.1, the contribution of gas convection increases with the velocity of the gas. There is no mechanism of heat transfer analogous to gas convection in gas-liquid systems. Hence in order to make both systems comparable (gas-liquid systems and gas fluidized beds), the contribution of gas convection should be as small as possible.

Because in incipiently fluidized systems gas velocities increase with the particle size[18], the contribution of gas convection is greater in gas fluidized beds of coarse particles. In the present set up the contribution of gas convection is given by the difference in heat transfer rates between cases of zero gas velocity and gas velocity at 95% of incipient fluidization.

Figure 6.7 shows that for the largest particles used in the present investigation (silica sand 4), with air as the gas phase, the contribution of gas convection to the total heat transfer is below 10%. Experiments were also conducted to determine the contribution of gas convection in beds of silica sand 1,2 and 3 (Table 6.1). There the contribution of gas convection is so small that it cannot be determined by the present experimental technique. Hence by using silica sand of size ranges below 600 μm, the contribution of gas convection can be kept small, and by using silica sand of size ranges below 300 μm, the contribution of gas convection can be neglected. This agrees well with experimental data of other investigators[5,54].

6.5.2. THE CONCEPT OF THE PROPERTY BOUNDARY LAYER.

The situation where the heat transfer probe is placed in an incipiently fluidized bed (stationary emulsion phase) of small particles has been discussed previously (Section 6.2.3). It has been shown that under these circumstances the only mechanism of heat transfer following a step heating input into the wire is emulsion conduction (Sections 6.2.3 and 6.5.1). Hence by comparing the experimental data on heat transfer with the theoretical results given by equation (6.1), the validity of the assumptions used for determining the functions H(R) and L(R), which specify the property boundary layer, can be tested.

Figures 6.8 to 6.15 demonstrate the very good agreement between experimental data and theoretical results. With exception of silica sand 4/air (Figure 6.11) and silica sand 2/helium (Figure 6.14), where the theoretical results fall below the experimental data, the theoretical results are on average about 10% higher than the corresponding experimental results.

The mean voidage of the emulsion phase ,ε_E, which is determined experimentally, varies from 0.40 (silica sand 4/air - Figure 6.11) to 0.49 (silica sand 2/helium - Figure 6.14). The latter voidage has been obtained in an expanded bed. As mentioned previously (Section 6.3.2), the mean voidage of the emulsion phase is determined experimentally, assuming that the voidage is uniform throughout the bed, from the volume of the whole bed. The validity of the assumption of constant voidage has been tested by calculating a controlling theoretical solution which is based on a different value of the mean voidage of the emulsion phase. This is done in Figure 6.8a where the controlling theoretical solution is included. This solution is based on an assumption that the voidage of the emulsion phase is $\varepsilon_E = 0.50$, which is much higher than the value of the mean voidage which is determined experimentally ($\varepsilon_E = 0.45$). The controlling solution is nearer to the experimental data but still overpredicts them by about 10%. This shows that in this region the theoretical solution is relatively insensitive to a change in the mean emulsion voidage and hence that the assumption that the emulsion voidage is uniform throughout the entire bulk of the bed can be used.

With increased particle size the experimental points get nearer to (Figures 6.8 to 6.10) or even above (Figure 6.11) the theoretical curve. This is due to the contribution of gas convection (Section 6.2.1) which increases with increasing particle size (Section 6.5.1) and hence causes an increase in experimental heat transfer rates, which is most prominent in the case of silica sand 4/air (Figure 6.11). Hence one can assume that were the effect of gas convection taken into account and subtracted (Section 6.5.1), all experimental results would then fall below the theoretical predictions (Figures 6.8 to 6.11).

Hence assuming that conduction is the only mechanism of heat transfer between the probe wire and the surrounding emulsion phase, the theoretical results are higher than the experimental data (with possible exception of silica sand 2/helium, where the contribution of gas convection was not determined) by, on average, about 11%.

Since it has been demonstrated previously that the numerical technique used here is sufficiently accurate (Sections 4.4.5 and 4.4.6), the above results indicate that some systematic error is being made during the theoretical calculation of functions H(R) and L(R), which define the property boundary layer. But considering the wide range of particle sizes used (75 to 600 μm) and the wide range of gas thermal conductivities (0.0097 to 0.148 W/mK), the agreement may be regarded as satisfactory. It is doubtful if any refinement of the method of calculating the functions H(R) and L(R) is required, since the present method gives good agreement with experimental data and is based on very simple geometrical considerations

(Section 6.2.2) and well established techniques[43] (Section 3.3.4).

The present theory has not been tested in gas fluidized beds of metal particles, because no clean partcles with well defined thermophysical properties were available. There is some scope for future work.

It has been argued in Section 6.2.3, that using the present probe, property boundary layer of the emulsion phase plays an important role in controlling the heat transfer rates. The importance of the property boundary layer is demonstrated in Figures 6.9 and 6.11. Each of these Figures contains also two theoretical solutions based on the respective assumptions that (a) the emulsion phase behaves as a liquid with zero thickness of the property boundary layer and (b) that only stationary gas, (and not solid particles), is present in the system. The theoretical solutions have been obtained from equation (4.63), using the thermophysical properties of the emulsion phase and of the gas respectively. One can observe that if the property boundary layer is not considered the theoretical predictions diverge greatly from the experimental results.

The excellent agreement between the theoretical and experimental results provides a very powerful argument for the justification of the concept of the property boundary layer and hence for the model of heat transfer in gas fluidized beds, developed in Chapter 3.

As seen from Figures 6.8 to 6.15, the theoretical heat transfer rates have not been calculated for emulsion phase residence times in excess of 1 sec. This is due to the complications with numerical calculations (Section 4.4.4), since very large computer times are required. Because heat transfer coefficients vary most rapidly for short emulsion phase residence times, the termination of the numerical calculations for residence times of about 1 sec is regarded as an acceptable compromise.

6.5.3. BUBBLE INDUCED INSTANTANEOUS AVERAGE WIRE TEMPERATURE.

The variations of the bubble induced instantaneous average wire temperature with time for various frequencies of bubble generation are shown in Figure 6.16. A typical bubble induced instantaneous average wire temperature versus time profile is shown in Figure 5.20 (but here the time coordinate points in the opposite direction). The explanation of this temperature-time profile is identical to that one made in Section 5.5.2. Similar results for the instantaneous probe temperature were obtained by Tuot and Clift[57].

The residence time of gas bubbles on the wire ,τ_b, corresponds to the time interval necessary for a bubble to pass the wire and is, in this case, of the order of 0.1 to 0.3 seconds. This again agrees well with the experimental observations of bubble sizes and velocities. The bubble diameter is about 30 mm and the bubble velocity about 200 mm/sec, implying the bubble residence time on the wire of about 0.15 sec.

Figure 6.16 demonstrates that the initial average wire temperature, T_{0A}, (point 0 - Figure 5.20) is in most cases approximately equal to the time-mean average wire temperature $(T_X)_m$. This value is used to determine the dimensionless temperatures $(W_2)_i$ and $(W_2)_m$ - Sections 4.4.6 and 6.2.4.

6.5.4. BUBBLE INDUCED HEAT TRANSFER.

As discussed in Section 5.5.4, the theoretically derived solutions for the instantaneous bubble induced heat transfer from the wire to the surrounding emulsion phase, based on transient conduction as the only mechanism of heat transfer, should result in heat transfer coefficients which are lower than those obtained experimentally. This must be so because the additional mechanisms of heat transfer (gas convection and emulsion convection), which increase the experimentally obtained heat transfer coefficients, are neglected in the theoretical analysis. Again, as in the case of bubbling liquids, the effect of emulsion convection should be most prominent for short emulsion residence times and hence for small values of the instantaneous Fourier number ,Fo. To decrease the influence of gas convection, particles of small diameters only have been used for the experimental investigation of the bubble induced heat transfer.

Experimental results of the instantaneous bubble induced heat transfer are shown in Figures 6.17 to 6.22. As seen from these Figures, the first approximation to the instantaneous bubble induced heat transfer is again (as in Section 6.5.3) calculated for residence times of up to 1 second. It has been mentioned previously (Section 4.4.6) that the numerical method used to calculate the temperature field in and around the wire due to the initial wire temperature, requires even larger amount of computer times than the numerical method which is used to calculate the first approximation to the bubble induced heat transfer. Hence the full theoretical solution for the instantaneous bubble induced heat transfer has been obtained for emulsion phase residence times of up to about 0.3 seconds. This is regarded as a good compromise, since for larger emulsion residence times the first approximation to the instantaneous bubble induced heat transfer becomes nearly identical with the full solution of the problem (Section 4.4.4).

From Figures 6.17 to 6.22, one can observe that as in the case of the wire response to a step heating input (Section 6.5.2), the theoretical results are higher, on average by about 10%, than the experimental data. Assuming, as in Section 6.5.2, that the reason for this anomaly is some systematic error made during the theoretical calculations of functions H(R) and L(R), which define the property boundary layer, a correction can readily be made to take this effect into account. The theoretical heat transfer coefficients for the instantaneous bubble induced heat transfer are decreased by an amount which is equal to the difference between the theoretical and experimental results of heat transfer, following a step heating input into the wire when submerged into an identical emulsion phase. This difference (or correction factor) can be obtained from Figures 6.8 to 6.10, 6.12 and 6.13. (The correction factor has not been determined for the bed of silica sand 1/argon - Figure 6.21.) The corrected theoretical results are also included in Figures 6.17, 6.18, 6.19, 6.20 and 6.22.

The corrected theoretical results and the experimental data for the instantaneous bubble induced heat transfer are, within the range of experimental errors, nearly identical. This is consistent with the assumption that transient conduction is the most important mechanism of the bubble induced heat transfer in gas fluidized beds of small particles. The present experimental results indicate that transient conduction is responsible for nearly 100% of the total heat transfer and that the contribution of emulsion convection is almost negligible. The reason for this feature of heat transfer in the present case could be that the bed is slightly below the value of incipient fluidization and that the movement of the bubble wakes might be restricted. But the fact that the bubbles can be generated and maintained in the middle section of the bed (Section 6.3) seems to indicate that what is called in this work 95% incipient fluidization over the whole cross section of the bed corresponds to incipiently fluidized conditions in the middle section of the bed. This then implies that the movement of the bubble wakes in the middle section of the bed is unrestricted.

Some of the experimentally obtained time-mean bubble induced heat transfer coefficients (in dimensionless form) are shown in Figures 6.23 to 6.26. The theoretically obtained results are also included. Because of the extremely large computer times required for the numerical calculations, the theoretical results cover only a small portion of the experimental range of the time-mean Fourier numbers, Fo_m. Using the method described above, the theoretical results are again corrected to take into account the systematic error made during the theoretical calculations of functions H(R) and L(R). Even after taking into account this correction, theoretical predictions are in the regions where the theoretical solutions have been obtained slightly higher (on average by about 10%) than the experimental data. This discrepancy is probably due to the finite residence times of gas bubbles on the surface of the wire, τ_b.

The theoretical solutions are based on the assumptions that the residence time of gas bubbles on the surface of the wire is zero and that only the bubble wakes (and not the bubble 'noses') are responsible for the renewal of the emulsion phase on the wire surface (Section 4.4.1). Since the heat capacity of the gas is much smaller than the heat capacity of the emulsion phase, heat transfer from the wire to the surrounding gas during the bubble presence on the wire is very small and can be neglected. The bubble residence time on the surface of the wire ,τ_b, was not measured directly but was estimated as between 0.1 and 0.3 seconds, giving a mean value of about 0.2 seconds ($\tau_b = d_b/U_b$).

If the bubble wakes only were responsible for the mechanism of surface renewal (Section 4.4.1), the experimental results would be considerably smaller than the theoretical ones, calculated on the assumption that the residence time of gas bubbles on the wire surface is zero. For example, for frequency of bubble generation of 2 bubbles per second, the residence time of the emulsion phase on the surface of the wire is only about 0.3 seconds out of the total periodic time of 0.5 seconds. The experimental results should then be, for a frequency of 2 bubbles per second, about 30 to 40% below the corrected theoretical predictions. Similarly, for frequency of 1 bubble per second, the experimental results should be about 15 to 20% below the theoretical predictions. It has been found during the present experimental work that the difference between the experimental and corrected theoretical results is much smaller; for frequencies of between 1 and 2 bubbles per second the difference has been found to be, on average, about 10%. The influence of the finite residence time of gas bubbles on the surface of the wire is more important for high frequencies of bubble generation when the ratio τ_b/τ is relatively large (Section 5.5.3). This then indicates that for high frequencies of bubble generation there must be an additional mechanism influencing the time-mean bubble induced heat transfer. This is the effect of the bubble 'noses', which, as in the case of gas bubbles in liquids - Section 5.5.2, provide an additional mechanism of surface renewal of the emulsion phase on the wire surface, thus increasing the time-mean heat transfer and hence opposing the effect of the decreased heat transfer rates during the residence of gas bubbles on the wire surface. The two effects, as in the case of gas-liquid systems, cancel, at least partially, each other out. This can be seen in Figure 6.16, where for the case of high frequencies of bubble generation the mutual elimination of both effects is best demonstrated.

The time-mean bubble induced heat transfer does, in general, depend on the volume of the gas bubbles. Since it has been found quite difficult to achieve reproducible bubble volumes, there is a considerable scatter of the experimental data of the time-mean bubble induced heat transfer (Figures 6.23 to 6.26). Because of the difficulties in keeping the bubble volumes constant and defining the bubble shapes and calculating their dimensions, it has not been considered practicable, in the present work, to investigate some of the behaviour of the system which was investigated in the case of bubbling liquids, as, for example, the exact mechanism of the surface renewal of the emulsion phase and the influence of the wire length/bubble diameter ratio.

As in the case of gas-liquid systems (Section 5.5.4), the frequency of bubble generation has been shown to have a very strong influence on the time-mean bubble induced heat transfer. In order to maximize it, the frequency of bubble generation should be as high as possible, but care should be taken to ensure that the decrease of the time-mean heat transfer due to the bubble residence on the wire surface does not outweigh the favourable effects of high frequencies of bubble generation.

6.6. CONCLUSIONS.

It has been shown that the heat transfer probe used in this work can be used to determine the contribution of gas convection to the overall mechanism of heat transfer.

Using the probe in incipiently fluidized beds, a further justification for the concept of the property boundary layer has been obtained. It has been found that the method of evaluating the property boundary layer, developed here, gives a very good agreement with the experimental data. The use of the present method results in theoretical heat transfer coefficients which are, on average, about 10% above the comparable experimental data.

Bubble induced heat transfer in simplified gas fluidized systems with controlled frequency of bubble generation has been investigated. It has been found that:

i) Surface renewal and penetration theory, as developed in Section 4.4, with the property boundary layer given by functions H(R) and L(R), calculated by the method of Section 6.2.2, can be used to describe the bubble induced heat transfer in the present system to a good degree of accuracy.

ii) The bubble wakes are primarily responsible for the renewal of the emulsion phase on the wire surface, while their 'noses' have been shown to be responsible for at least some surface renewal of the emulsion phase. The effect of the bubble residence time on the surface of the wire ,τ_b, on the time-mean bubble induced heat transfer is not as important as one might expect from the fraction of the bubble residence time over the whole periodic time ,τ_b/τ. This is due to the action of the bubble 'noses' which provide an additional mechanism of renewal on the wire surface, thus increasing the time-mean bubble induced heat transfer and hence cancelling, at least partially, the decrease of the heat transfer during the residence of gas bubbles on the surface of the wire. The theoretical time-mean heat transfer coefficients can then be calculated on the assumption that the bubble wakes only are responsible for the surface renewal of the emulsion phase and the effects of the bubble 'noses' and bubble residence times can be neglected. The theoretical results so obtained are in acceptable agreement with the experimental data obtained here.

iii) Transient conduction into the emulsion phase is the most important mechanism of the bubble induced heat transfer, being responsible - in the present case - for more than 90% of the total heat transfer. The remainder is provided by superimposed gas convection, whose contribution increases with mean particle size. The contribution of emulsion convection is shown to be very small and can be neglected.

iv) To maximize the time-mean bubble induced heat transfer the frequency of bubble generation should be as high as possible, but their volumes should be small so as to keep their residence time on the surface of the wire also small compared with the residence time of the emulsion phase there.

Chapter 7.

GENERAL CONCLUSIONS AND SUGGESTIONS FOR FURTHER WORK.

The purpose of this dissertation has been to investigate the analogy between fluidized beds and liquids from the point of view of heat transfer at heating or cooling of surfaces, and to determine the contribution of various modes to the mechanism of the bubble induced heat transfer in the two systems.

Experimental data available in the literature show that the presence of any constraining surface (and in particular, a heat transfer surface) in a bed of particles changes the packing of the solid particles in its vicinity and hence alters the voidage of the emulsion phase there. It has been demonstrated that the influence of the constraining surface on the voidage of the emulsion phase extends to a distance of about one particle diameter from the surface; beyond that its influence decreases rapidly and the voidage of the emulsion phase can be assumed to be un-influenced by the presence of the constraining surface and constant.

Since the thermophysical properties of the emulsion phase are functions of its voidage, the concept of a property boundary layer of the emulsion phase in the vicinity of the constraining surface has been introduced.

By introducing the concept of a property boundary layer, the liquid analogy has been extended to unify gas fluidized beds and bubbling liquids from the point of view of heat transfer. Both systems are unified by defining a general two-phase system consisting of a gas bubble discrete phase and a continuous dense phase which has constant thermophysical properties everywhere in the bed except in the vicinity of the heat transfer surface where a localized property boundary layer must be considered. In the case of bubbling liquids, liquid constitutes the dense phase and in the case of aggregative gas fluidized beds, the dense phase is provided by the emulsion phase. The main difference between gas fluidized beds and bubbling liquids is in the thickness of the property boundary layer which varies from relatively large (for gas fluidized beds of coarse particles) through relatively small (for gas fluidized beds of fine particles) to zero (for bubbling liquids).

A method of defining and calculating the property boundary layer is presented.

It has been demonstrated that in order to investigate the mechanism of the bubble induced heat transfer in more detail, the freely bubbling system must be simplified, in this work, by generating a single continuous stream of discrete gas bubbles into the stationary dense phase. Furthermore, a special heat transfer probe which can be used to discriminate between conductive and non-conductive modes of heat transfer has been designed.

A general model of the bubble induced heat transfer in a unified two-phase system has been developed; the model being based on the surface renewal and penetration theory with transient conduction into the dense phase as the only mechanism of heat transfer. Heat transfer from the probe to the surrounding dense phase when conduction is the only mode of heat transfer has been calculated theoretically to a high degree of accuracy, (as confirmed experimentally), so that the probe can be used to discriminate between conductive and non-conductive modes of heat transfer. The compound effect of the non-conductive modes of heat transfer is determined by comparing the experimentally observed heat transfer rates from the probe under mixed-mode conditions (conductive and non-conductive modes) with those obtained theoretically in which conduction is the only mode of heat transfer.

The theory of the bubble induced heat transfer developed here has been tested experimentally in both simplified, gas-liquid and gas fluidized, systems. The theories of this work have been justified experimentally, leading to the following conclusions:

i) The surface renewal and penetration theory can be used to describe the bubble induced heat transfer in the present system to a good degree of accuracy. Bubble wakes are primarily responsible for the renewal of the dense phase on the heat transfer surface and it is this frequent renewal of the dense phase which is the cause of the high rates of heat transfer at surfaces. Since the heat capacity of the gas is much smaller than that of the dense phase, heat transfer rates are decreased during the residence of gas bubbles on the surface of the wire. However, the bubble 'noses' are responsible for a partial surface renewal of the dense phase, thus providing an additional mechanism of heat transfer. The effect of the bubble 'noses' and of the bubble residence times partially cancel each other out in their influence on the time-mean bubble induced heat transfer. It is shown that when the theoretical coefficient of the time-mean bubble induced heat transfer is calculated on the assumption that only bubble wakes are responsible for the surface renewal of the dense phase, the effect of the bubble 'nose' and the bubble residence time on the surface of the heat transfer probe can be neglected without incurring a large error.

ii) The effect of gas within the bubbles on heat transfer was shown to be negligible, the heat transfer from the probe to the surrounding dense phase being primarily responsible for the bubble induced heat transfer. The modes of heat transfer from the probe to the surrounding dense phase can be classified as dense phase conduction, dense phase convection and, in the case of gas fluidized beds, superimposed gas convection. It has been demonstrated that for sand particles of sizes below 300 μm in diameter, the effect of gas convection can be neglected, and for sand particles of diameters between 300 μm and 600 μm, the gas convection contribution is below 10% of the total heat transfer. Hence for gas fluidized beds of small particles the effect of gas convection (which has no analogue in gas-liquid systems) can usually be neglected. Dense phase convection takes the form of emulsion phase convection in gas fluidized beds and liquid convection in bubbling liquids. Whereas liquid convection can be of two different forms (forced or natural), only forced emulsion phase convection is possible in gas fluidized beds. Forced dense phase convection is due to the dense phase moving with the bubble wake. In the case of gas fluidized beds, the effect of forced emulsion phase convection is negligible. In the case of bubbling liquids, liquid convection is responsible for about 25% of the bubble induced heat transfer. Hence dense phase conduction is the most important mechanism of bubble induced heat transfer in a general two-phase system investigated here. In the case of bubbling liquids, liquid conduction is responsible for about 75% of the bubble induced heat transfer, and in the case of gas fluidized beds of small particles operating below the radiative temperature level, emulsion conduction is responsible for more than 90% of the bubble induced heat transfer.

iii) In order to maximize the time-mean bubble induced heat transfer the frequency of bubble generation should be as high as possible. However, to allow high frequencies of bubble generation without bubble coalescence, the volume of generated bubbles should be as small as possible. During the process of maximisation of the time-mean bubble induced heat transfer, care should be taken to ensure that the adverse influence of the residence time of gas bubbles on the heat transfer surface on the time-mean bubble induced heat transfer is compensated by the action of the bubble 'noses'.

iv) The assumptions used for the mathematical description of the heat transfer probe used in the present work are correct to a high degree of accuracy.

v) The concept of a property boundary layer is a physically justified concept and the present method of its definition and calculation is acceptable for the prediction of surface-to-bed heat transfer rates.

Heat transfer in multi-phase systems is a very complex problem. The simplified system considered here is no exception. Some problems have not been considered, solutions of others have been only attempted and there are plenty of areas of future research among them the following:

i) The validity of the present work has not been justified conclusively in the case of fluidized beds of metal particles which, due to a layer of oxides on their surface which changes their effective thermophysical properties, introduce additional complications and hence provide the biggest scope for future research.

ii) Some more experimental data for the voidage variation in the vicinity of a constraining surface should be obtained, and further research would be also justified on improvement of the method of calculating the functions H(Z) and L(Z) which specify the property boundary layer.

iii) As demonstrated previously the heat transfer probe developed here is very versatile and can be used in many other heat transfer investigations as, for example, in determining the contribution of gas convection to the overall mechanism of heat transfer in high pressure gas fluidized systems.

iv) It has been shown that using the present set up, transient conduction is by far the most important mechanism of the bubble induced heat transfer in liquids. Since transient conduction is a function of the liquid thermal conductivity, as well as of liquid heat capacity which can be determined experimentally with little difficulties, some work has been done to use the present probe for rapid determination of thermal conductivities of liquids. It has been estimated that liquid conductivity can be determined with a probable error of about 7%. Since this application of the probe is of direct industrial use, some further research on this line is well justified.

The present work provides the first step in a more complicated investigation: to determine theoretically the mechanism of heat transfer in freely bubbling systems. The theories developed in this dissertation enable one to extend the validity of heat transfer solutions obtained in simpler gas-liquid systems into the regimes of aggregative gas fluidized beds.

	k	c_p	ρ
	W/mK	J/kgK	kg/m^3
helium	0.148	5200	0.165
air	0.026	1008	1.19
carbon dioxide	0.016	850	1.79
freon 12	0.0097	650	5.14
copper	380.0	385	8930.0
steel	45.0	480	7800.0
silica sand	1.87	860	2600.0
glass	0.85	765	2700.0
slag[21]	0.59	752	2720.0

Table 3.1: Thermophysical properties of solid particles and gases at 25°C.

k_E (W/mK)	helium	air	carbon dioxide	freon 12
copper	2.25	0.486	0.312	0.200
steel	1.51	0.374	0.245	0.159
silica sand	0.548	0.182	0.130	0.090
glass	0.363	0.139	0.103	0.0725
slag	0.300	0.122	0.090	0.065

Table 3.2: Calculated values of thermal conductivity of the emulsion phase for $\varepsilon_E = 0.41$. (Method of Kunii & Smith[43].)

	k	c_p	ρ	μ
	W/mK	J/kgK	kg/m^3	kg/ms
water	0.615	4180	1000	0.000895
n-heptane	0.140	2130	700	0.00042
50% aqueous solution of glycerol	0.420	3390	1125	0.0057

Table 5.1: Thermophysical properties of used liquids at 25°C.

	size range	mean diameter	k	c_p	ρ
	μm	μm	W/mK	J/kgK	kg/m^3
silica sand 1	75 - 90	82	1.87	860	2600
silica sand 2	125 - 180	150			
silica sand 3	250 - 300	274			
silica sand 4	500 - 600	548			
helium			0.148	5200	0.165
air			0.026	1008	1.19
argon			0.0177	520	1.63
carbon dioxide			0.016	850	1.79
freon 12			0.0097	650	5.14

Table 6.1: Thermophysical properties of solid particles and gases at 25°C.

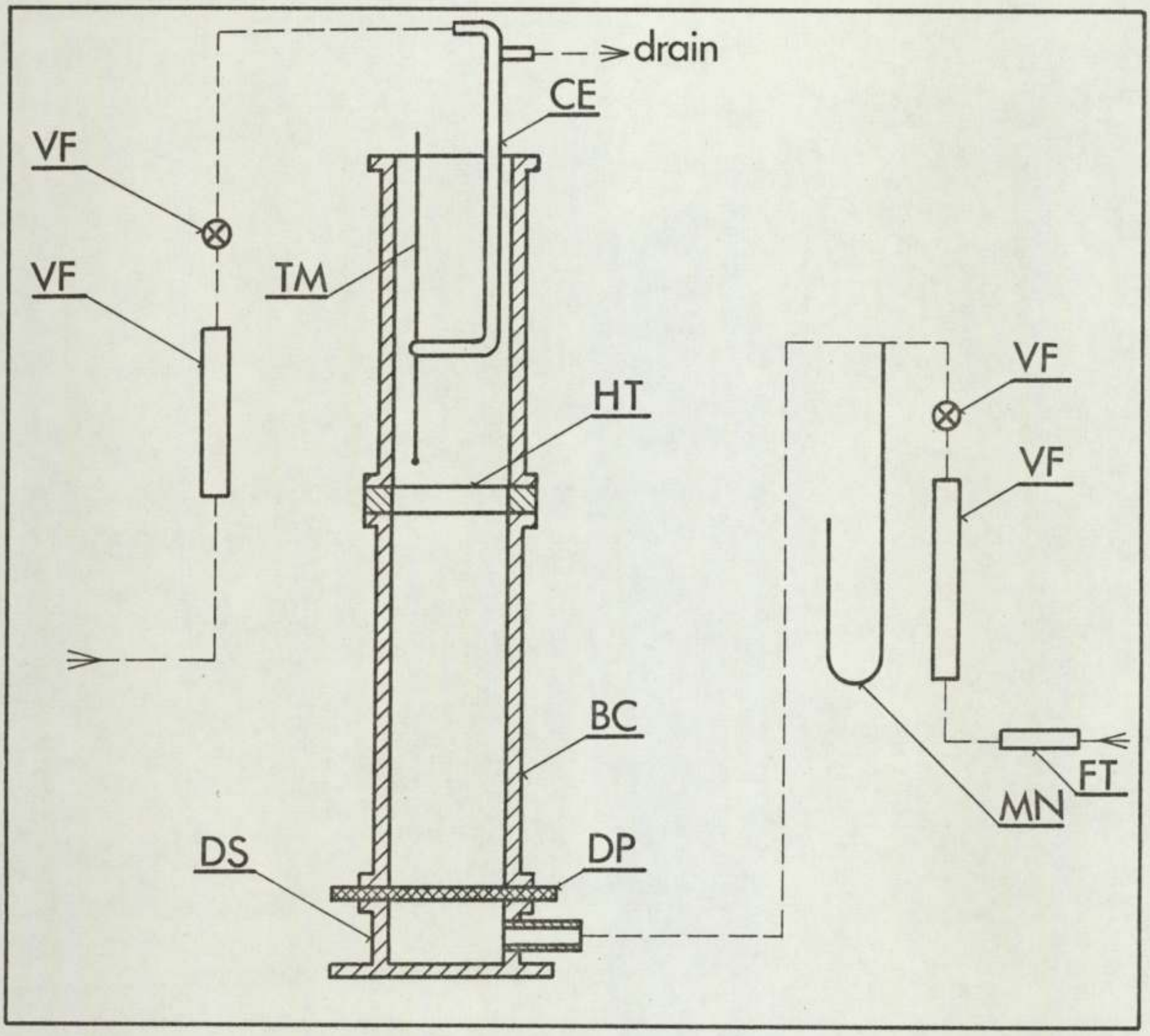

Fig. 2.1: Schematic diagram of the experimental apparatus used for the experimental investigation of heat transfer in two-phase gas-liquid systems.

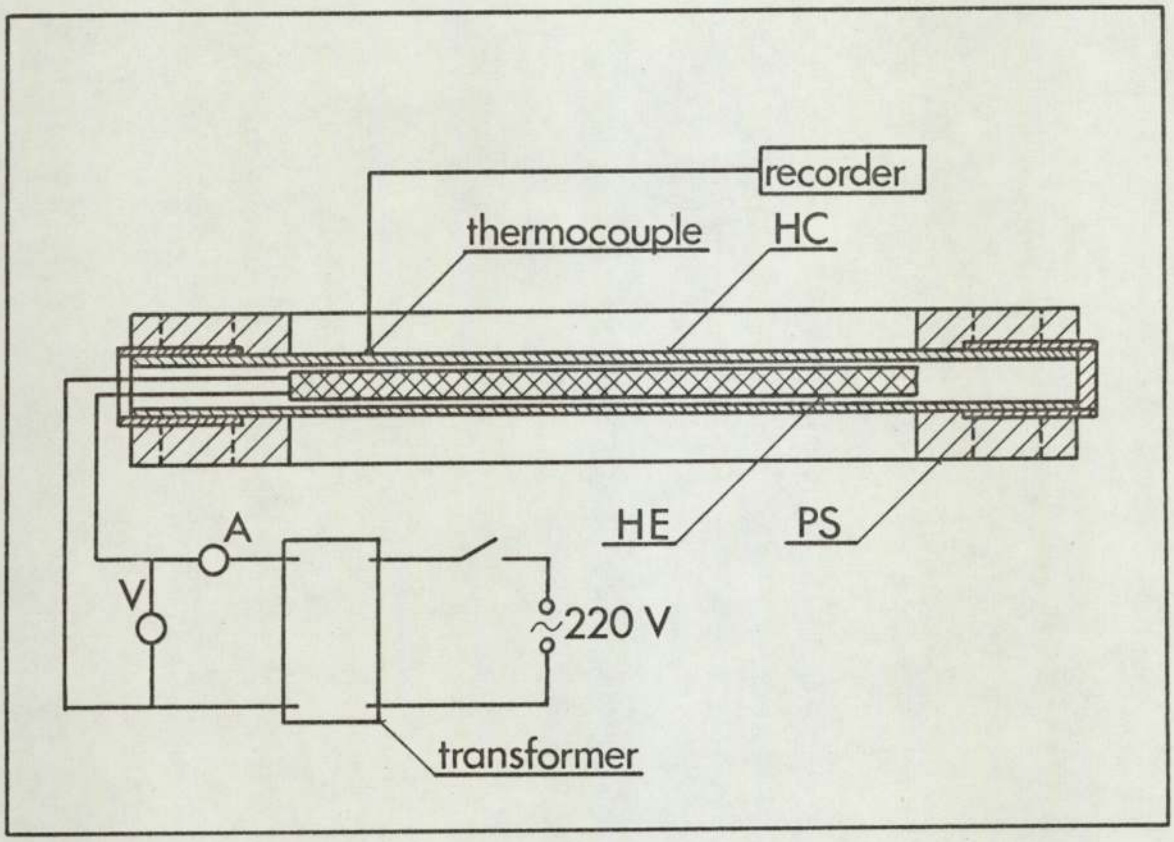

Fig. 2.2: Probe used in the investigation of heat transfer in two-phase gas-liquid systems.

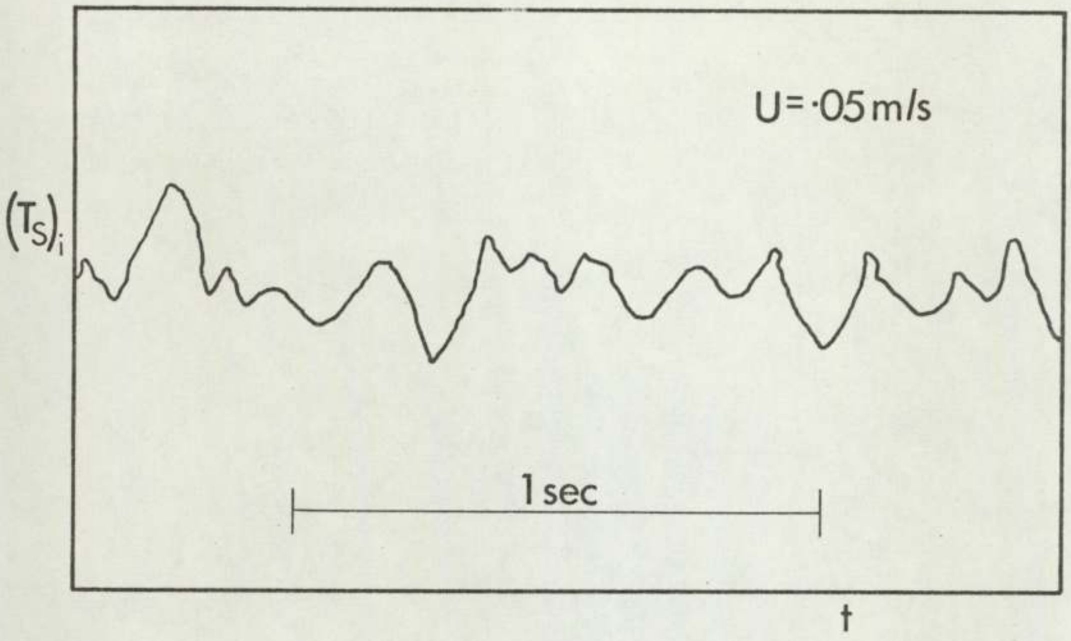

Fig. 2.3: A plot of a typical variation of the instantaneous surface temperature of the probe with time in a two-phase air-water system.

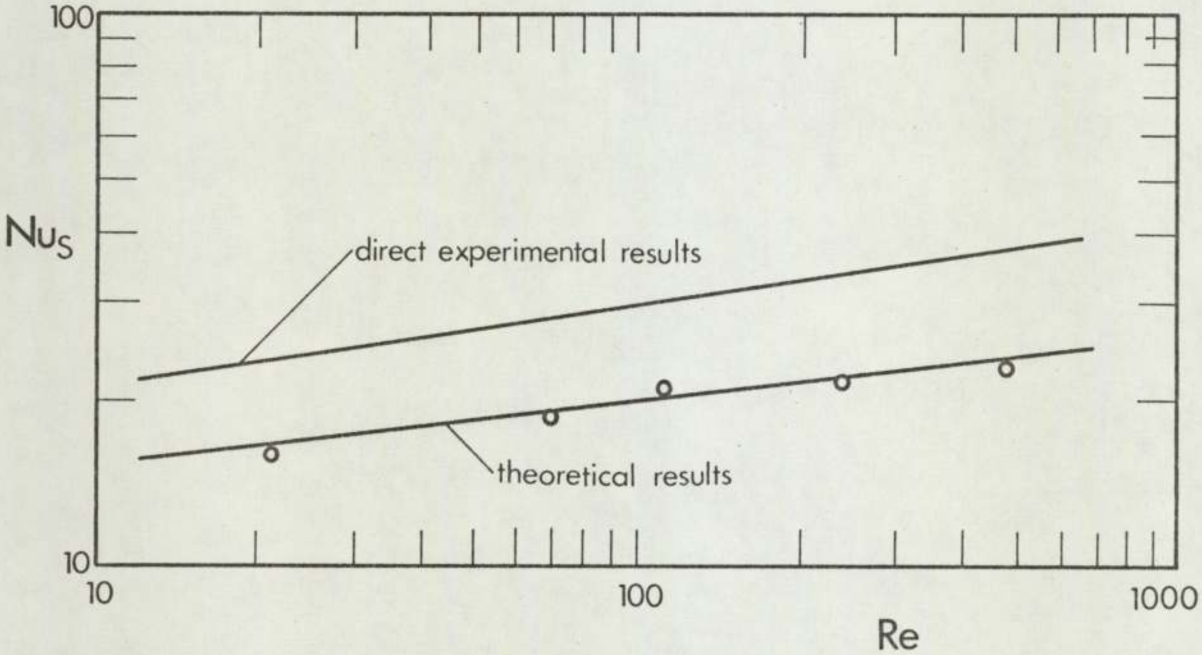

Fig. 2.4: Comparison of experimental data with the theoretical result for the time-mean heat transfer in a two-phase air-water system.

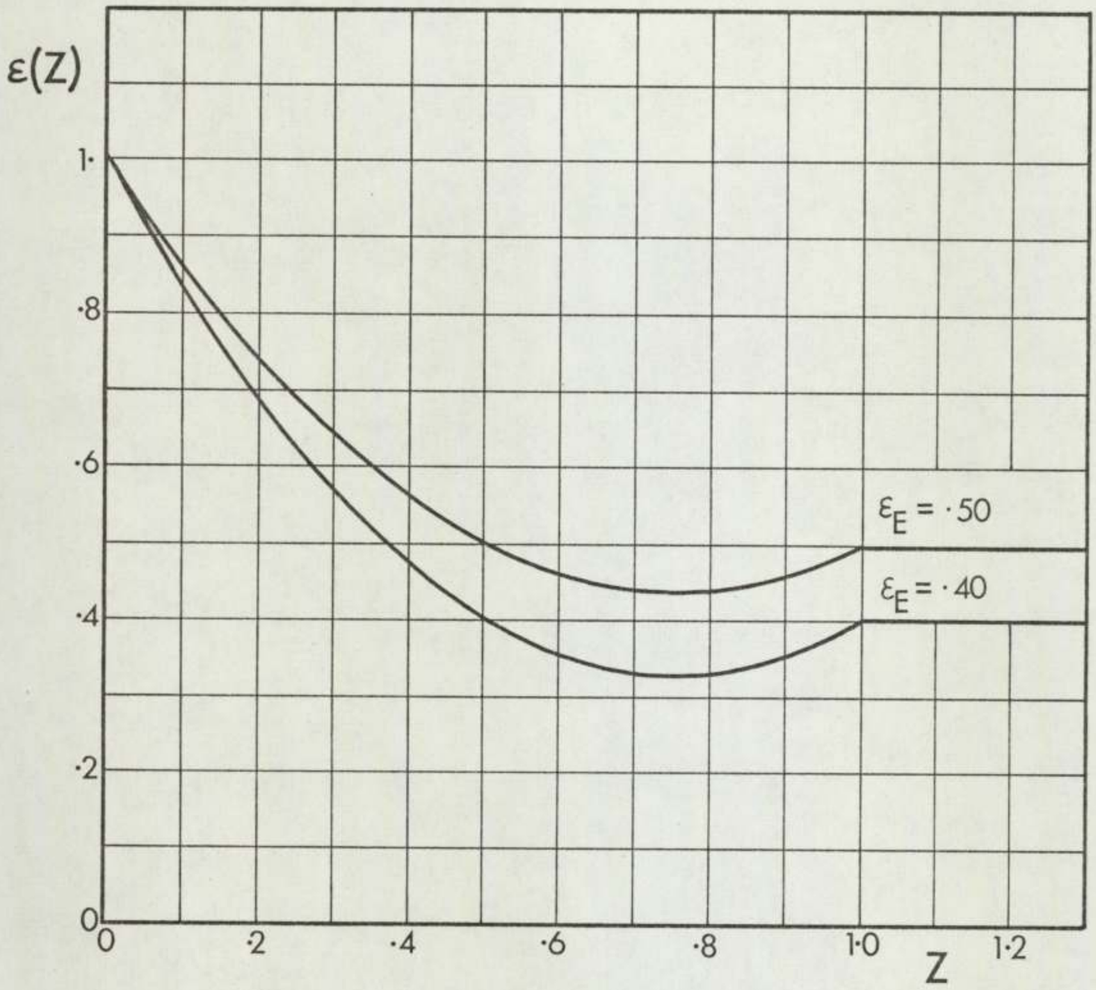

Fig. 3.1: Variation of the emulsion phase voidage in the vicinity of a flat surface.

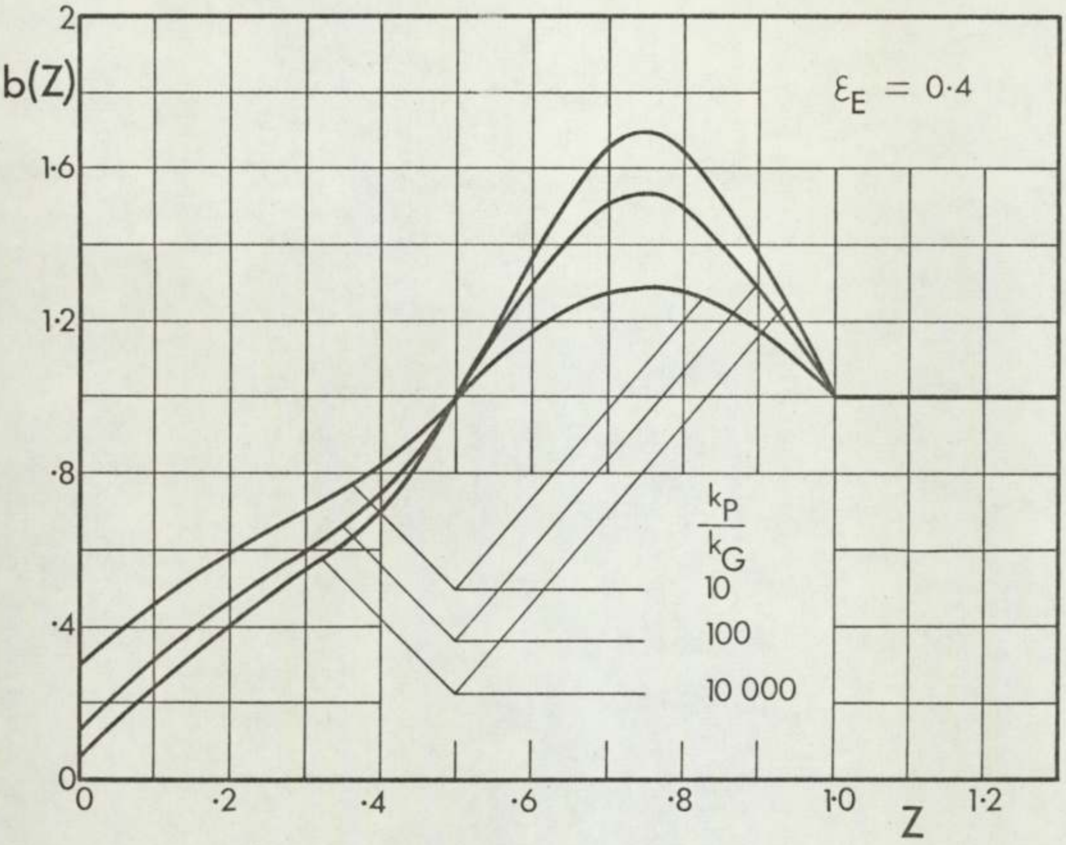

Fig. 3.2: Variation of the dimensionless conductivity b(Z) with Z for emulsion phase voidage $\varepsilon_E = 0.40$.

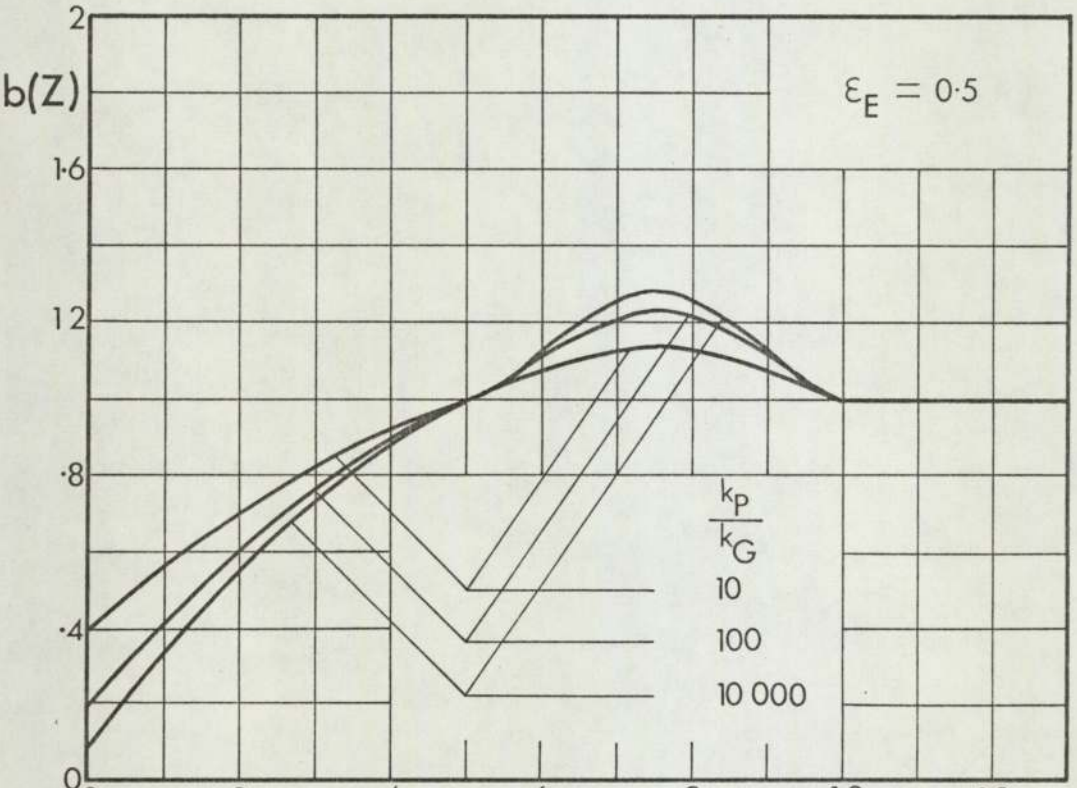

Fig. 3.3: Variation of the dimensionless conductivity b(Z) with Z for emulsion phase voidage $\varepsilon_E = 0.50$.

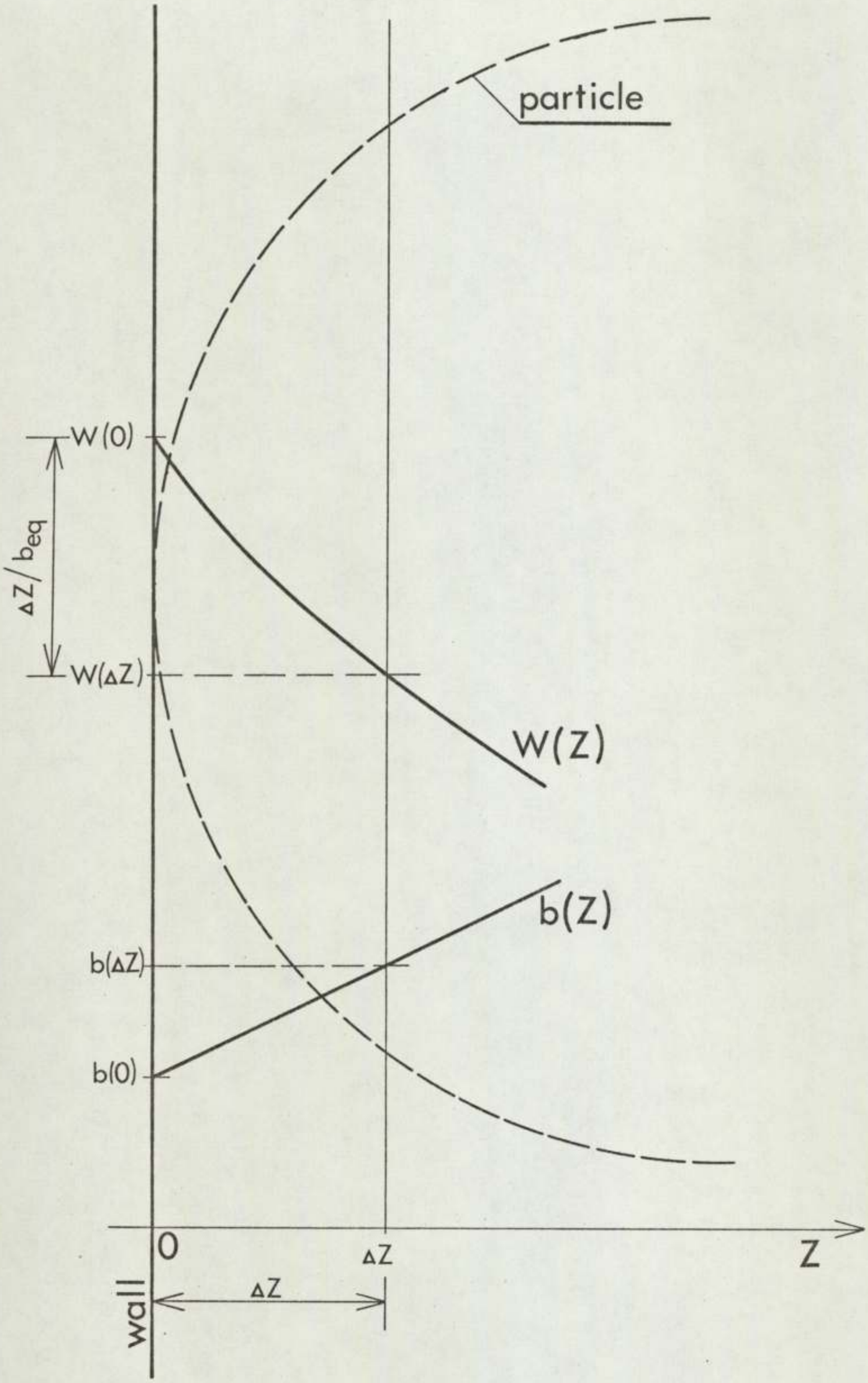

Fig. 3.4: Considerations for deriving b_{eq} used in the numerical calculations.

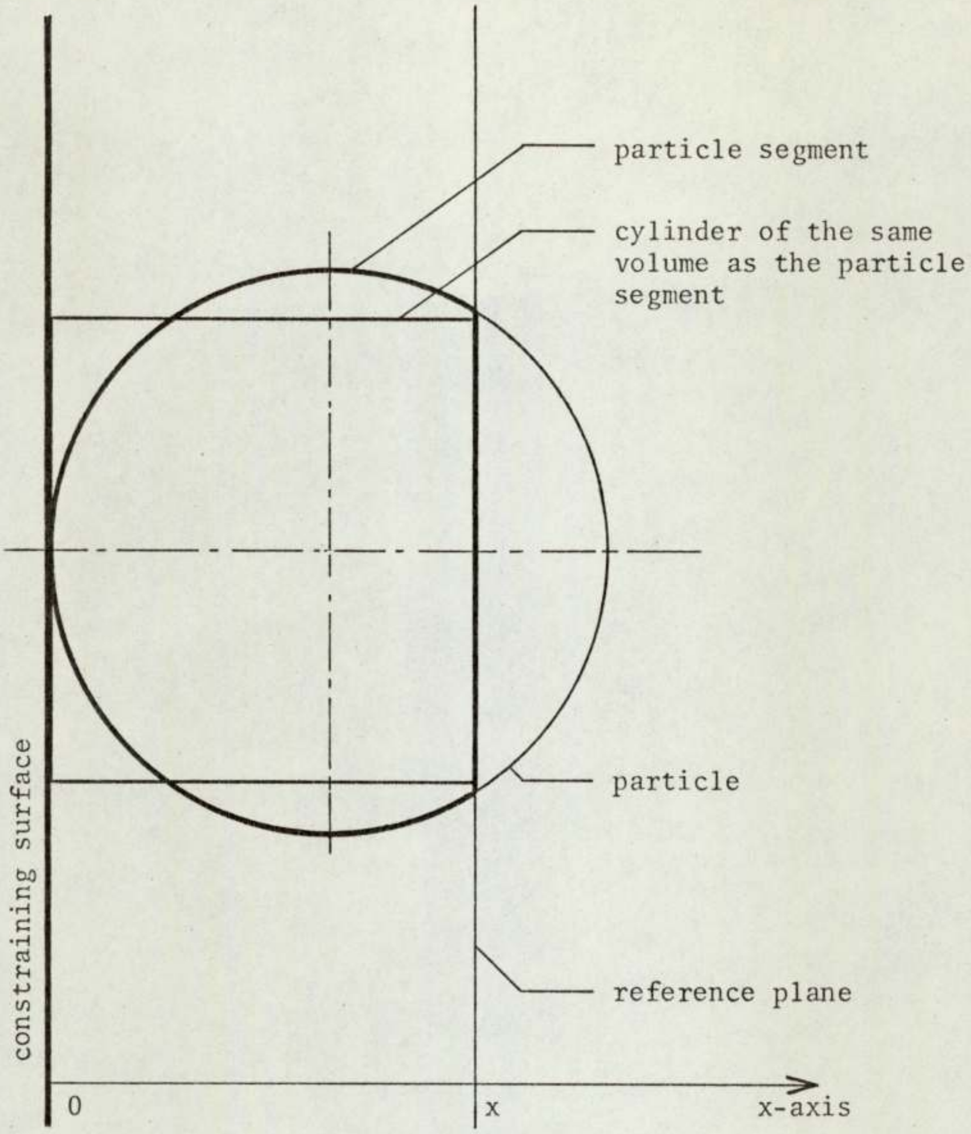

Fig. 3.4a: Considerations for describing the voidage distribution in the vicinity of a constraining surface.

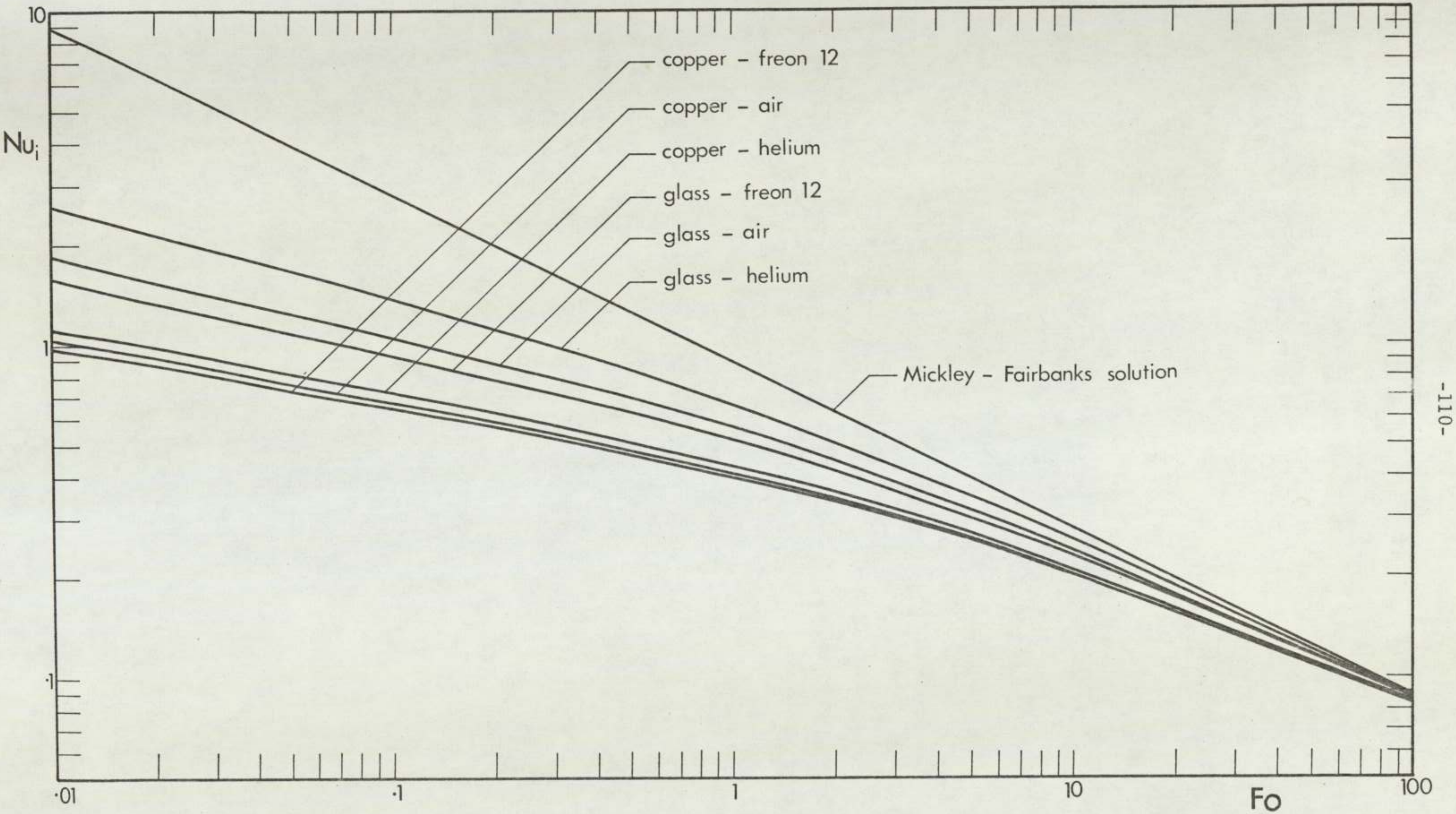

<u>Fig. 3.5:</u> A plot of the instantaneous Nusselt number as a function of the instantaneous Fourier number. (Emulsion phase voidage is assumed to be $\varepsilon_E = 0.41$.)

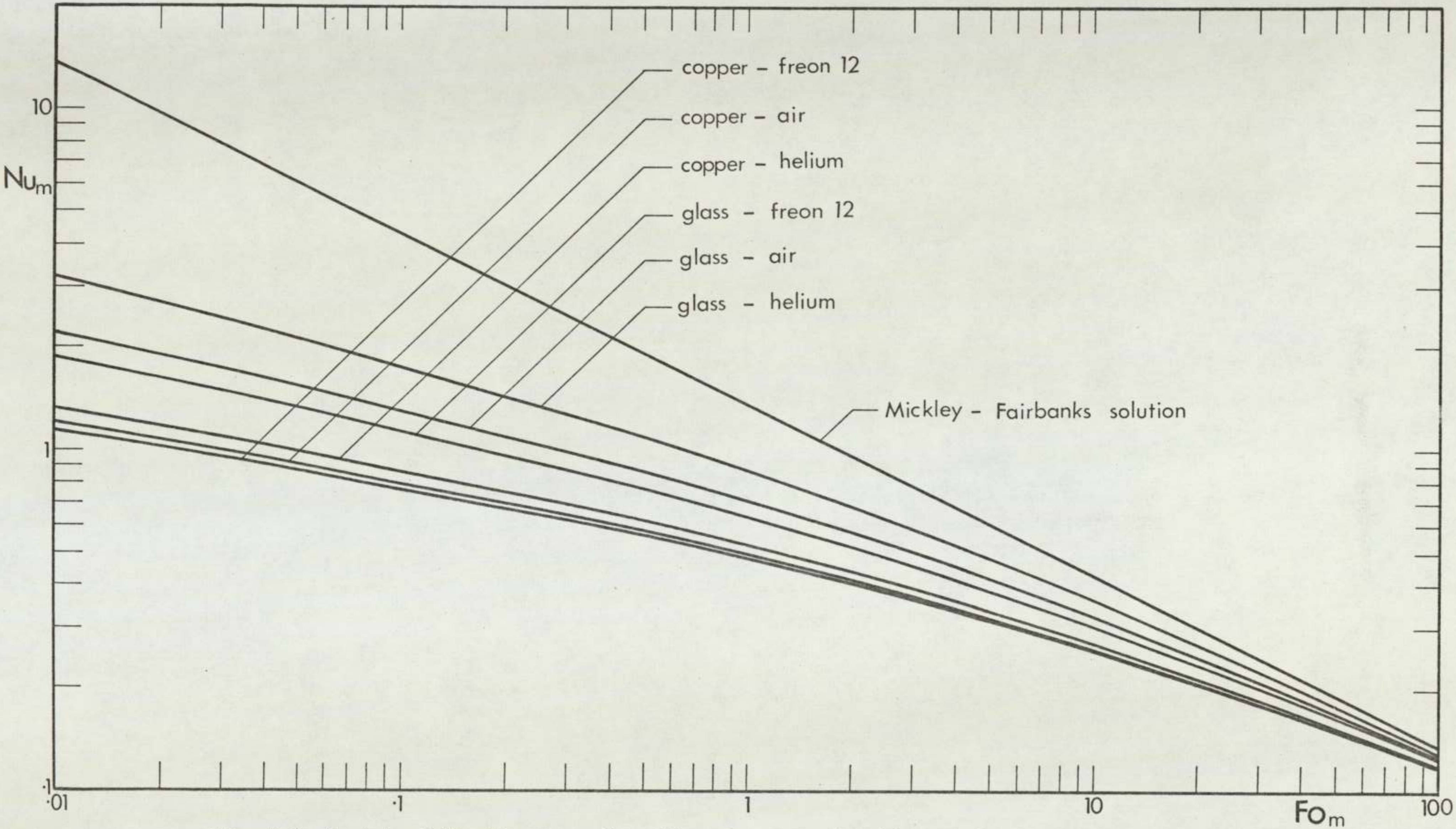

Fig. 3.6: A plot of the time-mean Nusselt number as a function of the time-mean Fourier number. (Emulsion phase voidage is assumed to be $\varepsilon_E = 0.41$.)

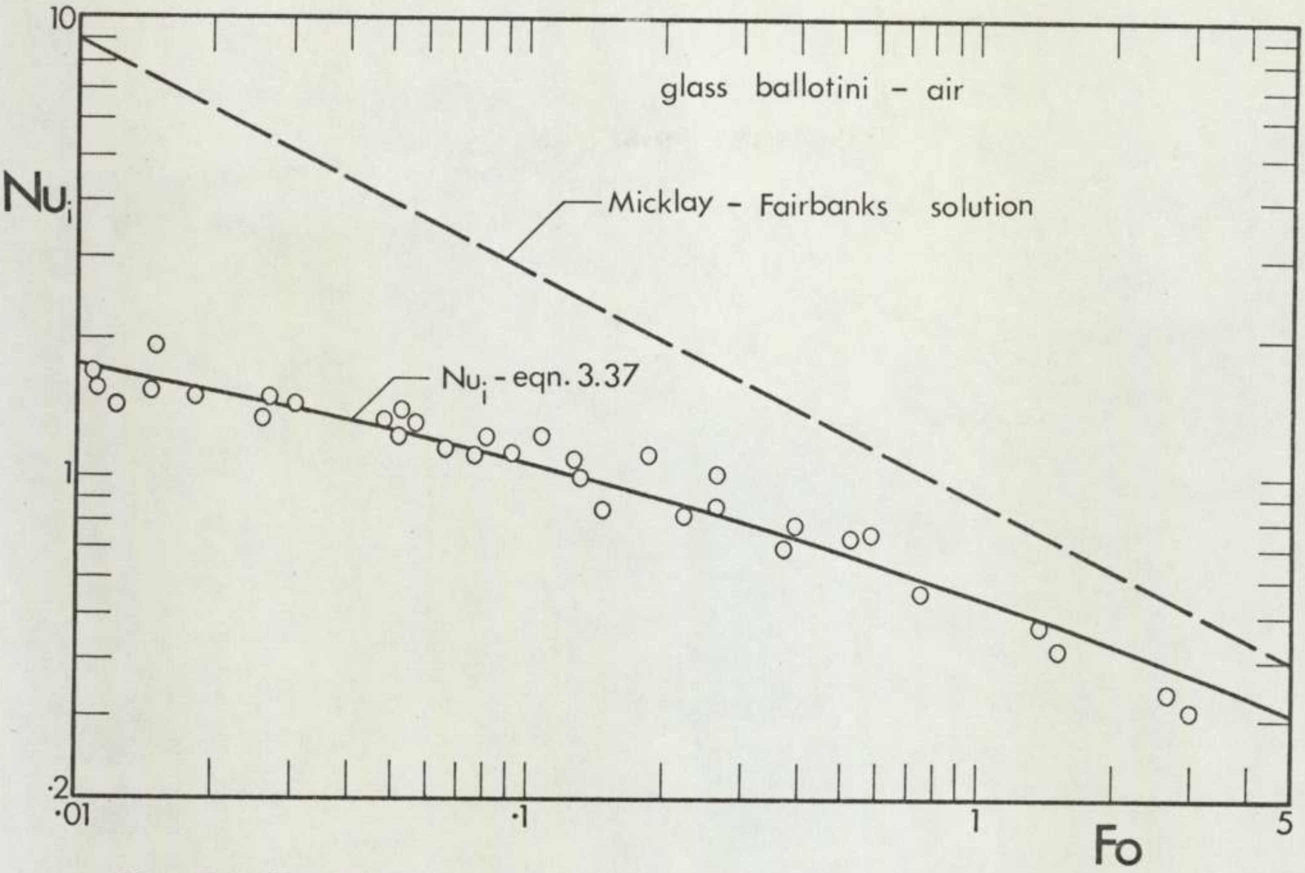

Fig. 3.7: Instantaneous heat transfer in the system glass ballotini-air. Comparison of the present theory with experimental data of Antonishin et al[2].

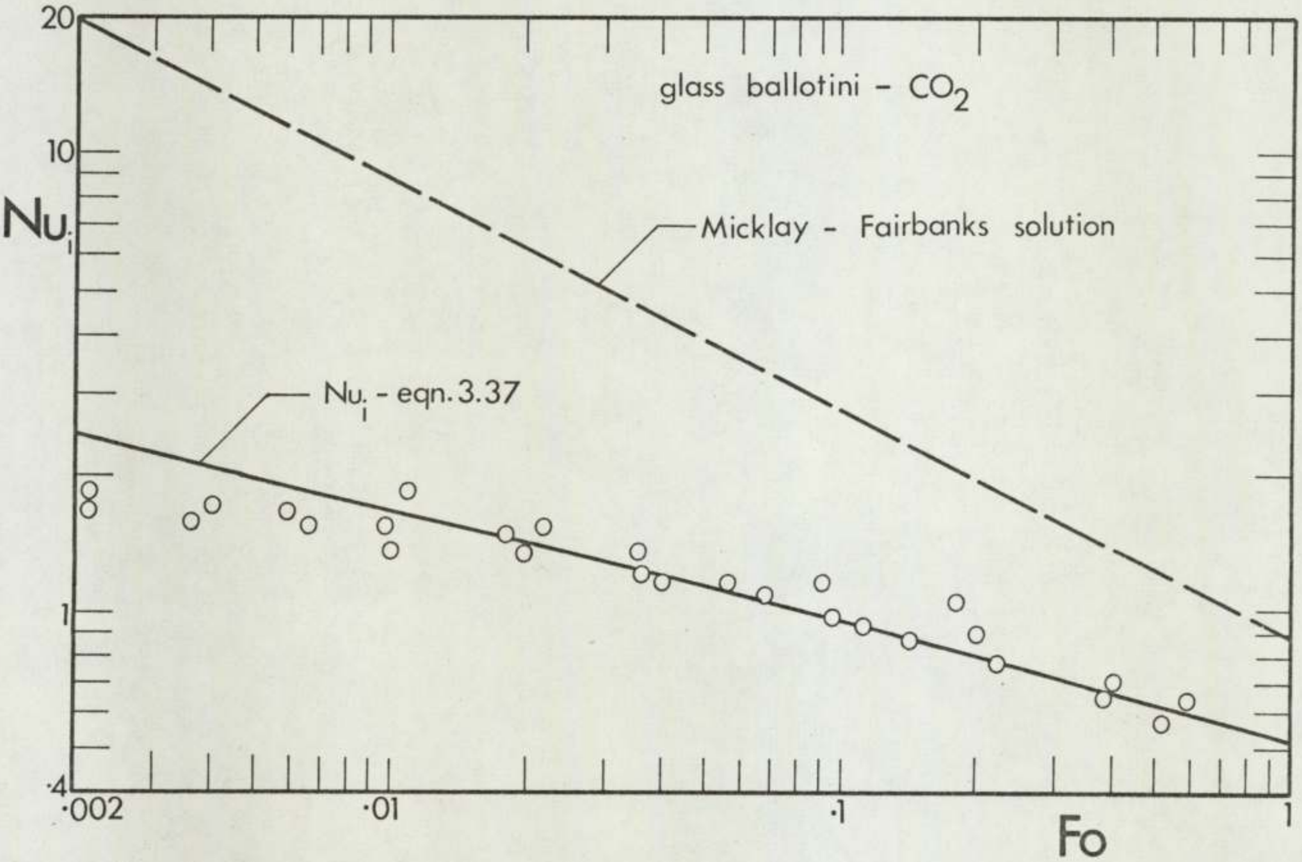

Fig. 3.8: Instantaneous heat transfer in the system glass ballotini-carbon dioxide. Comparison of the present theory with experimental data of Antonishin et al[2].

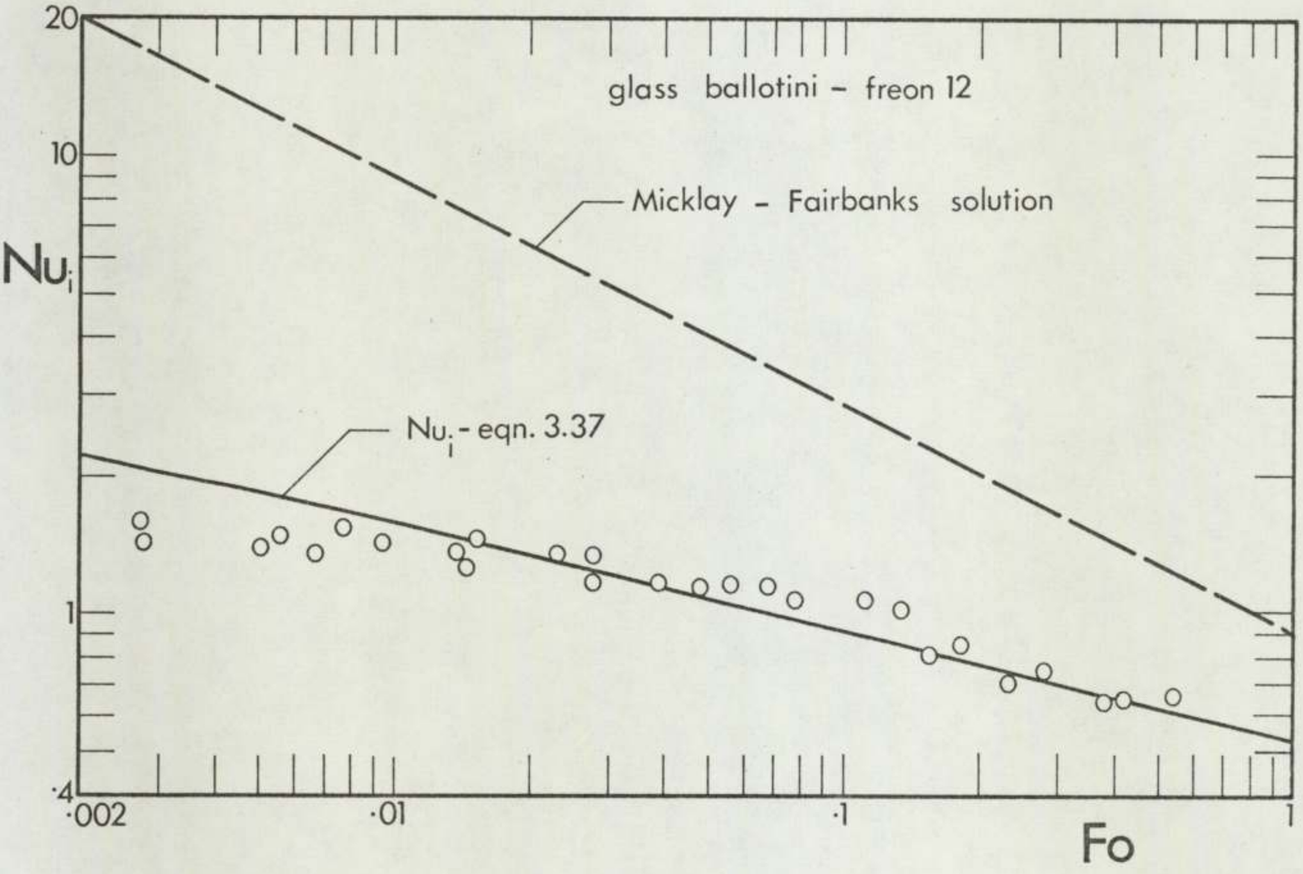

Fig. 3.9: Instantaneous heat transfer in the system glass ballotini-freon 12. Comparison of the present theory with experimental data of Antonishin et al[2].

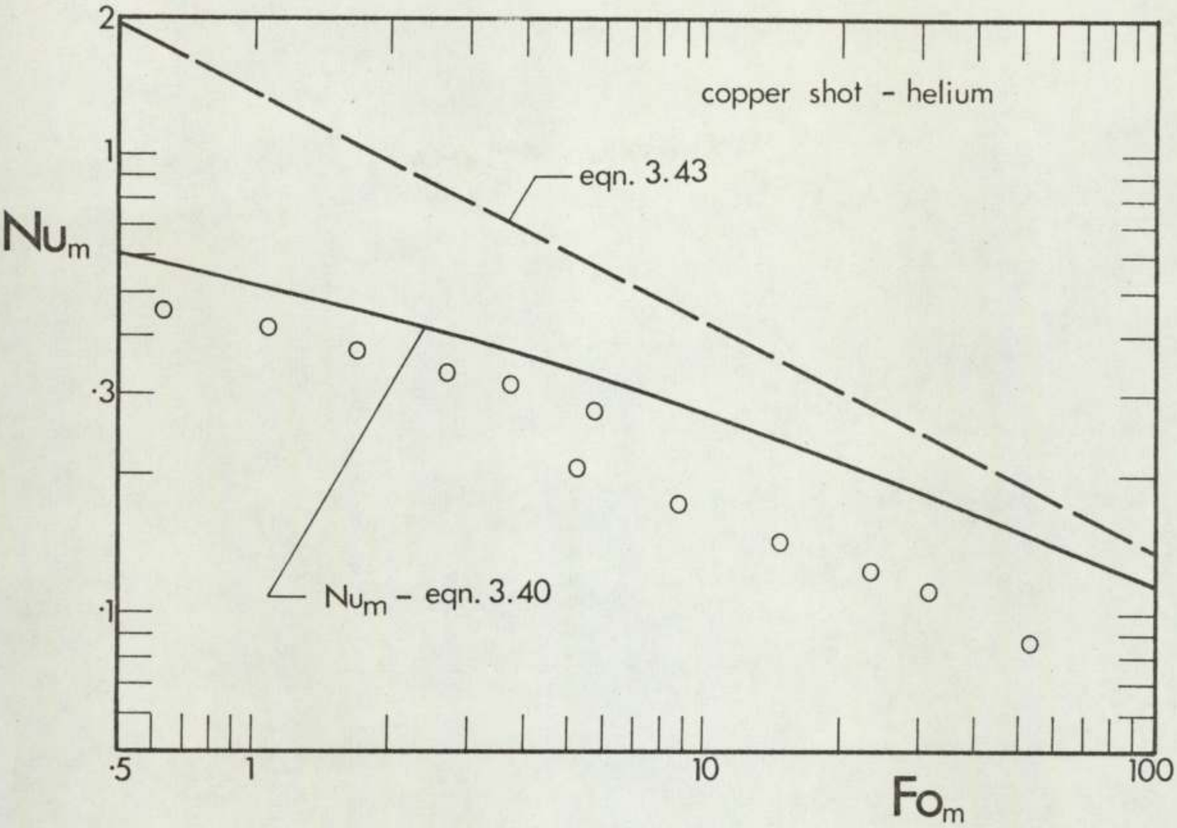

Fig. 3.10: Time-mean heat transfer in the system copper shot-helium. Comparison of the present theory with experimental data of Hampshire[30].

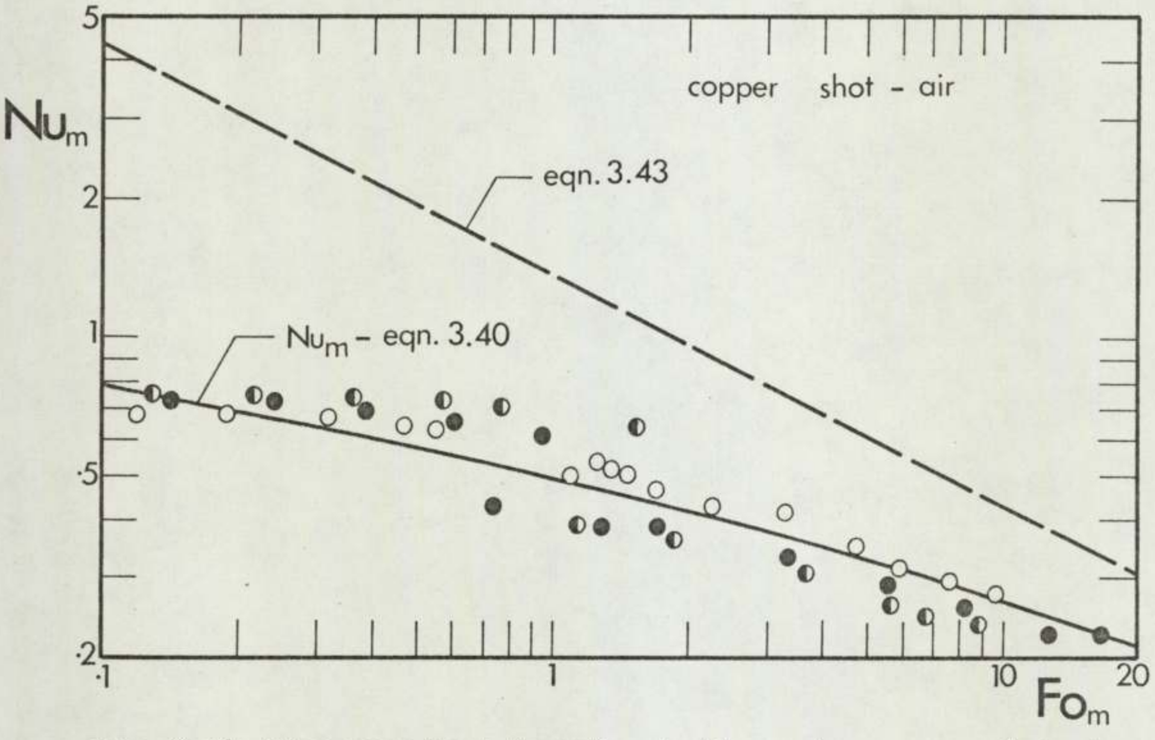

Fig. 3.11: Time-mean heat transfer in the system copper shot-air. Comparison of the present theory with experimental data of Butt[12] - o, Desai[20] - •, and Hampshire[30] - ◐.

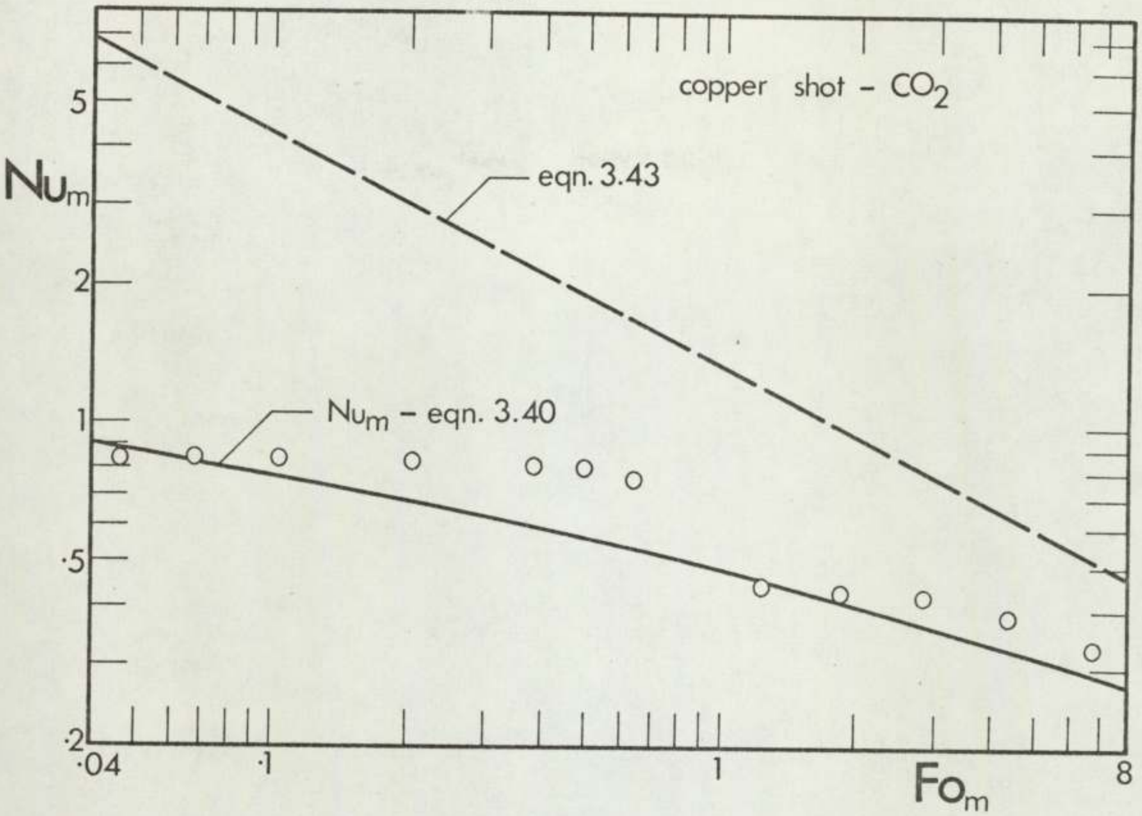

Fig. 3.12: Time-mean heat transfer in the system copper shot-carbon dioxide. Comparison of the present theory with experimental data of Desai[20].

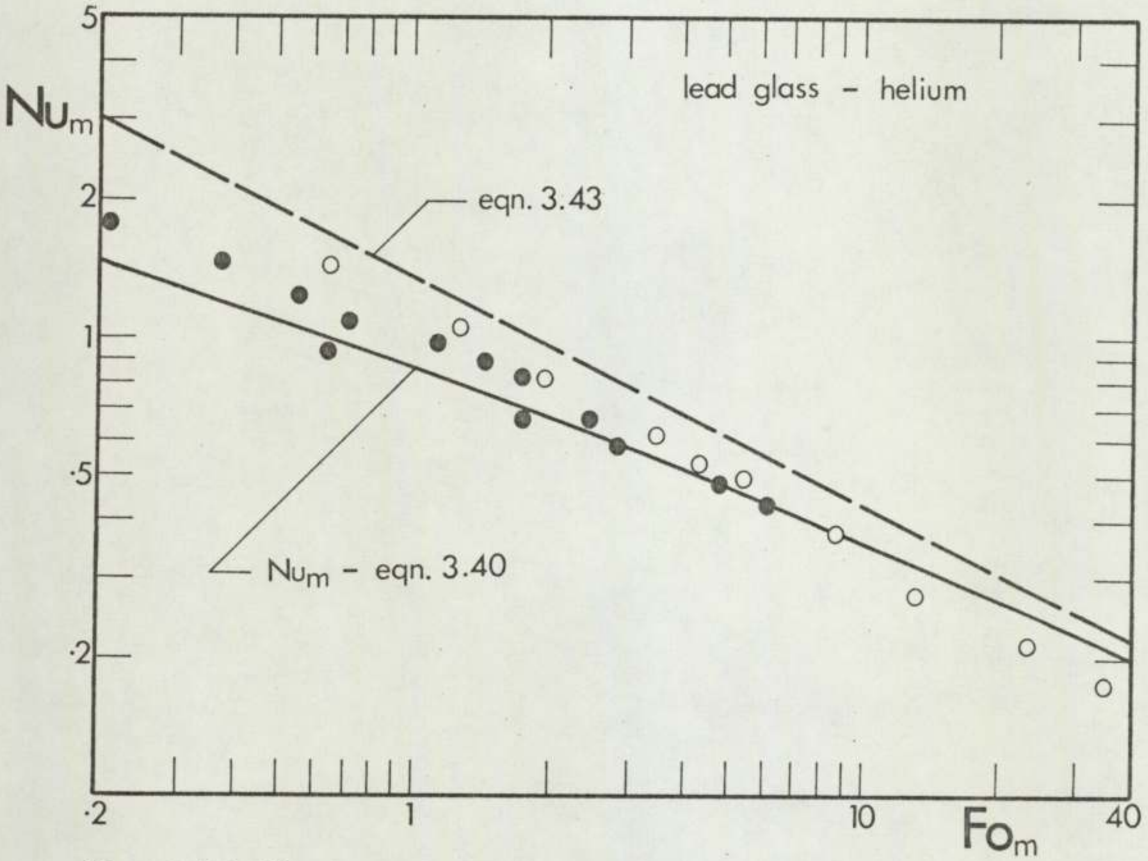

Fig. 3.13: Time-mean heat transfer in the system glass ballotini-helium. Comparison of the present theory with experimental data of Hampshire[30] - •, and Harakas & Beatty[31] - o.

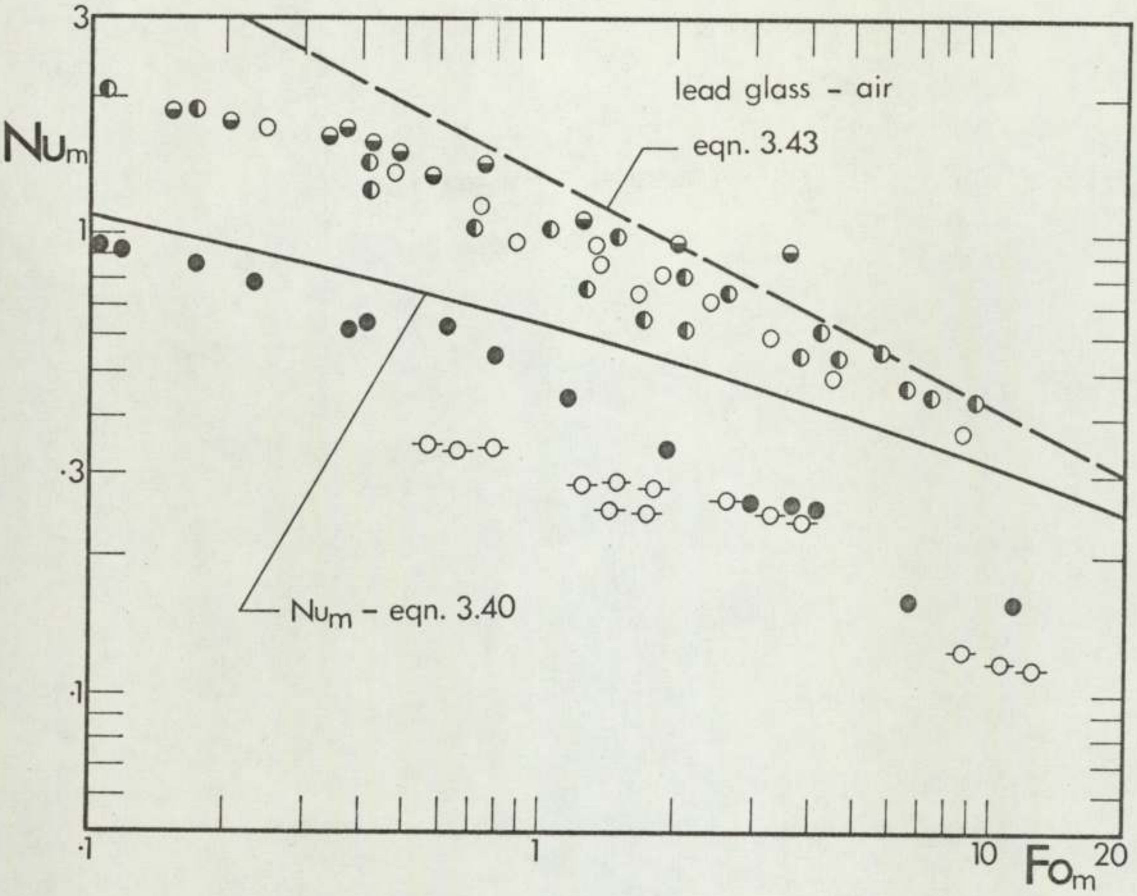

Fig. 3.14: Time-mean heat transfer in the system glass ballotini-air. Comparison of the present theory with experimental data of Butt[12] - ◐, Cain[13] - ●, Hampshire[30] - ◒, Harakas & Beatty[31] - o, and Williams & Smith[60] - -o-.

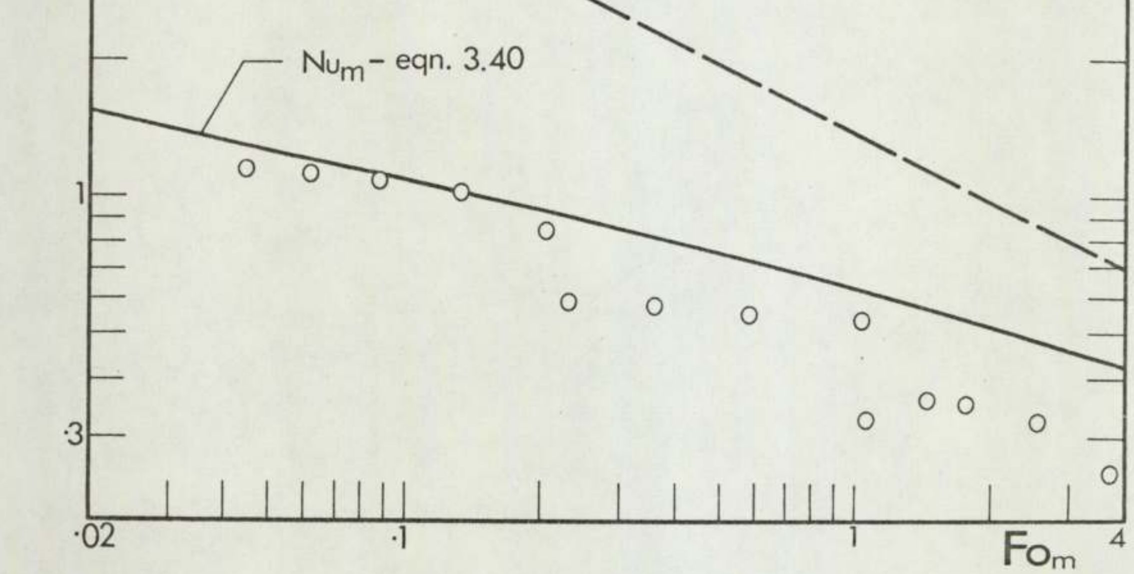

Fig. 3.15: Time-mean heat transfer in the system glass ballotini-freon 12. Comparison of the present theory with experimental data of Cain[13].

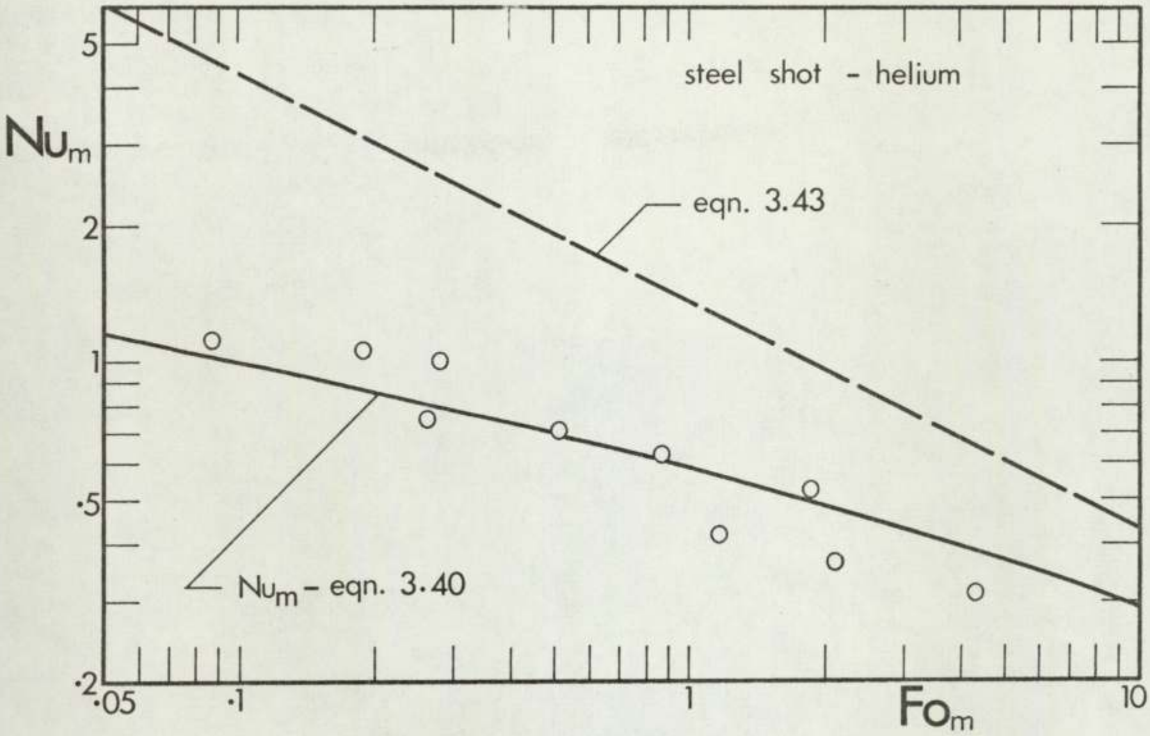

Fig. 3.16: Time-mean heat transfer in the system steel shot-helium. Comparison of the present theory with experimental data of Hampshire[30].

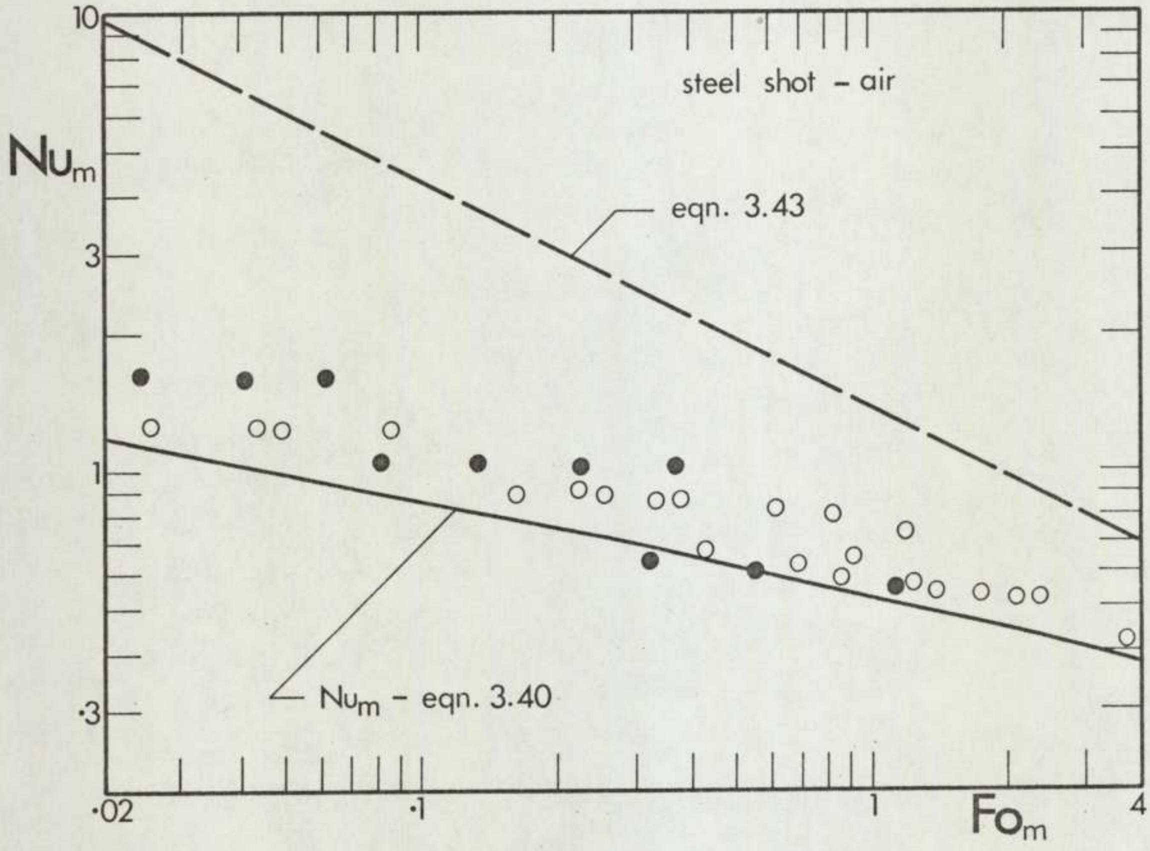

Fig. 3.17: Time-mean heat transfer in the system steel shot-air. Comparison of the present theory with experimental data of Butt[12] - o, and Hampshire[30] - •.

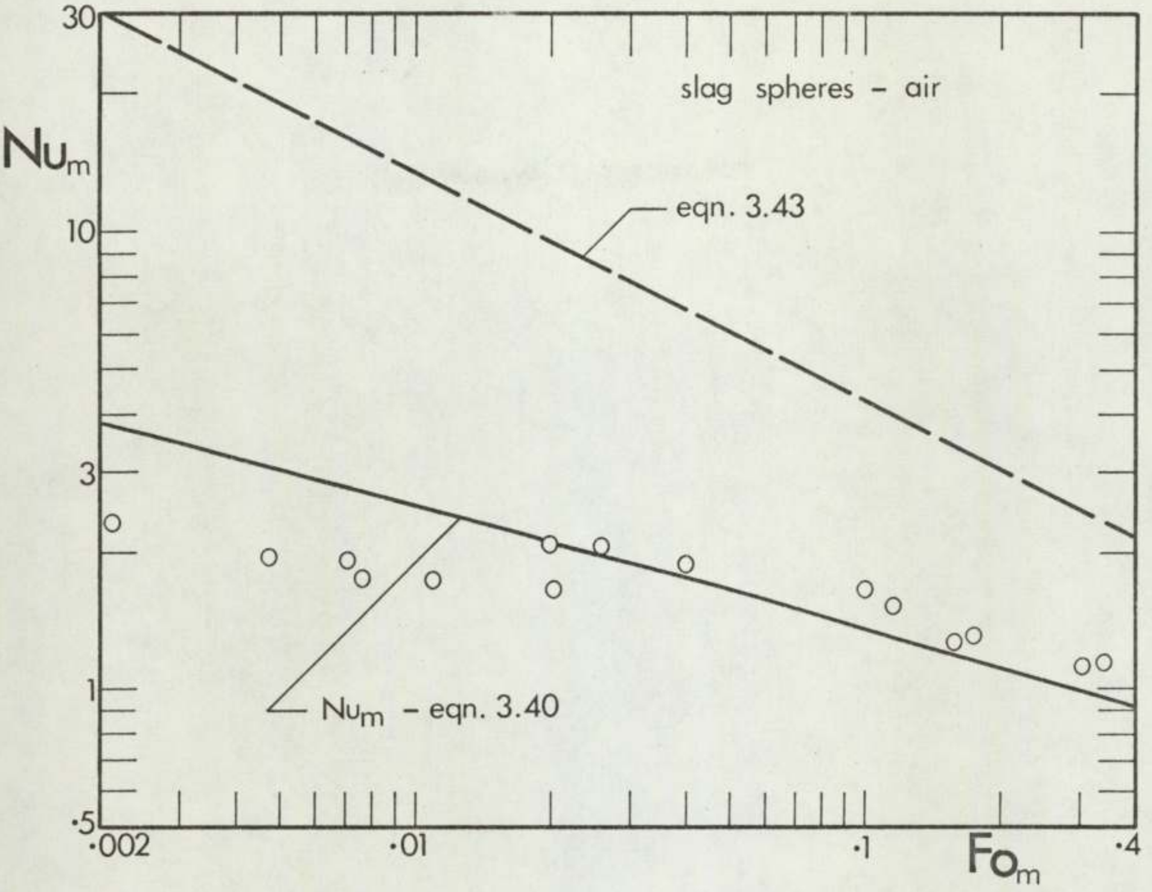

Fig. 3.18: Time-mean heat transfer in the system slag spheres-air. Comparison of the present theory with experimental data of Dunsky et al[21].

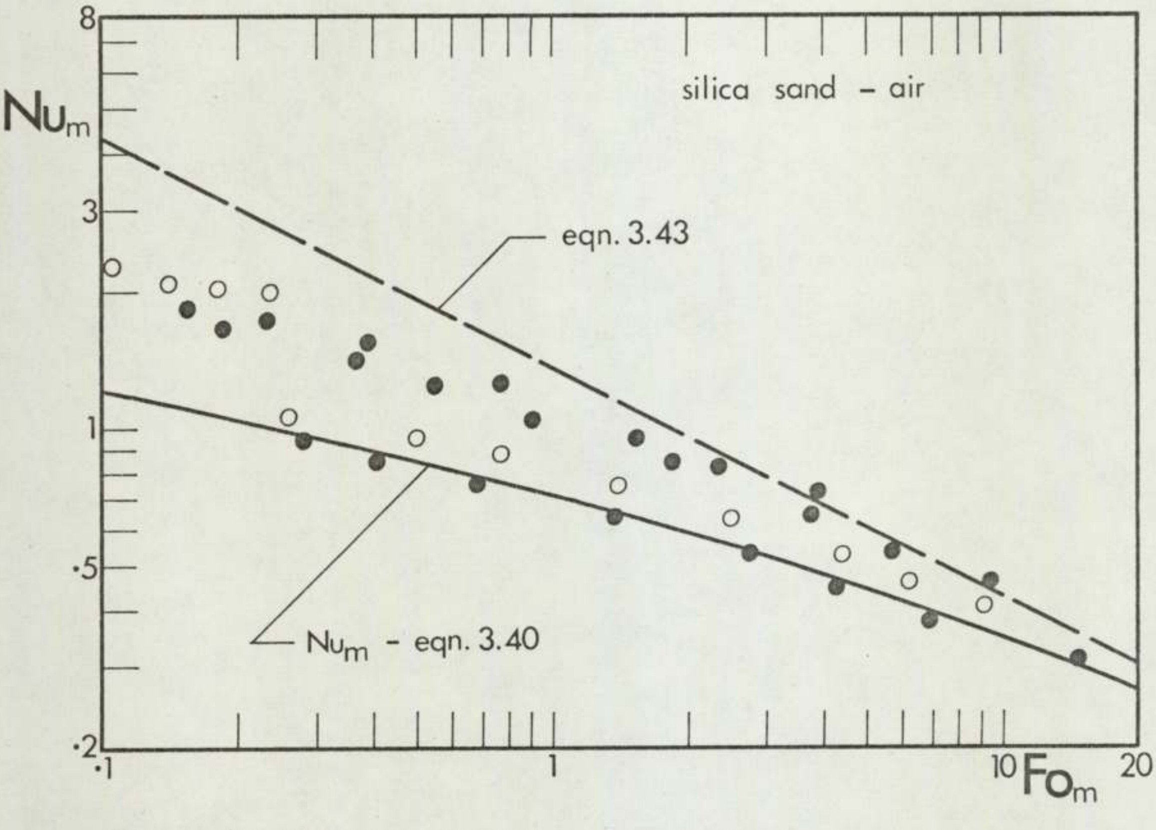

Fig. 3.19: Time-mean heat transfer in the system silica sand-air. Comparison of the present theory with experimental data of Desai[20] - o, and Ernst[24] - •.

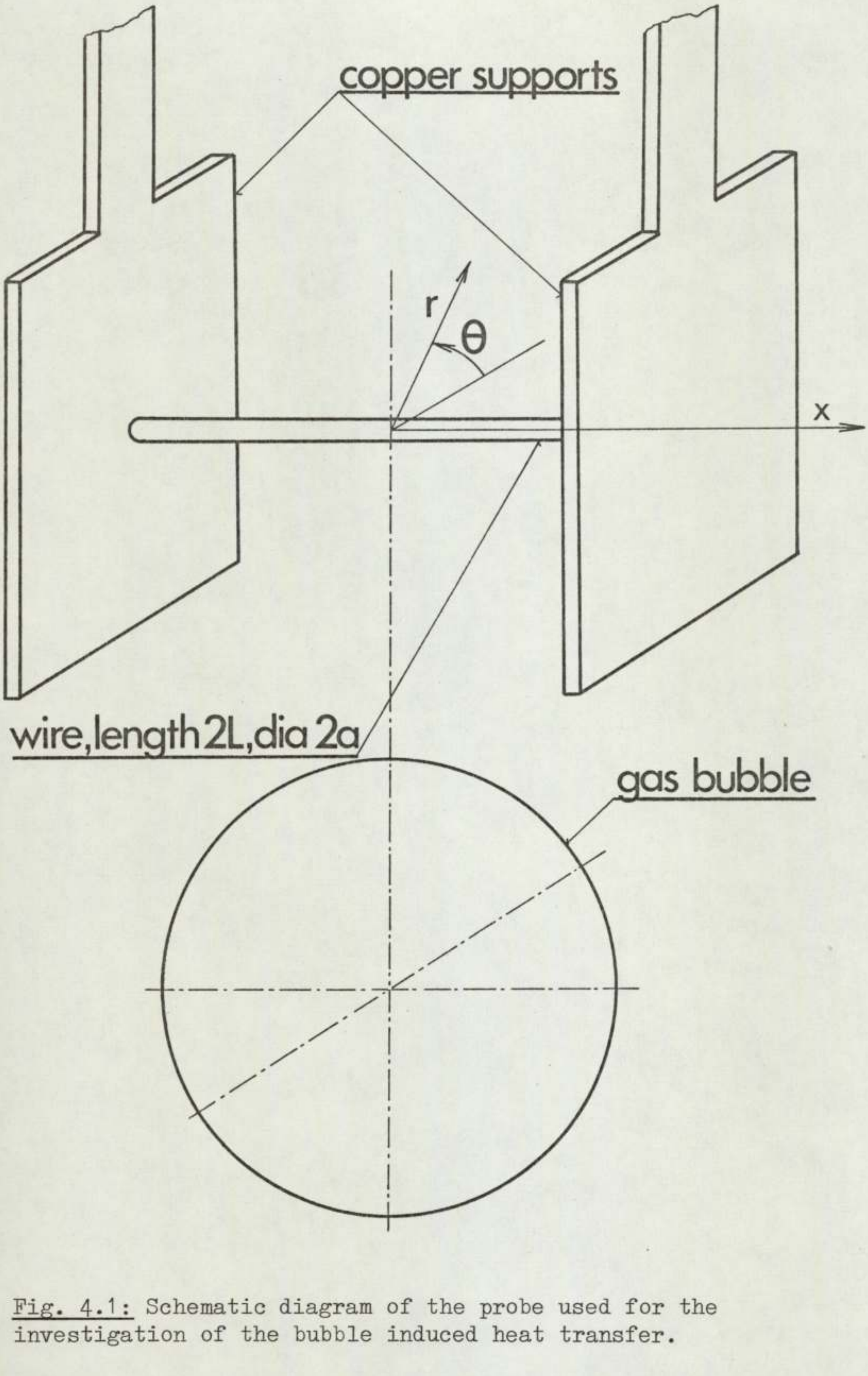

Fig. 4.1: Schematic diagram of the probe used for the investigation of the bubble induced heat transfer.

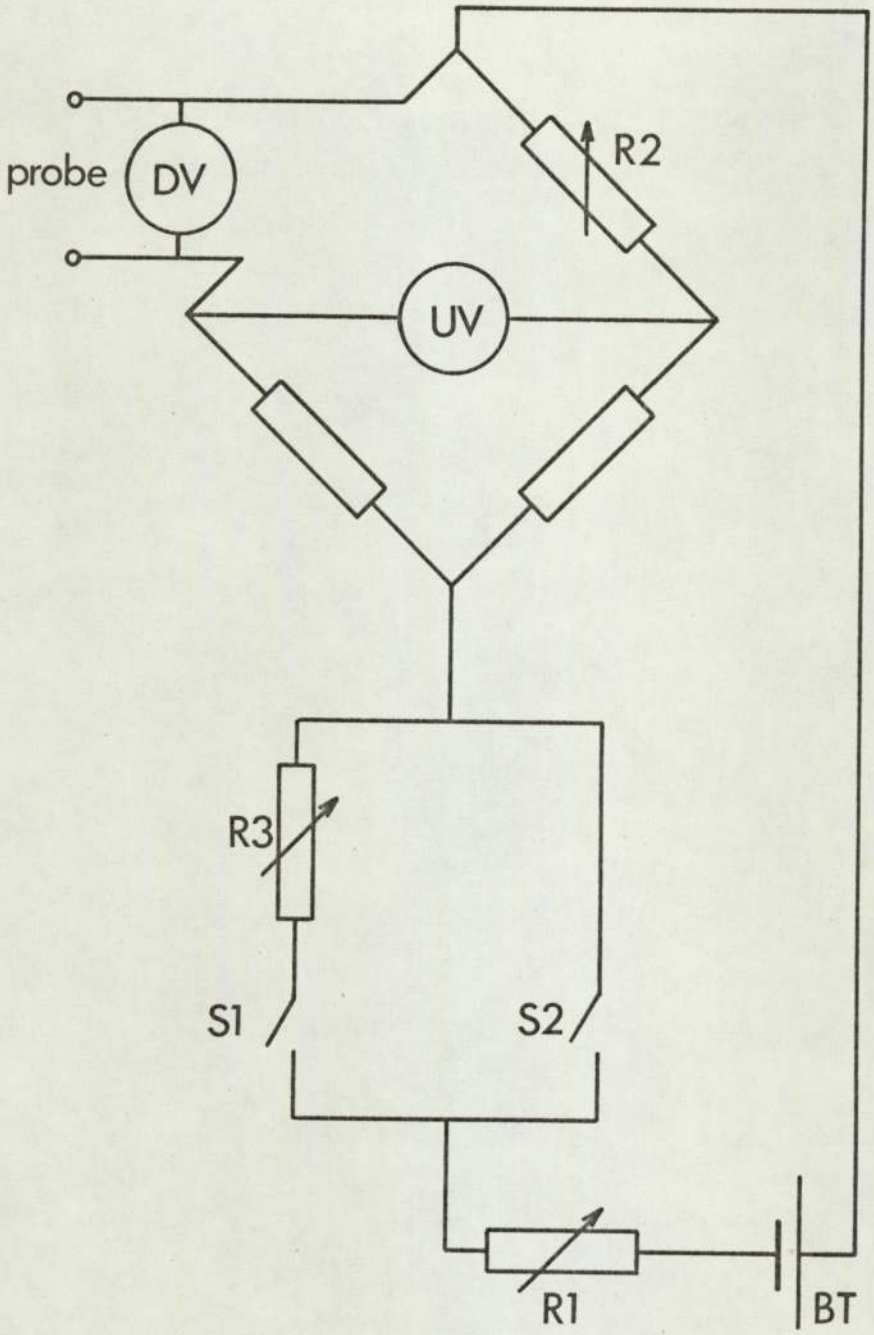

Fig. 4.2: Supporting bridge and instrumentation of the heat transfer probe.

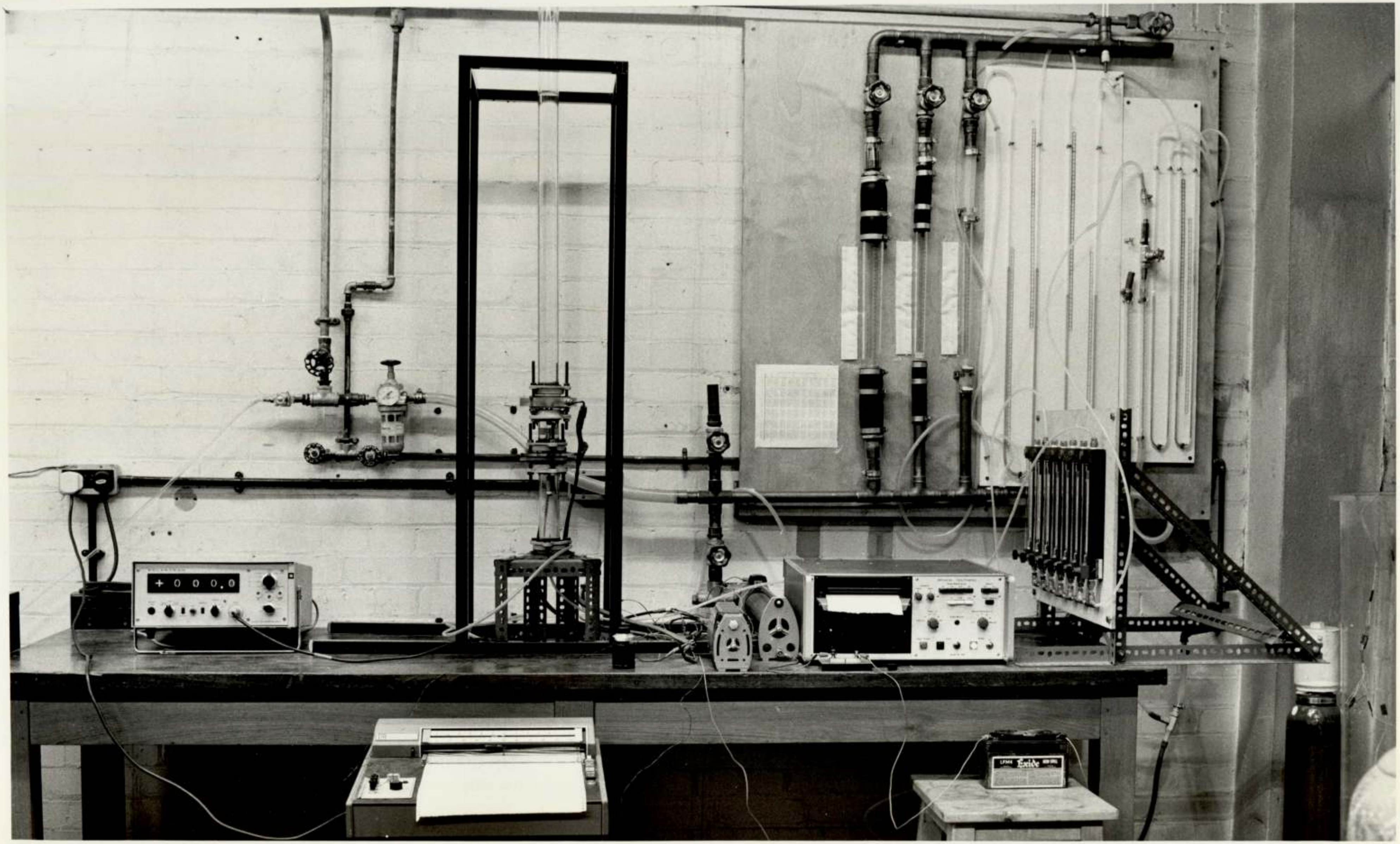

Fig. 5.1: Photograph of the experimental apparatus.

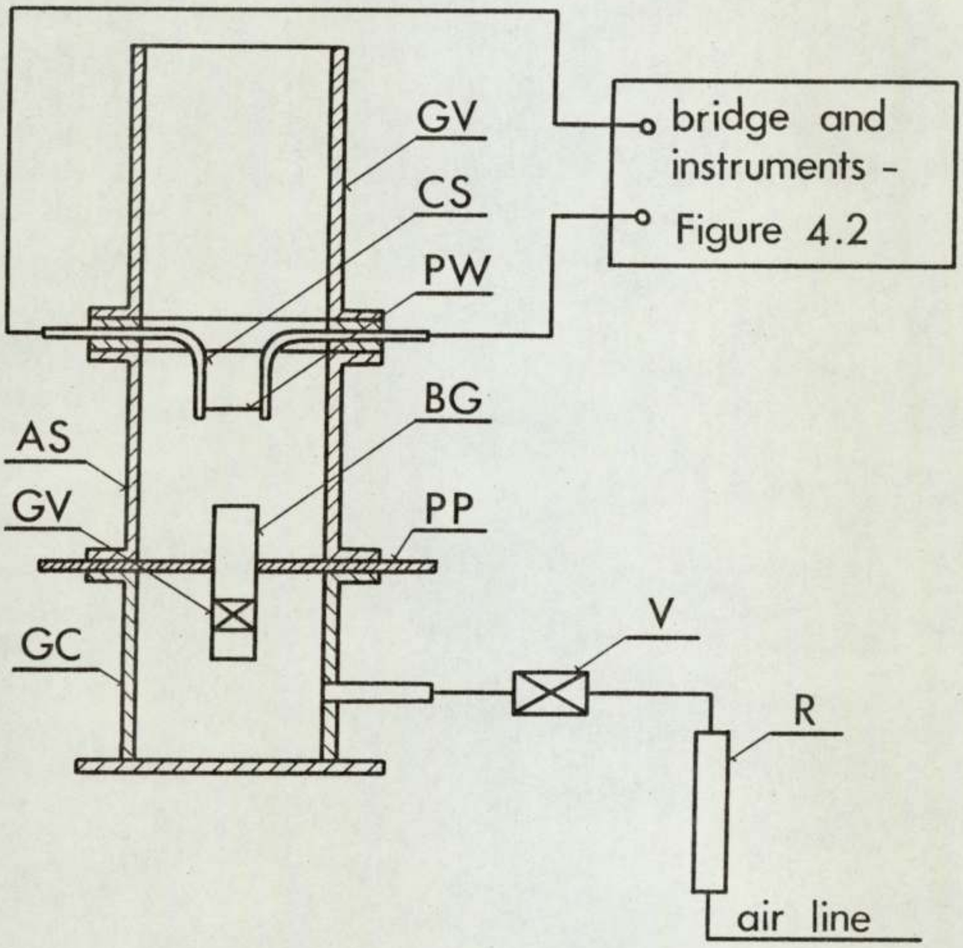

Fig. 5.2: Line diagram of the experimental apparatus.

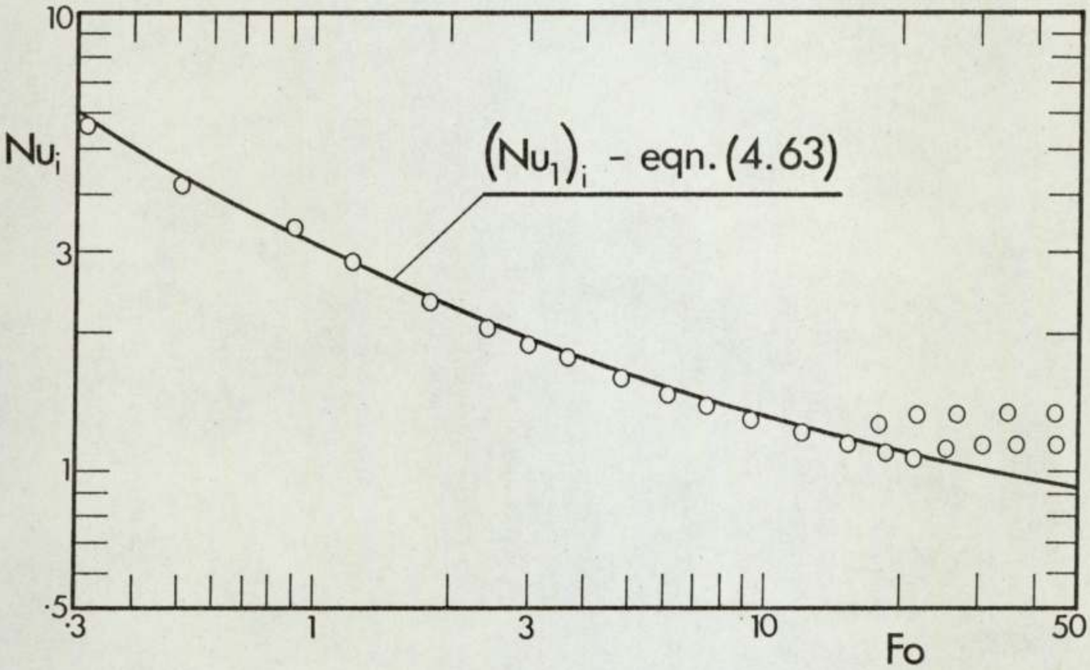

Fig. 5.3: Response of the probe wire, placed in stationary water, to a step heating input ($a = 152.5$ µm, $A = 113$, $T_\infty = 20^\circ C$).

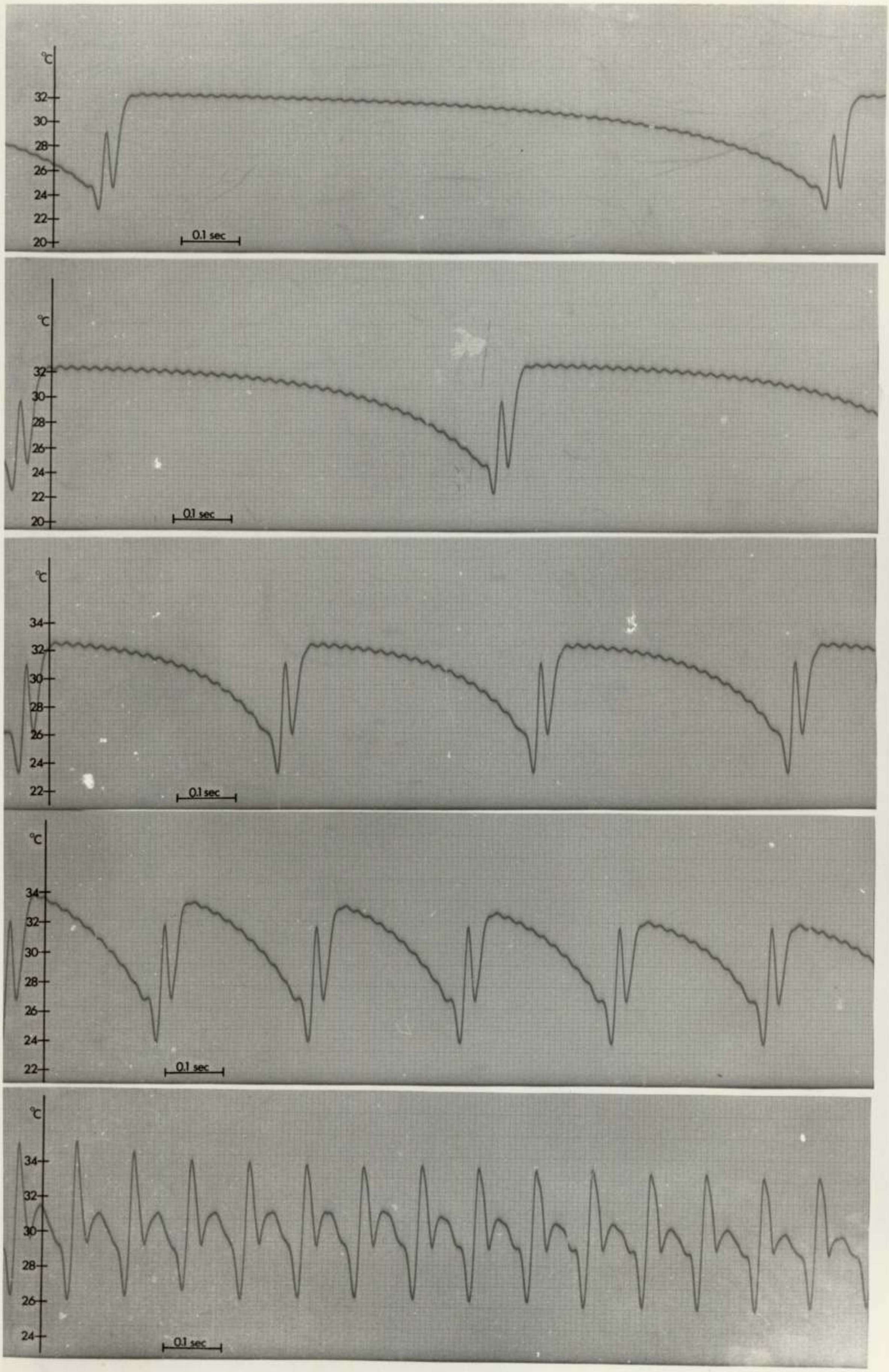

Fig. 5.4: Variation of the instantaneous average wire temperature with time (water, $a = 20.6\ \mu m$, $A = 108$, $T_\infty = 20^{o}C$, $\xi = 1.0$ to 1.1). From top to bottom: $f = 0.8$, 1.2, 2.3, 3.8, and 10.4 1/sec.

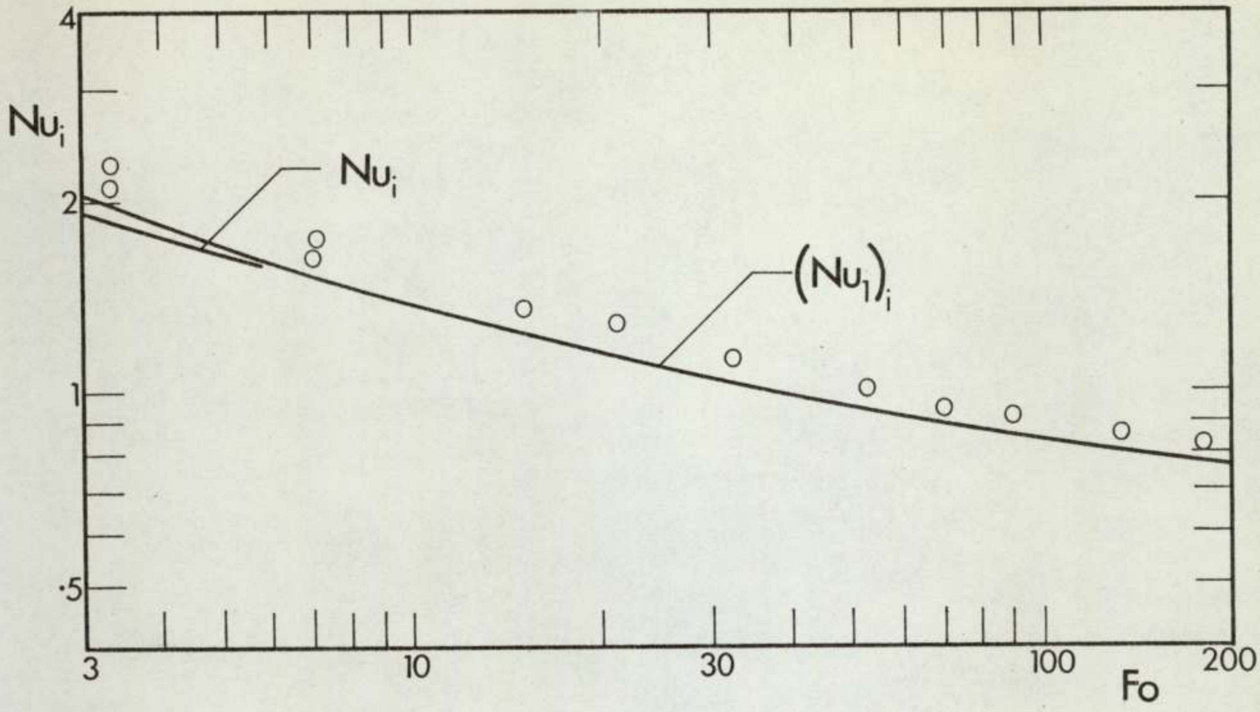

Fig. 5.5: Instantaneous bubble induced heat transfer from a 41.15 µm dia wire into water ($A = 108$, $\xi = 1.1$, $T_F = 25°C$).

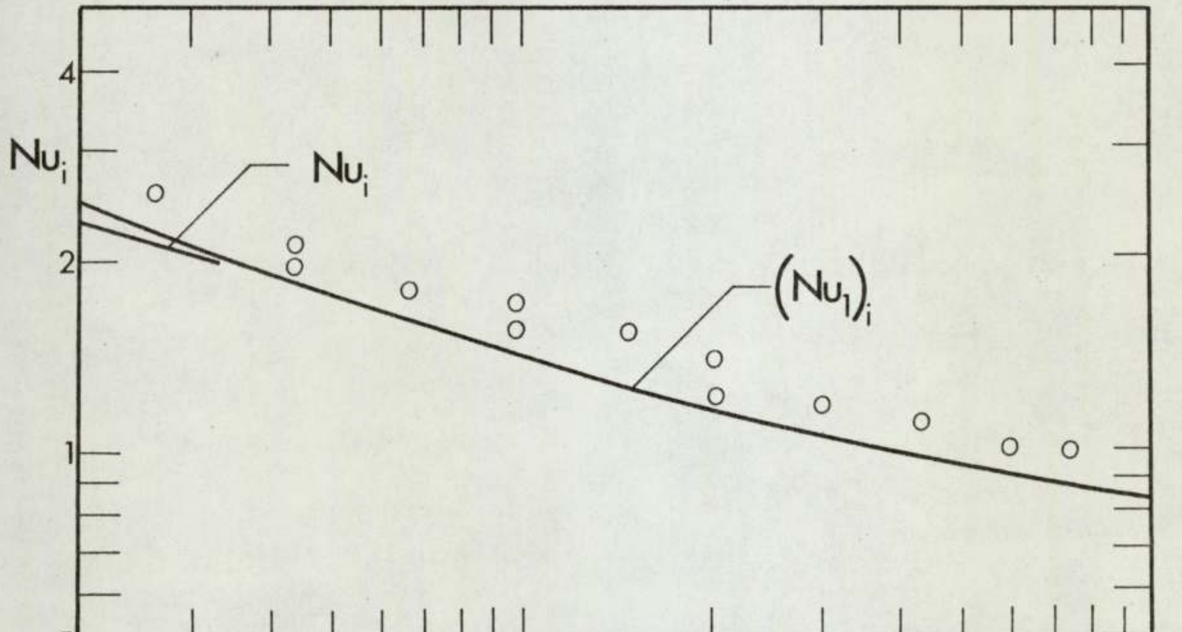

Fig. 5.6: Instantaneous bubble induced heat transfer from a 41.15 µm dia wire into 50% glycerol solution ($A = 108$, $\xi = 1.1$, $T_F = 25°C$).

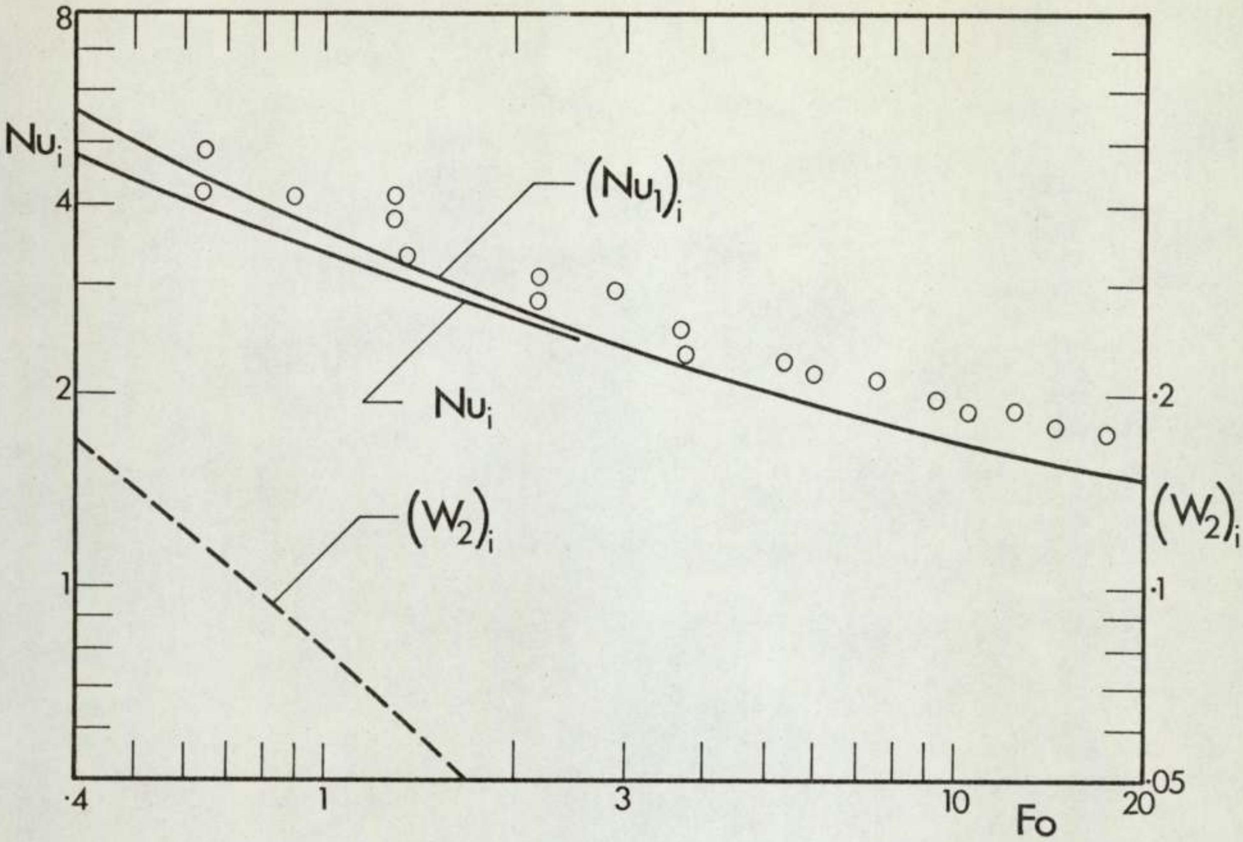

Fig. 5.7: Instantaneous bubble induced heat transfer from a 125 μm dia wire into water ($A = 35.6$, $\xi = 1.1$, $T_F = 25^oC$).

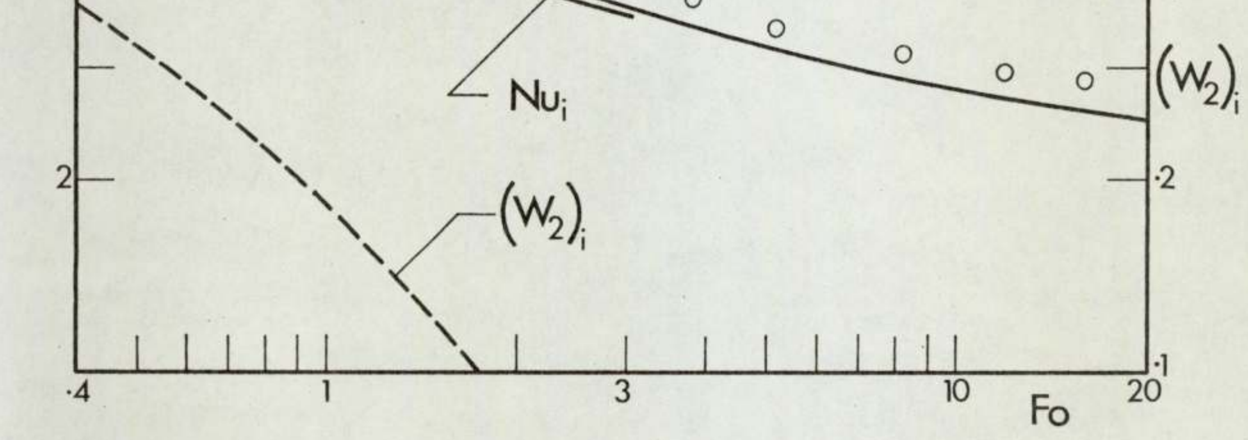

Fig. 5.8: Instantaneous bubble induced heat transfer from a 125 μm dia wire into n-heptane ($A = 35.6$, $\xi = 1.3$, $T_F = 25^oC$).

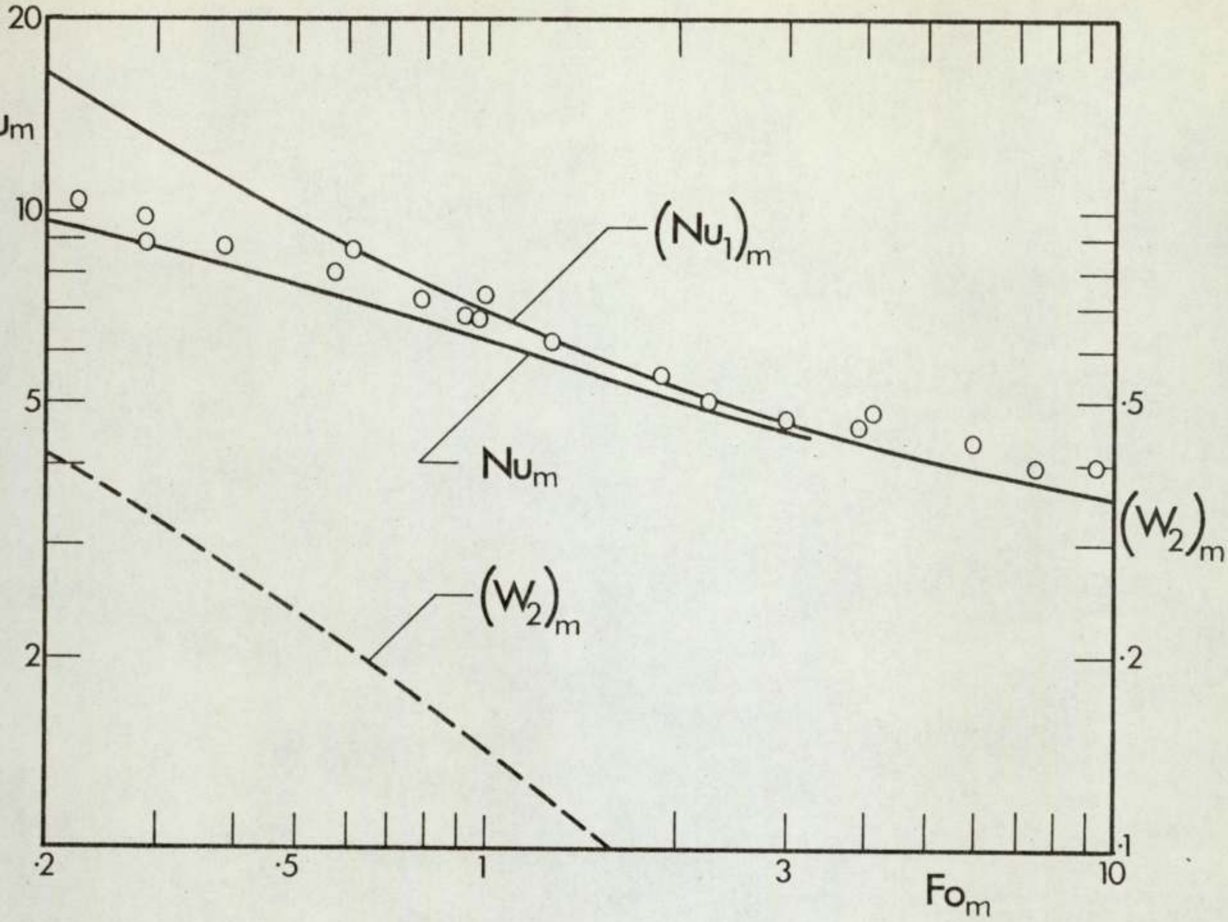

Fig. 5.9: Time-mean bubble induced heat transfer from a 305 µm dia wire into water ($A = 14.6$, $\xi = 1.1$, $T_F = 25°C$).

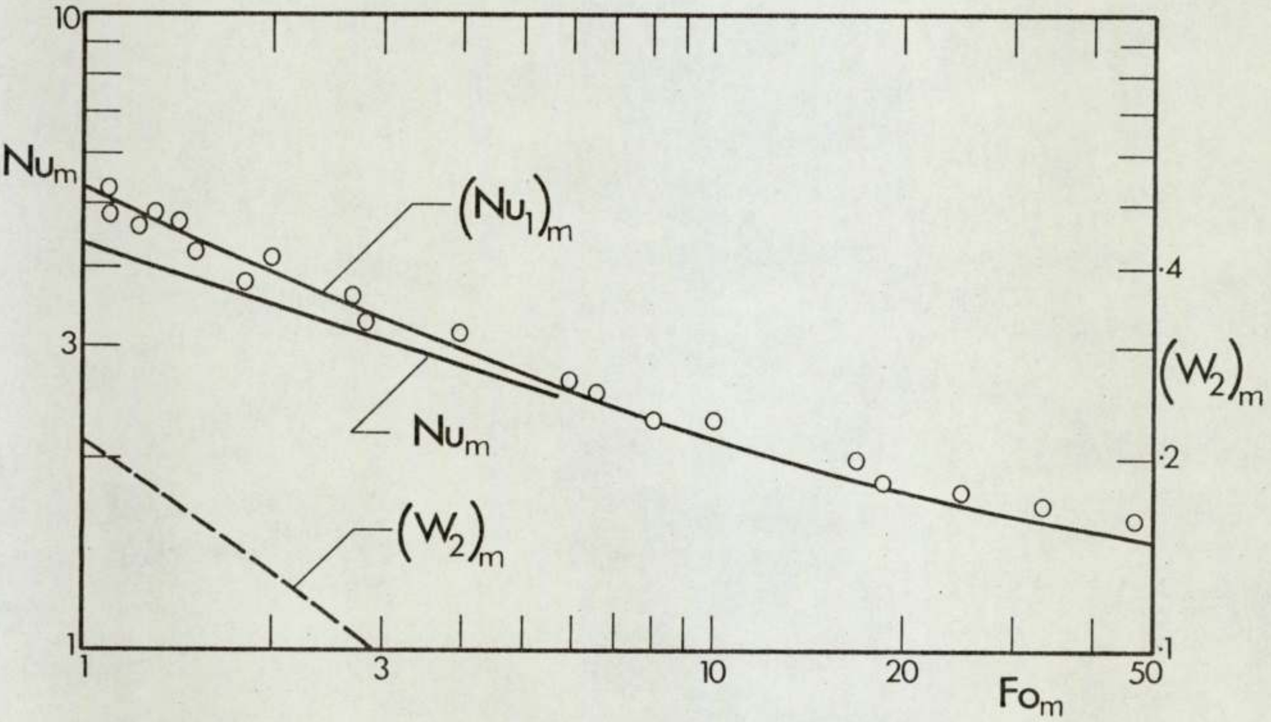

Fig. 5.10: Time-mean bubble induced heat transfer from a 125 µm dia wire into water ($A = 35.6$, $\xi = 1.1$, $T_F = 25°C$).

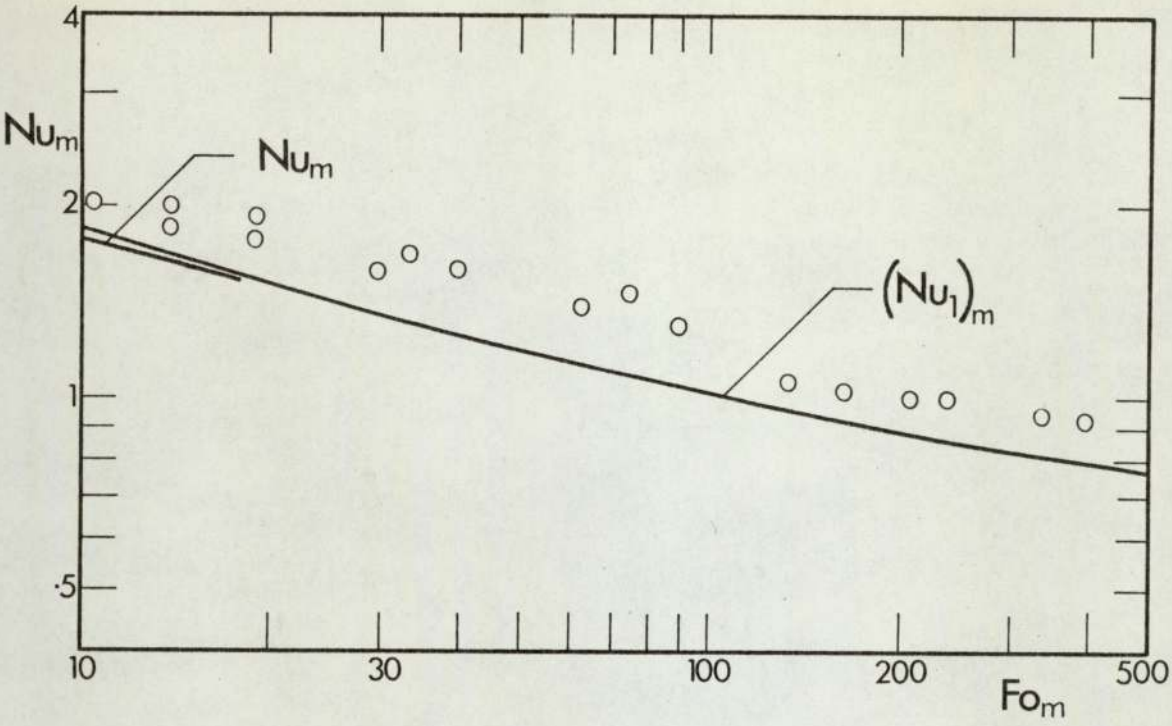

Fig. 5.11: Time-mean bubble induced heat transfer from a 41.15 μm dia wire into water (A = 108, $\xi = 1.1$, $T_F = 25^oC$).

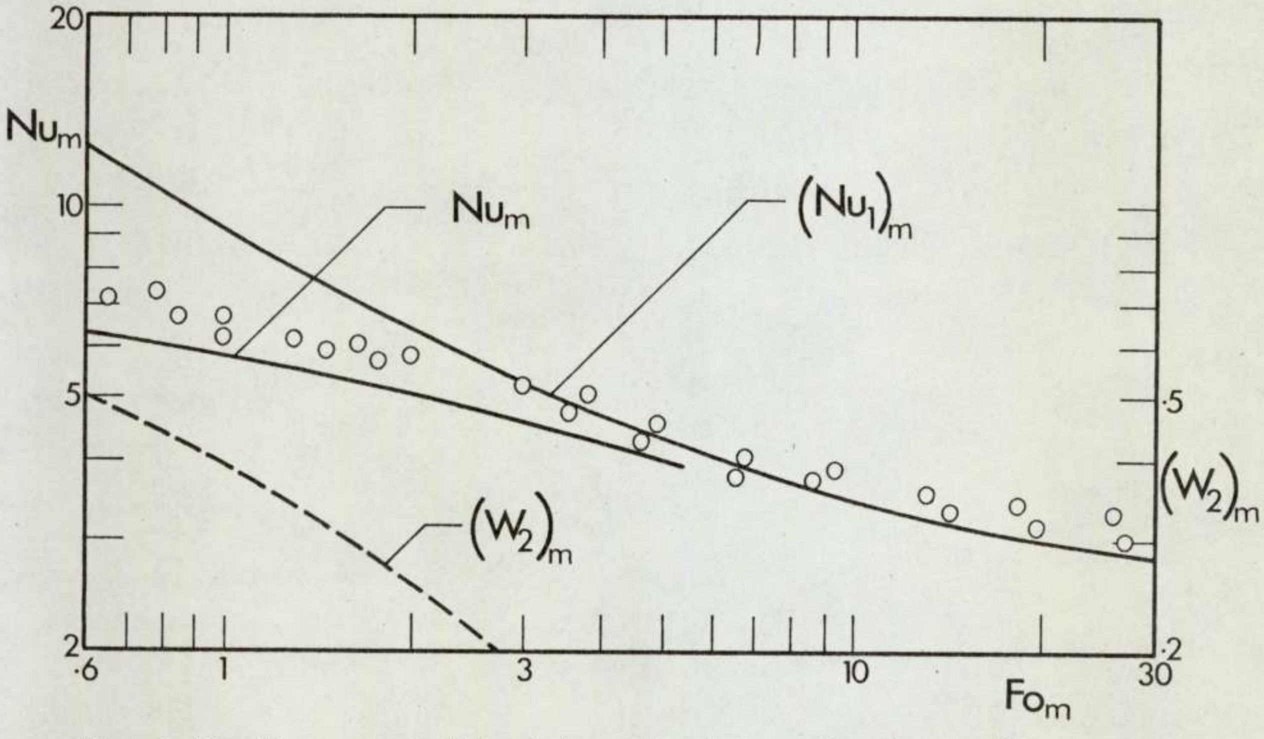

Fig. 5.12: Time-mean bubble induced heat transfer from a 125 μm dia wire into n-heptane (A = 35.6, $\xi = 1.3$, $T_F = 25^oC$).

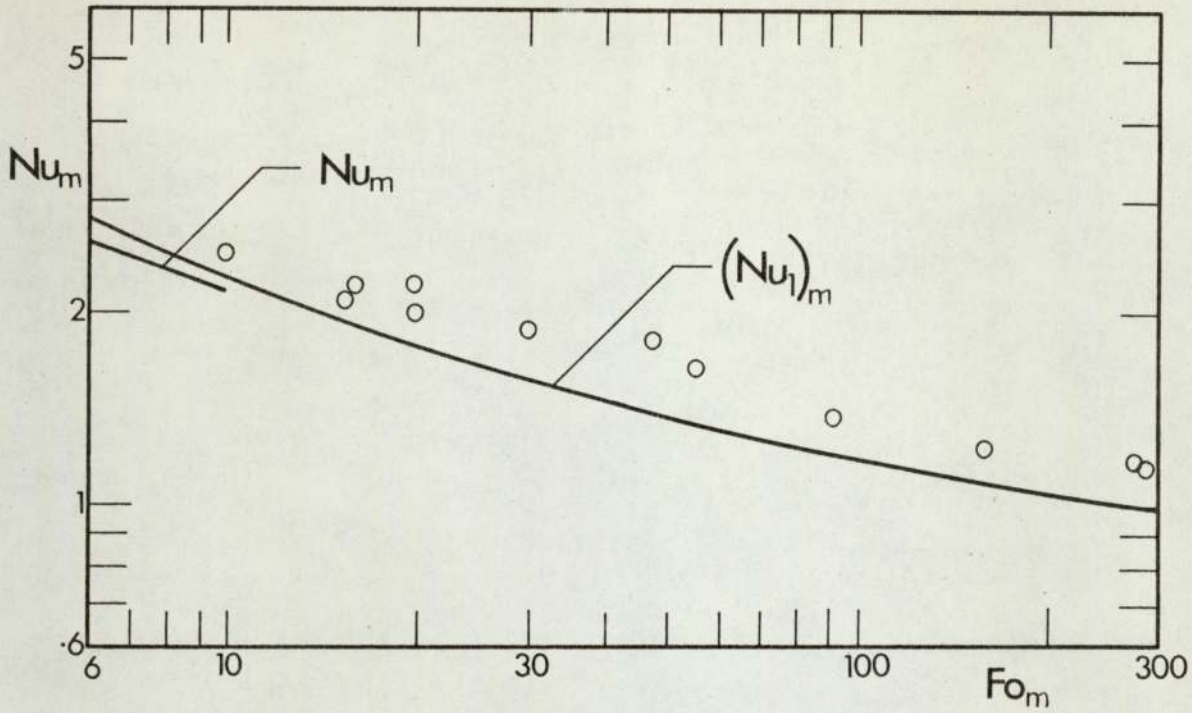

Fig. 5.13: Time-mean bubble induced heat transfer from a 41.15 μm dia wire into n-heptane ($A = 108$, $\xi = 1.3$, $T_F = 25^oC$).

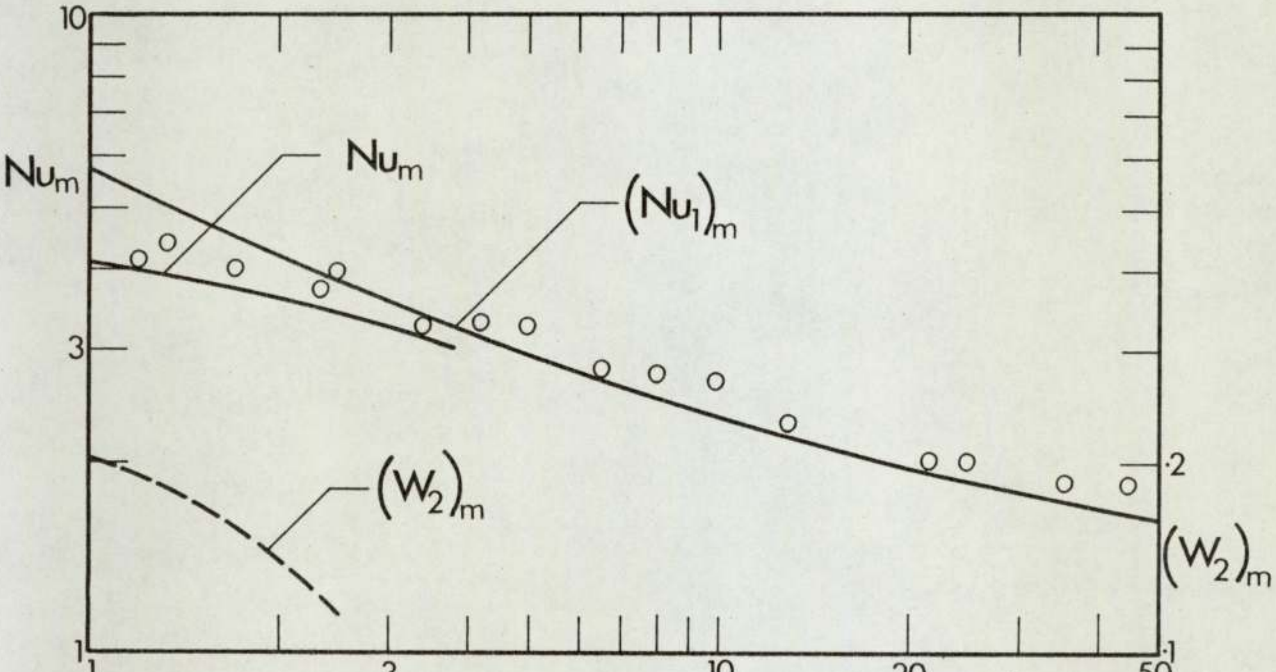

Fig. 5.14: Time-mean bubble induced heat transfer from a 125 μm dia wire into 50% solution of glycerol ($A = 35.6$, $\xi = 1.1$, $T_F = 25^oC$).

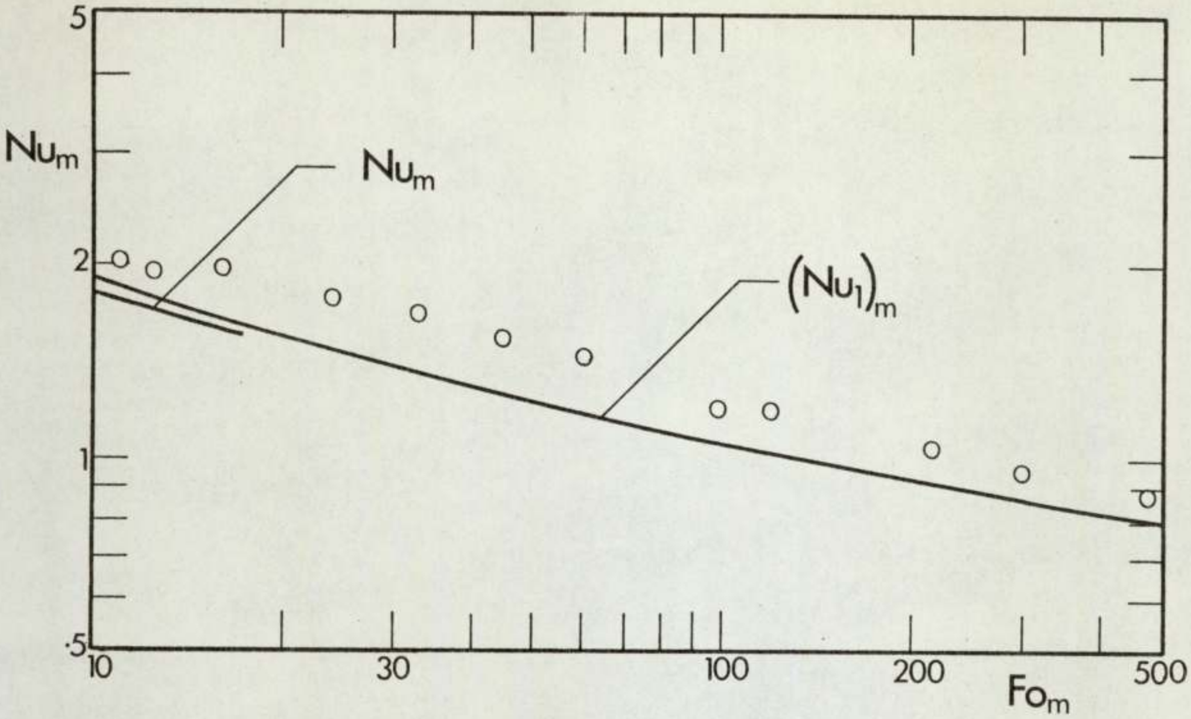

Fig. 5.15: Time-mean bubble induced heat transfer from a 41.15 μm dia wire into 50% solution of glycerol (A = 108, ξ = 1.1, T_F = 25°C).

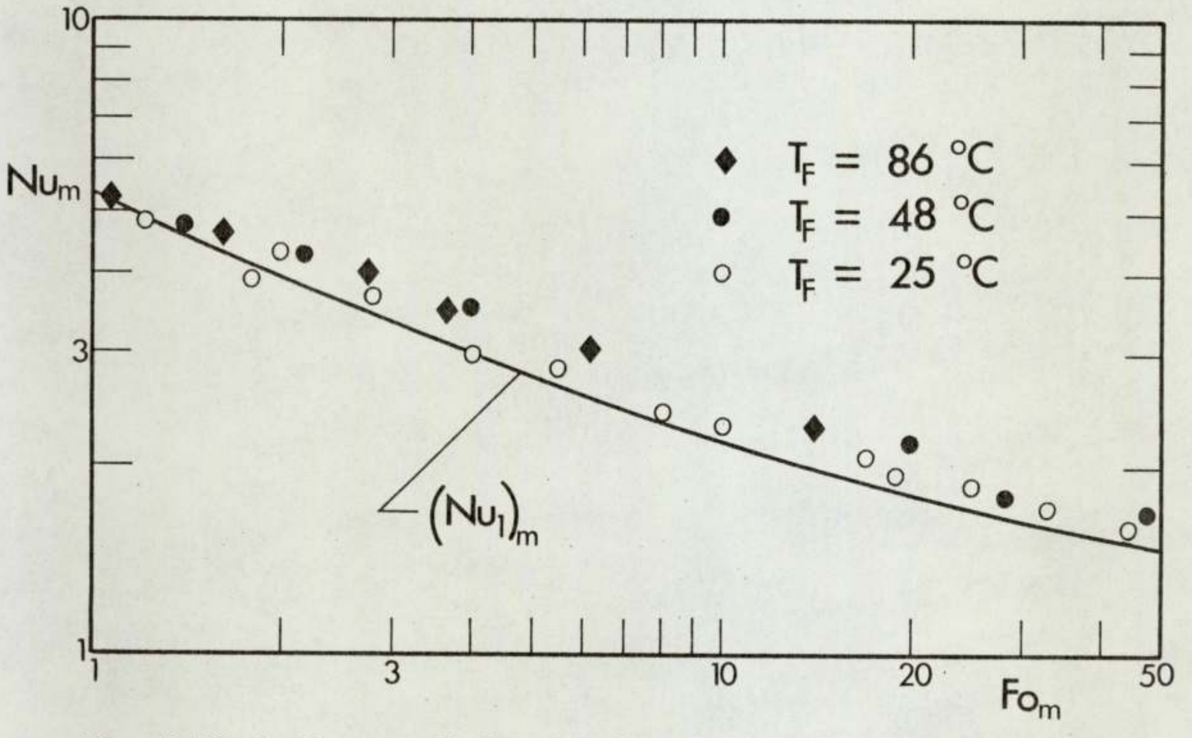

Fig. 5.16: Influence of elevated film temperatures on the time-mean bubble induced heat transfer from a 125 μm dia wire into water (A =35.6, ξ = 1.1 to 1.3).

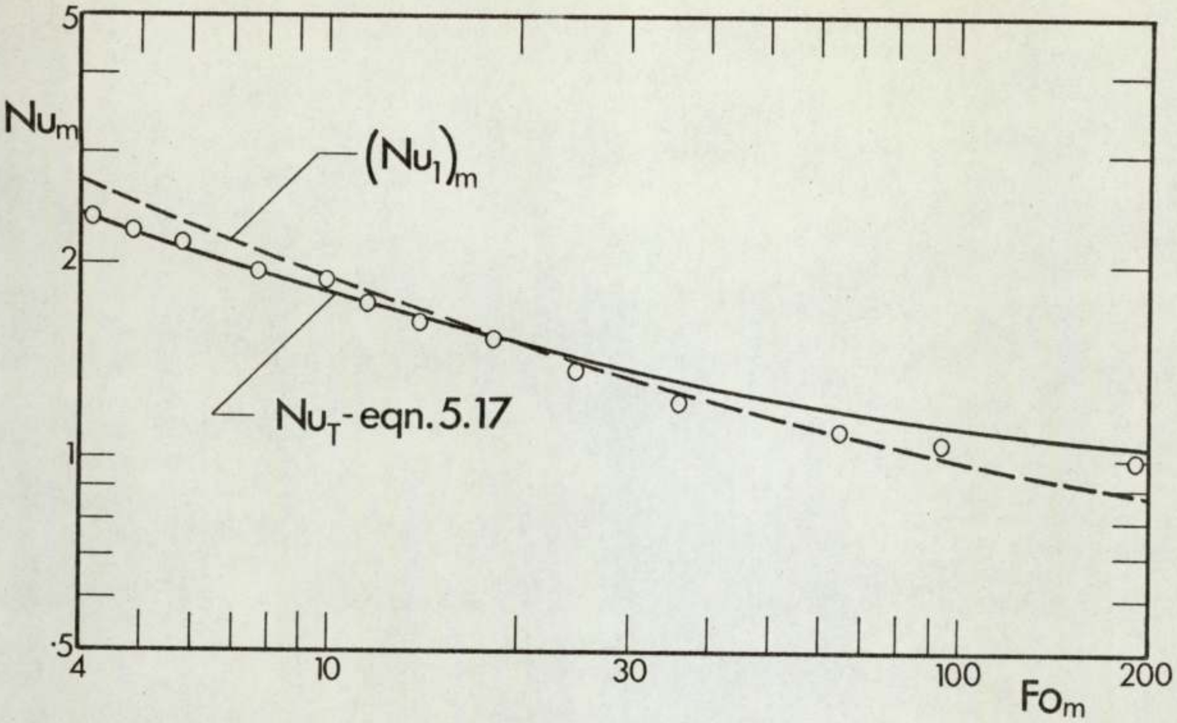

Fig. 5.17: Influence of ξ on the time-mean bubble induced heat transfer from a 101 μm dia wire into water (A = 128, ξ = 2.8, T_F = 25°C).

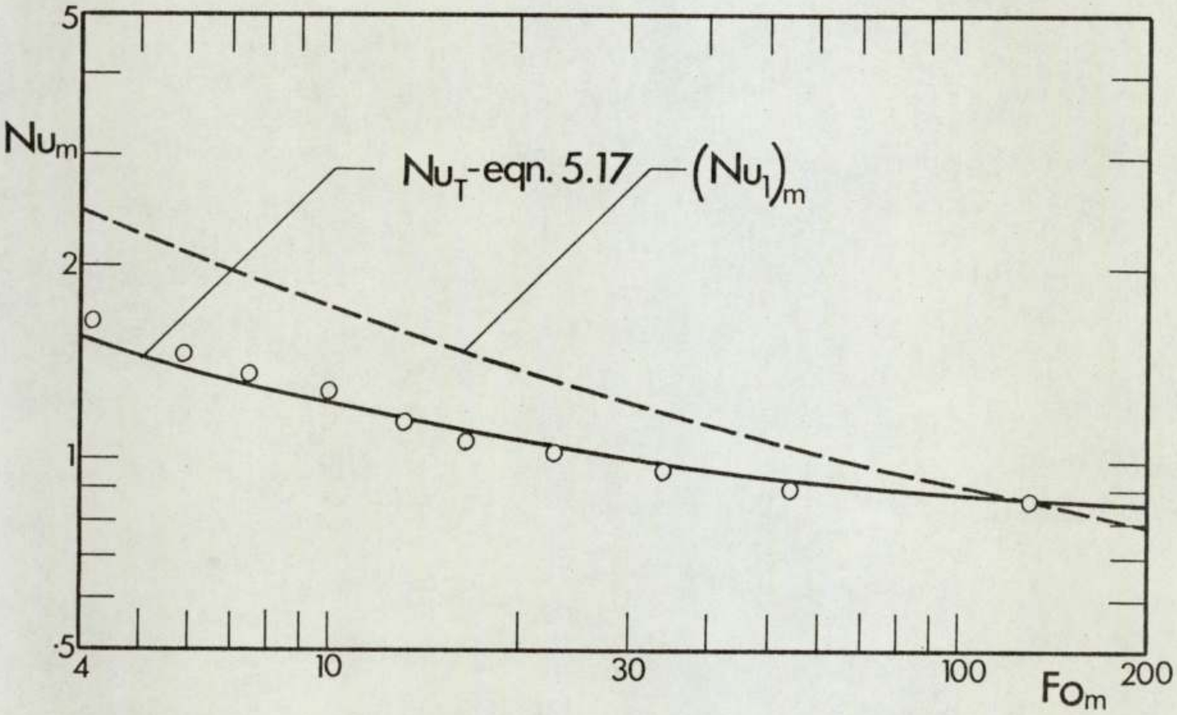

Fig. 5.18: Influence of ξ on the time-mean bubble induced heat transfer from a 101 μm dia wire into water (A = 264, ξ = 5.8, T_F = 25°C).

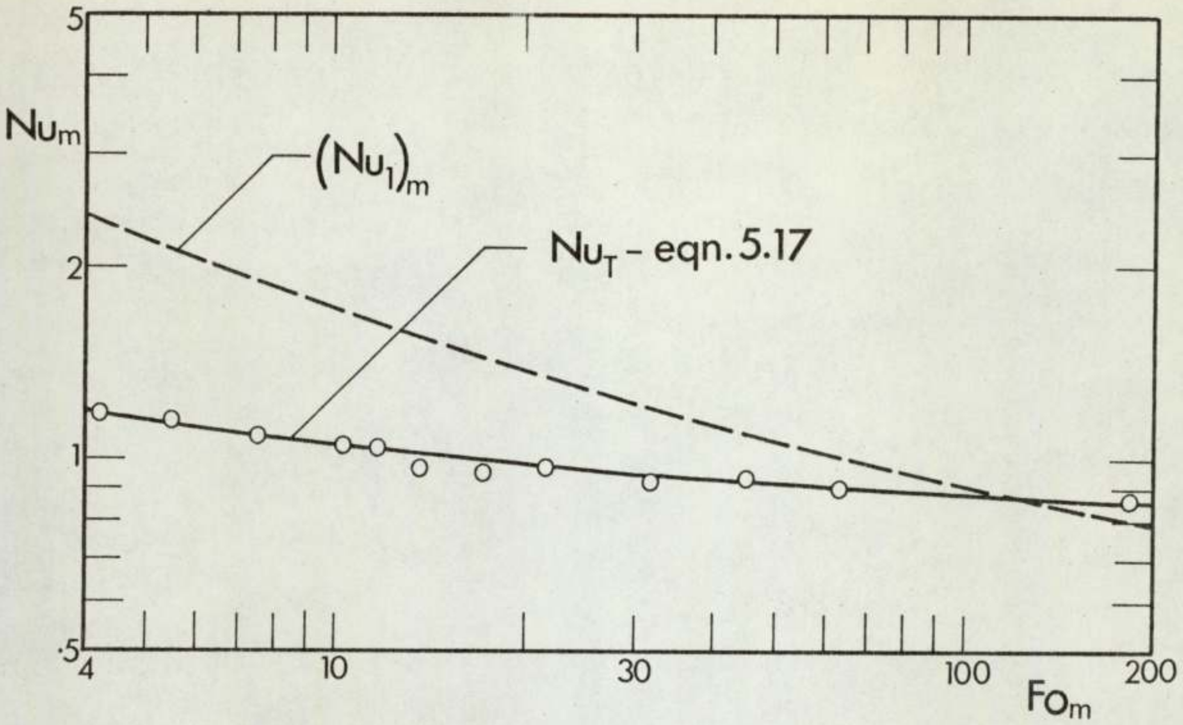

Fig. 5.19: Influence of ξ on the time-mean bubble induced heat transfer from a 101 μm dia wire into water (A = 264, ξ = 9.1, T_F = 25°C).

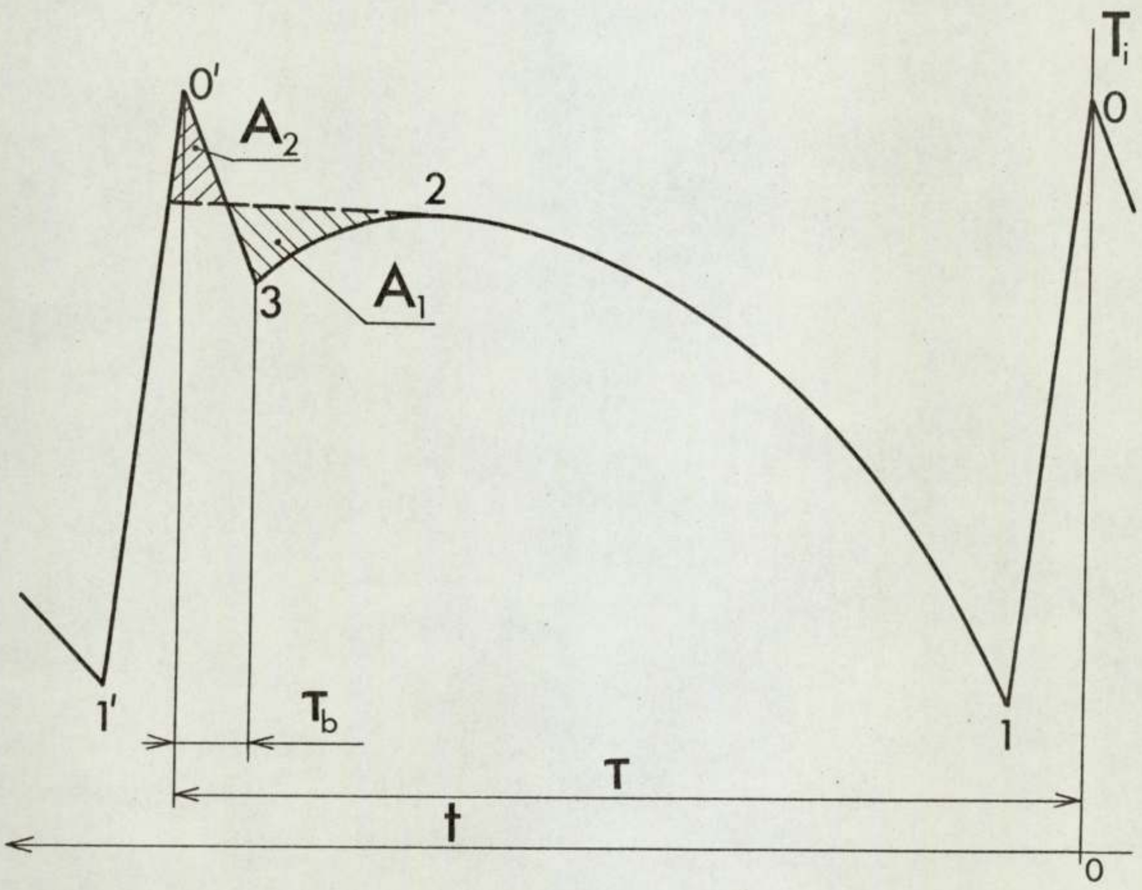

Fig. 5.20: A typical plot of the instantaneous average wire temperature as a function of time.

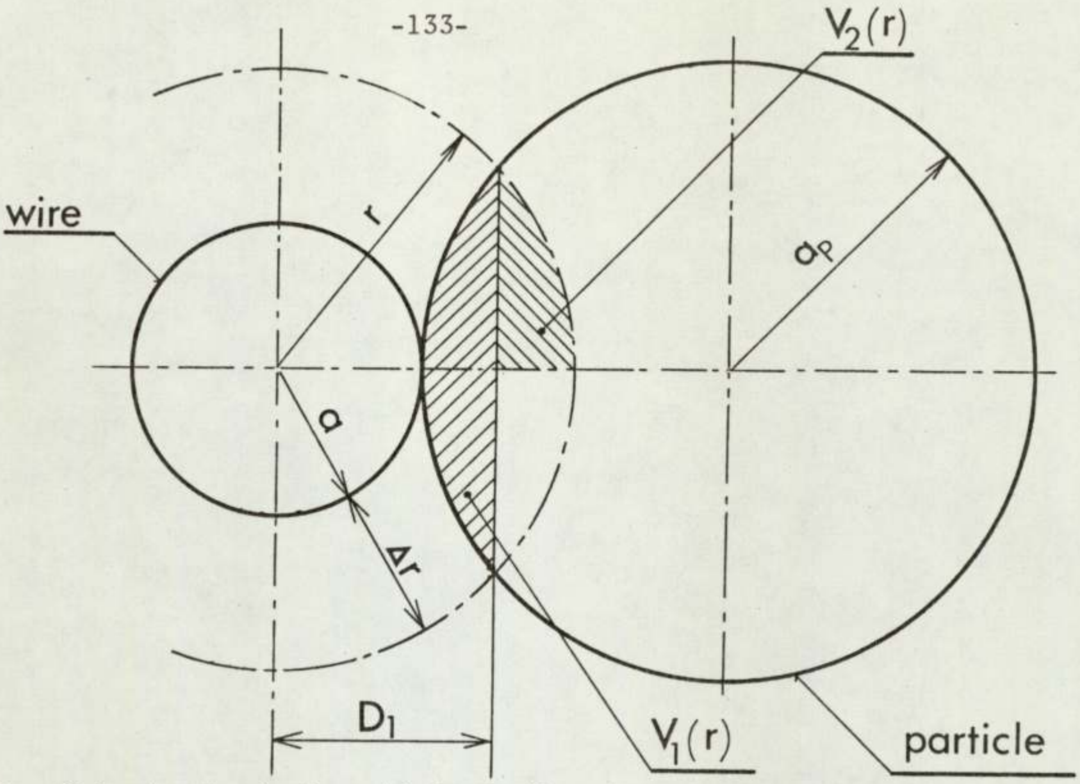

Fig. 6.1: A spherical particle in the wire vicinity.
Equation of the wire $r = a$.
Equation of the spherical particle $(r - a - a_P)^2 + x^2 = a_P^2$.

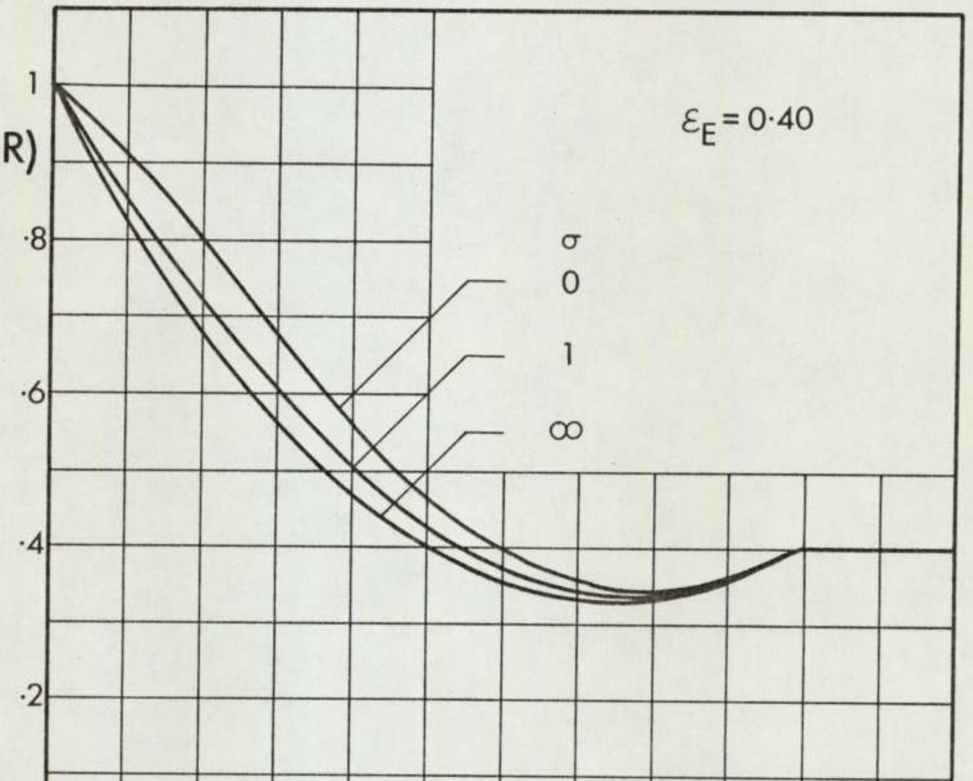

Fig. 6.2: Variation of the emulsion phase voidage in the wire vicinity for three different values of σ and $\varepsilon_E = 0.40$.

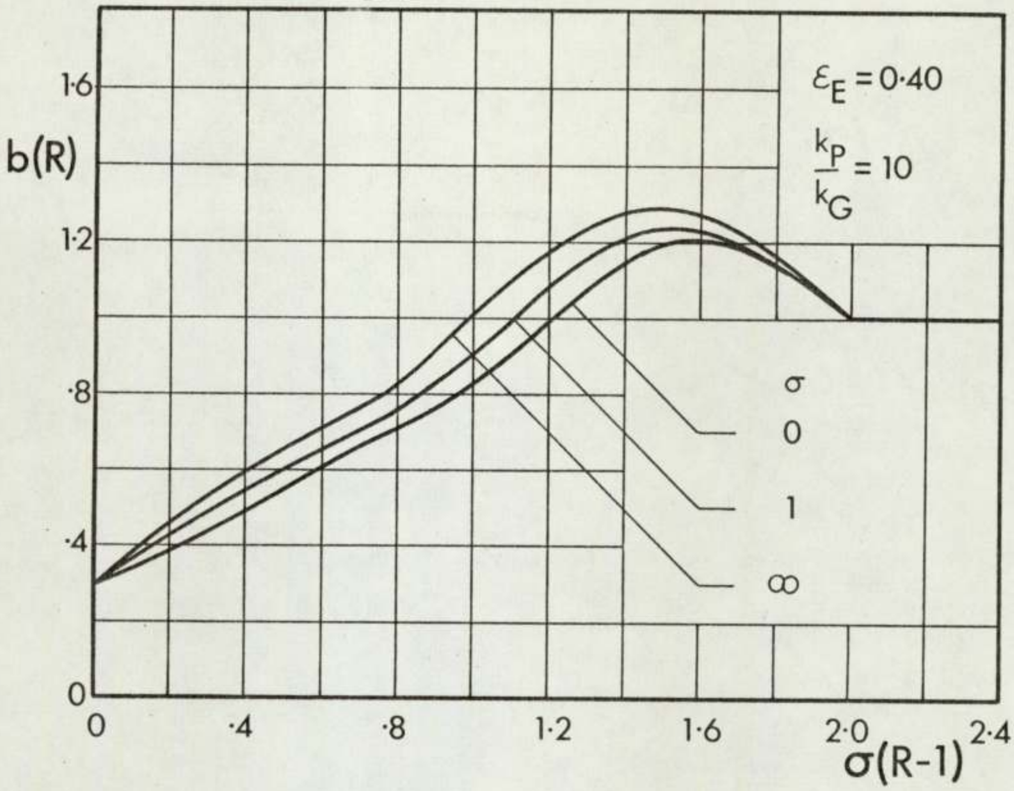

Fig. 6.3: Variation of the dimensionless conductivity b(R) in the wire vicinity for $\varepsilon_E = 0.40$, $k_P/k_G = 10$ and three values of σ .

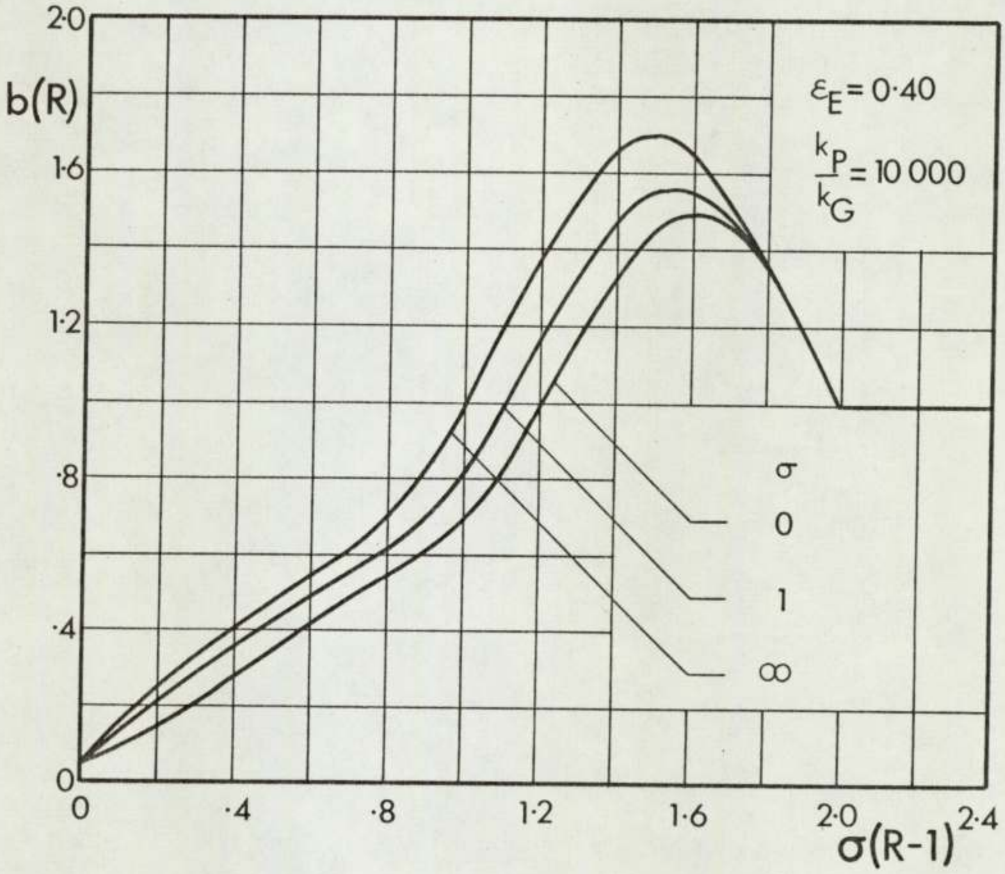

Fig. 6.4: Variation of the dimensionless conductivity b(R) in the wire vicinity for $\varepsilon_E = 0.40$, $k_P/k_G = 10\ 000$ and three values of σ .

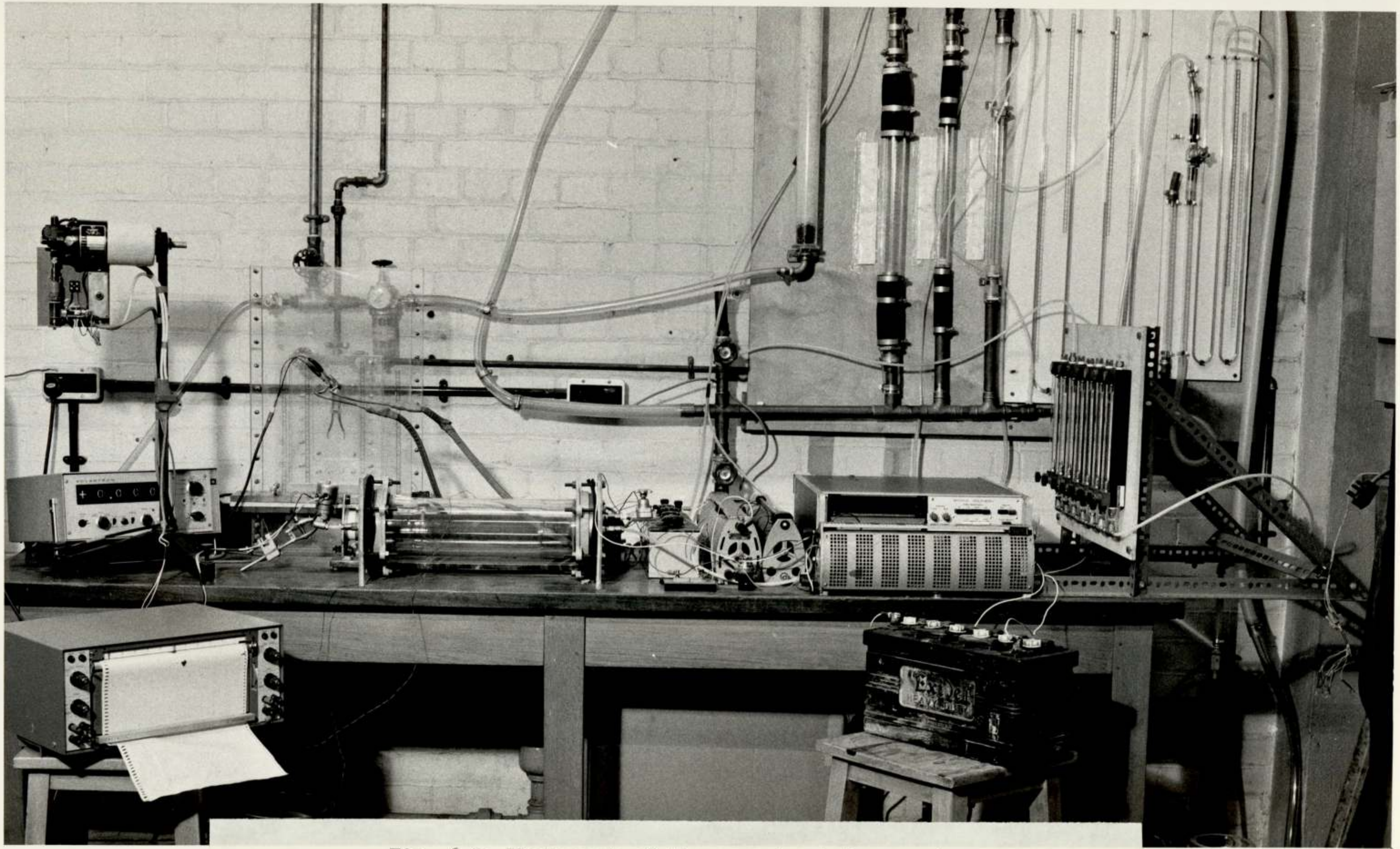

Fig. 6.5: Photograph of the experimental apparatus.

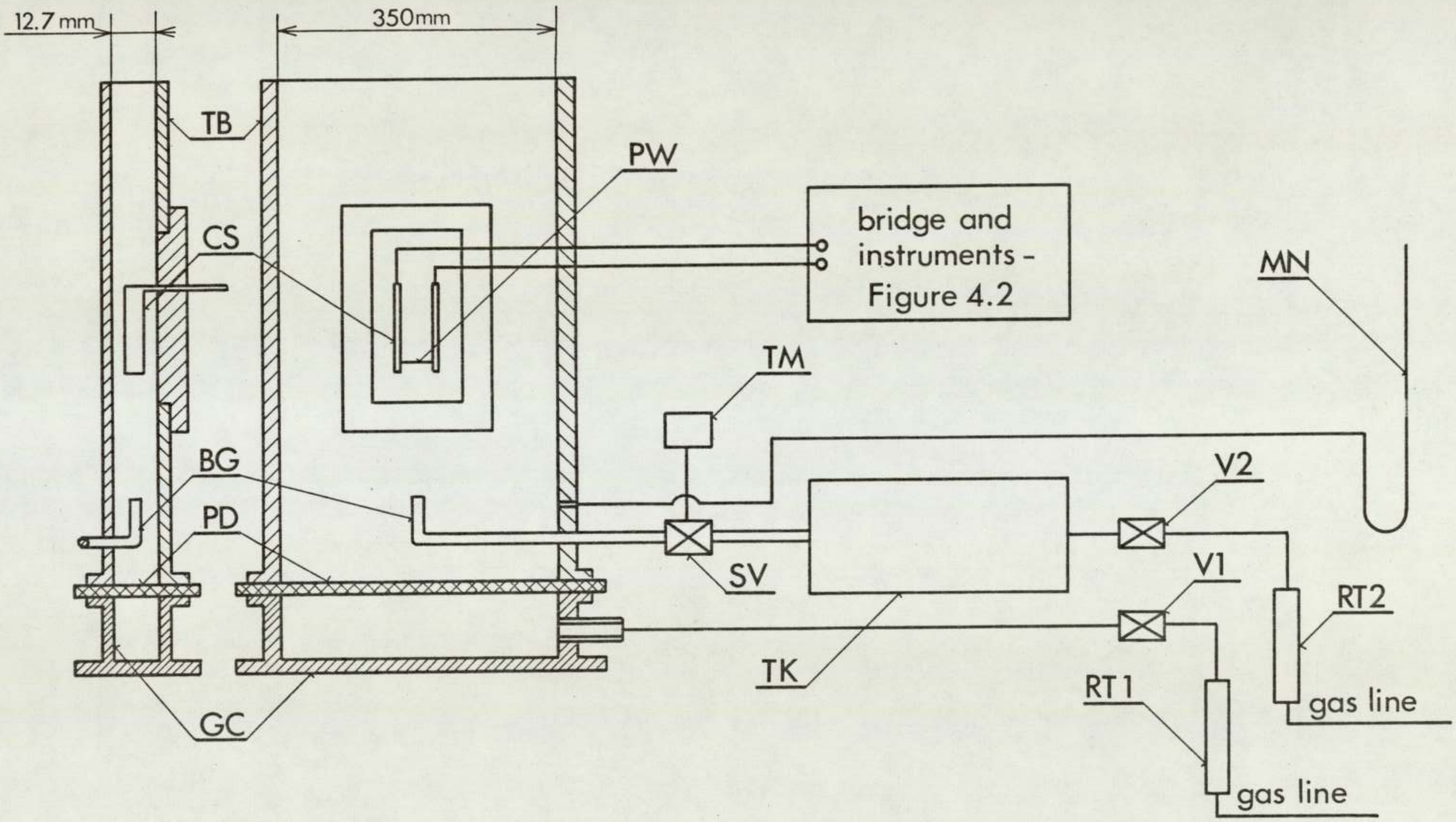

Fig. 6.6: Line diagram of the experimental apparatus.

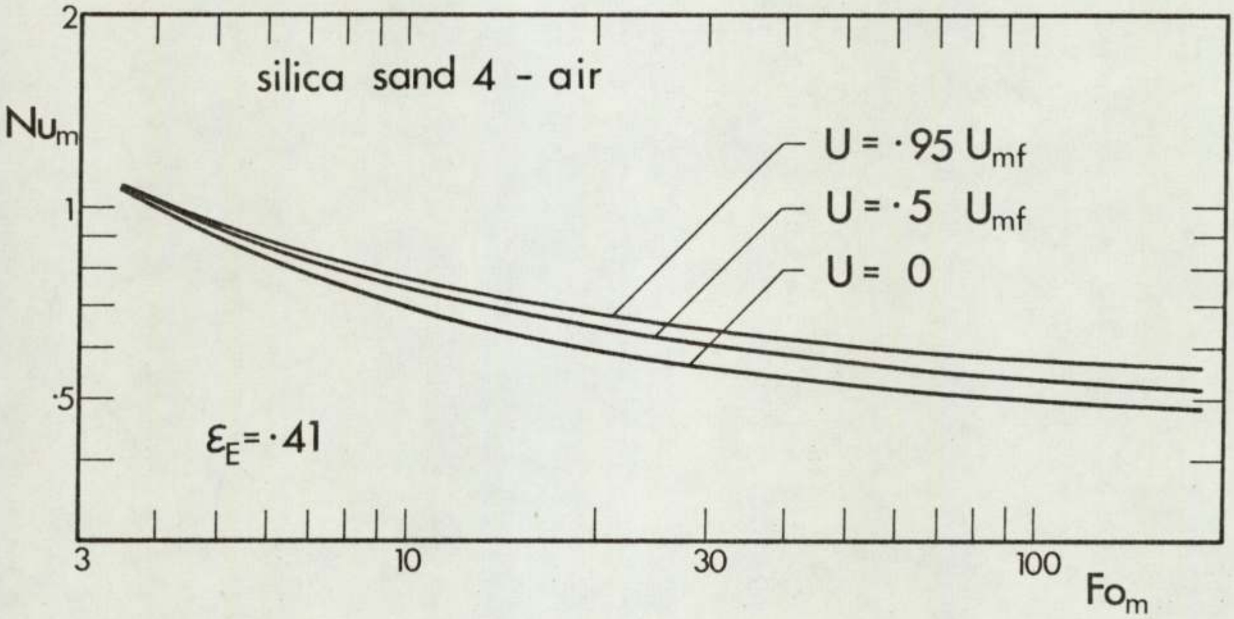

Fig. 6.7: Influence of gas velocity on the response of the wire, placed in the emulsion phase of silica sand 4 - air, to a step heating input.

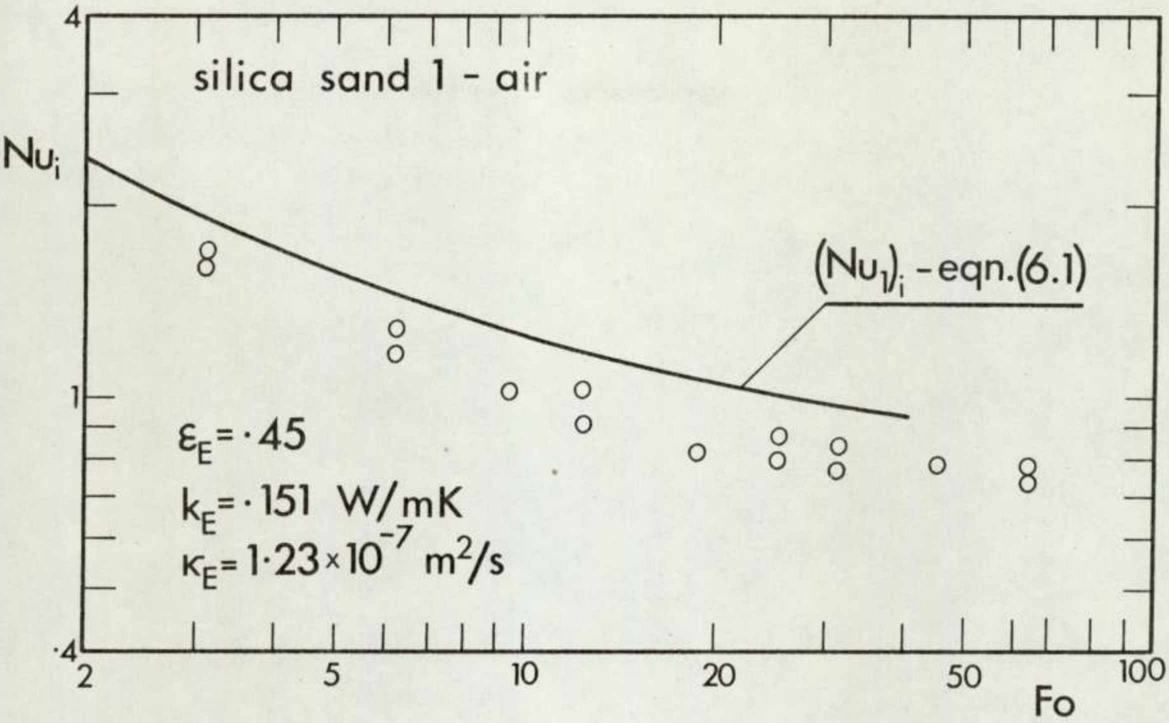

Fig. 6.8: Response of the wire, placed in an incipiently fluidized bed of silica sand 1 - air, to a step heating input. (Experimentally obtained value of the emulsion phase voidage.)

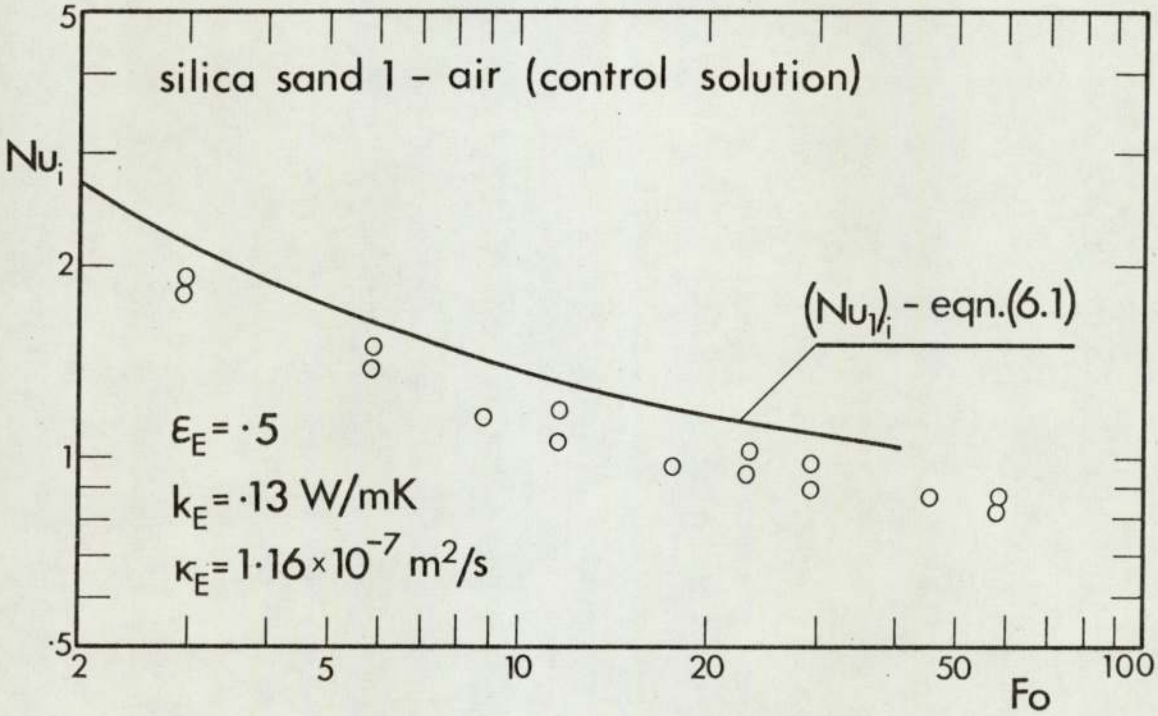

Fig. 6.8a: Response of the wire, placed in an incipiently fluidized bed of silica sand 1 - air, to a step heating input. (Results are based on an assumed value of the emulsion phase voidage.)

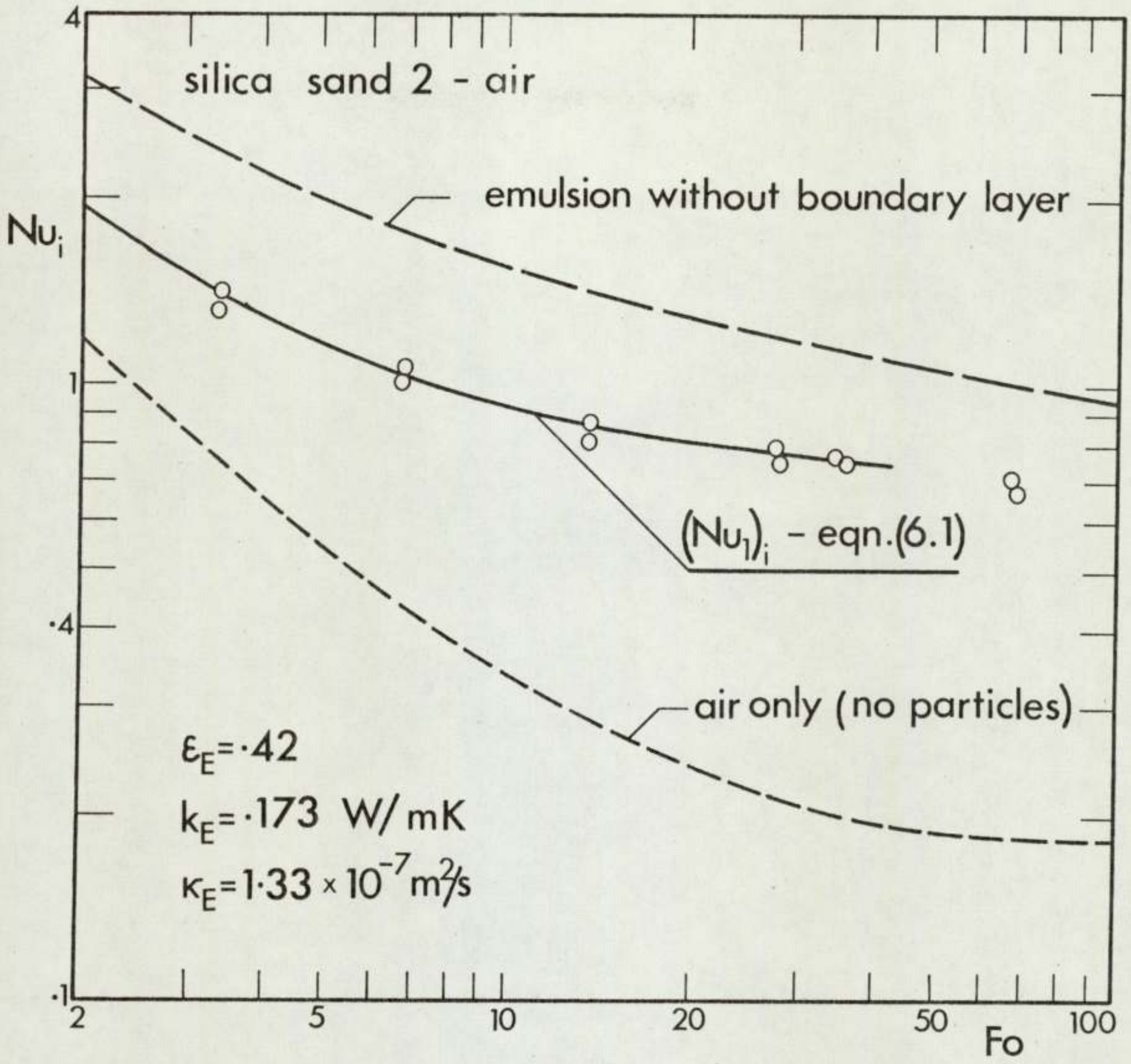

Fig. 6.9: Response of the wire, placed in an incipiently fluidized bed of silica sand 2 - air, to a step heating input.

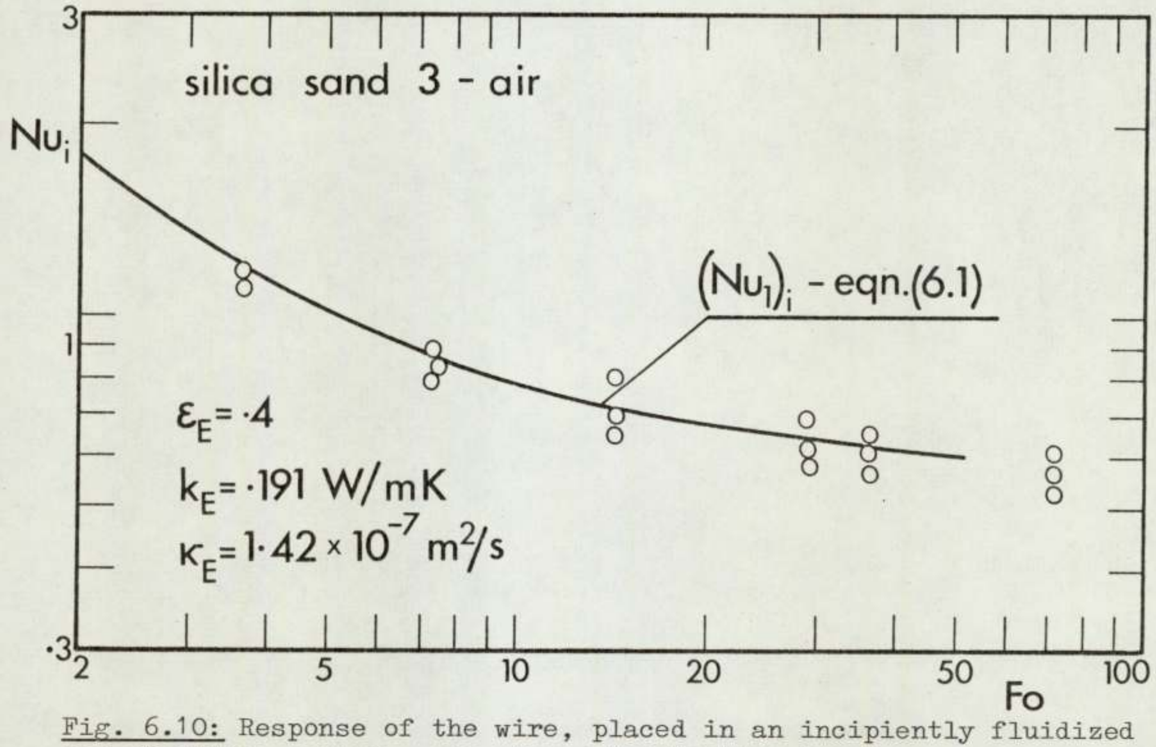

Fig. 6.10: Response of the wire, placed in an incipiently fluidized bed of silica sand 3 - air, to a step heating input.

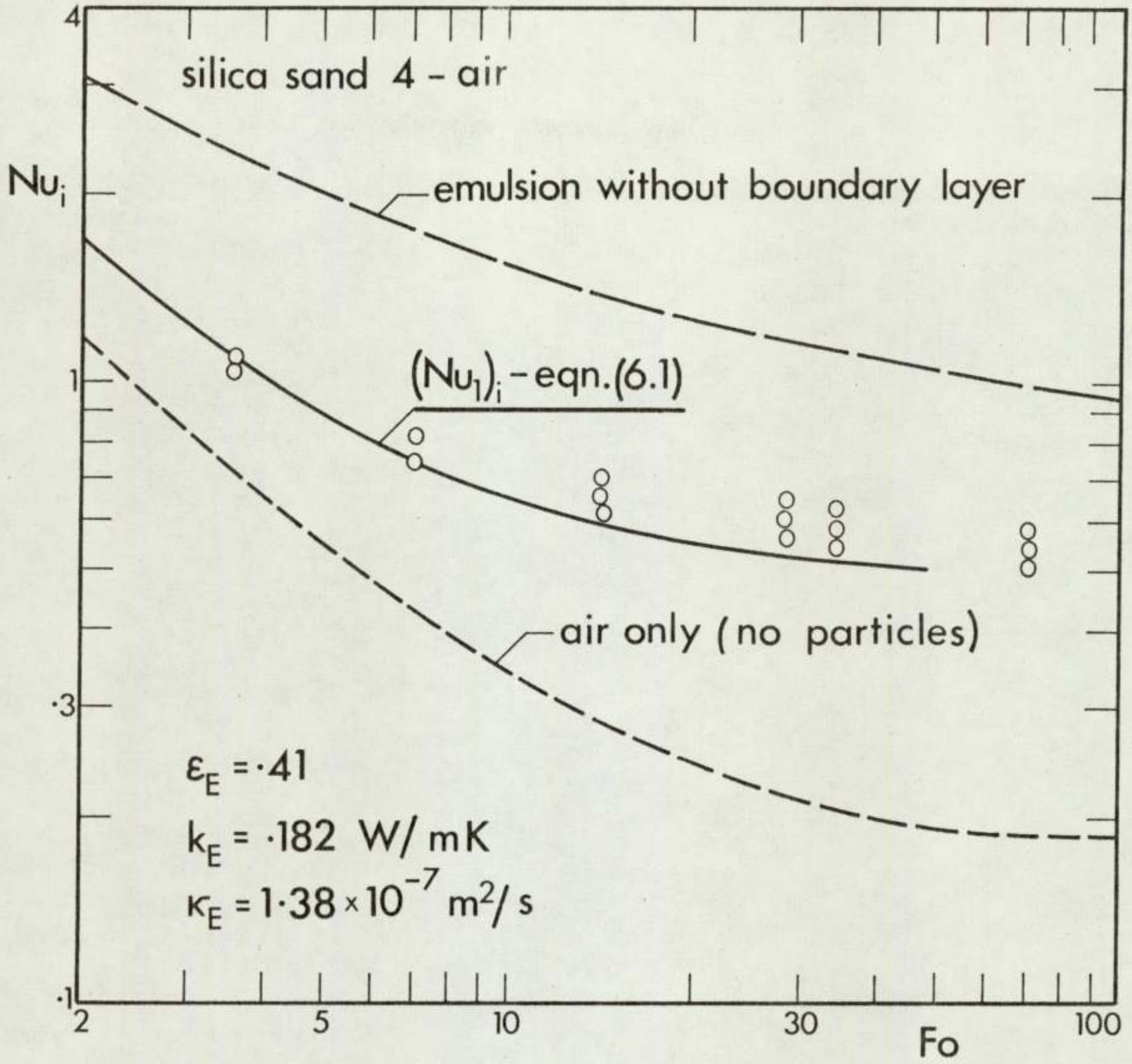

Fig. 6.11: Response of the wire, placed in an incipiently fluidized bed of silica sand 4 - air, to a step heating input.

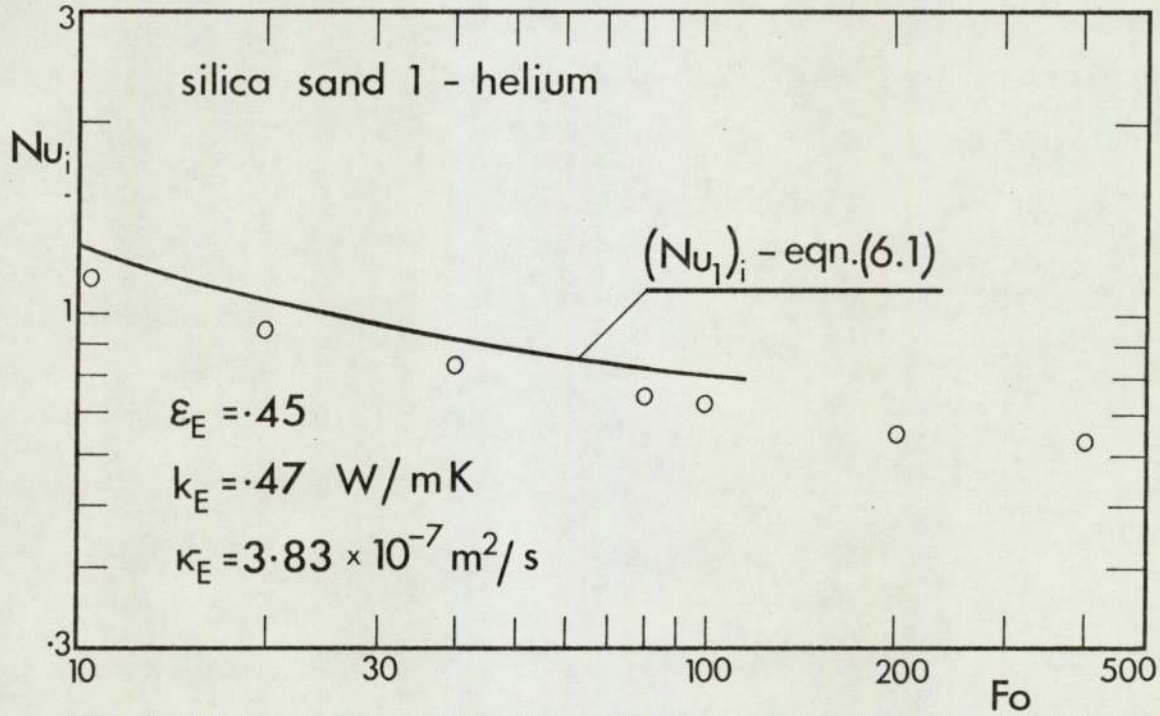

Fig. 6.12: Response of the wire, placed in an incipiently fluidized bed of silica sand 1 - helium, to a step heating input.

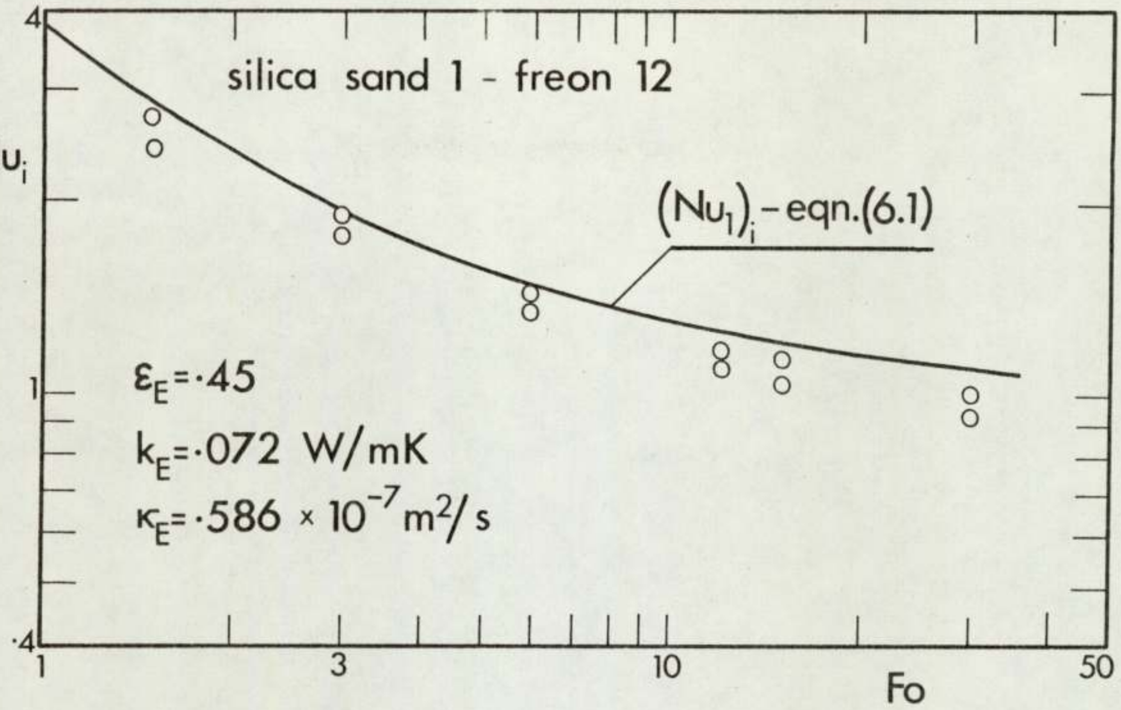

<u>Fig. 6.13:</u> Response of the wire, placed in an incipiently fluidized bed of silica sand 1 - freon 12, to a step heating input.

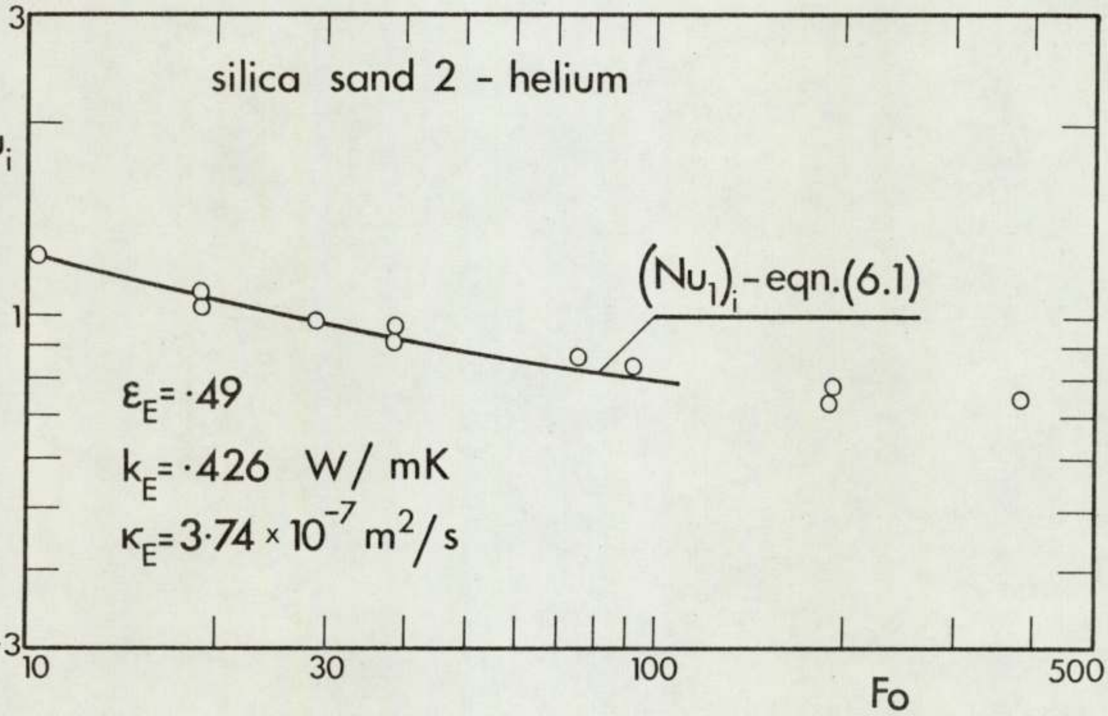

<u>Fig. 6.14:</u> Response of the wire, placed in an incipiently fluidized bed of silica sand 2 - helium, to a step heating input.

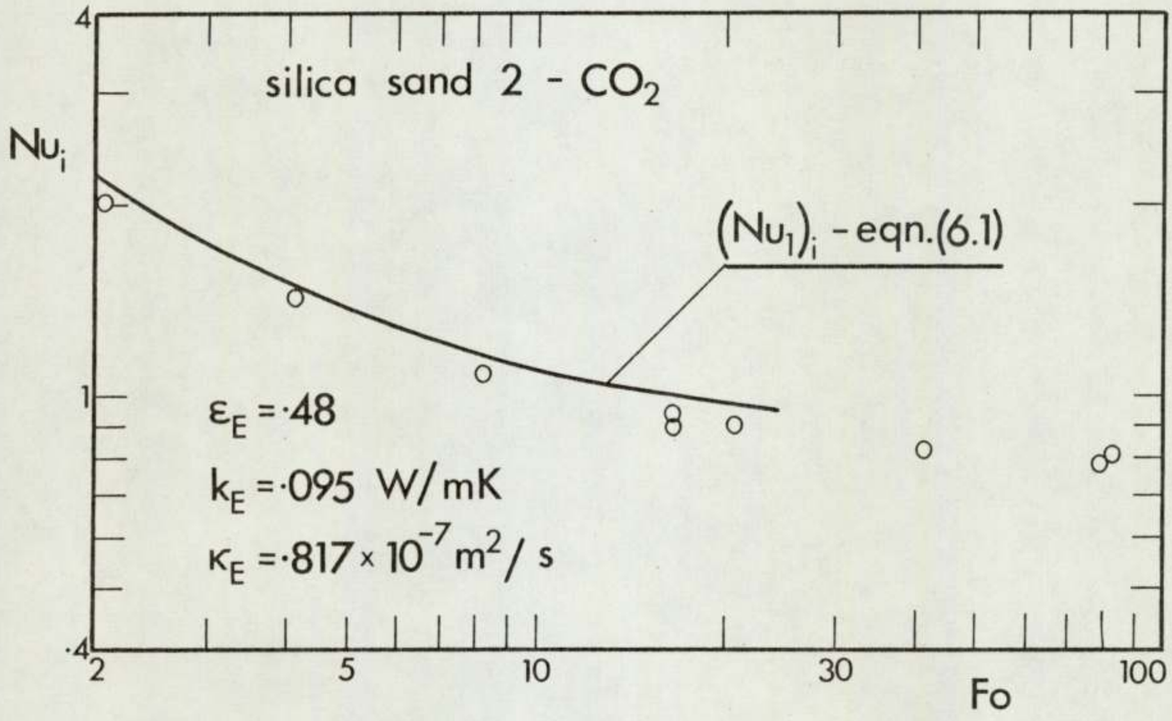

Fig. 6.15: Response of the wire, placed in an incipiently fluidized bed of silica sand 2 - carbon dioxide, to a step heating input.

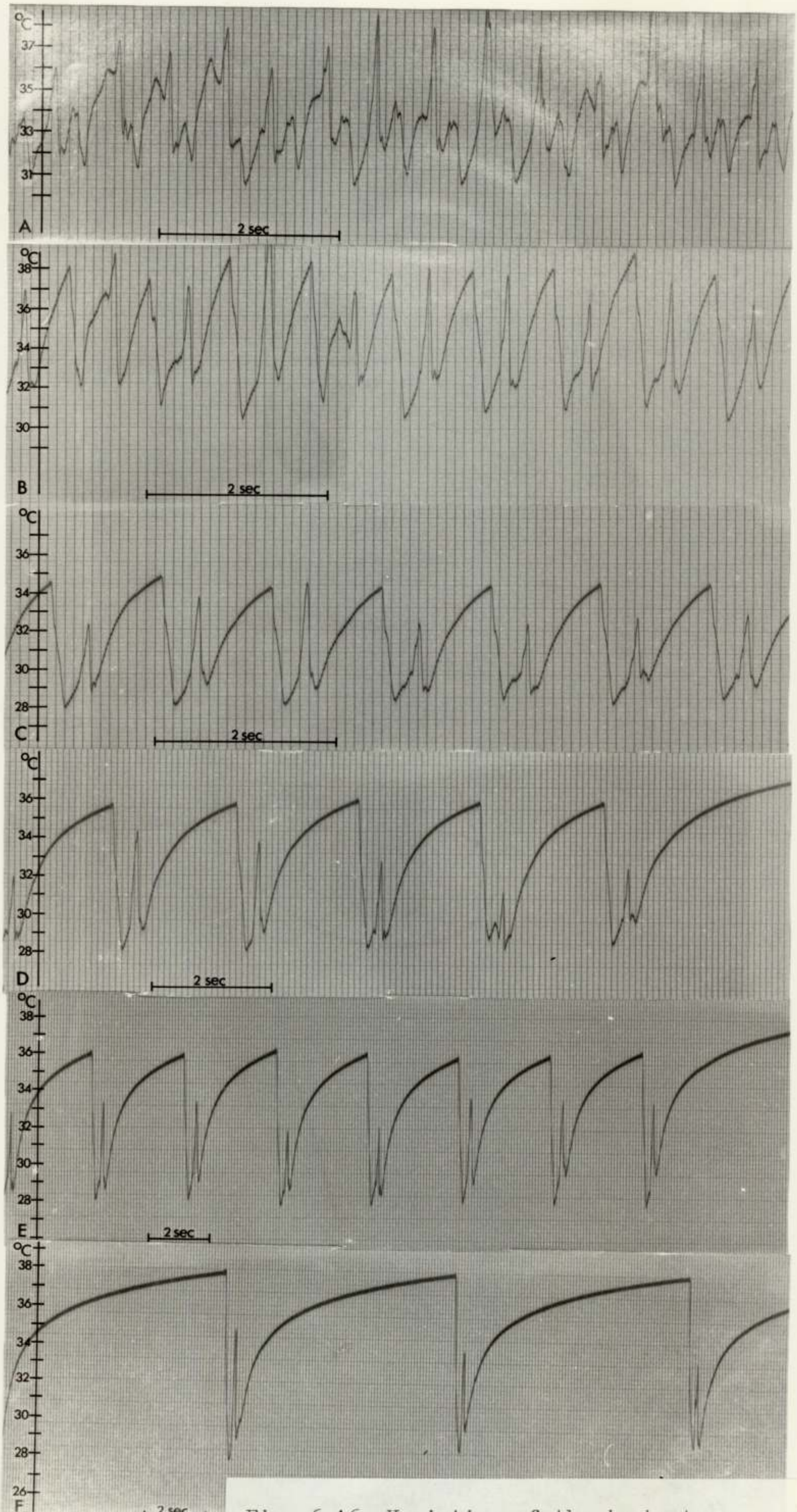

Fig. 6.16: Variation of the instantaneous average wire temperature with time (incipiently fluidized bed of copper shot - air). From top to bottom: f = 1.7, 1.1, 0.83, 0.49, 0.33 and 0.13 1/sec.

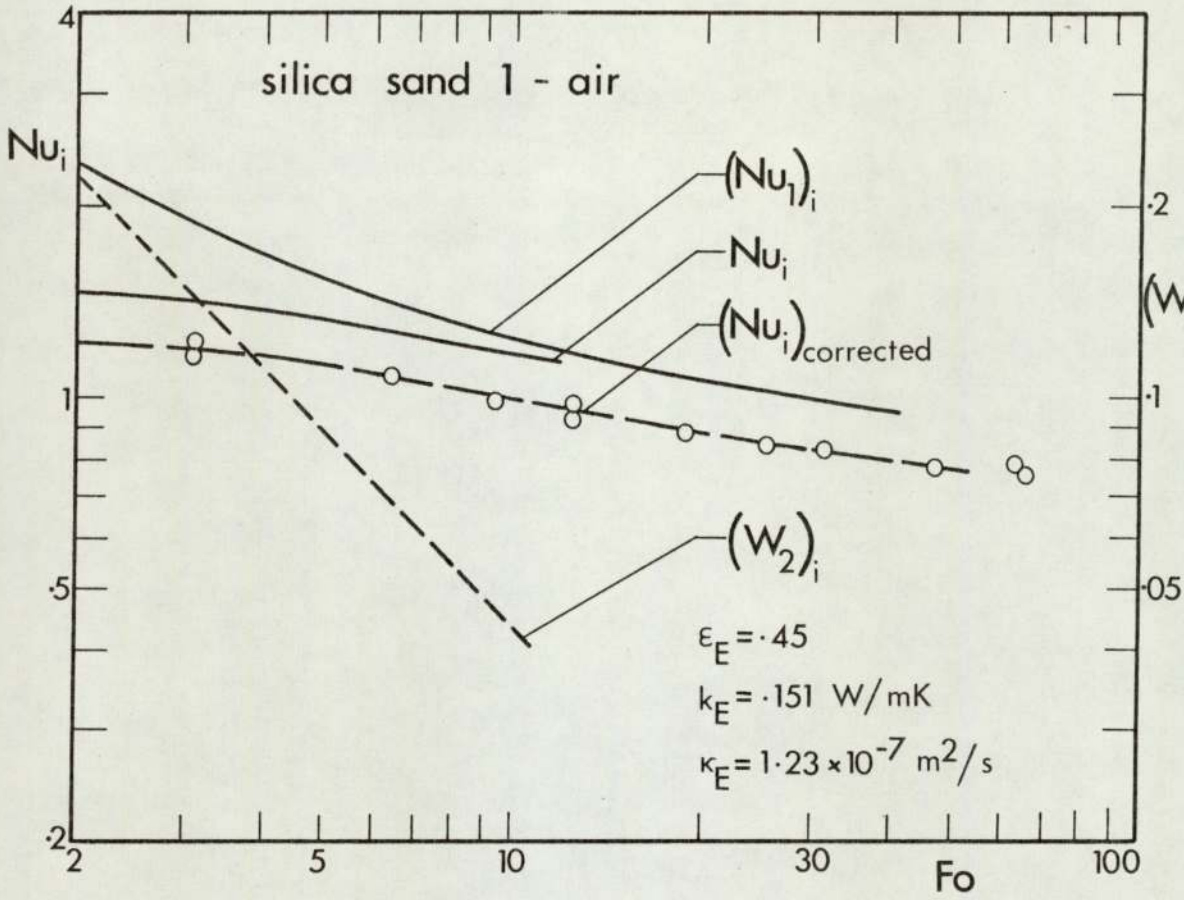

Fig. 6.17: Instantaneous bubble induced heat transfer from the wire into an incipiently fluidized bed of silica sand 1 - air.

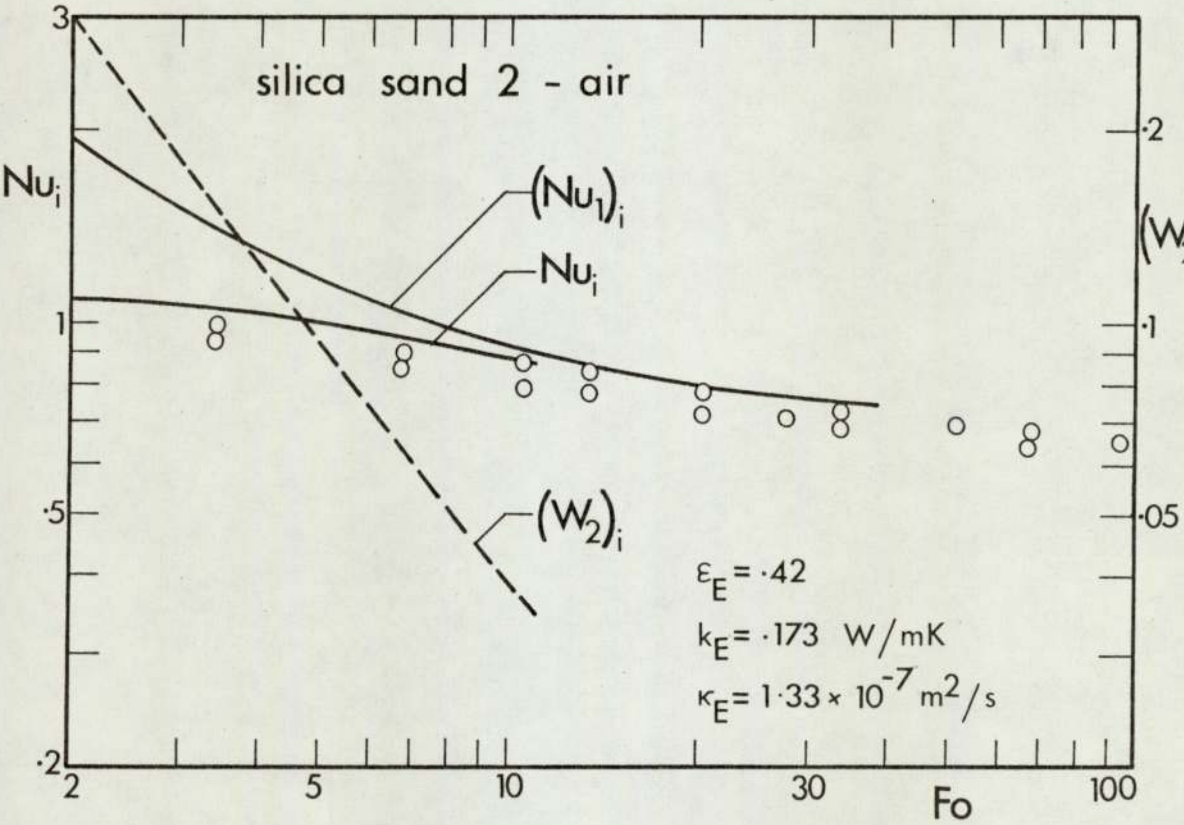

Fig. 6.18: Instantaneous bubble induced heat transfer from the wire into an incipiently fluidized bed of silica sand 2 - air.

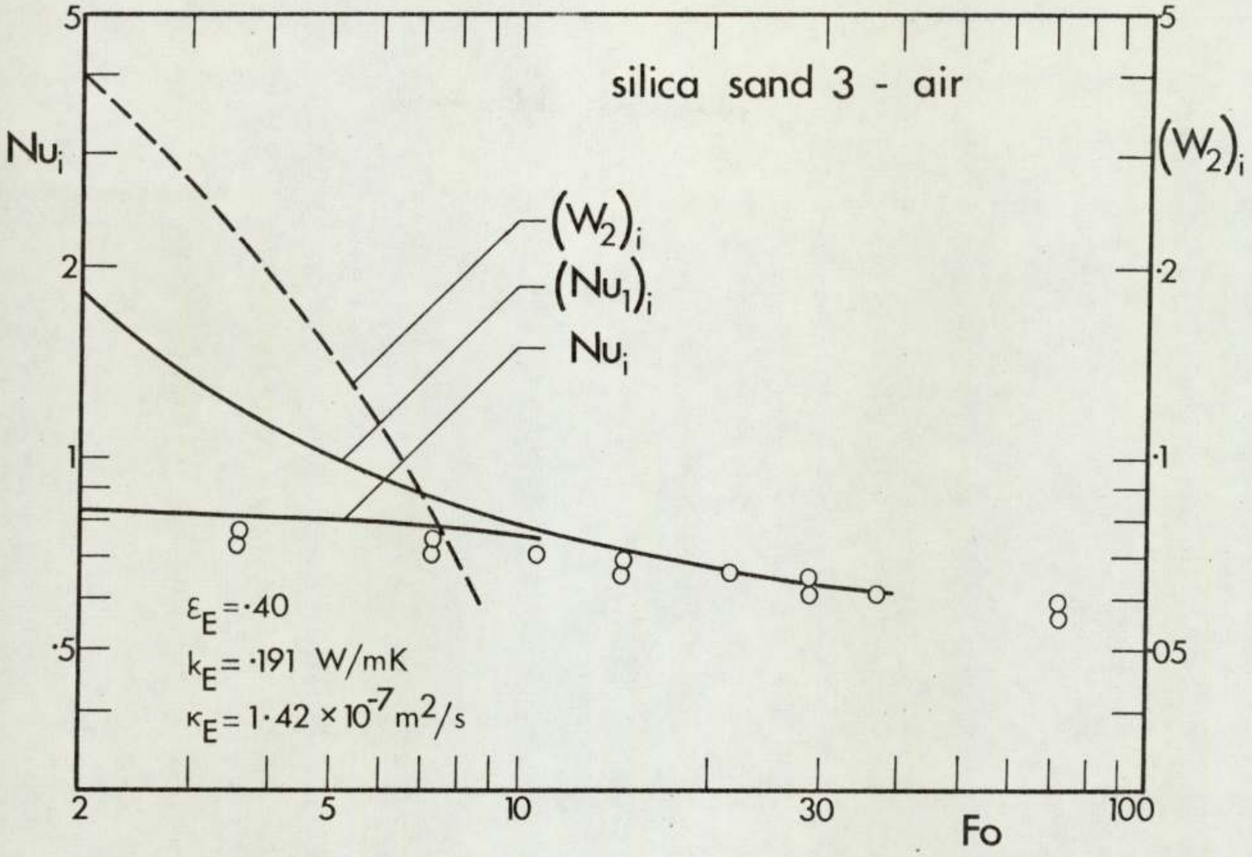

Fig. 6.19: Instantaneous bubble induced heat transfer from the wire into an incipiently fluidized bed of silica sand 3 - air.

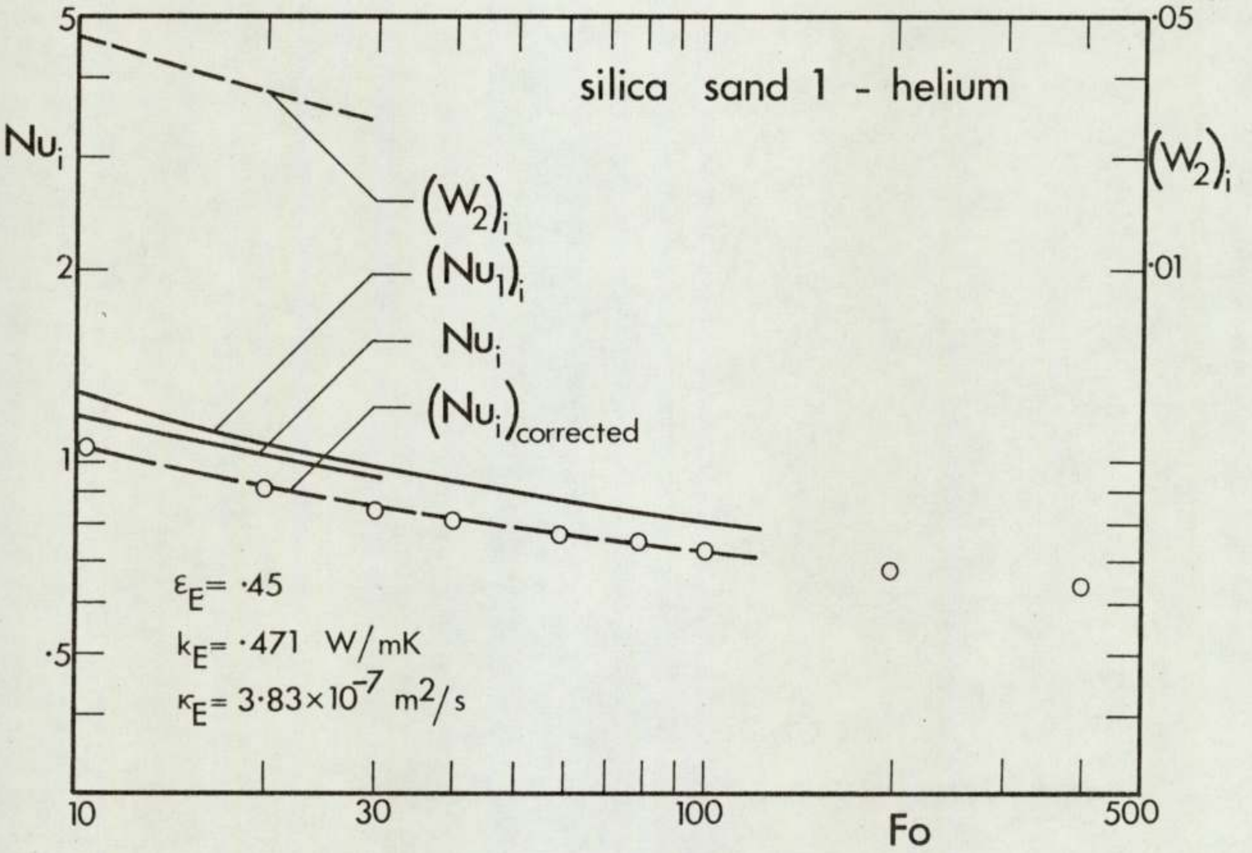

Fig. 6.20: Instantaneous bubble induced heat transfer from the wire into an incipiently fluidized bed of silica sand 1 - helium.

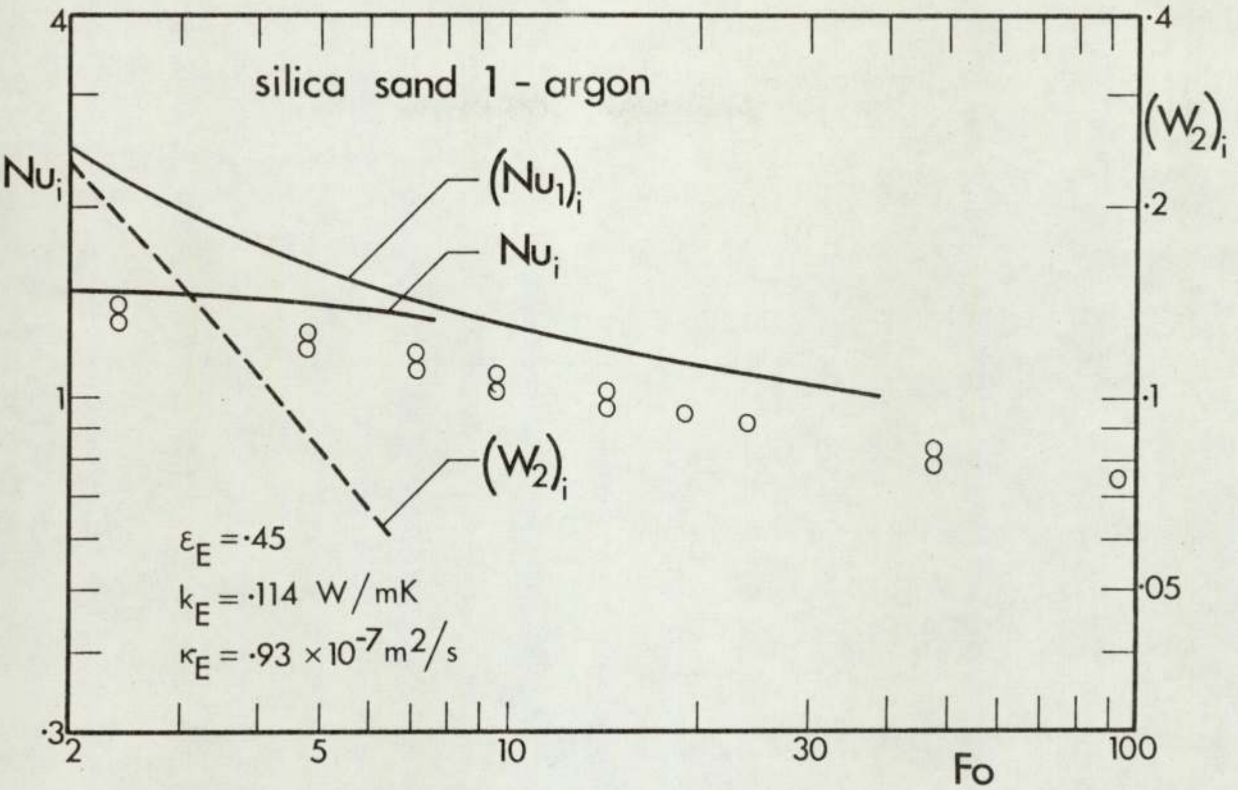

Fig. 6.21: Instantaneous bubble induced heat transfer from the wire into an incipiently fluidized bed of silica sand 1 - argon.

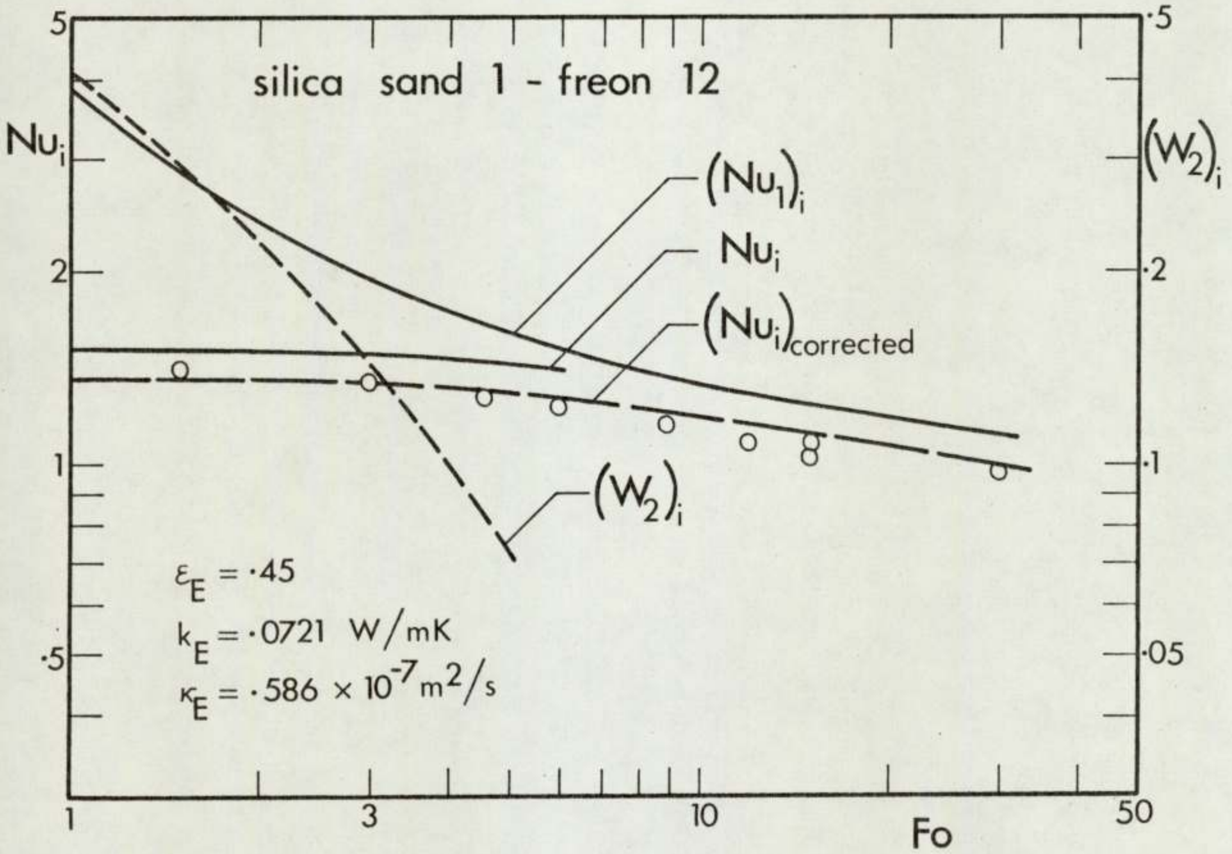

Fig. 6.22: Instantaneous bubble induced heat transfer from the wire into an incipiently fluidized bed of silica sand 1 - freon 12.

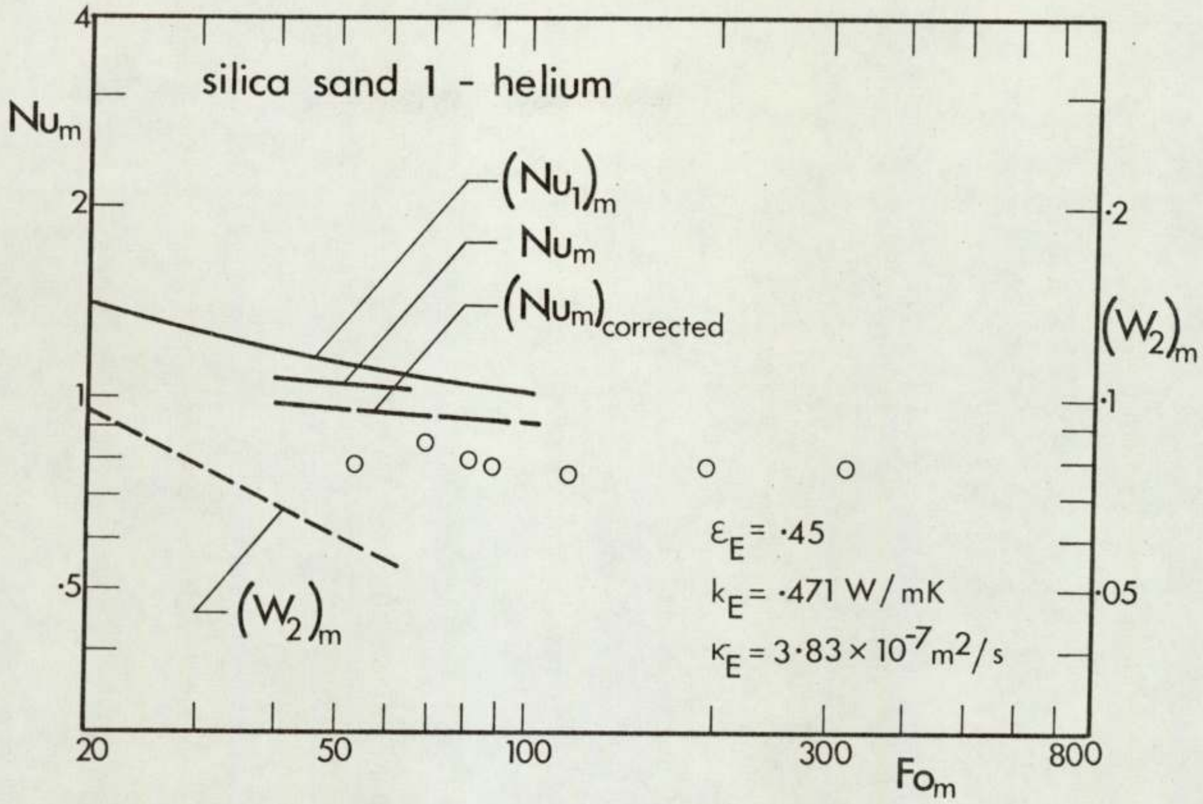

Fig. 6.23: Time-mean bubble induced heat transfer from the wire into an incipiently fluidized bed of silica sand 1 - helium.

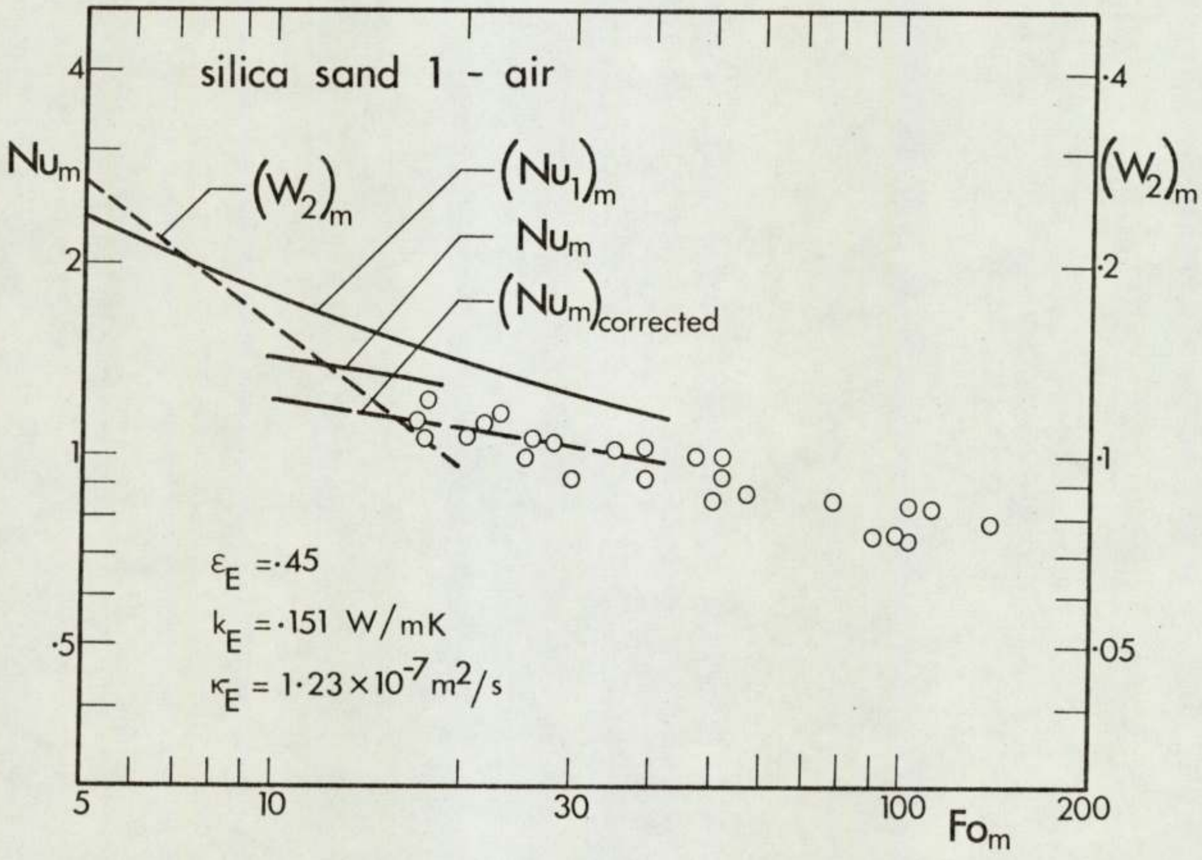

Fig. 6.24: Time-mean bubble induced heat transfer from the wire into an incipiently fluidized bed of silica sand 1 - air.

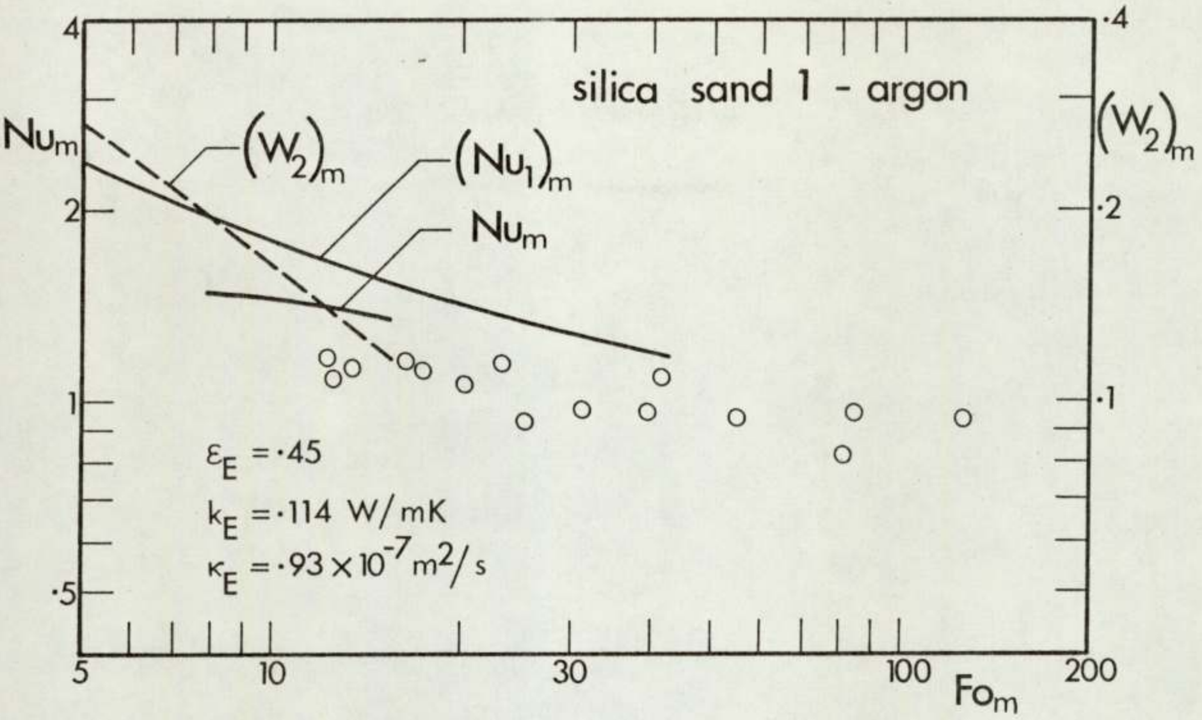

Fig. 6.25: Time-mean bubble induced heat transfer from the wire into an incipiently fluidized bed of silica sand 1 - argon.

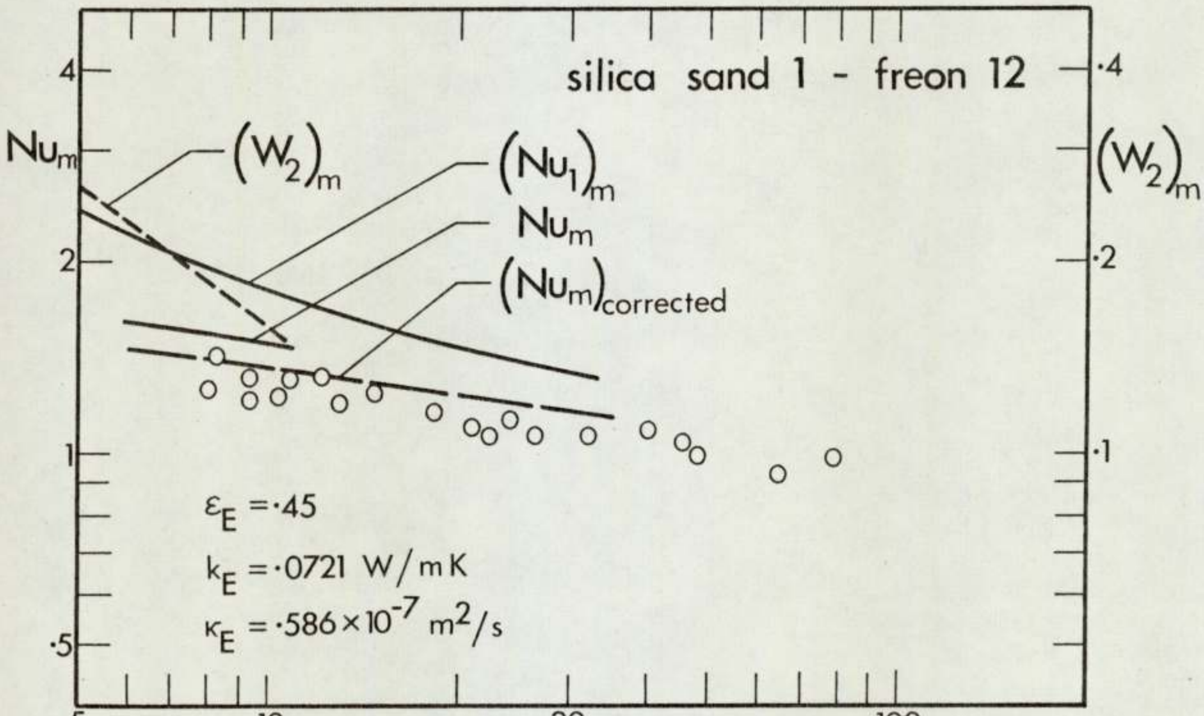

Fig. 6.26: Time-mean bubble induced heat transfer from the wire into an incipiently fluidized bed of silica sand 1 - freon 12.

References.

1. AGRAWAL S. & ZIEGLER E.N., On the optimum transfer coefficient at an exchange surface in a gas-fluidized bed, Chem.Engng.Sci. 24, 1235-40 (1969)

2. ANTONISHIN N.V., SIMCHENKO L.Y. & GORBACHEV L.V., Features of unsteady heat transfer in high rate short duration thermal action, Nauka i Technika Press, Minsk USSR, 5, 3-24 (1968)

3. BASKAKOV A.P., The mechanism of heat transfer between a fluidized bed and a surface, Intern.Chem.Engng. 4 (2), 320-323 (1964)

4. BASKAKOV A.P., Transfer of heat from an isothermal surface to a continuous flow of dispersed medium, Heat Transfer-Soviet Research 1 (6), 103-107 (1969)

5. BASKAKOV A.P. & SUPRUN V.M., The determination of the convective component of the coefficient of heat transfer to a gas in a fluidized bed, Intern.Chem.Engng. 12 (1), 53-55 (1972)

6. BENENATI R.F. & BROSILOW C.B., Void fraction distribution in beds of spheres, A.I.Ch.E. J. 8, 359-361 (1962)

7. BIOT M.A., Variational Principles in Heat Transfer, Oxford University Press (1970)

8. BOTTERILL J.S.M., BUTT M.H.D., CAIN G.L. & REDISH K.A., The effect of gas and solid properties on the rate of heat transfer to gas fluidized beds, Proceedings of the International Symposium on Fluidization, p.442, Netherlands University Press, Amsterdam (1967)

9. BOTTERILL J.S.M. & DESAI M., Limiting factors in gas fluidized bed heat transfer, Powder Technol. 6, 231-238 (1972)

10. BOTTERILL J.S.M. & WILLIAMS J.R., The mechanism of heat transfer to gas fluidized beds, Trans.Instn.Chem.Engrs. 41, 217-230 (1963)

11. BRADSHAW P. & JOHNSON R.F., Turbulence Measurements with Hot Wire Anemometers, Nat.Phys.Lab., HMSO London (1963)

12. BUTT M.H.D., The Effect of Particle Properties on Heat Transfer to Gas Fluidized Beds, Ph.D. Thesis, Dept. Chem. Engng., University of Birmingham, Dec. (1966)

13. CAIN. G.L., Heat Transfer to Gas Fluidized Beds, Ph.D. Thesis, Dept. Chem. Engng., University of Birmingham, June (1966)

14. CARSLAW H.S. & JAEGER J.C., Operational Methods in Applied Mathematics, Oxford University Press (1941)

15. CARSLAW H.S. & JAEGER J.C., Conduction of Heat in Solids, 2nd ed., Oxford University Press (1959)

16. CHUNG B.T.F., FAN L.T. & HWANG C.L., A model of heat transfer in fluidized beds, J. Heat Transfer, Feb., 105-110 (1972)

17. DAVIDSON J.F. & HARRISON D., Fluidized Particles, Cambridge University Press (1963)

18. DAVIDSON J.F. & HARRISON D., Fluidization, Academic Press, London and New York (1971)

19. DAVIES L. & RICHARDSON J.F., Gas interchange between bubbles and the continuous phase in a fluidized bed, Instn.Chem.Engrs.Trans. 44, 293-305 (1966)

20. DESAI M., Limiting Factors in Gas Fluidized Bed Heat Transfer, Ph.D. Thesis, Dept. Chem. Engng., University of Birmingham, Sept. (1970)

21. DUNSKY V.D., ZABRODSKY S.S. & TAMARIN A.I., On mechanism of heat transfer between a surface and a bed of moving particles, Proc. 3rd Intern. Heat Transfer Conf. AIChE, 3, 293-297 (1966)

22. ECKERT E.R.G. & DRAKE R.M., Analysis of Heat and Mass Transfer, McGraw-Hill, N.Y. and London (1972)

23. ERDELYI A. & KERMACK W.O., Note on the equation..., Proc. Camb. Phil. Soc. 41, 74-75 (1945)

24. ERNST R., Der Mechanismus des Warmeuberganges an Warmeaustauschern in Fliessbetten, Chem.Ing.Tech. 31, 166-173 (1959)

25. FURUKAWA J. & OHMAE T., Liquidlike properties of fluidized systems, Ind.Engng.Chem. 50, 821-828 (1958)

26. GABOR J.D., Wall-to-bed heat transfer in fluidized and packed beds, Chem.Engng.Progr.Symp. Series 66 (105), 76-86 (1970)

27. GELDART D., The Behaviour of Freely Bubbling Fluidized Beds. Ph.D. Thesis, University of Bradford, Nov. (1971)

28. GODARD K. & RICHARDSON J.F., Bubble velocities and bed expansions in freely bubbling fluidized beds, Chem.Engng.Sci 24, 663-670 (1969)

29. GRACE J.R., The viscosity of fluidized beds, Canad. J. Chem. Engng. 48, 30-33 (1970)

30. HAMPSHIRE L.N., The Effect of Gas Properties on Wall to Bed Heat Transfer in a Flowing Bed, M.Sc. Thesis, Dept. Chem. Engng., University of Birmingham, Sept. (1967)

31. HARAKAS N.K. & BEATTY K.O., Effect of interstitial gas with fine particles, Chem.Engng.Progr.Symp. Series 59 (41), 122-128 (1963)

32. HIGBIE R., The rate of absorption of a pure gas into a still liquid during short periods of exposure, AIChE Trans. 31, 365-389 (1935)

33. HILDEBRAND F.B. Finite-difference Equations and Simulations, Englwood Cliffs: Prentice-Hall (1968)

34. HUGHES E., Electrical Technology, 4th ed. Longmans, London (1969)

35. JACKSON M.A., The mechanism of fluidized beds: Part I: The stability of the state of uniform fluidization, Instn.Chem.Engrs. Trans. 41, 13-21 (1963)

36. JAEGER J.C., Conduction of heat in a solid in contact with a thin layer of a good conductor, Quart.J.Mech.Appl.Math. 8, 101-106 (1955)

37. KONDUKOV N.B., KORNILAEV A.N., SKACHKO I.M., AKHROMENKOV A.A. & KRUGLOV A.S., An investigation of the parameters of moving particles in a fluidized bed by a radioisotopic method, Intern.Chem.Engng. 4, 43-47 (1964)

38. KOPPEL L.B., PATEL R.D. & HOLMES J.T., Statistical model for surface renewal in heat and mass transfer: Part I. Dependence of average transport coefficients on age distribution, A.I.Ch.E. J. 12 (5), 941-946 (1966)

39. KOROLEV V.N. & SYROMYATNIKOV N.Y., Heat transfer from a surface to a fluidized bed, Heat Transfer-Soviet Research 3 (4), 112-116 (1971)

40. KOROLEV V.N., SYROMYATNIKOV N.Y. & TOLMACHEV E.M., Structure of a fixed and a fluidized granular bed near a wall immersed into it, J. Engng. Physics 21 (6), 973 (1971)

41. KUBIE J., Heat transfer in two-phase gas/liquid systems, Proc. Symp. on Multi-Phase Flow Systems, I.Mech.E. & I.Chem.E., Glasgow, April (1974)

42. KUNII D. & LEVENSPIEL O., Fluidization Engineering, John Wiley & Sons, N.Y. (1969)

43. KUNII D. & SMITH J.M., Heat transfer characteristics of porous rocks, A.I.Ch.E. J. 6, 71-78 (1960)

44. LEVA M., Fluidization, McGraw-Hill, N.Y. (1959)

45. McADAMS W.H., Heat Transmission, 3rd ed. McGraw-Hill (1954)

46. MICKLEY H.S. & FAIRBANKS D.F., Mechanism of heat transfer to fluidized beds, A.I.Ch.E. J. 1, 374-384 (1955)

47. MICKLEY H.S., FAIRBANKS D.F. & HAWTHORN R.D., The relation between the transfer coefficient and thermal fluctuations in fluidized bed heat transfer, Chem.Engng.Progr.Symp. Series 32 (57), 51-60 (1961)

48. MURRAY J.D., On the mathematics of fluidization, Part 2. Steady motion of fully developed bubbles., J.Fluid Mech. 22 (part 1), 57-80 (1965)

49. PIGFORD R.L. & BARON T., Hydrodynamic stability of a fluidized bed, Ind.Engng.Chem.Fund. 4, 81-87 (1965)

50. REKTORYS K., Survey of Applicable Mathematics, ILIFFE, London (1969)

51. RIDGWAY K. & TARBUCK K.J., The random packing of spheres, Brit.Chem. Engng. 12 (3), 384-388 (1967)

52. ROBLEE L.H.S., BAIRD R.M. & TIERNEY J.W., Radial porosity variations in packed beds, A.I.Ch.E. J. 4, 460-464 (1958)

53. SCHUGERL K., MERZ M. & FETTING F., Rheologische Eigenschaften von gasdurchstromten Fliessbettensystemen, Chem.Engng.Sci. 15, 1-38 (1961)

54. SHIRAI T., YASHITOME H., SHAJI Y., TANAKA S., HOJO K. & YOSHIDA S., Heat and mass transfer on the surface of solid spheres fixed with fluidized beds, Kagaku Kogaku (Chem.Engng.Japan) 29, 880-884 (1965)

55. TAMARIN A.I., The origin of self-excited oscillations in fluidized beds, Intern.Chem.Engng. 4, 50-54 (1964)

56. TOOMEY R.D. & JOHNSTONE H.F., Gaseous fluidization of solid particles, Chem.Engng.Progr. 48, 220-226 (1952)

57. TUOT J. & CLIFT R., Heat transfer around single bubbles in a two-dimensional fluidized bed, Chem.Engng.Progr.Symp. Series 69 (128), 78-83 (1973)

58. VREEDENBERG H.A., Heat transfer between a fluidized bed and a horizontal tube, Chem.Engng.Sci. 9, 52-60 (1958)

59. WILHELM R.H. & KWAUK M., Fluidization of solid particles, Chem.Engng. Progr. 44, 201-218 (1948)

60. WILLIAMS J.A. & SMITH V.C., Heat transfer in mechanically stirred gas-fluidized systems, Symposium on Fluidization and Fluid Particle Technology, Part I., 61st Annual Meating AIChE, Los Angeles, Dec. (1968)

61. YOSHIDA K., KUNII D. & LEVENSPIEL O., Heat transfer mechanism between wall surface and fluidized bed, Int.J.Heat Mass Transfer 12, 529-536 (1969)

Appendix 1.

EQUIVALENT CONDUCTIVITY OF THE FIRST SLAB.

Constant flux condition at the surface of the heat transfer probe is given by equation (3.8) as

$$\frac{\partial W}{\partial Z} = - \frac{1}{b(0)} \quad . \qquad (A1.1)$$

Equation (A1.1) is valid only at the surface of the heat transfer probe (Z = 0). If a finite difference numerical method is used, with a finite material slab thickness, equation (A1.1) is not applicable and must be modified as

$$\frac{\partial W}{\partial Z} = - \frac{1}{b_{eq}} \quad , \qquad (A1.2)$$

where b_{eq} is the equivalent dimensionless thermal conductivity of the first slab (Figure 3.4).

Referring to Figure 3.4, the temperature at the wall, W(0), can be calculated from temperature W(ΔZ) at point Z = ΔZ as[15]

$$W(0) = W(\Delta Z) + \frac{\Delta Z}{b_{eq}} \quad . \qquad (A1.3)$$

Equation (A1.3) is based on the assumption that the first slab of material remains at steady state throughout the heating process. The same assumption can be applied on a material slab of variable conductivity by solving the following equations:

$$\frac{d}{dZ} [b(Z) \frac{dW}{dZ}] = 0 \qquad (A1.4)$$

subject to

$$Z = 0 \qquad -b(0) \frac{dW}{dZ} = 1 \qquad (A1.5)$$

$$Z = \Delta Z \qquad W = W(\Delta Z) \tag{A1.6}$$

It is further assumed that, because the slab thickness is small compared with the particle diameter, the variation of the dimensionless thermal conductivity can be, in the first slab, approximated by a linear function satisfying the following conditions:

$$Z = 0 \qquad b(Z) = b(0) \tag{A1.7}$$

$$Z = \Delta Z \qquad b(Z) = b(\Delta Z) \tag{A1.8}$$

The function $b(Z)$ can then be approximated in the first slab by

$$b(Z) = b(0) + \frac{b(\Delta Z) - b(0)}{\Delta Z} Z \quad . \tag{A1.9}$$

The solution of equation (A1.4) subject to equations (A1.5) and (A1.6) with $b(Z)$ given by equation (A1.9) is

$$W(Z) = W(\Delta Z) + \frac{\Delta Z}{b(\Delta Z) - b(0)} \ln \frac{\Delta Z + \dfrac{b(0)\ \Delta Z}{b(\Delta Z) - b(0)}}{Z + \dfrac{b(0)\ \Delta Z}{b(\Delta Z) - b(0)}} \ , \tag{A1.10}$$

from which the wall temperature $W(0)$ can be calculated as

$$W(0) = W(\Delta Z) + \frac{\Delta Z}{b(\Delta Z) - b(0)} \ . \ \ln \frac{b(\Delta Z)}{b(0)} \quad . \tag{A1.11}$$

Finally comparing equations (A1.3) and (A1.11), the expression for the equivalent dimensionless thermal conductivity of the first slab is obtained as

$$b_{eq} = \frac{b(\Delta Z) - b(0)}{\ln \dfrac{b(\Delta Z)}{b(0)}} \quad . \tag{A1.12}$$

Appendix 2.

SPACE AVERAGE WIRE TEMPERATURE.

The wire used in the present work is made of platinum. Because the wire temperature fluctuations are small, the relationship between the wire temperature and the wire resistance may be approximated with sufficient accuracy by a linear function. It is assumed that the radial distribution of temperature within the wire is uniform (Section 4.3.2); hence the wire temperature and wire resistance vary along the wire length only.

Let R_∞ and R_W be the values of wire resistance per unit length at temperatures T_∞ and T_W respectively and let α be a temperature coefficient of resistance of the wire material.

Then

$$R_W - R_\infty = \alpha(T_W - T_\infty) \qquad \text{(A2.1)}$$

and because the wire resistance per unit length varies along the wire length only, the total wire resistance, R_T, which is measured when the wire is used in the present application, is given by the following expression:

$$R_T = \int_{-L}^{L} R_W \, dx \qquad \text{(A2.2)}$$

The total wire resistance, R_T, corresponds to a space-average wire resistance per unit length, R_a, defined by

$$R_a = \frac{1}{2L} R_T \qquad \text{(A2.3)}$$

and to a space-average wire temperature, T, defined by

$$R_a - R_\infty = \alpha(T - T_\infty) \quad . \qquad \text{(A2.4)}$$

Comparing equations (A2.1), (A2.2), (A2.3) and (A2.4), the space-average wire temperature is finally obtained as

$$T = \frac{1}{2L} \int_{-L}^{L} T_W \, dx \quad . \qquad \text{(A2.5)}$$

Appendix 3.

SIMPLIFICATION OF EQUATIONS (4.16) TO (4.25).

Since the wire is approximated by a finite rod with uniform radial temperature distribution, equations (4.17) and (4.25) are not applicable. Energy balance on an element of the wire shows that for

$t \geq 0,\ r = a,\ |x| \leq L$

$$\frac{k_W}{\kappa_W}\frac{\partial T_{W1}}{\partial t} = k_W \frac{\partial^2 T_{W1}}{\partial x^2} - \frac{2}{a} f_S + Q \tag{A3.1}$$

where f_S is the heat flux which is being dissipated from the outer surface of the probe wire by conduction into the surrounding dense phase and hence

$$f_S = - k(a)\left[\frac{\partial T_{D1}}{\partial r}\right]_{r=a} \quad . \tag{A3.2}$$

Equation (A3.2) is substituted into equation (A3.1):

$$\frac{1}{\kappa_W}\frac{\partial T_{W1}}{\partial t} = \frac{\partial^2 T_{W1}}{\partial x^2} + \frac{2k(a)}{ak_W}\left[\frac{\partial T_{D1}}{\partial r}\right]_{r=a} + \frac{Q}{k_W} \quad . \tag{A3.3}$$

Equation (4.24) is then substituted into equation (A3.3) to obtain for

$t \geq 0,\ r = a,\ |x| \leq L$

$$\frac{1}{\kappa_W}\frac{\partial T_{D1}}{\partial t} = \frac{\partial^2 T_{D1}}{\partial x^2} + \frac{2k(a)}{ak_W}\frac{\partial T_{D1}}{\partial r} + \frac{Q}{k_W} \quad . \tag{A3.4}$$

Equation (A3.4) constitutes an additional boundary condition for equation (4.16). Hence the wire and the dense phase temperatures are uncoupled and the dense phase temperature can be obtained by solving equation (4.16) subject to equations (4.18), (4.20), (4.22) and (A3.4).

The wire temperature, T_{W1}, is calculated from equation (4.24) as

$$T_{W1} = [T_{D1}]_{r=a}. \tag{A3.5}$$

Appendix 4.

METHOD OF NUMERICAL SOLUTION OF EQUATIONS (4.41) TO (4.45).

First it is assumed that functions H(R) and L(R) are known. The grid used for the numerical calculation is shown in Figure A4.1. Since the probe and the surrounding dense phase are symmetric about a plane parallel to the copper supports and passing through the origin (Figure 4.1), only one half of the whole domain is considered. Subscripts x and y refer to the R- and Z-coordinate respectively and superscript p refers to time such that

$$Fo = \Delta Fo \cdot p \tag{A4.1}$$

and all the remaining notation is shown in Figure A4.1. To make the notation in this Appendix simpler, symbol W is used instead of W_{D1}.

All derivatives are rewritten, using a standard difference technique[15], as follows:

$$\frac{\partial W^p_{x,y}}{\partial Fo} = \frac{W^{p+1}_{x,y} - W^p_{x,y}}{\Delta Fo} \tag{A4.2}$$

$$\frac{\partial W^p_{x,y}}{\partial R} = \frac{W^p_{x+1,y} - W^p_{x,y}}{2\ \Delta R} \tag{A4.3}$$

$$\frac{\partial^2 W^p_{x,y}}{\partial R^2} = \frac{W^p_{x+1,y} - 2W^p_{x,y} + W^p_{x-1,y}}{(\Delta R)^2} \tag{A4.4}$$

$$\frac{\partial^2 W^p_{x,y}}{\partial Z^2} = \frac{W^p_{x,y+1} - 2W^p_{x,y} + W^p_{x,y-1}}{(\Delta Z)^2} \tag{A4.5}$$

Using the notation

$$M = \frac{\Delta Fo}{(\Delta R)^2} \tag{A4.6}$$

$$N = \frac{(\Delta R)^2}{(\Delta Z)^2} \quad , \tag{A4.7}$$

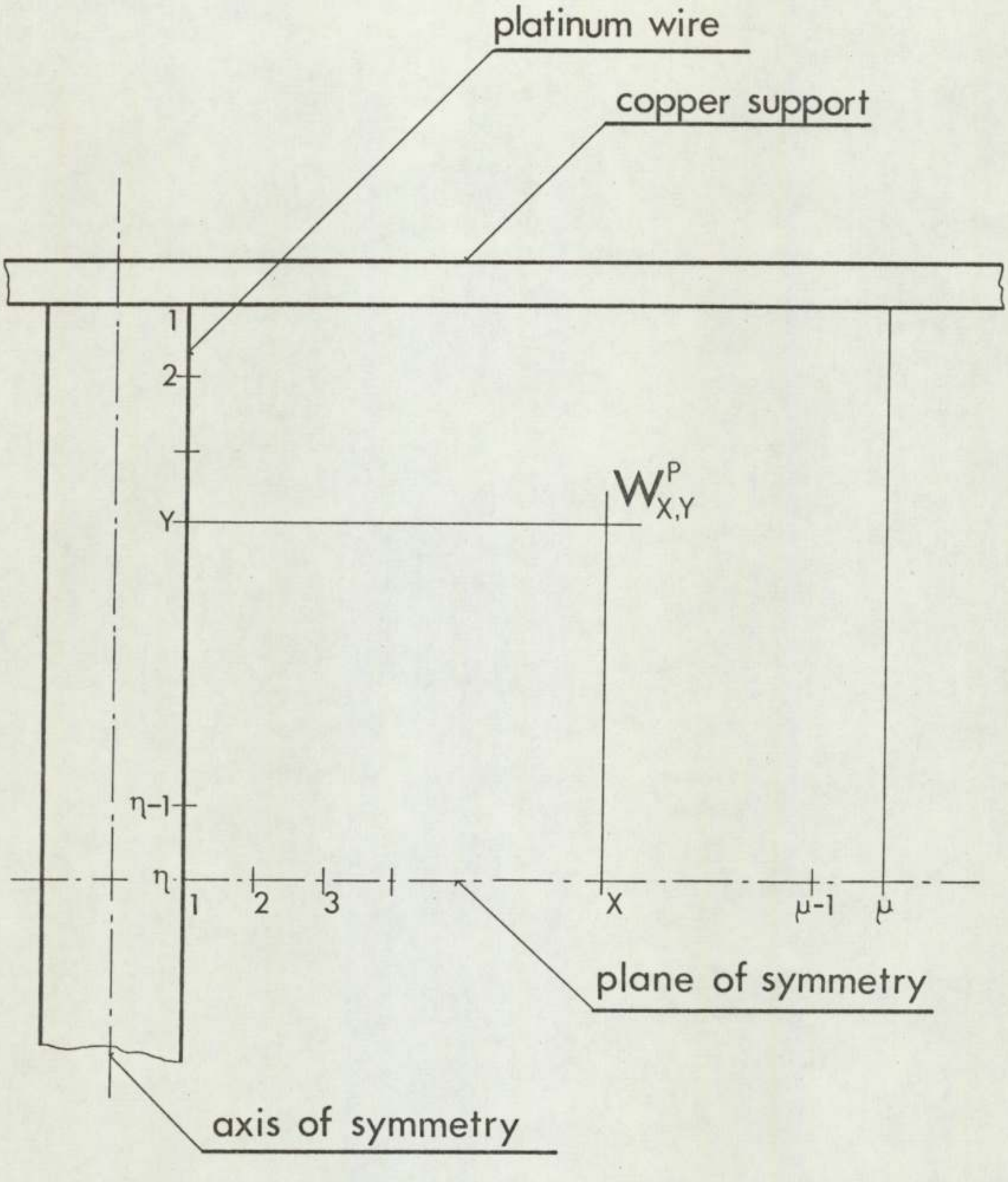

Fig. A4.1: Grid used for the numerical calculation.

the following system of equations can be substituted for equations (4.41) to (4.45):

$p = 0,\ 1 \le x \le \mu,\ 1 \le y \le \eta$

$$W^0_{x,y} = 0 \tag{A4.8}$$

$p \ge 0,\ 1 < x < \mu,\ 1 < y < \eta$

$$W^{p+1}_{x,y} = W^p_{x+1,y}[C_1(x)+C_2(x)+C_3(x)]+W^p_{x-1,y}[C_2(x)-C_1(x)-C_3(x)] + [W^p_{x,y+1}+W^p_{x,y-1}]C_4(x)+W^p_{x,y}[1-2\{C_2(x)+C_4(x)\}] \tag{A4.9}$$

$p \ge 0,\ x = 1,\ 1 < y < \eta$

$$W^{p+1}_{1,y} = W^p_{1,y}[1-2(C_5+C_6)]+[W^p_{1,y+1}+W^p_{1,y-1}]C_5+C_6W^p_{2,y}+C_7 \tag{A4.10}$$

$p \ge 0,\ 1 \le x \le \mu,\ y = 1$

$$W^p_{x,1} = 0 \tag{A4.11}$$

$p \ge 0,\ x = \mu,\ 1 < y \le \eta$

$$W^p_{\mu,y} = W^p_{\mu-1,y} \tag{A4.12}$$

$p \ge 0,\ 1 \le x \le \mu,\ y = \eta$

$$W^p_{x,\eta} = W^p_{x,\eta-1} \tag{A4.13}$$

where

$$C_1(x) = M\cdot\Delta R\cdot L(x)/2 \tag{A4.14}$$

$$C_2(x) = M\cdot H(x) \tag{A4.15}$$

$$C_3(x) = 0.5M\cdot H(x)\cdot\Delta R/[1+(x-1)\Delta R] \tag{A4.16}$$

$$C_4(x) = M\cdot N\cdot H(x)/A^2 \tag{A4.17}$$

$$C_5 = M\cdot N/(\kappa_0 A^2) \tag{A4.18}$$

$$C_6 = 2M\cdot\Delta R\cdot k_0\cdot b(1)/\kappa_0 \tag{A4.19}$$

$$C_7 = M\cdot k_0\cdot(\Delta R)^2/\kappa_0 \tag{A4.20}$$

Similarly to Section 3.4.1, it is desirable to redefine the constant C_6. Equation (4.45) is valid only at the surface of the probe wire. In order to solve the difference equations accurately, very small space (and hence time) increments must be used, because the function b(Z) varies very rapidly near the surface. In order to overcome this complication, while not sacrificing much accuracy, the equivalent thermal conductivity of the first slab, b_{eq}, is used (see Section 3.4.1). Hence equation (A4.19) is redefined as

$$C_6 = 2M\cdot\Delta R\cdot k_0\cdot b_{eq}/\kappa_0 \quad , \tag{A4.21}$$

where b_{eq} is calculated as in Appendix 1, but the curvature of the first slab is also taken into account. The equation to be solved is

$$\frac{d}{dR}\,[R\cdot b(R)\cdot\frac{dW}{dR}] = 0 \tag{A4.22}$$

subject to

$$R = 1 \qquad -b(1)\frac{dW}{dR} = 1 \tag{A4.23}$$

$$R = 1 + \Delta R \qquad W = W(1 + \Delta R) \tag{A4.24}$$

and where $b(R)$ is approximated by a linear function (Appendix 1) which satisfies the following conditions:

$$R = 1 \qquad b(R) = b(1) \tag{A4.25}$$

$$R = 1 + \Delta R \qquad b(R) = b(1+\Delta R) \tag{A4.26}$$

Hence function $b(R)$ can be calculated and equations (A4.22) to (A4.24) can be solved. Similarly to Appendix 1, the equivalent dimensionless thermal conductivity of the first slab can then be defined as

$$b_{eq} = \frac{\Delta R\cdot e_2}{\ln\dfrac{(1+e_3)(1+\Delta R)}{1+e_3+\Delta R}} \tag{A4.27}$$

where

$$e_1 = [b(1+\Delta R)-b(1)]/\Delta R \tag{A4.28}$$

$$e_2 = b(1)-e_1 \tag{A4.29}$$

$$e_3 = e_2/e_1 \quad . \tag{A4.30}$$

Next by standard methods[33], convergence conditions are determined as

$$\Delta R \le \frac{2}{\dfrac{1}{1+(x-1)\Delta R} + \dfrac{L(x)}{H(x)}} \tag{A4.31}$$

$$M \le \min\{\ \frac{1}{2H(x)\,[1+N/A^2]}\ ;\ \frac{1}{2\,[N/\kappa_0 A^2 + \Delta R\cdot k_0\cdot b_{eq}/\kappa_0]}\ \}. \tag{A4.32}$$

For each time interval, the temperature field is calculated until a point (on the plane of symmetry) is reached at which the dimensionless temperature, W, becomes smaller than 10^{-10}. At this point the calculation is terminated and restarted for the next time interval. It has been found that the accuracy of the numerical solution is relatively insensitive to the size of ΔR-increments and $\Delta R = 0.25$ or 0.2 can be used to achieve sufficient accuracy. On the other hand, the accuracy of the solution is very sensitive to the size of ΔZ-increments, but too small values of ΔZ step-size require very large computer times. Hence a compromise has been reached by using $\Delta Z = 0.33333$ or $\Delta Z = 0.25$. The error is then kept below 5% (as confirmed by decreasing the ΔZ step-size to obtain a check).

The instantaneous wire temperature is defined by equation (A3.5). The instantaneous space-average wire temperature is calculated from equation (4.1) and the time-mean space-average wire temperature from equation (4.57).

Appendix 5.

METHOD OF SOLUTION OF EQUATIONS (4.58) TO (4.62).

Equation (4.58) subject to equations (4.59) to (4.62) was first solved by Jaeger[36], who obtained a solution for the maximum instantaneous temperature only. Despite an extensive literature search, the author has been unable to find a complete solution to the problem. The solution of equations (4.58) to (4.62) is, in principle, simple and will be shown only briefly. It is more convenient to use the original notation given by equations (4.36) to (4.40), which for the present case simplify to:

$t \geq 0,\ r \geq a,\ |x| \leq L$

$$\frac{\partial T_{L1}}{\partial t} = \kappa_L\left(\frac{\partial^2 T_{L1}}{\partial r^2} + \frac{1}{r}\frac{\partial T_{L1}}{\partial r} + \frac{\partial^2 T_{L1}}{\partial x^2} \right) \qquad \text{(A5.1)}$$

subject to

$$t = 0,\ r \geq a,\ |x| \leq L \qquad T_{L1} = 0 \qquad \text{(A5.2)}$$

$$t \geq 0,\ r \geq a,\ |x| = L \qquad T_{L1} = 0 \qquad \text{(A5.3)}$$

$$t \geq 0,\ r \geq a,\ x = 0 \qquad \frac{\partial T_{L1}}{\partial x} = 0 \qquad \text{(A5.4)}$$

$$t \geq 0,\ r = a,\ |x| \leq L \qquad \frac{1}{\kappa_W}\frac{\partial T_{L1}}{\partial t} = \frac{\partial^2 T_{L1}}{\partial x^2} + \frac{2k_L}{ak_W}\frac{\partial T_{L1}}{\partial r} + \frac{Q}{k_W} \qquad \text{(A5.5)}$$

First, the Laplace Transformation of equations (A5.1) to (A5.5) with respect to time is

$$r \geq a,\ |x| \leq L \qquad \frac{\partial^2 \Phi}{\partial r^2} + \frac{1}{r}\frac{\partial \Phi}{\partial r} - q^2\Phi + \frac{\partial^2 \Phi}{\partial x^2} = 0 \qquad \text{(A5.6)}$$

subject to

$$r \geq a,\ |x| = L \qquad \Phi = 0 \qquad \text{(A5.7)}$$

$$r \geq a,\ x = 0 \qquad \frac{\partial \Phi}{\partial x} = 0 \qquad \text{(A5.8)}$$

$$r = a,\ |x| \leq L \qquad \frac{p}{\kappa_W}\Phi = \frac{\partial^2 \Phi}{\partial x^2} + \frac{2k_L}{ak_W}\frac{\partial \Phi}{\partial r} + \frac{Q}{pk_W} \qquad \text{(A5.9)}$$

where Φ is the Laplace Transformation of T_{L1} defined by

$$\Phi = \int_0^\infty e^{-pt} \, T_{L1} \, dt \tag{A5.10}$$

and

$$q^2 = \frac{p}{\kappa_L} \quad . \tag{A5.11}$$

Next Φ and 1 are expanded using a cosine Fourier series

$$\Phi = \sum_{n=0}^{\infty} R_n(r) \cos \frac{sx}{L} \tag{A5.12}$$

$$1 = 2 \sum_{n=0}^{\infty} \frac{(-1)^n}{s} \cos \frac{sx}{L} \tag{A5.13}$$

where $R_n(r)$ is a function of r only and

$$s = \frac{2n + 1}{2} \pi \quad . \tag{A5.14}$$

Equations (A5.12) and (A5.13) are substituted into equations (A5.6) to (A5.9) which must be identically satisfied for all values of x. This is possible only if for

$$r \geq a \qquad \frac{d^2R_n}{dr^2} + \frac{1}{r}\frac{dR_n}{dr} - \left(q^2 + \frac{s^2}{L^2}\right) R_n = 0 \tag{A5.15}$$

subject to

$$r = a \qquad \frac{p}{\kappa_W} R_n = - \frac{s^2}{L^2} R_n + \frac{2k_L}{ak_W}\frac{dR_n}{dr} + \frac{2Q}{pk_W} \frac{(-1)^n}{s} \quad . \tag{A5.16}$$

Equation (A5.15) is a modified Bessel equation of the zeroth order; using the implied condition that the temperature at infinity is finite, Bessel functions of the first kind are excluded and the solution of equations (A5.15) and (A5.16) is then obtained in the following form:

r ≥ a

$$R_n(r) = \frac{2Q\kappa_W}{psk_W} \frac{(-1)^n \, K_0(\beta r)}{\left[p + \kappa_W \frac{s^2}{L^2}\right] K_0(\beta a) + \frac{2k_L \kappa_W}{ak_W} \beta K_1(\beta a)} \tag{A5.17}$$

where

$$\beta^2 = q^2 + \frac{s^2}{L^2} \tag{A5.18}$$

and $K_0(\beta a)$ and $K_1(\beta a)$ are modified Bessel functions of the second kind.

Substituting (A5.17) into (A5.12) and using the Inversion Theorem for the Laplace Transformation[14], an expression for T_{L1} is then obtained:

$r \geq a, \; |x| \leq L$

$$T_{L1} = \frac{1}{2\pi i}\int_{\gamma-i\infty}^{\gamma+i\infty} e^{pt} \left[\frac{2Q\kappa_W}{pk_W} \sum_{n=0}^{\infty} \frac{1}{s} \frac{(-1)^n K_0(\beta r) \cos\frac{sx}{L}}{(p + \kappa_W\frac{s^2}{L^2})K_0(\beta a) + \frac{2k_L\kappa_W}{ak_W}\beta K_1(\beta a)}\right] dp \quad (A5.19)$$

Reversing the order of integration and summation, using the theorem for the Laplace Transformation of an integral[14] and writing

$$p' = p + \kappa_L \frac{s^2}{L^2} \quad (A5.20)$$

$$(q')^2 = \beta^2 = \frac{p'}{\kappa_L} \quad (A5.21)$$

equation (A5.19) then simplifies to

$$T_{L1} = \frac{2Q\kappa_W}{k_W} \sum_{n=0}^{\infty} \frac{(-1)^n}{s} \cos\frac{sx}{L} \int_0^t \exp[-\kappa_L(\tfrac{s}{L})^2\lambda] w(\lambda)\, d\lambda \quad (A5.22)$$

where

$$w(\lambda) = \frac{1}{2\pi i}\int_{\gamma'-i\infty}^{\gamma'+i\infty} e^{p'\lambda} \frac{K_0(q'r)}{[p' + (\kappa_W - \kappa_L)\frac{s^2}{L^2}]K_0(q'a) + \frac{2k_L\kappa_W}{ak_W} q'K_1(q'a)} dp' \cdot \quad \ldots (A5.23)$$

Because the integrand of (A5.23) has a branch point at the origin, a contour shown in Figure A5.1 is used for evaluating of (A5.23). It is known that if $\kappa_W > \kappa_L$ (which is the case for most liquids) there are no poles of the integrand inside this region and on its boundaries[23]; the integrand is also a single valued function inside the closed contour. It is simple to show that integral (A5.23) round the small circle tends to zero as $r_c \to 0$ and that this integral along the contours A to B and E to F (Figure A5.1) also tends to zero as $R_c \to \infty$. Thus when $r_c \to 0$ and $R_c \to \infty$, integral (A5.23) can be substituted by the sum of real infinite integrals over BC and DE. To obtain the real infinite equivalent of (A5.23), $\kappa_L(\frac{y}{a})^2 e^{-i\pi}$ and $\kappa_L(\frac{y}{a})^2 e^{+i\pi}$ are substituted for p' (equation (A5.20)) on

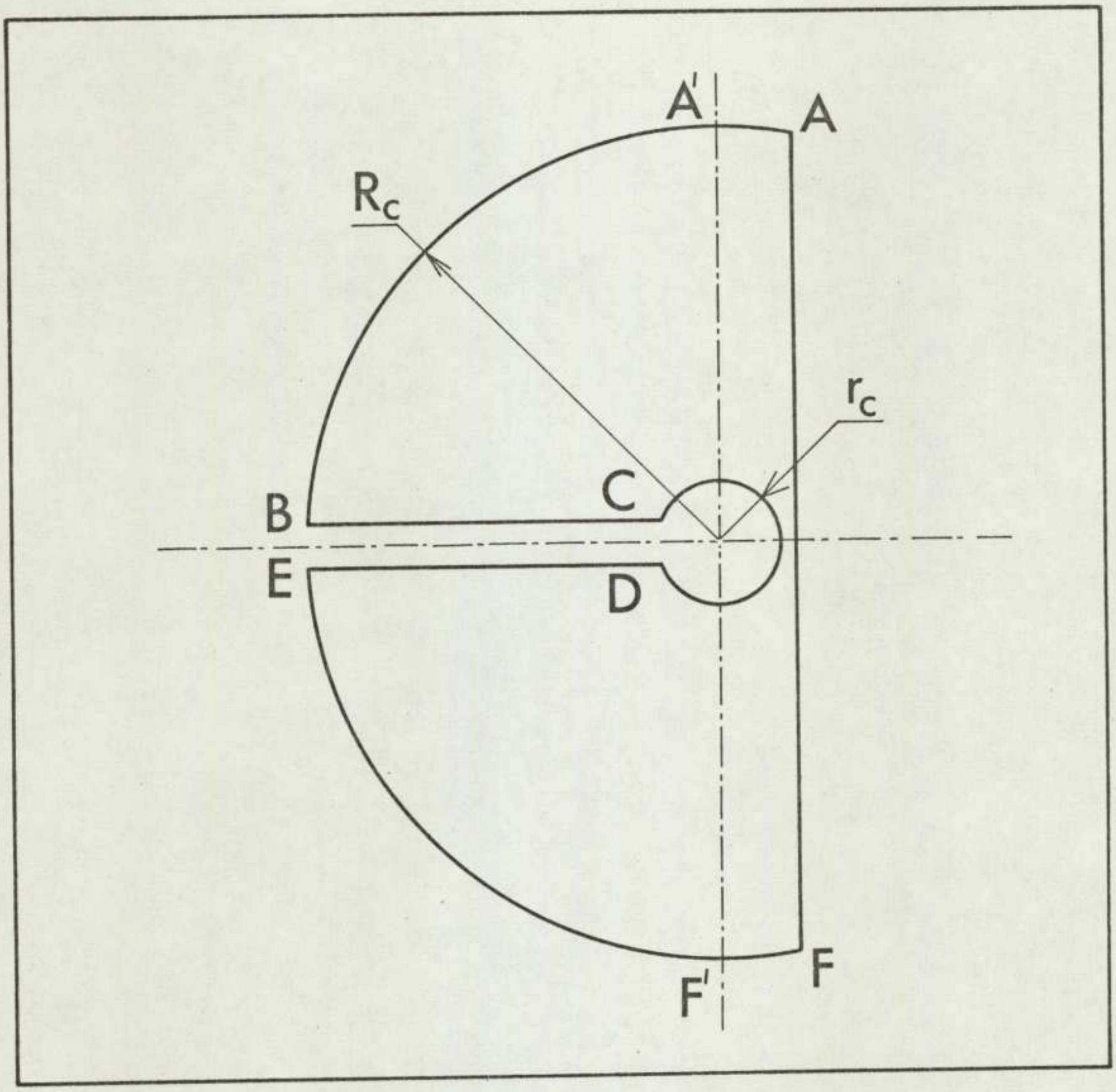

Fig. A5.1: Contour used for the inversion of function (A5.23).

contours (DE) and (BC) respectively (Figure A5.1) and the following identities[15] are used:

$$K_0\left(\frac{r}{a}y\ e^{0.5\pi i}\right) = 0.5\pi i\ \left[-J_0\left(\frac{r}{a}y\right) + iY_0\left(\frac{r}{a}y\right)\right] \tag{A5.24}$$

$$K_1\left(y\ e^{0.5\pi i}\right) = 0.5\pi\ \left[-J_1(y) + iY_1(y)\right] \tag{A5.25}$$

The result is then substituted into equation (A5.22). Changing the order of integrations and finally integrating with respect to time leads to an expression for the temperature field in the medium surrounding the wire in the following form

$t \geq 0,\ r \geq a,\ |x| \leq L$

$$\frac{T_{L1}k_L}{Qa^2} = \sum_{n=0}^{\infty} \frac{(-1)^n}{s} \cos\frac{sx}{L} \int_0^{\infty} \left(1 - e^{-y_1 Fo}\right) \frac{Y_0\left(\frac{r}{a}y\right)\psi - J_0\left(\frac{r}{a}y\right)\phi}{y_1(\phi^2+\psi^2)}\, y\,dy \tag{A5.26}$$

where

$$\phi = yY_1(y) + CY_0(y) \tag{A5.27}$$

$$\psi = yJ_1(y) + CJ_0(y) \tag{A5.28}$$

$$C = \frac{1}{2k_0}\left[\left(\frac{s}{A}\right)^2 - y_1\kappa_0\right] \tag{A5.29}$$

$$y_1 = y^2 + \left(\frac{s}{A}\right)^2 \tag{A5.30}$$

and where y is the integration parameter, Fo is the instantaneous Fourier number and Bessel functions have their usual meanings.

Temperature of the wire is obtained from equation (A5.26) with r=a (equation(A3.5)). Using equation (4.1), the first approximation to the dimensionless instantaneous average wire temperature, $(W_1)_i$, is then calculated as

$$(W_1)_i = \frac{4}{\pi^2} \sum_{n=0}^{\infty} \frac{1}{s^2} \int_0^{\infty} \left[1 - e^{-y_1 Fo}\right] \frac{y\ dy}{y_1(\phi^2 + \psi^2)}\ ; \tag{A5.31}$$

and finally using equation (4.57), the first approximation to the dimensionless time-mean average wire temperature, $(W_1)_m$, is obtained in the following form

$$(W_1)_m = \frac{4}{\pi^2} \sum_{n=0}^{\infty} \frac{1}{s^2} \int_0^{\infty} \left\{1 - \frac{1}{y_1 Fo_m}\left[1 - e^{-y_1 Fo_m}\right]\right\} \frac{y dy}{y_1(\phi^2 + \psi^2)}\ . \tag{A5.32}$$

Appendix 6.

CALIBRATION OF THE UV-RECORDER TRACES.

In Figure A6.1, R denotes the resistance of the probe, R_R the resistance of the centre branch (including the galvanometer) and the other resistances refer to the remaining branches. The bridge is originally balanced so that

$$R \cdot R_3 = R_2 \cdot R_4 \tag{A6.1}$$

$$I_R = 0 \tag{A6.2}$$

and the equilibrium average wire temperature ,T, is determined from the resistance R_2 and the wire calibration curve. Let the average wire temperature increase by δT. This causes an increase of the wire resistance by δR from R to R + δR. The current I_R has a non-zero value and using Kirchhoff's Laws[34] can be calculated as

$$I_R = a_2 \frac{R + R_4 + \delta R}{(R + \delta R)(b_2 - a_2 R_4)} V \tag{A6.3}$$

where

$$a_2 = \frac{\delta R \cdot R_3}{(R_2 + R_3)(R + R_4 + \delta R)} \tag{A6.4}$$

$$b_2 = \frac{R_4(R + \delta R)}{R + R_4 + \delta R} + R_R + \frac{R_2 R_3}{R_2 + R_3} \tag{A6.5}$$

and where V is the voltage across the probe wire. Neglecting small values of δR as compared with larger values of other resistances, equations (A6.3) to (A6.5) can be simplified to

$$\frac{I_R}{\delta R} = \frac{a_1}{b_1} \frac{R + R_R}{R} V \tag{A6.6}$$

where

$$a_1 = \frac{R_3}{(R_2 + R_3)(R + R_4)} \tag{A6.7}$$

$$b_1 = R_R + \frac{R_2 R_3}{R_2 + R_3} + \frac{R R_4}{R + R_4} \quad . \tag{A6.8}$$

For probe wires made of platinum and small temperature changes, the

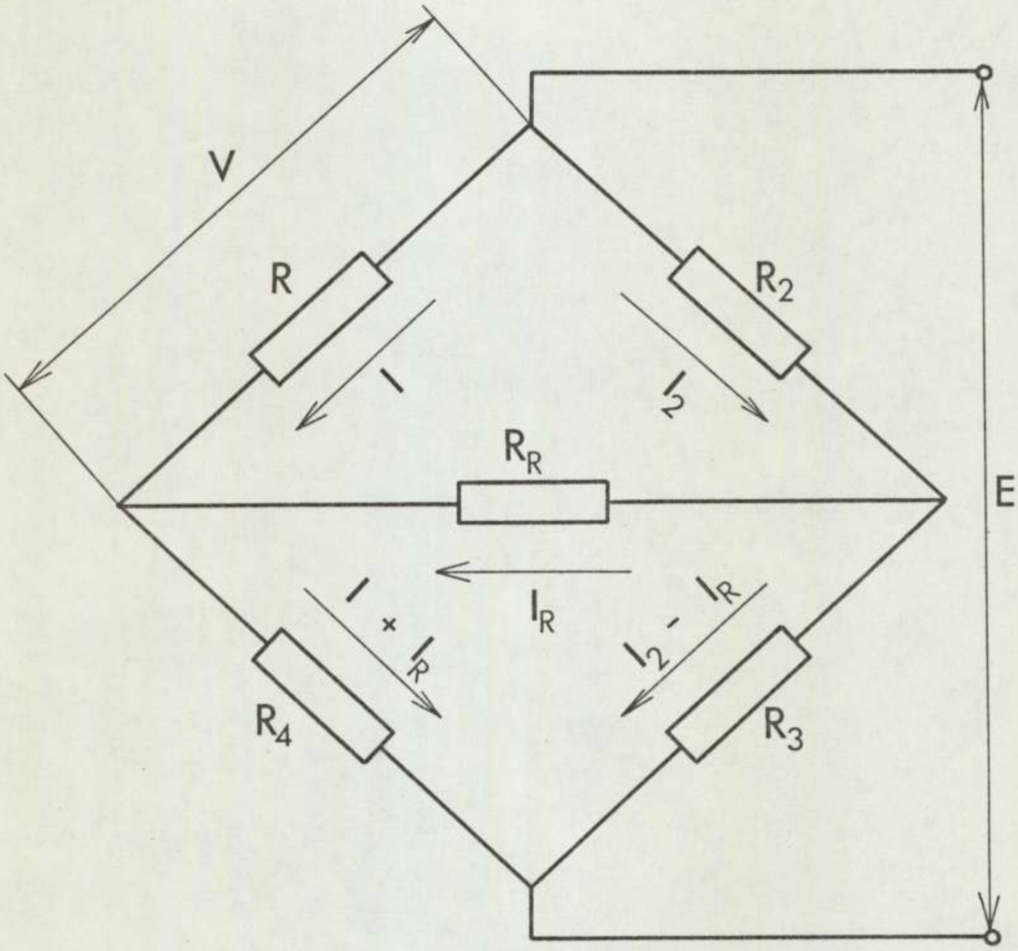

Fig. A6.1: Schematic diagram of the bridge incorporating the heat transfer probe.

calibration curve for the average wire temperature may be approximated by a straight line, so that

$$\frac{\delta T}{\delta R_2} = S_W \tag{A6.9}$$

where S_W is a calibration constant which is determined experimentally. Furthermore, the calibration constant of the galvanometer is given by

$$S_g = \frac{\delta x}{I_R} \tag{A6.10}$$

where δx is the deflection of the UV-recorder from its equilibrium position. Constant S_g is either obtained from tables or determined experimentally.

Hence the calibration constant of a UV-recorder trace, defined by

$$S_t = \frac{\delta T}{\delta x} \quad , \tag{A6.11}$$

can be rewritten as

$$S_t = \frac{\delta T}{\delta R_2} \frac{\delta R_2}{\delta R} \frac{\delta R}{I_R} \frac{I_R}{\delta x} \tag{A6.12}$$

where

$$\frac{\delta R_2}{\delta R} = \frac{R_3}{R_4} \quad . \tag{A6.13}$$

Finally comparing equations (A6.6) to (A6.13), the final result for the calibration curve of the UV-recorder traces is

$$S_t = \frac{S_W}{V \cdot S_b \cdot S_g} \tag{A6.14}$$

where

$$S_b = \frac{R_4}{R_3} \frac{R + R_4}{R} \frac{a_1}{b_1} \quad . \tag{A6.15}$$

Appendix 7.

VOIDAGE DISTRIBUTION IN THE WIRE VICINITY.

The material concentration, $\beta(r)$, is given analogously to equations (3.23) and (3.24) as

$$\Delta r \leq d_P \qquad \beta(r) = (1-\varepsilon_E)\,\frac{d_P}{\Delta r}\,\frac{V(r)}{V_P} \tag{A7.1}$$

$$\Delta r > d_P \qquad \beta(r) = (1-\varepsilon_E) \tag{A7.2}$$

where

$$\Delta r = r - a \tag{A7.3}$$

and where $V(r)$, the volume of that part of a spherical particle which can be found in the annulus of the reference and the constraining cylinder, is calculated as follows (Figure 6.1):

Let

$$V(r) = V_1(r) + 4V_2(r) \tag{A7.4}$$

where $V_1(r)$ is the volume of that segment of the particle which is cut by a plane distance D_1 from the origin and $V_2(r)$ is the volume of a quarter of the remaining part of $V(r)$.

$V_1(r)$ is given by standard textbooks[50] as,

$$V_1(r) = 0.5\pi(r^2 - D_1^2)\cdot(D_1 - a) + \frac{1}{6}\pi\,(D_1 - a)^3 \tag{A7.5}$$

and $V_2(r)$ is calculated as follows

$$V_2(r) = \int_{D_1}^{r} \int_{0}^{\theta(r)} \int_{0}^{x(r,\theta)} r\,dx\,d\theta\,dr \tag{A7.6}$$

where

$$x(r,\theta) = [a_P^2 - (r - a - a_P)^2]^{0.5} \tag{A7.7}$$

$$\theta(r) = \arctan\,[(\frac{r}{D_1})^2 - 1\,]^{0.5} \quad . \tag{A7.8}$$

Next, the integrations with respect to x and θ are performed,

$$V_2(r) = \int_{D_1}^{r} r\,\theta(r)\,x(r,\theta)\,dr\ , \tag{A7.9}$$

and equation (A7.9) is rearranged as

$$V_2(R) = a_P^3 \int_{\delta}^{\sigma R} \eta[1 - (\eta-\sigma-1)^2]^{0.5}\arctan[(\tfrac{\eta}{\delta})^2 - 1]^{0.5}\, d\eta \qquad (A7.10)$$

where

$$R = r/a \qquad (A7.11)$$

$$\sigma = a/a_P \qquad (A7.12)$$

$$\delta = \frac{\sigma^2(R + 1) + 2\sigma}{2(\sigma + 1)} \quad . \qquad (A7.13)$$

From equations (A7.1), (A7.2), (A7.4), (A7.5) and (A7.10), the final result for the voidage distribution in the wire vicinity is obtained as

$R \leq 1 + \frac{2}{\sigma}$

$$\varepsilon(R) = 1 - \frac{3(1-\varepsilon_E)}{2\pi\sigma(R-1)}\{0.5\pi(\sigma^2R^2 - \delta^2)(\delta - \sigma) + \frac{1}{6}\pi(\delta - \sigma)^3$$

$$+ 4\int_{\delta}^{\sigma R} \eta[1 - (\eta - \sigma - 1)^2]^{0.5} \arctan[(\tfrac{\eta}{\delta})^2 - 1]^{0.5} d\eta\} \qquad (A7.14)$$

$R > 1 + \frac{2}{\sigma}$

$$\varepsilon(R) = \varepsilon_E \quad . \qquad (A7.15)$$

The numerical values of the voidage are obtained by the numerical integration of equation (A7.14). The method of the numerical integration is shown in Appendix 8.

Appendix 8.

PROGRAMME FOR THE NUMERICAL SOLUTION OF EQUATIONS (4.41) TO (4.45).

This programme is used to calculate the first approximation to the average temperature of the wire which is placed in an emulsion phase of solid particles and the fluidizing gas. Certain modifications of the programme are required when the wire is placed in a liquid. The modifications are discussed at the end of this Appendix.

```
      MASTER ALENA
      DIMENSION A(100,10),B(100,10),ALPHA(100),BETA(100),H(100),
     XG(100),DERH(100),C1(100),C2(100),C3(100),C4(100)
C     MP = number of steps in the R-direction
C     NP = (number of steps in the Z-direction) + 1
C     DELTA = step size in fractions of the wire radius
C     AKG = thermal conductivity of the fluidizing gas
C     AKS = thermal conductivity of solid particles
C     AKW = thermal conductivity of the wire material
C     AKPG = thermal diffusivity of the fluidizing gas
C     AKPS = thermal diffusivity of solid particles
C     AKPW = thermal diffusivity of the wire material
C     ASP = aspect ratio of the probe wire
C     AW = radius of the probe wire
C     AP = mean equivalent radius of the solid particles
C     VOID = mean voidage of the emulsion phase
C     FI1 = function of (AKG,AKS) given by Kunii and Smith43
C     FI2 = function of (AKG,AKS) given by Kunii and Smith43
C     SOME ADDITIONAL PARAMETERS
      AKGS=AKG/AKS
      AKPGS=AKPG/AKPS
      ASP2=ASP*ASP
      DELTA2=DELTA*DELTA
      RATWP=AW/AP
      AN=(DELTA*(NP-1.0))**2.0
      ANASP2=AN/ASP2
      CONC=1.0-VOID
      MP1=MP-1
      MP2=MP-2
      NP1=NP-1
      NP2=NP-2
      Y=0.0
      SUMMN=0.0
      DELTR=DELTA*RATWP
C     THERMOPHYSICAL PROPERTIES OF THE EMULSION PHASE - KUNII & SMITH (43)
C     AKB = THERMAL CONDUCTIVITY OF THE EMULSION PHASE
C     AKPB = THERMAL DIFFUSIVITY OF THE EMULSION PHASE
      IF(VOID.GT.0.476)FI=FI1
      IF(VOID.LE.0.476.AND.VOID.GE.0.260)FI=FI2+(FI1-FI2)
     X*(VOID-0.260)/0.216
      IF(VOID.LT.0.260)FI=FI2
      AKB=AKG*(VOID+0.95*CONC/(FI+0.66666*AKGS))
      AKPB=(AKB*AKPS)/(AKS*CONC)
```

```
C     SOME ADDITIONAL PARAMETERS
      AKGB=AKG/AKB
      AKBW=AKB/AKW
      AKPBW=AKPB/AKPW
C     CALCULATIONS OF PROPERTIES
      DO 100 J1=1,MP
      RD=(J1-1.0)*DELTR
      IF(RD.LT.0.0000001) GO TO 208
      IF(RD.GE.2.0) GO TO 101
      DELTAP=1.0+RATWP
      ZETA=RD+RATWP
      ZETA2=ZETA*ZETA
      ZETA0=0.5*(ZETA2+2.0*RATWP+RATWP*RATWP)/DELTAP
      ZB=ZETA0-RATWP
      VOL1=1.5708*(ZETA2-ZETA0*ZETA0)*ZB+0.5236*ZB*ZB*ZB
      DZETA=ZETA-ZETA0
      IF(DZETA.LT.0.000001) GO TO 810
      DET=DZETA/20.0
      ETA=ZETA0-DET
      SVOL=0.0
      DO 8400 K=1,21
      ETA=ETA+DET
      EZ0=ETA/ZETA0
      EZ02=EZ0*EZ0
      IF(EZ02.LE.1.0) AGT=0.0
      IF(EZ02.GT.1.0) AGT=(EZ02-1.0)**0.5
      ETD=ETA-DELTAP
      SX=ETA*DET*((1.0-ETD*ETD)**0.5)*ATAN(AGT)
      IF(K.EQ.1.OR.K.EQ.21) SX=0.5*SX
      SVOL=SVOL+SX
 8400 CONTINUE
      GO TO 820
  810 VOL2=0.0
      GO TO 830
  820 VOL2=4.0*SVOL
  830 BERTA1=0.47746*(VOL1+VOL2)/RD
      GO TO 850
  208 BERTA1=0.0
  850 ERTA=1.0-CONC*BERTA1
      IF(ERTA.GT.0.476)FI=FI1
      IF(ERTA.LE.0.476.AND.ERTA.GE.0.260)FI=FI2+4.63*(FI1-FI2)*
     X(ERTA-0.260)
      IF(ERTA.LT.0.260)FI=FI2
      G(J1)=AKGS*(1.0/CONC-BERTA1)/AKPGS+BERTA1
      H(J1)=AKGB*(ERTA+(0.95*(1.0-ERTA))/(FI+0.66667*AKGS))
      GO TO 100
  101 G(J1)=1.0
      H(J1)=1.0
  100 CONTINUE
      DO 200 J2=2,MP1
      DERH(J2)=(H(J2+1)-H(J2-1))/(2.0*DELTA)
      ALPHA(J2)=DERH(J2)/G(J2)
  200 BETA(J2)=H(J2)/G(J2)
C     CONVERGENCE CONDITIONS
      HMAX=AMAX1(BETA(2),BETA(3),BETA(4),BETA(5),BETA(6),
     XBETA(7),BETA(8),BETA(9),BETA(10),BETA(11),BETA(12),
     XBETA(13),BETA(14),BETA(15),BETA(16),BETA(17),BETA(18),
     XBETA(19),BETA(20),BETA(21),BETA(22),BETA(23),BETA(24),
     XBETA(25),BETA(26),BETA(27),BETA(28),BETA(29),BETA(30),
     XBETA(31),BETA(32),BETA(33),BETA(34),BETA(35),BETA(36),
     XBETA(37),BETA(38),BETA(39),BETA(40),BETA(41),BETA(42))
```

```
      AM1=0.5/(HMAX*(1.0+ANASP2))
      AM2=0.5/(ANASP2/AKPBW+H(1)*AKBW*DELTA/AKPBW)
      AM=AMIN1(AM1,AM2)
      FMULT=AM*DELTA2
      DELTCHCK=2.0/(1.0+ALPHA(2)/BETA(2))
      WRITE(2,1000) AM,FMULT,AM1,AM2,DELTCHCK,H(1),G(1)
C     AM = given by equation (A4.6)
C     FMULT = step size in the Fo-direction; equation (A4.1)
      IF(DELTCHCK.LT.DELTA) STOP
      WRITE(2,1001)
      DO 300 J3=2,MP1
      C1(J3)=0.5*AM*DELTA*ALPHA(J3)
      C2(J3)=AM*BETA(J3)
      C3(J3)=0.5*AM*DELTA*BETA(J3)/(1.0+(J3-1.0)*DELTA)
      C4(J3)=AM*ANASP2*BETA(J3)
  300 WRITE(2,1002)H(J3),G(J3),DERH(J3),ALPHA(J3),BETA(J3),
     XC1(J3),C2(J3),C3(J3),C4(J3)
C     C1(J3) = given by equation (A4.14)
C     C2(J3) = given by equation (A4.15)
C     C3(J3) = given by equation (A4.16)
C     C4(J3) = given by equation (A4.17)
      WRITE(2,1001)
C     CALCULATION OF THE EQUIVALENT CONDUCTIVITY OF THE FIRST SLAB
      CSB=(H(2)-H(1))/DELTA
      CSA=H(1)-CSB
      RAB=CSA/CSB
      HEFF=(DELTA*CSA)/(ALOG((1.0+RAB)*(1.0+DELTA)/(1.0+RAB+DELTA)))
      WRITE(2,1010) H(1),HEFF,H(2)
C     HEFF = equivalent conductivity given by equation (A4.27)
      WRITE(2,1001)
      H(1)=HEFF
      C5=AM*ANASP2/AKPBW
      C6=2.0*AM*H(1)*DELTA*AKBW/AKPBW
      C7=AM*DELTA2*AKBW/AKPBW
C     C5 = given by equation (A4.18)
C     C6 = given by equation (A4.21)
C     C7 = given by equation (A4.20)
C     INITIAL VALUES
      DO 10 K1=1,MP
      DO 10 L1=1,NP
      A(K1,L1)=0.0
   10 B(K1,L1)=0.0
C     DIFFERENCE EQUATIONS
      DO 20 J20=1,200000
      F=FMULT*J20
      DO 30 K3=1,MP2
      DO 40 L4=1,NP2
   40 B(1+K3,1+L4)=A(2+K3,1+L4)*(C1(1+K3)+C2(1+K3)+C3(1+K3))+
     XA(K3,1+L4)*(C2(1+K3)-C1(1+K3)-C3(1+K3))+C4(1+K3)*
     X(A(1+K3,2+L4)+A(1+K3,L4))+A(1+K3,1+L4)*(1.0-2.0*(C2(1+K3)+
     XC4(1+K3)))
      B(1+K3,NP)=B(1+K3,NP1)
      IF(B(1+K3,NP).LT.0.0000000001) GO TO 50
   30 CONTINUE
      K3=MP2
   50 AJ2=J20
      DO 60 L6=1,NP2
      B(1,1+L6)=A(1,1+L6)*(1.0-2.0*C5-C6)+C5*(A(1,2+L6)+A(1,L6))+
     XC6*A(2,1+L6)+C7
   60 B(MP,1+L6)=B(MP1,1+L6)
      B(1,NP)=B(1,NP1)
```

```
      B(MP,NP)=B(MP,NP1)
      K7F=K3+2
      DO 70 K7=1,K7F
      DO 70 L7=2,NP
   70 A(K7,L7)=B(K7,L7)
      ANU=0.5*A(1,NP)
      DO 11 J=2,NP1
   11 ANU=ANU+A(1,J)
      ANU=ANU/NP1
      SUMMN=SUMMN+ANU
      Z=10.0*ALOG10(AJ2)-Y
      IF(Z.LT.1.0) GO TO 20
      Y=Y+1.0
      ANUM=FMULT*SUMMN/F
      WRITE(2,1003)F,ANU,ANUM,K3
C     F = instantaneous Fourier number
C     ANU = instantaneous average wire temperature
C     ANUM = time-mean average wire temperature
      WRITE(2,1004) ((A(I8,J8),J8=2,NP),I8=1,66,5)
      WRITE(2,1001)
   20 CONTINUE
 1000 FORMAT(7E15.6)
 1001 FORMAT(/)
 1002 FORMAT(9E11.4)
 1003 FORMAT(3E20.7,10X,I7)
 1004 FORMAT(3E11.3)
 1010 FORMAT(3E20.8)
      STOP
      END
      FINISH
```

If the wire is placed in a liquid, the liquid constitutes the dense phase and hence the thermophysical properties of the dense phase do not have to be calculated.

The input parameters then are:

MP
NP
DELTA
ASP
AW
AKW
AKPW
AKB = thermal conductivity of the liquid
AKPB = thermal diffusivity of the liquid
H(J) = 1, for all J
G(J) = 1, for all J
ALPHA(J) = 0, for all J
BETA(J) = 1, for all J

The modified programme is then obtained by using the above input parameters and the original program from the statement

CONVERGENCE CONDITIONS.

Appendix 9.

PROGRAMME FOR THE NUMERICAL SOLUTION OF EQUATIONS (4.67) TO (4.76).

This programme is used to calculate the temperature of the wire which is placed in an emulsion phase of solid particles and the fluidizing gas. Certain modifications of the programme are required when the wire is placed in a liquid. The modifications are analogous to those discussed in Appendix 8.

```
      MASTER ALENA
      DIMENSION A(100,10),B(100,10),ALPHA(100),BETA(100),H(100),
     XG(100),DERH(100),C1(100),C2(100),C3(100),C4(100),C5(100),
     XC6(100)
C     L = number of steps in the R-direction
C     NP = (number of steps in the Z-direction) + 1 ; taken as 4
C     DELTA = step size in fractions of the wire radius
C     AKG = thermal conductivity of the fluidizing gas
C     AKS = thermal conductivity of solid particles
C     AKW = thermal conductivity of the wire material
C     AKPG = thermal diffusivity of the fluidizing gas
C     AKPS = thermal diffusivity of solid particles
C     AKPW = thermal diffusivity of the wire material
C     ASP = aspect ratio of the probe wire
C     AW = radius of the probe wire
C     AP = mean equivalent radius of the solid particles
C     VOID = mean voidage of the emulsion phase
C     FI1 = function of (AKG,AKS) given by Kunii and Smith[43]
C     FI2 = function of (AKG,AKS) given by Kunii and Smith[43]
C     SOME ADDITIONAL PARAMETERS
      AKGS=AKG/AKS
      AKPGS=AKPG/AKPS
      ASP2=ASP*ASP
      LPH=1/DELTA+1
      DELTA2=DELTA*DELTA
      RATWP=AW/AP
      AN=(DELTA*3.0)**2.0
      ANASP2=AN/ASP2
      CONC=1.0-VOID
      L1=L-1
      LPH2=LPH-1
      LPH3=LPH+1
      LPH4=LPH+2
      Y=0.0
      SUM=0.0
      DELTR=DELTA*RATWP
C     THERMOPHYSICAL PROPERTIES OF THE EMULSION PHASE - KUNII & SMITH (43)
C     AKB = THERMAL CONDUCTIVITY OF THE EMULSION PHASE
C     AKPB = THERMAL DIFFUSIVITY OF THE EMULSION PHASE
      IF(VOID.GT.0.476)FI=FI1
      IF(VOID.LE.0.476.AND.VOID.GE.0.260)FI=FI2+(FI1-FI2)
     X*(VOID-0.260)/0.216
      IF(VOID.LT.0.260)FI=FI2
      AKB=AKG*(VOID+0.95*CONC/(FI+0.66666*AKGS))
      AKPB=(AKB*AKPS)/(AKS*CONC)
```

```
C     SOME ADDITIONAL PARAMETERS
      AKGB=AKG/AKB
      AKBW=AKB/AKW
      AKPBW=AKPB/AKPW
C     CALCULATIONS OF PROPERTIES
      DO 100 J1=LPH,L
      RD=(J1-LPH)*DELTR
      IF(RD.GE.2.0) GO TO 101
      IF(RD.LT.0.000001) GO TO 208
      DELTAP=1.0+RATWP
      ZETA=RD+RATWP
      ZETA2=ZETA*ZETA
      ZETAO=0.5*(ZETA2+2.0*RATWP+RATWP*RATWP)/DELTAP
      ZB=ZETAO-RATWP
      VOL1=1.5708*(ZETA2-ZETAO*ZETAO)*ZB+0.5236*ZB*ZB*ZB
      DZETA=ZETA-ZETAO
      IF(DZETA.LT.0.000001) GO TO 810
      DET=DZETA/20.0
      ETA=ZETAO-DET
      SVOL=0.0
      DO 8400 K=1,21
      ETA=ETA+DET
      EZO=ETA/ZETAO
      EZO2=EZO*EZO
      IF(EZO2.LE.1.0) AGT=0.0
      IF(EZO2.GT.1.0) AGT=(AZO2-1.0)**0.5
      ETD=ETA-DELTAP
      SX=ETA*DET*((1.0-ETD*ETD)**0.5)*ATAN(AGT)
      IF(K.EQ.1.OR.K.EQ.21) SX=0.5*SX
      SVOL=SVOL+SX
 8400 CONTINUE
      GO TO 820
  810 VOL2=0.0
      GO TO 830
  820 VOL2=4.0*SVOL
  830 BERTA1=0.47746*(VOL1+VOL2)/RD
      GO TO 850
  208 BERTA1=0.0
  850 ERTA=1.0-CONC*BERTA1
      IF(ERTA.GT.0.476)FI=FI1
      IF(ERTA.LE.0.476.AND.ERTA.GE.0.260)FI=FI2+4.63*(FI1-FI2)*
     X(ERTA-0.260)
      IF(ERTA.LT.0.260)FI=FI2
      G(J1)=AKGS*(1.0/CONC-BERTA1)AKPGS+BERTA1
      H(J1)=AKGB*(ERTA+(0.95*(1.0-ERTA))/(FI+0.66667*AKGS))
      GO TO 100
  101 G(J1)=1.0
      H(J1)=1.0
  100 CONTINUE
      DO 200 J2=LPH3,L1
      DERH(J2)=(H(J2+1)-H(J2-1))/(2.0*DELTA)
      ALPHA(J2)=DERH(J2)/G(J2)
  200 BETA(J2)=H(J2)/G(J2)
C     CONVERGENCE CONDITIONS
      HMAX=AMAX1(BETA(LPH3),BETA(LPH4))
      AM1=0.5/(HMAX*(1.0+ANASP2))
      AM2=0.5*AKPBW/(1.0+ANASP2)
      AM=AMIN1(AM1,AM2)
      FMULT=AM*DELTA2
      DELTCHCK=2.0/(1.0+ALPHA(LPH3)/BETA(LPH3))
```

```
      WRITE(2,1000)AM,AM1,AM2,FMULT,DELTCHCK,H(LPH),G(LPH)
      WRITE(2,1001)
      IF(DELTCHCK.LT.DELTA) STOP
      AMKAP=AM/AKPBW
      C7=AMKAP*ANASP2
      C8=1.0-2.0*AMKAP*(1.0+ANASP2)
      WRITE(2,1002)C7,C8
      WRITE(2,1001)
      DO 400 J4=2,LPH2
      C5(J4)=AMKAP*(1.0+0.5/(J4-1))
      C6(J4)=AMKAP*(1.0-0.5/(J4-1))
  400 WRITE(2,1003)J4,C5(J4),C6(J4)
      WRITE(2,1001)
      DO 300 J3=LPH3,L1
      C1(J3)=0.5*AM*DELTA*ALPHA(J3)
      C2(J3)=AM*BETA(J3)
      C3(J3)=0.5*AM*DELTA*BETA(J3)/(1.0+(J3-LPH)*DELTA)
      C4(J3)=AM*ANASP2*BETA(J3)
  300 WRITE(2,1004)J3,H(J3),G(J3),DERH(J3),ALPHA(J3),BETA(J3),
     XC1(J3),C2(J3),C3(J3),C4(J3)
      WRITE(2,1001)
C     CALCULATION OF THE EQUIVALENT CONDUCTIVITY OF THE FIRST SLAB
      CSB=(H(LPH3)-H(LPH))/DELTA
      CSA=H(LPH)-CSB
      RAB=CSA/CSB
      HEFF=(-1.0)*CSA*ALOG(1.0-DELTA)/(ALOG((1.0+RAB)*(1.0+DELTA)/
     X(1.0+RAB+DELTA)))
      AKAST=AKBW*HEFF
      AKAST1=AKAST+1.0
      WRITE(2,1005)H(LPH),HEFF,H(LPH3),AKAST
      WRITE(2,1001)
C     INITIAL VALUES
      DO 9100 M1=1,LPH
      A(M1,1)=1.286
      A(M1,2)=1.286
      A(M1,3)=0.964
 9100 A(M1,4)=0.0
      DO 9200 M2=LPH3,L
      DO 9200 N2=1,4
      A(M2,N2)=0.0
 9200 B(M2,N2)=0.0
C     DIFFERENCE EQUATIONS
      DO 9300 L3=1,100000
      F=FMULT*L3
      DO 9400 M4=2,LPH2
      DO 9400 N4=2,3
 9400 B(M4,N4)=C5(M4)*A(M4+1,N4)+C6(M4)*A(M4-1,N4)+C7*(A(M4,N4+1)+
     XA(M4,N4-1))+C8*A(M4,N4)
      DO 9500 M5=LPH3,L1
      DO 9501 N5=2,3
 9501 B(M5,N5)=A(M5+1,N5)*(C1(M5)+C2(M5)+C3(M5))+A(M5-1,N5)*
     X(C2(M5)-C1(M5)-C3(M5))+C4(M5)*(A(M5,N5+1)+A(M5,N5-1))+
     XA(M5,N5)*(1.0-2.0*(C2(M5)+C4(M5)))
      IF(B(M5,1).LT.0.0000000001) GO TO 9600
 9500 CONTINUE
      M5=L
 9600 AL3=L3
      M7F=M5
      DO 9601 N=2,3
 9601 B(LPH,N)=(AKAST*B(LPH3,N)+B(LPH2,N))/AKAST1
      DO 9602 M=2,LPH2
```

```
 9602 B(M,1)=B(M,2)
      DO 9603 M=LPH3,M7F
 9603 B(M,1)=B(M,2)
      DO 9604 N=2,3
 9604 B(1,N)=B(2,N)
      DO 9605 N=1,3
 9605 B(L,N)=B(L1,N)
      B(1,1)=0.5*(B(1,2)+B(2,1))
      B(LPH,1)=0.5*(B(LPH,2)+(B(LPH2,1)+AKAST*B(LPH3,1))/AKAST1)
      TEM=0.375*(B(LPH,2)+B(LPH,3))+0.125*B(LPH,1)
      DO 9700 M7=1,M7F
      DO 9700 N7=1,3
 9700 A(M7,N7)=B(M7,N7)
      SUM=SUM+TEM
      Z=10.0*ALOG10(AL3)-Y
      IF(Z.LT.1.0) GO TO 9300
      Y=Y+1.0
      TEMTM=SUM*FMULT/F
      WRITE(2,1006)F,TEM,TEMTM,M7F
C     F = Fourier number
C     TEM = instantaneous temperature given by equation (4.87)
C     TEMTM = time-mean temperature given by equation (4.88)
      WRITE(2,1001)
 9300 CONTINUE
 1000 FORMAT(7E12.5)
 1001 FORMAT(/)
 1002 FORMAT(2E20.5)
 1003 FORMAT(I5,2E12.5)
 1004 FORMAT(I5,9E12.5)
 1005 FORMAT(4E25.10)
 1006 FORMAT(3E20.8,I10)
      STOP
      END
      FINISH
```